Advanced miniaturised electrochemical detection for flow-based analytical systems

A thesis submitted in fulfilment of the requirements for the degree of Doctor of Philosophy

Muhammed Ariful Islam (Arif)

B. Sc in Applied Chemistry and Chemical Engineering

MSc in Chemical Engineering

PhD Candidate in Chemical Sciences, ACROSS, Chemistry

ACROSS - Australian Centre for Research on Separation Science

School of Natural Sciences | College of Sciences and Engineering

University of Tasmania, Private Bag 75, Hobart 7001, Australia

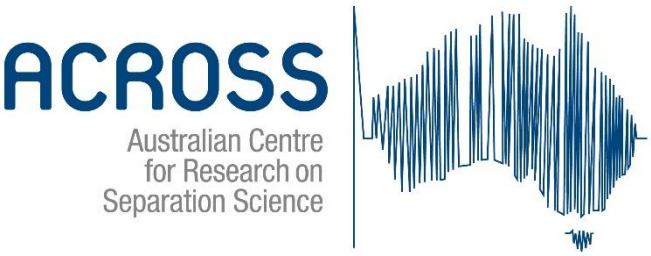

April 2020

Statements and declarations

The thesis contains a declaration of originality and the appropriate authority of access statement.

Declaration of Originality

"This thesis contains no material which has been accepted for a degree or diploma by the University or any other institution, except by way of background information and duly acknowledged in the thesis, and to the best of my knowledge and belief no material previously published or written by another person except where due acknowledgement is made in the text of the thesis, nor does the thesis contain any material that infringes copyright."

Muhammed Ariful Islam

Authority of Access Statement

This thesis may be made available for loan. Copying and communication of any part of this thesis is prohibited for two years from the date this statement was signed; after that time limited copying and communication is permitted in accordance with the Copyright Act 1968.

Muhammed Ariful Islam

Statement regarding Published work contained in the Thesis

"The publishers of the papers comprising Chapters 1-4 hold the copyright for that content, and access to the material should be sought from the respective journals. The remaining non-published content of the thesis may be made available for loan and limited copying and communication in accordance with the Copyright Act 1968."

Muhammed Ariful Islam

Statement of Co-Authorship

The following people are contributed to the below works undertaken as part of this thesis:

Chapter 1: Muhammed Ariful Islam was the primary author and wrote the chapter. The co-authors (Dr Parvez Mahbub, Prof. Pavel N. Nesterenko, Prof. Brett Paull, and Prof. Mirek Macka) contributed a total of 20% to the work. All co-authors contributed to ideas, formalisation, refinement and presentation. We the undersigned agree with the above stated "proportion of work undertaken" for the above submitted scripts contributing to this thesis.

Chapter 2: Muhammed Ariful Islam was the primary author and conducted all the experiments, analysed data and wrote the chapter. The co-authors (Shing Chung Lam, Yan Li, and Mostafa A. Atia) offered experimental assistance. The co-authors (Shing Chung Lam, Yan Li, Mostafa A. Atia, Dr Parvez Mahbub, Prof. Pavel N. Nesterenko, Prof. Brett Paull, and Prof. Mirek Macka) contributed a total of 40% to the work. All co-authors contributed to ideas, formalisation, refinement and presentation. We the undersigned agree with the above stated "proportion of work undertaken" for the above submitted scripts contributing to this thesis.

Chapter 3: Muhammed Ariful Islam was the primary author and conducted all the experiments, analysed data and wrote the chapter. The co-author (Mostafa A. Atia) offered experimental assistance. The co-authors (Mostafa A. Atia, Prof. Mirek Macka, Professor Brett Paull, and Dr Parvez Mahbub,) contributed a total of 20% to the work. All co-authors contributed to ideas,

formalisation, refinement and presentation. We the undersigned agree with the above stated "proportion of work undertaken" for the above submitted scripts contributing to this thesis.

Chapter 4: Muhammed Ariful Islam was the primary author and conducted all the experiments, analysed data and wrote the chapter. The co-authors (Aleksandra N. Koreshkova and Vipul Gupta) offered experimental assistance. The co-authors (Dr Trevor Lewis, Prof. Mirek Macka, Prof. Brett Paull, and Dr Parvez Mahbub) contributed a total of 20% to the work. All co-authors contributed to ideas, formalisation, refinement and presentation. We the undersigned agree with the above stated "proportion of work undertaken" for the above submitted scripts contributing to this thesis.

List of Publications

The research works described in this thesis have been reported in the following publications:

1. M.A. Islam, P. Mahbub, P.N. Nesterenko, B. Paull, M. Macka, Prospects of pulsed amperometric detection in flow-based analytical systems - A review, Anal. Chim. Acta, 1052 (2019) 10-26.

   DOI: https://doi.org/10.1016/j.aca.2018.10.066

   This journal paper comprises the Chapter 1 (reproduced with permission, © 2018 Elsevier B.V).

2. M.A. Islam, S.C. Lam, Y. Li, M.A. Atia, P. Mahbub, P.N. Nesterenko, B. Paull, M. Macka, Capillary gap flow cell as capillary-end electrochemical detector in flow-based analysis, Electrochim. Acta, 303 (2019) 85-93.

   DOI: https://doi.org/10.1016/j.electacta.2019.02.026

   This journal paper comprises the Chapter 2 (reproduced with permission, © 2018 Elsevier B.V).

3. M.A. Islam, S.C. Lam, P. Mahbub, P.N. Nesterenko, B. Paull, M. Macka, Electrochemical detection in miniaturised capillary separation platforms: Gap cell for amperometric detection for portable liquid chromatography, XVIII. Workshop of Biophysical Chemists and Electrochemists, Masaryk University, 2018, pp. 12.

   URL: http://www.sci.muni.cz/~labifel/files/soubory/sbornik_2018.pdf

   This conference paper comprises a small section of the Chapter 2.

4. M.A. Islam, M.A. Atia, M. Macka, B. Paull, P. Mahbub, Electrochemical characterisation of nanoparticulate zirconium dioxide-on-gold electrode for electrochemical detection in flow-based analytical systems, Electrochim. Acta, 318 (2019) 61-68.

   DOI: https://doi.org/10.1016/j.electacta.2019.06.031

   This paper comprises the Chapter 3 (reproduced with permission, © 2018 Elsevier B.V).

5. M.A. Islam, A. Koreshkova, V. Gupta, T. Lewis, M. Macka, B. Paull, P. Mahbub, Fast pulsed amperometric waveform for miniaturised flow-through electrochemical detection: Application in monitoring graphene oxide reduction, Electrochim. Acta, 328 (2019) 135087.

   DOI: https://doi.org/10.1016/j.electacta.2019.135087

   This paper comprises the Chapter 4 (reproduced with permission, © 2018 Elsevier B.V).

We undersigned agree with the above stated contribution of work undertaken for each of the above published (or submitted) peer-reviewed manuscripts contributing to this thesis.

17.10.2019	18.10.2019	18-10-2019
Muhammed Ariful Islam	***Prof. Brett Paull***	***Prof. Jason A Smith***
PhD Candidate	Primary Supervisor	Acting Head of School
School of Natural Sciences	School of Natural Sciences	School of Natural Sciences
University of Tasmania	University of Tasmania	University of Tasmania

List of Conferences

Parts of research works described in this thesis have been reported in the following conference presentations:

1. M.A. Islam, P. Mahbub, M. Macka, B. Paull, Disposable zirconium-gold electrode for sensitive electrochemical detection in HPLC, 48th International Symposium on High-Performance Liquid Phase Separations and Related Techniques, Milan, Italy (16-20 Jun 2019).

   www.hplc2019-milan.org

2. M.A. Islam, P. Mahbub, T. Lewis, M. Macka, B. Paull, Monitoring chemical reduction of graphene oxide using pulsed amperometric waveform in ion chromatography, 9th edition of the largest European Conference and Exhibition in Graphene and 2D materials 2019, Rome, Italy (25-28 Jun 2019).

   www.grapheneconf.com/2019

3. M.A. Islam, S.C. Lam, P. Mahbub, P.N. Nesterenko, B. Paull, M. Macka, Portable electrochemical detection in miniaturised capillary separation platforms: Gap cell for amperometric detection for portable liquid chromatography, Workshop of Biophysical Chemists and Electrochemists, Brno, Czech Republic (12-13 Sep 2018) (Oral presentation by Prof. Mirek Macka).

   www.sci.muni.cz/~labifel

4. M.A. Islam, P. Mahbub, P.N. Nesterenko, B. Paull, M. Macka, End-capillary gap flow cell as electrochemical detector in capillary LC-hyphenated detection system, 25th Annual RACI R&D Topics Conference in Analytical and Environmental Chemistry, Hobart, Australia (03-06 Dec 2017).

   www.rndtopics.com

5. M.A. Islam, P. Mahbub, P.N. Nesterenko, B. Paull, M. Macka, Analysis of electrochemical cell efficiency and effective cell volume of a gap flow cell as a tool for end-capillary electrochemical detection, 8th Australia New Zealand Nano-Microfluidics Symposium (ANZNMF), Hobart, Australia (26-29 Jun 2017).

   www.anznmf.com

6. M.A. Islam, P.N. Nesterenko, B. Paull, M. Macka, Gap flow cell for end-capillary electrochemical detection, 24th Annual RACI R&D Topics Conference in Analytical and Environmental Chemistry, Sydney, Australia (05-07 Dec 2016). www.rndtopics.com

7. M.A. Islam, P.N. Nesterenko, B. Paull, M. Macka, Pulsed electrochemical detection in microfluidic and paperfluidic platforms, 23rd Annual RACI R&D Topics Conference in Analytical and Environmental Chemistry, Melbourne, Australia (06-09 Dec 2015).

   www.rndtopics.com

Acknowledgements

I would like to thank following people for their support during the last few years in my PhD work.

My primary supervisor Prof. Brett Paull for his supervision, encouragements and for supporting me to become a better scientist during the whole work of my PhD. Thank you, for giving me the chance to work with you and learn from you.

My co-supervisors Dr Parvez Mahbub and Dr Trevor Lewis, and research advisor Prof. Mirek Macka for their supervision, encouragements and supporting me during the countless hours of working in the laboratory. Thank all of you for giving me an insight into your ways of working and teaching me how to break big scientific problems down into small ones.

My colleagues in the Australian Centre for Research on Separation Science (ACROSS), department of Chemistry for making an exceptionally empowering workplace especially glad to Murray Frith (former Laboratory Manager, Chemistry), Carol Jacob (former Manager, ACROSS), and Dr Petr Smejkal (Research technician, ACROSS).

My beloved family members, specially my wife Merin Nigar and son Arshan Mehmet, for their support and for being so empathic and understanding always. The author MAI dedicates the thesis to his all family members for their continued support to keep things in perspective that made the completion of this work possible.

The authors gratefully acknowledge the Tasmanian graduate research scholarship (TGRS) awarded to MAI.

Table of Contents

List of Abbreviations

2,3-DHBA	2,3-dihydroxybenzoic acid
A	Electrode geometric area
A_s	Peak asymmetry factor
ACN	Acetonitrile
AD	Amperometric detection
Ag	Silver
APAD	Activated pulsed amperometric detection
C	Concentration [mol L^{-1}]
C^4D	Capacitively-coupled contactless conductivity detector
CE	Capillary electrophoresis
CV	Cyclic voltammetry
DC	Direct current
dN/dt	Rate of change of number of moles
E_{det}	Detection potential
E_{red}	Reduction potential
EC	Electrochemical
F	Faraday constant [C mol^{-1}]
$[Fe(CN)_6]^{4-}$	Ferrocyanide
FC	Flow cell
FIA	Flow injection analysis
FWHM	Full width at half maximum
GO	Graphene oxide
rGO	Reduced graphene oxide
HPAEC	High-performance anion exchange chromatography
HPLC	High-performance liquid chromatography
I	Measured current [A]
I_0	Theoretical current corresponding to full conversion [A]
IC	Ion chromatography

IPAD	Integrated pulsed amperometric detection
LC	Liquid chromatography
LODs	Limits of detection
MPAD	Multiplex-pulsed amperometric detection
n	Number of electrons transferred per mole of solute
η	EC conversion efficiency [%]
N	Number of moles of solute oxidised or reduced
N_P	Plate number
NaOH	Sodium hydroxide
NMs	Nanomaterials
NPs	Nanoparticles
PAD	Pulsed amperometric detection
PBS	Phosphate buffer solution
PED	Pulsed electrochemical detection
PEEK	Polyether ether ketone
Pt	Platinum
Q	Flow rate [L min^{-1}]
QPAD	Quadrupole pulsed amperometric detection
r	Determination coefficient
RDE	Rotating disk electrode
RE	Reference electrode
Redox	Reduction and oxidation
RP	Reversed phase
RPAD	Reverse pulsed amperometric detection
S/N	Signal-to-noise
SEM	Scanning electron microscopy
SIPAD	Six-potential integrated pulsed amperometric detection
SPEs	Screen-printed electrodes
t	Time [min]

t_{del}	Delay time
t_{det}	Detection time
t_{int}	Integration time
t_{red}	Reduction time
t_R	Retention time
TEM	Transmission electron microscopy
TL-FC	Thin-layer flow cell
V_C	Volume of capillary
V_D	Volume of the detector (gap-FC)
V_E	Effective cell volume
V_I	Void volume contribution by the injector
$w_{h/2}$	Width of the peak at half height
w_L	Distance from leading edge of the peak to peak midpoint
w_R	Distance from peak midpoint to trailing edge of the peak
WE	Working electrode
WJ-FC	Wall-jet flow cell
ZrO_2	Zirconium dioxide

List of Figures

Page No.

List of Tables

Page No.

Abstract

Electrochemical (EC) detection has grown in popularity across the chemical sciences over the last three decades, leading to significant advances in EC techniques for the detection of a wide range of analytes in the liquid phase. EC techniques are being constantly improved, and pulsed amperometric detection (PAD) is considered one of the most advanced EC technique to-date for flow-based analysis. However, a conventional EC system—incorporating a heavy potentiostat with large flow cells (FCs), large electrodes or microelectrodes with complex modification techniques and limited stability, and a long pulsed waveform is typically required to perform PAD for the sensitive detection of most target analytes. Herein, a miniaturised EC detector, rapidly modified disposable electrodes with high stability, and a fast-pulsed waveform have been studied to understand their capabilities and potential to perform advanced PAD within a miniaturised format for flow-based analytical systems.

Initially, a miniaturised gap-FC was demonstrated as a replacement for commonly used larger scale EC detectors (i.e., wall-jet (WJ) or thin-layer (TL) FCs), and its capability for PAD within a miniaturised format explored. The gap-FC overcame the difficulties in miniaturisation of the EC system [1-3], i.e., the rigid construction of the WJ- and TL-FCs [4-9], and the fact that the conventional system was incapable of being coupled with analytical systems operating at nano- to microlitre per minute flow rates. The gap-FC provides a low gap distance (30 µm from capillary outlet to electrode) for the formation of a very thin layer of electrolyte on the electrode surface, achieving high EC conversion efficiency and low effective cell volume. The gap-FC demonstrated the highest efficiency (*ca.* 16-times than reported in [10]) and lowest effective cell volume (35 nL) to-date. With the use of the gap-FC with LC, the sensitivity of the detector for test solutes (namely, ascorbic acid, 2,3-dihydroxybenzoic acid, pyrocatechol and dopamine) was greater than the value reported in the literature (*ca.* 4 to 25-times higher than UV and 2-times higher than previous EC detection). This work provides a comprehensive EC characterisation of miniaturised gap-FC for flow-based analytical systems, which will be beneficial for the advancement of the PAD technique.

Disposable electrodes, rapidly modified with nanoparticles (i.e., ZrO_2 NPs, modification time approximately 10 min), were investigated as a replacement for the commonly applied metal electrodes. The existing electrodes used with the PAD are very sensitive to electroactive analytes but require time-consuming complex modification techniques [11-14], and have limited stability [15, 16]. Furthermore, the effective surface area of the electrode, EC reversibility, and stability of the modified electrodes in continuous flow have not been reported in the literature. In this study, the electrodes modified with ZrO_2 NPs showed a 100% increase of effective surface area as compared to bare electrodes, due to the formation of a porous electrode surface. In addition, a 95 to 180-times improvement of current was achieved due to the formation of the large effective surface area and the minimisation of the capacitance of the double layer. Also, the modified electrodes showed high stability (8.5 hr during continuous-flow and 45 days during intermittent use in flow-through systems) and *ca.* 2-times higher sensitivity to the above-mentioned test solutes to that reported in the literature. The use of ZrO_2 NPs facilitates electrocatalytic properties, stability, and good electrical conductivity. This work has also provided a comprehensive EC characterisation of both the bare and modified electrodes for flow-based analytical systems, which will further advance the PAD technique.

Finally, a fast-pulsed waveform (2-steps at +400 mV and -400 mV, 10 ms each, and 50 Hz cycle repetition) was developed, and the first miniaturised PAD was performed using gap-FC-incorporating modified electrodes in the liquid phase. The technique allowed miniaturised EC detection coupled with fast flow-through systems (such as FIA, LC, and IC in this study) for the first time, and overcame limitations such as the difficulties with data acquisition at high frequency (50 Hz) [17], and the loss of useful data during a long cleaning step (e.g., 560 ms [18]) for the removal of surface oxide. The developed high frequency

waveforms (15 to 45-times fast than existing waveforms [17-21]) result in an improved electroactivity of the electrode and facilitated the rapid establishment of baseline stability, higher current, and high detection sensitivity to electroactive solutes (such as obtaining *ca.* 100-times lower LOD for hydrazine than the lowest reported value in the literature [22]). The analytical application of the developed waveform was demonstrated by monitoring the consumption of reducing agents (hydrazine and ascorbic acid) during the graphene oxide (GO) reduction process.

In conclusion, a new miniaturised EC detector (gap-FC), using highly stable disposable electrodes rapidly modified with NPs (ZrO_2), and a fast-pulsed waveform (2-step, 20 ms, and 50 Hz) has been developed and resultant capabilities and potential to perform advanced miniaturised EC detection for flow-based analytical systems has been demonstrated.

Introduction

1. Background

Electrochemical (EC) detection continues to receive significant research interest due to its high selectivity through the proper choice of detection potential and/or electrode material [23], and potential high sensitivity towards electroactive compounds [24]. In 1973, Kissinger *et al.* [25] laid the foundation for the incorporation of EC detection within flow-based analytical systems. The versatility of EC detection techniques (including detector designs, electrodes, and detection modes) meets the requirements for flow-based analysis [26]. EC detection techniques include a variety of mechanisms, such as the measurement of current at fixed or variable potentials, or as a function of time (amperometry, pulsed amperometry, and voltammetry), or the measurement of Nernstian potential (potentiometry) [26]. Amongst these techniques, amperometry and pulsed amperometry have been widely used in flow-based analysis because of their high sensitivity [24] and instrumental simplicity [27]. These techniques are ideally suited to miniaturisation [27] due to their compatibility with simple instrumentation, low electrical power requirements for in-field use, low cost, and robustness [28]. The details of EC detection (including principles, detection modes, advantages, disadvantages, detector designs, electrodes, and technological advances) for each of these techniques are compared and contrasted in Chapter 1 (published as review article [29]).

2. Current status of EC detection

Pulsed amperometric detection (PAD) has been relatively adopted as an advanced EC detection technique for flow-based analytical systems [30]. PAD uses variable potentials during oxidation and subsequent reduction steps that facilitate potentiostatic cleaning and reactivation of the electrode surface after each measurement cycle, on a time scale of milliseconds [29, 30]. PAD based techniques are being constantly improved, and significant advances in waveform designs incorporating disposable electrodes (see details in Chapter 1 [29]) have been observed over the past few years. However, widely used PAD systems [29] incorporate heavy potentiostats, large flow-cells (FCs), large electrodes or limited stability microelectrodes prepared with complex modification techniques, and long pulsed waveforms.

Commonly used EC detectors for PAD are based upon wall-jet (WJ) or thin-layer (TL) FCs (see details in Chapter 1 [29]), where significant challenges for flow-through EC detection exist. These include difficulties in the miniaturisation of the EC system [1-3], a high effective cell volume, an inability to couple with analytical systems operating at nano- to millilitre range flow rates [1, 10, 31-35], and no possibility for the formation of a very thin layer of electrolyte on the electrode surface to achieve high efficiency EC conversion. Recently, gap-based FCs as the basis on the EC detector have been introduced to overcome the above challenges for miniaturised EC detection within analytical systems operating at nano- to millilitre range flow rates (see Chapter 3 [36]). The typical EC systems have flow cell volumes of 0.1-1 µL and electrode diameter 2-4 mm [4-9]. The diameters of microelectrodes range 0.2-50 µm, which allows extremely small detection cell volumes without loss of detection sensitivity [37].

Conventional large electrodes are widely used within PAD (see details in Chapter 1 [29]). However, similar or better capabilities have been found with disposable electrodes (see Chapter 1). Also, significant modifications of electrodes have been performed advancing EC detection. These advanced modified electrodes are very sensitive to electroactive species, but require time-consuming modification techniques such as electrodeposition [11, 12] and sol-gel processes [13, 14], and in some cases the use of large quantities of materials (e.g. *ca.* 965 mg [38]). These electrodes have a limited stability, usually 5-7 days [15, 16].

These issues significantly hinder the potential of using modified electrodes within PAD. There have been no reports of using rapidly modified electrodes for EC detection in analytical flow techniques. In addition, the EC reversibility, effective surface area, and stability of modified electrode surfaces in continuous-flow have, to our knowledge, not been extensively experimentally investigated [39, 40]. Therefore, the integration of disposable electrodes within flow-based analytical systems requires accurate characterisation of bare and modified electrodes in terms of current, EC reversibility, effective surface area, and stability in continuous flow use, as well as intermittent use within an analytical platform. Recently, a rapid process of disposable electrode modification with ZrO_2 NPs was investigated, where high sensitivity to test solutes and high stability of the electrodes in a continuous flow system was reported for the first time (see Chapter 3 [41]).

While a commonly used pulsed waveform for PAD is the three-step waveform (see details in Chapter 1 [29]), a number of other pulsed waveforms have been introduced to overcome challenges for EC detection in analytical systems (see details in Chapter1). Kotnik *et al.* [17] envisaged that the prospect of obtaining a 50 Hz potential cycle could be a great benefit in fast-eluting flow-based analytical systems. The development of a fast-pulsed waveform within a miniaturised EC detection system, coupled with fast-eluting systems is challenging, particularly due to loss of useful data when a long cleaning step (such as 560 ms reported in [18]) is required for the removal of large oxide layers from the electrode surface. Large oxide layers on the electrode surface result from the use of high potentials (700–1250 mV [19-21]), high flow rates (1–1.2 mL min^{-1} [17-21]), and high sample volumes (20 µL [21]) for sensitive EC detection, and the maximum calculated frequency is *ca.* 3.3 Hz [21] for most simple PAD techniques incorporating 2-step pulsed waveforms [17-21]. Low frequency waveforms result in longer analysis times, and consequently the formation of large surface-oxide layers and the poor stability of electrodes. The development of high frequency waveforms incorporated within a miniaturised flow-through EC detector could be advantageous for the rapid analysis of target solutes (such as hydrazine [42], which has gained interest for different applications).

In brief, a miniaturised EC detector incorporating rapidly modified disposable electrodes with high stability, and a fast pulsed waveform would overcome all abovementioned drawbacks and challenges associated with the existing EC detection techniques and would result in a significant advancement in EC detection systems within flow-based analytical systems.

3. Research problem

To-date, the challenges of EC detection have restricted its use, especially when working with microfluidic systems. Miniaturised FCs have relatively low EC conversion efficiency, high effective cell volumes, and are incapable of being coupled with analytical systems operating at nano- to millilitre range flow rates. Furthermore, complex modification processes have been used to enhance the surface electroactivity of electrodes, but the limited stability of the modified surface significantly hinders the potential of using modified electrodes in flow-based analytical systems. Low frequency prolonged/complex pulsed waveforms within large conventional EC detection systems result in longer analysis times, and consequently the formation of large surface oxide layers and the low stability of electrodes. As discussed above, advanced miniaturised EC detection techniques in flow-through systems can overcome these challenges while offering new possibilities and opportunities in the field of chemical sciences. Accordingly, in this thesis, the use of a new miniaturised EC detector incorporating modified electrodes with high stability, and a fast-pulsed waveform has been studied to overcome the limitations of using miniaturised EC detection for flow-through systems.

4. Research aims

The research aimed to obtain the following:

- A better understanding of the difficulties in performing miniaturised EC detection, including the design of FCs, electrodes, and pulsed waveforms, and their compatibility of being coupled with chromatographic separation platforms operating at nano- to millilitre range flow rates
- Characterisation of a new type of miniaturised FC, coupling it with nano- to millilitre range flow-through systems, and evaluation of the performance of EC detection using this miniaturised system compared to those reported using other EC or UV techniques
- Identification of a rapid electrode modification process with stable nanomaterials that could improve the response of EC detection as well as the stability of the surface in continuous flow-through systems
- Development of a fast-pulsed waveform within the miniaturised flow-through EC detection system, and consequently the reduction of the formation of surface oxide layers thus increasing the stability of the electrode surface

5. Research questions

Throughout the thesis, various research questions have been addressed, including:

- How can the drawbacks of EC techniques be overcome to perform a miniaturised EC detection?

  (addressed in Chapter 2: see section 1)
- How can the performance of EC detection be improved compared to other reported EC/UV techniques?

  (addressed in Chapter 2: see section 3.2)
- How can the FC be coupled with analytical platforms operating at nano- to millilitre flow rates?

  (addressed in Chapter 2: see section 3.1)
- How can the gap distance be adjusted to facilitate the formation of a thin layer of electrolyte on the electrode?

  (addressed in Chapter 2: see section 3.1)
- How does the gap distance in the EC detector affect the efficiency of EC conversion and effective cell volume?

  (addressed in Chapter 2: see section 3.1.2)
- How can the effective cell volume be determined experimentally?

  (addressed in Chapter 2: see section 3.1.3)
- How can the low-cost NPs and rapid modification process be selected for electrodes?

  (addressed in Chapter 3: see section 1)
- How do NPs enhance the EC response as an electrocatalyst?

  (addressed in Chapter 3: see section 1)

- How can the effective surface area of the electrode and EC reversibility be experimentally determined?

  (addressed in Chapter 3: see section 3.1)

- How stable is the modified surface of the electrode in continuous flow within an analytical platform?

  (addressed in Chapter 3: see section 3.3)

- How can the fast-pulsed waveform be developed within the miniaturised EC arrangement for different applications?

  (addressed in Chapter 4: see section 3.1)

6. Research hypothesis

The knowledge and understanding gathered from the investigation of EC detection have been used in different analytical formats (such as FIA, capillary to standard format LCs, and IC operating at nano- to millilitre range flow rates). The benefits have been demonstrated with various commonly used EC techniques (such as cyclic voltammetry, amperometry, and pulsed amperometry) in terms of the rapid and sensitive analysis of target solutes in the liquid phase. Moreover, EC characterisations such as EC conversion efficiency, effective cell volume, and effective surface area have been experimentally investigated for the first time. The work presented here will provide the groundwork for the future development of EC detection in microformats and encourage further technological advancement of the chemical sciences.

7. Outline of the thesis chapters

The overall research is divided into four chapters:

Introduction introduces the research topic. The development of a high frequency waveform incorporated within a miniaturised flow-through EC detector and rapidly modified disposable electrodes with high stability could be an advantage for the rapid and sensitive analysis of target solutes.

In Chapter 1 (published as review article [29]), recent knowledge (from 1997 to 2018) regarding the advances in EC detection of a wide range of analytes in the liquid phase is collected. This review addressed the advances in different EC detectors (including conventional/large and miniaturised) and electrodes (including conventional/large and microelectrodes), with emphasis on the PAD in flow-based analytical systems.

In Chapter 2 (published as research article [36]) a new FC has been used for miniaturised EC detection for the first time. Comprehensive EC characterisation has been demonstrated in FIA. The FC also demonstrated great potential when coupled with capillary and standard LCs. The FC also overcome significant difficulties for miniaturised EC detection.

In Chapter 3 (published as research article [41]), the rapid modification of electrodes with the use of low-cost NPs to circumvent the limitations of electrodes in the liquid phase is described. The NPs were selected based on electrocatalytic properties that can enhance improved EC detection. The comprehensive EC characterisation of bare and modified electrodes for flow-based analytical systems has been investigated. The performance of NPs in terms of the formation of a porous electrode surface, minimisation of the capacitance of the double layer, creation of a large effective (electroactive) surface area, and EC reversibility were compared both with bare electrodes and results in the existing literature. The stability of the modified electrodes was tested in continuous flow-through systems. The modified electrodes overcame significant challenges and difficulties for miniaturised EC detection.

In Chapter 4 (published as research article [43]), the development of a fast pulsed waveform for miniaturised flow-through EC detection systems is described. For the development of the waveform, an emphasis was placed on short analysis times without compromising the electrode cleaning (from surface oxide), the electrode stability, and the high sensitivity to target solutes. The prospects of the developed waveform are promising.

Finally, conclusions provides the overall conclusions of this research study with directions for future research.

Chapter 1. Literature review

Prospects of pulsed amperometric detection in flow-based analytical systems - A Review

Muhammed Ariful Islam [a], Parvez Mahbub [a, b], Pavel N. Nesterenko [a, c], Brett Paull [a, d], Mirek Macka [a, e, f, *]

[a] Australian Centre for Research on Separation Science (ACROSS) and School of Natural Sciences, University of Tasmania, Private Bag 75, Hobart 7001, Australia

[b] Institute for Sustainable Industries and Liveable Cities, Victoria University, Footscray Park Campus, Melbourne, Victoria 3011, Australia

[c] Department of Chemistry, Lomonosov Moscow State University, 1-3 Leninskie Gory, 119991 Moscow, Russian Federation

[d] ARC Training Centre for Portable Analytical Separation Technologies (ASTech), School of Natural Sciences, University of Tasmania, Private Bag 75, Hobart 7001, Australia

[e] Department of Chemistry and Biochemistry, Mendel University in Brno, Zemedelska 1, CZ-613 00 Brno, Czech Republic

[f] Central European Institute of Technology, Brno University of Technology, Purkynova 123, CZ-612 00 Brno, Czech Republic

*Email: mirek.macka@utas.edu.au

Graphical abstract

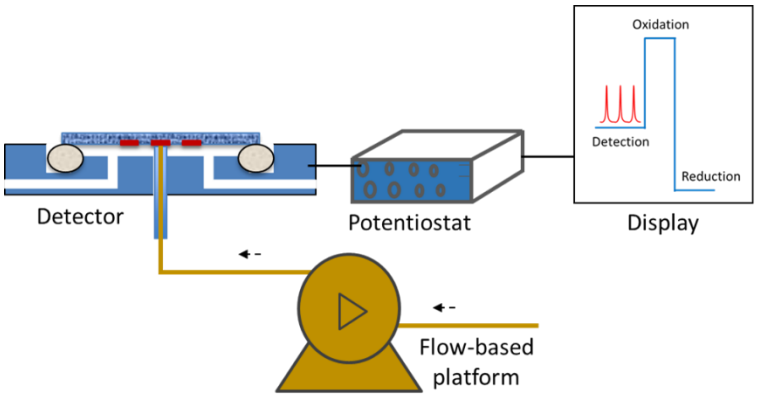

Highlights

- The fundamentals and waveform designs of pulsed amperometric detection (PAD).
- Electrochemical (EC) detector designs are commonly used for PAD.
- The technological advancement of PAD and its selected applications since 1997-2018.
- Future directions of PAD such as 3D printed EC detector, nanomaterials, multi-modal EC detection.

Abstract

Electrochemical (EC) detection techniques in flow-based analytical systems such as flow injection analysis (FIA), capillary electrophoresis (CE), and liquid chromatography (LC) have attracted continuous interest over the last three decades, leading to significant advances in EC detection of a wide range of analytes in the liquid phase. In this context, the unique advantages of pulsed amperometric detection (PAD) in terms of high sensitivity and selectivity, and electrode cleaning through the application of pulsed potential for noble metal electrodes (e.g. Au, Pt), have established PAD as an important detection technique for a variety of electrochemically active compounds. PAD is especially valuable for analytes not detectable by

ultraviolet (UV) photometric detection, such as organic aliphatic compounds and carbohydrates, especially when used with miniaturised capillary and chip-based separation methods. These applications have been accomplished through advances in PAD potential waveform design, as well as through the incorporation of nanomaterials (NMs) employed as microelectrodes in PAD. PAD allows on-line pulsed potential cleaning and coupling with capillary or standard separation techniques. The NMs are largely employed in microelectrodes to speed up mass and electron transfer between electrode surfaces and to perform as reactants in EC analysis. These advances in PAD have improved the sensitive and selective EC detection of analytes, especially in biological samples with complex sample matrices, and detection of electro-inactive compounds such as aliphatic organic compounds (i.e., formic acid, acetic acid, maleic acids, and β-cyclodextrin complexes). This review addresses the fundamentals of PAD, the role of pulsed sequences in AD, the utilization of different EC detectors for PAD, technological advancements in PAD waveforms, utilisation of microelectrodes in PAD techniques, advances in the use of NMs in PAD, the applications of PAD, and prospects for EC detection, with emphasis on PAD in flow-based systems.

Keywords

Electrochemical detector

Flow-based analytical systems

Pulsed amperometric detection

1. Introduction

The use of electrochemical (EC) detection techniques and corresponding EC detectors in flow-based analytical systems such as flow injection analysis (FIA), capillary electrophoresis (CE), and liquid chromatography (LC) has attracted the interest of analytical chemists over the last three decades [4-6, 44, 45]. The pioneering work of Kissinger *et al.* [25] laid the foundation for the incorporation of EC detection modes and EC detectors with flow-based analytical techniques.

EC detection is ideally suited to miniaturised analytical systems [27] due to the compatibility of EC detection techniques in general with miniaturisation, simple instrumentation, low electrical power requirements for in-field use, low cost, and robustness [28]. EC detection offers high selectivity through the proper choice of detection potential and/or electrode material [23], and high sensitivity towards electroactive compounds (a material electrically active or responsive) [24]. The versatility of EC detector designs and detection modes meets most of the requirements of flow-based analysis [26].

EC detection techniques include a variety of detection mechanisms to determine target analytes in a liquid stream such as measurement of current at fixed or variable potential or as a function of time (amperometry, voltammetry or coulometry, respectively), measurement of Nernstian potential (potentiometry) and measurement of conductivity [26]. Amongst these different EC detection techniques, amperometric detection (AD) has been widely used in flow analysis systems because of its high sensitivity [24] and instrumental simplicity [27]. However, a major disadvantage of the AD is the deposition of solution impurities or EC reaction by-products on the electrode surface. To enhance the performance of electrodes in the AD, a pulsed potential is often applied during amperometric measurements, hence the term pulsed amperometric detection (PAD) [26]. PAD has been drawing the attention of analytical researchers over the last 30 years and has become an alternative detection technique for the quantitative detection of numerous organic compounds such as carbohydrates [30]. Noble metal electrodes (e.g. Au, Pt) offer partially unsaturated d-orbitals, which enhances adsorption of the analytes (e.g. carbohydrates) on the

electrode surface and subsequent detection by PAD. PAD is generally based on a triple potential waveform that facilitates potentiostatic cleaning [26] of the electrocatalytic solid anodic electrodes (e.g. C, Au, and Pt) [30] and reactivation of the electrode surface after each measurement cycle, on a time scale of milliseconds, allowing rapid measurements in dynamic systems including detection in flow-based analytical methods. Thus, PAD can be used to reduce fouling of the electrode surface that otherwise results in a loss of electrode activity over time [26].

AD in non-pulsed mode uses direct current (DC) for the detection of a variety of organic and inorganic compounds [30]. In DC amperometry, during detection in an oxidative mode using the anodic detection electrode (also designated the working electrode), many organic aromatic compounds demonstrate high electroactivity (i.e., standard reduction potentials). The high electroactivity demonstrated by aromatic compounds is attributed to inherent π-resonance, functioning to stabilise the free radical intermediates during the oxidative reactions at the electrode surface [46]. As a consequence, the activation energy barrier of the EC oxidation reaction decreases significantly, resulting in a higher rate of oxidation of the analyte at the surface of the electrode [46]. On the other hand, organic aliphatic compounds have functional group such as hydroxyl (e.g. carbohydrates, alcohols, and alditols), and hydroxyl/amine (e.g. amine, amino acids, aminosugars, aminoglycosides, peptides, and proteins) demonstrate low electroactivity (i.e., standard reduction potentials), and hence, there is no possibility of stabilization of free-radical intermediates via π-resonance. For this reason, low oxidation rates resulting from the increased activation energy barrier of EC oxidation are observed for aliphatic compounds at inert electrode surfaces during the DC amperometric-based detection process. However, the activation energy barrier of EC oxidation for organic aliphatic compounds was reported to reduce greatly when noble metal electrodes such as Pt or Au were used [46]. Hence, the adsorption of analytes on the electrode surface increases, resulting in the gradual inactivation of the electrode surface for further use [30]. In this context, PAD applies an alternate cathodic and anodic potential in a cyclic order to reactivate and maintain clean electrode surfaces and to enhance the sensitivity and reproducibility of the EC signal. Hence, aliphatic compounds can easily be detected in a sensitive manner by the use of DC amperometric techniques in pulsed mode [30]. At present, the PAD technique remains under the overarching categorisation of pulsed electrochemical detection (PED), which encompasses all waveform applications of metal electrodes for amperometric-based detection [30].

During the last two decades (1997-2018), approximately 423 journal papers, including 5 reviews on PAD have been published (see Fig. 1). Amongst these reviews, in 2004 Jandik *et al.* [47] covered topics including developments in the area of analysis of amino acid-carbohydrate mixtures by high-performance anion exchange chromatography (HPAEC), and in 2005 LaCourse *et al.* [37] discussed the detection modes of PED and general PED waveform design at microelectrodes, and microelectrode applications in microchromatographic and electrophoretic separation techniques. In 2011, Trojanowicz [48] discussed about the PAD waveforms and microelectrode materials (such as gold, platinum, silver, and graphite) and reported their applications in liquid chromatography. Then in 2012 Corradini *et al.* [49] described HPAEC coupled with PED techniques for carbohydrate determination, in 2015 Fedorowski *et al.* [30] outlined the development of advanced waveforms of PED and the use of microsystems in combination with PED. Fedorowski *et al.* [30] also discussed advancements in PED technology, such as improvements to waveforms and microelectrodes, as well as the advanced analysis of carbohydrates including the fingerprinting of bioproducts and characterization of enzymatic processes.

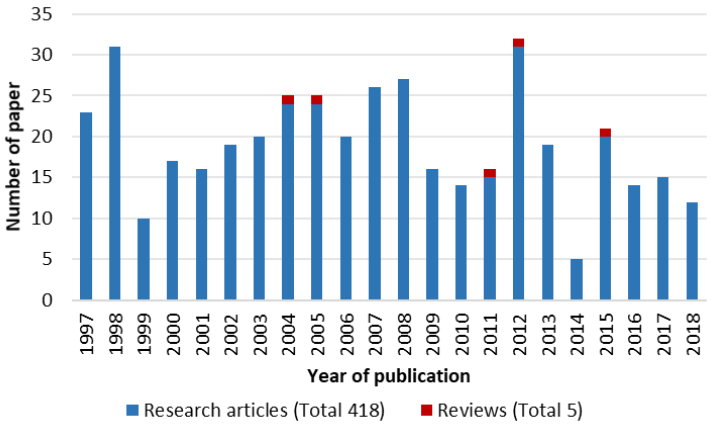

Fig. 1. Number of published articles related to PAD in flow-based systems such as CE, FIA, and LC from 1997 to 2018 (Title searched phrases: "pulsed amperometric detection" and "pulsed electrochemical detection").

As the applications of PAD in flow-based analytical systems is increasing continuously (*ca.* 67 journal articles published during the period of 2014-2018 as demonstrated in Fig. 1), it is necessary to collate recent knowledge regarding the advanced waveforms, NMs, and microelectrodes in PAD incorporated within flow-based systems. Therefore, the following sections of this review will cover the fundamentals of PAD, the role of pulsed sequences in AD, the utilization of different EC detectors, microelectrodes, NMs, technological advances in PAD, the applications of PAD to aqueous-based separation techniques, such as CE, FIA, and LC systems from 1997-2018, and future directions for EC detection, with emphasis on PAD in flow-based systems.

2. Fundamentals of PAD

2.1 Amperometric detection

Amperometric detection (AD) is a widely reported EC detection technique in CE, FIA, and LC [26]. The AD is performed using a two or three electrode EC cell, with a working electrode, a reference electrode, and an auxiliary electrode [50]. This technique is carried out by applying a constant potential to the working electrode and the resulting current is measured as a function of time. This technique is different from cyclic voltammetry (CV), which is performed by cycling the potential of a working electrode and measuring the resulting current [50]. At the surface of the working electrode, the redox (reduction and oxidation) reactions of the analytes take place by the application of a potential where the output current is proportional to the analyte's concentration [27, 51]. The mathematical expression that relates the amount of analyte oxidised or reduced at the working electrode surface to the resulting current is established according to Faraday's law (Equation 1) [27]:

$$I_t = \frac{dQ}{dt} = nF\frac{dN}{dt} \qquad (1)$$

where I_t is the yielded current at the working electrode surface at time t, Q is the charge at the working electrode surface, t is the time, n is the number of electrons transferred per mole of analyte, F is the Faraday constant (96485 C mol^{-1}), and N is number of moles of analyte oxidised or reduced [52].

2.2 Pulsing sequences in PAD

PAD utilises electrocatalytic surfaces to stabilise (mainly aliphatic) free radical intermediates. However, large amounts of catalytic activity promote the accumulation of interferents at the working electrode Pt or Au surface during the redox reaction [30]. To sustain a clean and reactive electrode surface for continuous reproducible detection a cyclic potential waveform in

PAD must have at least three principal steps: (1) application of a potential to promote electrocatalytic oxidation of the analyte of interest, (2) oxidation *via* a large positive anodic potential resulting in the formation of a surface oxide, and (3) reduction to restore the activity of the electrode *via* a large negative cathodic potential, resulting in removal of the surface oxide [53].

Furthermore, for the analysis of simple carbohydrates, Neuburger and Johnson [54] established that PAD with an Au electrode in basic media resulted in a lower limit of detection and a higher sensitivity compared to PAD with a Pt electrode. Therefore, at present most PAD applications take these advantages of using an Au electrode for the detection of the target analyte of interest in basic media.

2.3 PAD detection modes

All PAD detection modes include an oxidation step i.e., a large positive anodic potential result in the formation of a surface oxide. PAD enhances the electrode reactivation, including oxide formation and its removal at the surface of the metal electrode. These mechanisms can be achieved through three detection modes as shown in Fig. 2.

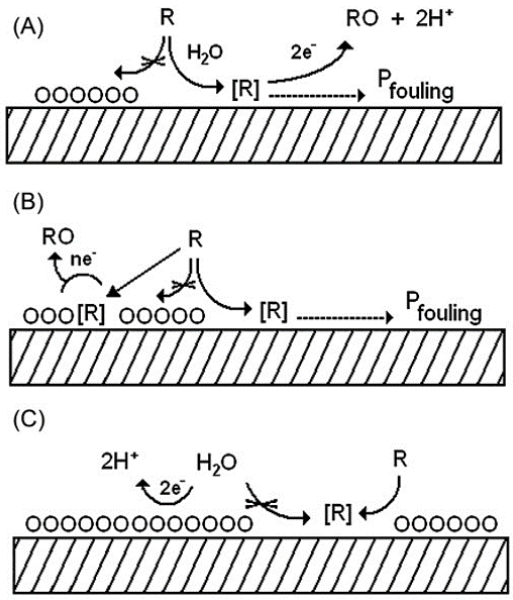

Fig. 2. Schematic diagram of the three different detection modes A, B, and C, of PAD respectively (reproduced with permission) [30]. In (A), reactant R is adsorbed on the oxide-free surface of the electrode resulting in either oxidation to RO or the fouling ($P_{fouling}$) of the electrode. In (B), R is adsorbed on the electrode surface which may result in oxidation simultaneously with the formation of surface oxide or fouling. In (C), reactant R is adsorbed on the electrode surface, suppressing oxide formation and resulting in a negative response [30].

2.3.1 Mode A: Direct detection of analytes at oxide-free surfaces

In the absence of a surface oxide, electrocatalytic noble metal electrode surfaces can adsorb organic aliphatic compounds (see Fig. 2A). Convective diffusion-based mass transport mechanisms bring the analytes to the electrode surface and the electrode drives the oxidation of the compounds with little or no concurrent formation of surface oxide. The oxidised products exit the diffusion layer and then readsorb for further oxidation or fouling of the electrode surface [30, 55]. The response from the analyte using detection mode A is larger than the baseline signal or background response [30]. This detection mode is used for the determination of carbohydrates with either Au electrode in alkaline solutions or Pt electrode in acidic solutions [46].

2.3.2 Mode B: Direct oxide-catalysed detection of analytes

This detection mode is accomplished by the concurrent formation of a surface oxide and oxidation of the analyte at a metal electrode [37]. In Fig. 2B convective diffusional mass transport brings the analytes to the electrode surface and catalytic oxidation of the compounds occurs. The primary analytical signal results from the oxidation of pre-adsorbed analytes. The products formed by the oxidation of analytes may either foul the electrode surface or leave the diffusional layer. The continuous and significant signal generated from surface oxide formation at the electrode makes a large contribution to the background signal (larger than in mode A), ultimately resulting in a decreased signal- to-noise (S/N) [30, 55]. This detection mode is used for the determination of both aliphatic amines and amino acids using Au or Pt electrodes (in alkaline solutions), and various sulfur compounds with Au (in alkaline solutions) or with Pt electrodes (in acidic solutions) [37].

2.3.3 Mode C: Indirect detection of analytes at oxide surfaces

The indirect analyses require analyte preadsorption at the electrode surface prior to analyte oxidation [56]. This detection mode (Fig. 2C) is used for electro-inactive analytes, which can interfere with the formation of surface oxides. Electro-inactive analytes suppress the baseline signal resulting from anodic currents due to surface oxide formation. This suppression generates the negative peak for the analyte due to the prevention of surface oxide formation [30, 55]. The suppression of these anodic currents presented an indirect detection scheme for PAD that was dependent on analyte adsorption. Mode C is typically applied for the detection of inorganic and sulfur-containing organic compounds [37].

3. PAD waveform design

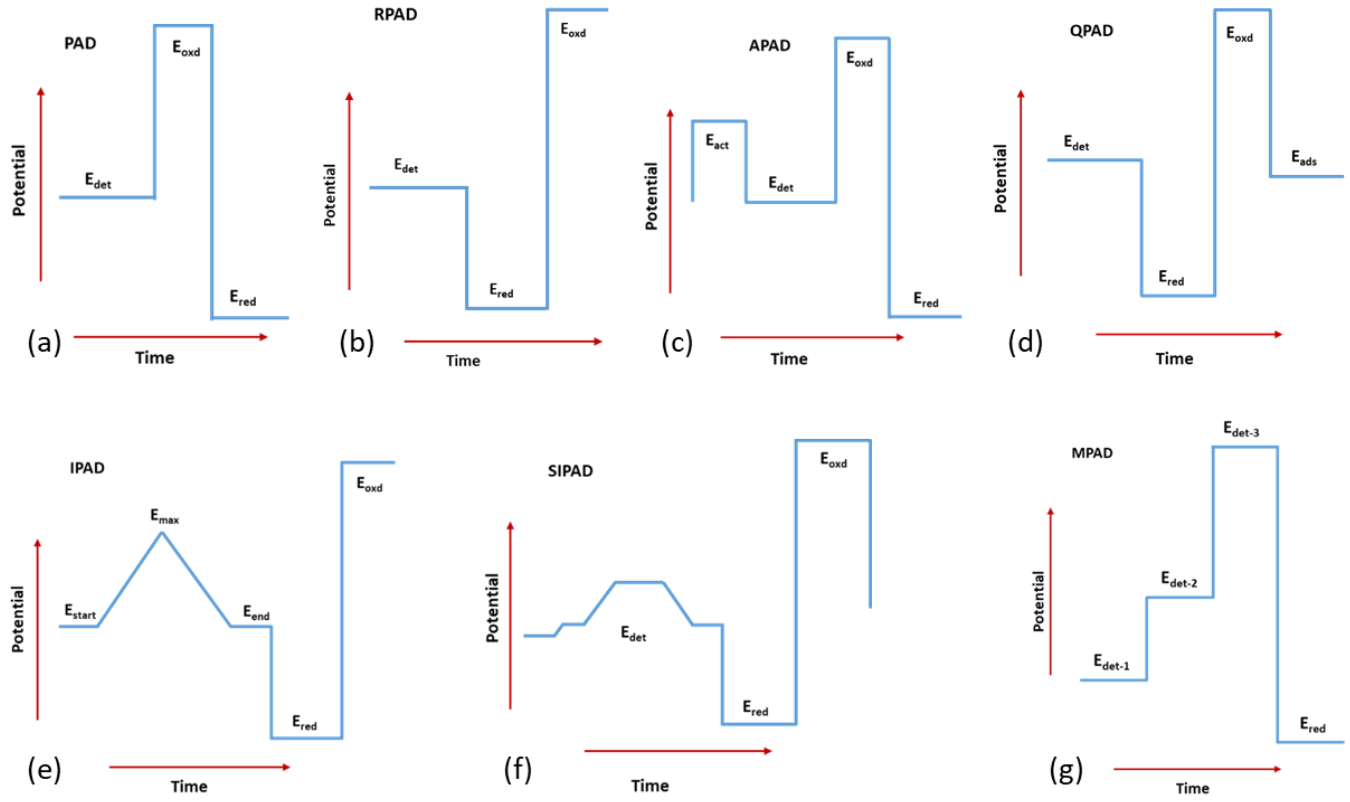

Fig. 3. Schematic diagrams of (a) PAD, (b) RPAD, (c) APAD, (d) QPAD, (e) IPAD, (f) SIPAD, and (g) MPAD waveforms. The regions of E_{act}, E_{ads}, E_{det}, E_{red}, and E_{ox} correspond to activation potential, potential to disrupt the adsorption, detection potential, reduction potential, and oxidation potential respectively (reproduced and redrawn with permission) [30, 57].

The simplest PAD waveform, Fig. 3a [30, 46, 58] includes three different potential steps. The analyte of interest is detected by the application of the detection potential (E_{det}) at the Au or Pt electrode for a certain time (t_{det}). Then the anodic oxidative potential (E_{oxd}) is applied for a time (t_{oxd}), to produce a surface oxide on the electrode surface with simultaneous oxidative desorption of adsorbed carbonaceous materials. In the last step, a cathodic reductive potential (E_{red}) is applied to reactivate the electrode [59]. This type of waveform with detection mode A is used to determine alcohol-containing compounds such as alcohols, amino-glycosides, alditols, and carbohydrates with an Au electrode (in alkaline solutions) and a Pt electrode (under both alkaline and acidic conditions) [60-63]. The application of the PAD waveform with detection mode B was reported to produce inferior results to that with detection mode A [46].

The analytical response in detection mode A is larger than the baseline signal (background response) [30]. In the detection mode B, a continuous significant current is generated by the oxide surface, contributing significantly to the background or baseline signal resulting in baseline drift [64]. To overcome this situation Gilroy [64] demonstrated that the use of a lower potential can slow down surface oxide formation and diminish its contribution to the background signal. Later on, Polta and Johnson [65] reversed the PAD waveform potential steps E_{oxd} and E_{red} to obtain similar or better result, known as reverse pulsed amperometric detection (RPAD, see Fig. 3b) [30, 46, 58]. Nevertheless, this waveform with detection mode B achieved lower baseline for the detection of sulfur compounds and poor oxidative cleaning performance [46].

Prior to applying E_{det} in RPAD, it became necessary to introduce a fourth potential pulse (E_{act}) to ensure sufficient oxidative cleaning of the electrode surface [66]. This is known as activated pulsed amperometric detection (APAD, see Fig. 3c) [30, 67]. This initial potential step accelerated the activation of the surface oxide after which switching to a low detection potential satisfied detection mode B [30]. APAD waveforms were used by Williams *et al.* [66] to determine arsenic (III), and by Johll *et al.* [68] to determine cysteine with Pt electrodes in acidic conditions.

In quadrupole pulsed amperometric detection (QPAD, Fig. 3d) [30, 69], after the detection step (E_{det}) an additional cathodic electrode surface cleaning step (E_{red}) is used to reduce each partially solvated species of Au, which finally returns to metallic Au. Then a brief potential E_{oxd} is introduced to activate the electrode surface and finally a negative potential (E_{ads}, t_{ads}) to disrupt the adsorption of the analyte on the electrode surface [70].

In integrated pulsed amperometric detection (IPAD, Fig. 3e) [30, 53], the onset of a cyclic scan precedes the oxidation of the analyte and gradually progresses with the positive scan through an oxide formation region that follows the detection by mode B. As the potential progresses out of the oxide formation region through the negative scan, the oxide background signal is rejected, whilst the analyte signal is recorded. This integrated pulsed waveform can eliminate drift and changes due to the small variations of mobile phase composition, pH, and application of gradients in chromatography [47]. IPAD with detection mode B has been utilised to determine amino acids, amines, proteins, peptides, and thiol compounds at both Au and Pt electrodes [63, 71-73].

Fedorowski *et al.* [30] and Clarke *et al.* [74] reported the utilisation of six-potential integrated pulsed amperometric detection (SIPAD, Fig. 3f) [69, 74] for the determination of amino acids and amino sugars, without any additional pre-column or post-column derivatization, in LC. In the optimisation step, the gradual erosion of gold from the surface of the electrode was reduced by incorporating a large negative potential prior to the waveform integration period. The addition of a short adsorption step in six-potential IPAD resulted in a highly efficient cycle which overcame the limitations of amino sugars and amino acids analysis.

Multiplex-pulsed amperometric detection (MPAD, Fig. 3g) [46, 70, 75] uses multiple potential pulses as a function of time to monitor the current at several applied potentials, which makes it feasible to detect different compounds, both individually and simultaneously [76, 77]. It is also used for the introduction of internal standard addition in the FIA system with AD [78], and for increasing the selectivity of the EC method for the detection of the products of oxidation or reduction, even in the presence of interfering species [57]. Additionally, the MPAD detection mode enables the simultaneous determination of electroactive compounds that partly overlap and cannot be determined by voltammetric techniques. Besides the application of a potential pulse for analyte detection, this technique also enables the constant application of a cleaning potential pulse at the end of the cycle [77].

4. EC detector designs for PAD

The term EC detector has been mainly used in relation to amperometric or coulometric detectors. EC detectors respond only to those species which can be oxidised or reduced by the applied potential on the electrode material used in the detectors. The working electrode of these detectors is kept at a constant potential against a suitable reference electrode, and the current flowing across the working electrode is measured. Current depends on the concentration of an analyte in the carrier stream but also largely on the flow pattern of the carrier stream near the electrode. For these reasons, the design of the flow geometry is particularly important in EC detectors. Two geometries such as thin-layer FC (TL-FC, Fig. 4(a, b)) and wall-jet FC (WJ-FC, Fig. 4(c, d)) have been frequently utilised in EC detection [9, 79], depending on the type of the working electrode, the shape of the inlet capillary nozzle and the distance between the nozzle and the electrode surface [4-6].

In a TL-FC (Fig. 4 (a,b)) [1], the solution flows through a thin flat channel parallel to the electrode surface which is contained in one of the channel walls [4-6]. In a WJ-FC (Fig. 4 (c, d)) [1], the carrier stream exits through a small orifice into a liquid-filled space and forms a jet that impinges on the electrode surface [1, 9] and the solution is drained away from the vicinity of the electrode after contact.

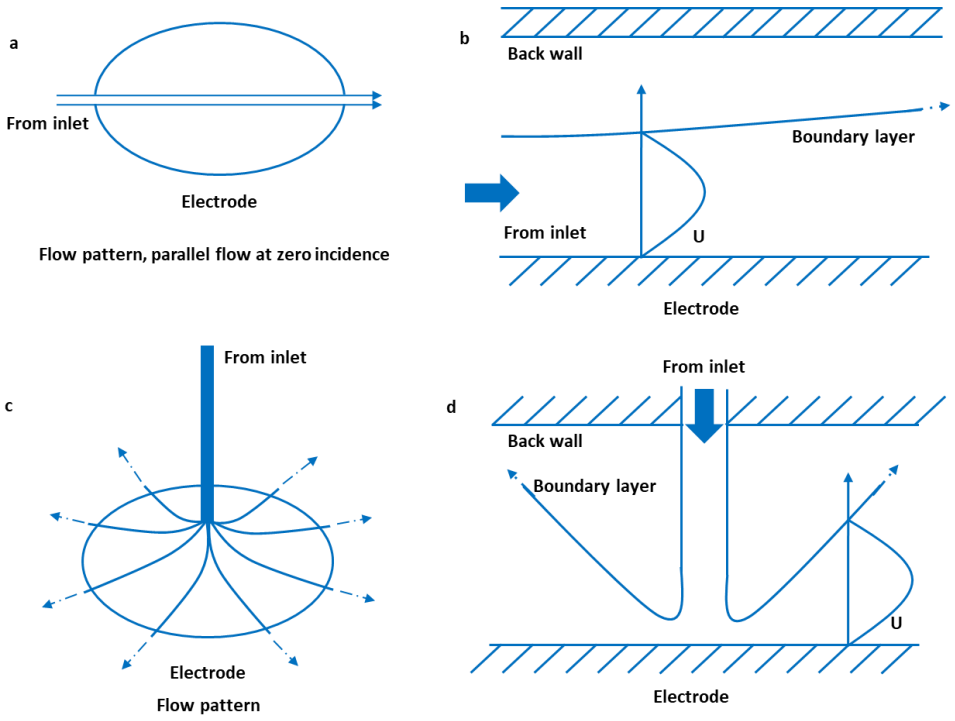

Fig. 4. Schematic diagram of flow patterns, and boundary layers: (A, B) thin layer flow cell, and (C, D) WJ-FC. U, indicates the rate of flow at the surface of the electrode, which is the radial flow velocity for the WJ-FC (reproduced and redrawn with permission) [1].

WJ configuration appears to be the most suitable for continuous-flow monitoring. In particular, it shows high sensitivity in the millilitre flow rate range [80, 81]. It also has several desirable features such as ease of maintenance and a simple and robust design. As shown by Albery *et al.* [82] and Gunasingham *et al.* [83], the WJ electrode affords an attractive alternative to the RDE for fundamental EC studies, despite the fact that it does not have a uniformly accessible surface. Perhaps the most useful aspect of the WJ electrode in this respect is the fact that it can be used in a continuous-flow system. The WJ electrode is an attractive configuration for EC detectors for LC on account of its high convective mass transfer characteristics [1]. It offers many useful features such as well-defined hydrodynamic properties, low void volume, good sensitivity, fast response, ease of operation, and low cost [84, 85].

5. Technical advances

5.1 Faster waveforms

The requirement of using PAD at a high frequency was necessitated by the rapid advances in CE- and LC-based flow systems. Neuburger *et al.* [86] achieved an increased S/N for carbohydrate detection by expanding the current integration time period (t_{int}) duration from 16.7 ms to 200 ms, which eliminated the noise resulting from the 60 Hz power supply. Later, LaCourse and Johnson [38] used pulsed voltammetry to optimise the PAD waveform potential and time, with the waveform frequency of 1 Hz at t_{int} equal to 200 ms. Additionally, Roberts *et al.* [87] succeeded in the detection of carbohydrates by increasing the waveform frequency from 0.5 to 6.2 Hz. This was accomplished by minimising the time for oxidative cleaning and reductive reactivation of the electrode surface without changing the t_{int} (200 ms) for ideal current sampling. Additionally, Jensen and Johnson [88] applied a 6.7 Hz frequency waveform by incorporating the cathodic reduction potential ideal for removing the products formed during the glucose oxidation. This waveform for detecting glucose in an LC-PAD system established a sub-picomole limit of detection (LOD) with a linear dynamic range that covered more than three orders of magnitude [30].

5.2 Microelectrodes in PAD

PAD depends on reactions at the electrode surface, which makes it suitable for use with micro-separation platforms. EC detection allows miniaturisation with technological advancements in the fabrication of microelectrodes. The diameters of microelectrodes range 0.2-50 µm which results in extremely small detection cell volumes without loss of detection sensitivity [37]. Howell *et al.* [89] showed the benefits of utilising disk shaped 7 µm Au and Pt micro-voltammetric electrodes in a high resistance solution without any instrumental correction procedures to correct ohmic potential (iR) effects. Additionally, Chen *et al. [90]* employed pulsed potential at a Pt microelectrode to determine glucose, potassium ferrocyanide and various catechols in biological environments. Afterwards, initial reports of carbohydrate detection utilising an Au microelectrode in CE-PAD systems were published [91-93]. CE-IPAD utilising an Au microelectrode was first introduced by Holland *et al.* [94] and LaCourse *et al.* [95] for the determination of sulfur-containing compounds and amines. Since then, several reviews have been published about the applications and advances of PAD utilising microelectrodes combined with aqueous media based separation systems [37, 96, 97].

5.3 Disposable screen-printed electrode

In flow-through EC cells, a cheap microfabrication technique is realised by printing the working electrode onto a polymeric substance, which allows the routine use of disposable working electrodes [30]. Cheng *et al.* [98] initially described stable detection for at least one week using a disposable Au microelectrode with PAD and IPAD waveforms. Detected analytes included carbohydrates, amines and sulfur-containing compounds. Liang *et al. [99]* made a comparison between disposable and conventional Ag working electrodes for the determination of iodide using PAD waveforms. According to the report, disposable electrodes provided better results in terms of equilibration, detection limit, reproducibility, and calibration linearity. Cheng *et al*. [100] showed similar investigation results for the analysis of alcohols, aldehydes, cyanides, sulphides, sulphites, sulfoxides and ketones.

6. Applications of PAD in flow-based analytical systems

Since 1997, PAD applications have progressed due to advancements in electrode technology and potential waveforms. The applications percentage of PAD in flow-based systems from 1997 to 2018 are illustrated in Fig. 5 and Table 1. The significant applications of PAD include the determination of carbohydrates, alditols, EPA priority pollutants, amino acids, aminoglycosides, antibiotics, and biogenic amines. The remaining applications such as determination of sulfur-containing compounds, aliphatic carboxylates, nonsteroidal anti-inflammatory drugs etc.

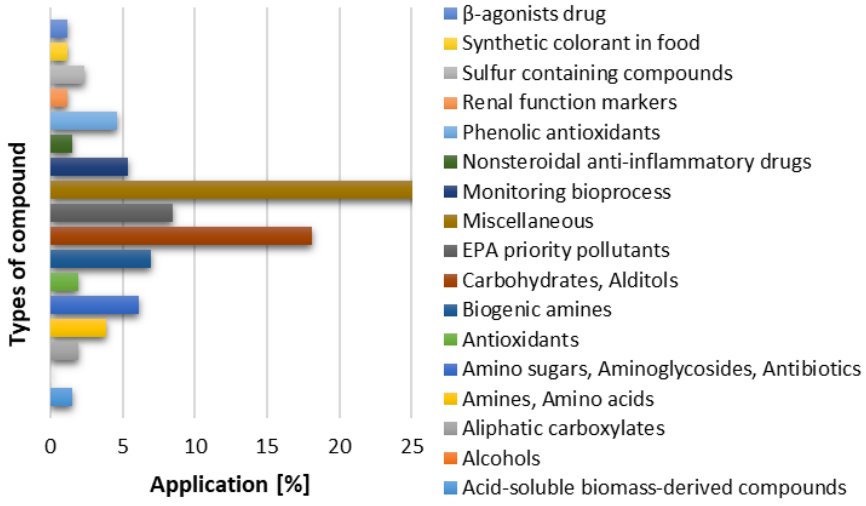

Fig. 5. Applications of PAD in flow-based systems such as CE, FIA, and LC (1997-2018).

Table 1. Selected applications of PAD in flow-based systems (1997-2018).

Year	Application	Sample matrix	Solvent; pH	Instrument	Detector	WE, RE, AE	Mode	LOD [μg L^{-1}]	Ref.
Amines/amino acids									
2001	Bialaphos	Urine, serum	NaOH, Na_2CO_3	HPAEC	TL-FC	Au, Ag/AgCl, Ti	IPAD	51	[101]
2001	Glufosinate	Urine, serum	NaOH, Na_2CO_3	HPAEC	TL-FC	Au, Ag/AgCl, Ti	IPAD	18	[101]
2001	Glyphosate	Urine, serum	NaOH, Na_2CO_3	HPAEC	TL-FC	Au, Ag/AgCl, Ti	IPAD	65	[101]
2002	Amino acids	Food	Water, NaOH, Na Ac; 7	HPAEC	TL-FC	Au, pH electrode	IPAD	-	[102]
2003	Amino acids	Plant litter, soil	MSA or HCl	HPAEC	TL-FC	Au, Ag/AgCl, Ti	IPAD	-	[103]
2004	Taurine	Milk	NaOH	HPAEC	TL-FC	Au, Ag/AgCl, Ti	IPAD	62	[104]
2007	4-hydroxyproline	Gelatine	NaOH; 8	HPAEC	TL-FC	Au, pH-Ag/AgCl	IPAD	10	[105]
2007	Proline	Gelatine	NaOH, Ba AC	HPAEC	TL-FC	Au, pH-Ag/AgCl	IPAD	10	[105]
2009	Amino acids	Commercial	NaOH	HPAEC	-	Au, Ag/AgCl, Pt	In. PAD	0.2-3	[56]
2009	Proteins	Commercial	NaOH	HPAEC	-	Au, Ag/AgCl, Pt	In. PAD	0.2-3	[56]
Biogenic amines									
2003	Biogenic amines	Milk	NaOH, Citrate buffer; 3.5	CE	TL-FC	Au, Ag/AgCl, Ti	PAD	20-400	[106]
2005	Histamine	Commercial	$NaClO_4$, $HClO_4$, H_2O	HPLC	-	Au-GC, Ag/AgCl, -	PAD	67	[19]
2006	Cysteine	Commercial	Na phosphate, NaOH; 10	FIA	-	Au, Ag/AgCl, Pt	PAD	60.5	[107]
2007	Agmatine	Alcoholic beverages	MSA, NaOH	CEC	-	Au, pH-Ag/AgCl, Ti	IPAD	17	[108]

2007	Biogenic amines	Meat products	MSA; 12.7	CEC	TL-FC	Au, pH-Ag/AgCl, Ti	IPAD	700-2000	[109]
2007	Cadaverine	Alcoholic beverages	MSA, NaOH	CEC	-	Au, pH-Ag/AgCl, Ti	IPAD	69	[108]
2007	Dopamine	Alcoholic beverages	MSA, NaOH	CEC	-	Au, pH-Ag/AgCl, Ti	IPAD	21	[108]
2007	Histamine	Alcoholic beverages	MSA, NaOH	CEC	-	Au, pH-Ag/AgCl, Ti	IPAD	28	[108]
2007	Phenylethylamine	Alcoholic beverages	MSA, NaOH	CEC	-	Au, pH-Ag/AgCl, Ti	IPAD	39	[108]
2007	Putrescine	Alcoholic beverages	MSA, NaOH	CEC	-	Au, pH-Ag/AgCl, Ti	IPAD	39	[108]
2007	Spermidine	Alcoholic beverages	MSA, NaOH	CEC	-	Au,pH-Ag/AgCl, Ti	IPAD	62	[108]
2007	Spermine	Alcoholic beverages	MSA, NaOH	CEC	-	Au, pH-Ag/AgCl, Ti	IPAD	36	[108]
2007	Tyramine	Alcoholic beverages	MSA, NaOH	CEC	-	Au, pH-Ag/AgCl, Ti	IPAD	73	[108]
2014	Dopamine	Commercial	KCl	-	-	rGO-GC, Ag/AgCl, Pt	PAD	107.2	[11]
2014	Dopamine	Commercial	PPB; 7	-	-	Au/rGO/GC, SCE, Pt	PAD	214.4	[11]
2018	Cysteamine	River water, serum	H_2SO_4	FIA	-	BDD, Ag/AgCl, Pt	MPAD	0.77	[110]
2018	Dopamine	Commercial	$HClO_4$, CH_3COONa	RP-HPLC	TL-FC	-	IPAD	2×10^{-5}	[111]
2018	Dopamine	River water, serum	H_2SO_4	FIA	-	BDD, Ag/AgCl, Pt	MPAD	1.5	[110]
Amino sugars/aminoglycosides/antibiotics									
1997	Kanamycin sulphate	Commercial	SOSP, SS, THF, PPB; 3	HPAEC	-	Au, Ag/AgCl, SS	PAD	150-200	[112]
1998	Netilmicin sulfate	Commercial	SOSP, SS, THF, PPB; 3	HPAEC	-	Au, Ag/AgCl, SS	PAD	200-300	[113]
2000	Galactosamine	Seawater	BA, NaOH	HPAEC	TL-FC	Au, pH-Ag/AgCl	PAD	-	[114]

2000	Glucosamine	Seawater	BA, NaOH	HPAEC	TL-FC	Au, pH-Ag/AgCl	PAD	0.18	[114]
2000	Mannosamine	Seawater	BA, NaOH	HPAEC	TL-FC	Au, pH-Ag/AgCl	PAD	0.72	[114]
2000	Tobramycin	Commercial	SOSP, SS, THF, PPB; 3	HPAEC	-	Au, Ag/AgCl, SS	PAD	80-200	[115]
2002	Lincomycin	Commercial	SOSP, SS, THF, PPB; 3	RP-LC	-	Au, Ag/AgCl, SS	PAD	35-175	[116]
2002	Spectinomycin	Commercial	PFPA, PDHP, THF; 6.25	RP-LC	TL-FC	Au, Ag/AgCl, SS	PAD	50	[117]
2003	Tetracycline	Pharmaceutical tablets	PDHP, PPA, NaOH; 2-10	FIA	TL-FC	Pt, Ag/AgCl, SS	PAD	0.01	[118]
2006	Etimicin sulfate	Commercial	OA, HFBA, ACN; 3.4	LC	-	Au, Ag/AgCl, SS	PAD	200	[119]
2006	Neomycin	Commercial	SOSP, SS, THF, PPB; 3	RP-LC	TL-FC	Au, H, C filled PTFE	PAD	-	[120]
2006	Tobramycin	Commercial	KOH	HPAEC	TL-FC	Au, pH, -	PAD	1.87	[15]
2007	Amikacin	Commercial	SOSP, SS, THF, PPB; 3	RP-LC	TL-FC	Au, H, C filled PTFE	PAD	200	[121]
2008	Amikacin	Cerebrospinal fluid	SOSP, SS, THF, PPB; 3	RP-HPLC	-	Au, H, C filled PTFE	PAD	50	[122]
2010	Netilmicin	Commercial	SOSP, SS, THF, PPB; 3	RP-LC	TL-FC	Au, H, C filled PTFE	PAD	130	[123]
2013	Micronomicin	Commercial	ACN, TFA, PFPA, NaOH; 2.6	LC	TL-FC	Au, Ag/AgCl, Ti	PAD, QPAD, SPAD	80	[124]
2015	Gentamicin	Commercial	SOSP, SS, THF, PPB; 3	HPAEC	-	Au, Ag/AgCl, SS	PAD	1000	[30]
Carbohydrates/alditols									
2000	Galactinol	Olive plant extracts	NaOH	HPAEC	TL-FC	Au, Ag/AgCl, Ti	PAD	-	[125]
2000	Myo-inositol	Olive plant extracts	NaOH	HPAEC	TL-FC	Au, Ag/AgCl, Ti	PAD	-	[125]
2000	Raffinose	Olive plant extracts	NaOH	HPAEC	TL-FC	Au, Ag/AgCl, Ti	PAD	-	[125]

2000	Saccharides	Wastewater	NaOH	HPAEC	TL-FC	Au, -, -	IPAD	-	[126]
2004	Alkylglycosides surfactants	Detergent formulation	NaOH	RP-LC	TL-FC	Au, Ag/AgCl, SS	PAD	26	[127]
2004	Arylglycosides surfactants	Detergent formulation	NaOH	RP-LC	TL-FC	Au, Ag/AgCl, SS	PAD	13	[127]
2004	Glucose	Blood	Borate, NaOH; 9.4	CE	-	Au, Pt, Pt	PAD	0.0002	[128]
2004	Lactulose	Milk (Heat treated)	NaOH, $Ba(OAc)_2$	HPAEC	TL-FC	Au, pH-Ag/AgCl	PAD	411	[128]
2005	Glucose	Blood	NaOH	HPAEC	TL-FC	Au, Ag/AgCl, Ti	PAD	0.92	[129]
2005	Isomaltose	Blood	NaOH	HPAEC	TL-FC	Au, Ag/AgCl, Ti	PAD	12.90	[129]
2005	Levoglucsoan	Smoke samples	$Na_2B_4O_7$; 12.30	CE	TL-FC	Au, Ag/AgCl, Pt	IPAD	2707	[130]
2005	Maltose	Blood	NaOH	HPAEC	TL-FC	Au, Ag/AgCl, Ti	PAD	10.30	[129]
2005	Ribose	Blood	NaOH	HPAEC	TL-FC	Au, Ag/AgCl, Ti	PAD	7.50	[129]
2006	Galactosan	Biomass aerosol	NaOH	HPAEC	TL-FC	Au, -, -	IPAD	2	[131]
2006	Levoglucsoa	Biomass aerosol	NaOH	HPAEC	TL-FC	Au, -, -	IPAD	2	[131]
2006	Mannosan	Biomass aerosol	NaOH	HPAEC	TL-FC	Au, -, -	IPAD	2	[131]
2007	Sugar phosphates	Blood	NaOH, Na_2CO_3	HPAEC	-	Au, Ag/AgCl, SS	PAD	10-30	[132]
2008	Carbohydrate	Geophytes	NaOH	HPAEC	TL-FC	Au, -, -	PAD	-	[133]
2009	Sorbitol	Blood	NaOH	HPAEC	-	Au, Ag/AgCl, SS	PAD	0.003	[134]
2010	Galactose	Blood	NaOH, NaOAc, Na_2CO_3	HPAEC	-	Au, Ag/AgCl, SS	PAD	36-72	[135]
2014	Lactose, lactulose	Dairy products	KOH	HPAEC	-	-, pH-Ag/AgCl, -	PAD	-	[136]
2015	3’-sialyllactose	Commercial	NaOH	HPAEC	-	Au, PH-Ag/AgCl, -	PAD	220	[137]

2015	6’-sialyllactosamine	Commercial	NaOH	HPAEC	-	Au, PH-Ag/AgCl, -	PAD	100	[137]
2015	6’-sialyllactose	Commercial	NaOH	HPAEC	-	Au, PH-Ag/AgCl, -	PAD	30	[137]
2015	β-D-Glucans	Glucose	-	HPAEC	-	-	PAD	-	[138]
2016	Sugar	Pet food	ACN, MeOH, EtOH, water	HPAEC	-	Au, AgCl, -	PAD	-	[139]
2017	Arabinose	Spirulina platensis	NaOH, Na Ac, water	HPAEC	-	Au, PH-Ag/AgCl, -	PAD	0.02	[140]
2017	Arabinose	Astragalus residue	-	HPAEC	TL-FC	Au, Ag, -	IPAD	67	[141]
2017	Carbohydrate	Grass samples	NaOH	HPAEC	-	-	PAD	-	[140]
2017	Fructose	Spirulina platensis	NaOH, Na Ac, water	HPAEC	-	Au, PH-Ag/AgCl, -	PAD	0.02	[140]
2017	Fucose	Spirulina platensis	NaOH, Na Ac, water	HPAEC	-	Au, PH-Ag/AgCl, -	PAD	0.02	[140]
2017	Galactose	Spirulina platensis	NaOH, Na Ac, water	HPAEC	-	Au, PH-Ag/AgCl, -	PAD	0.02	[140]
2017	Galactose	Astragalus residue	-	HPAEC	TL-FC	Au, Ag, -	IPAD	82	[141]
2017	Galacturonic acid	Spirulina platensis	NaOH, Na Ac, water	HPAEC	-	Au, PH-Ag/AgCl, -	PAD	0.01	[140]
2017	Glucose	Spirulina platensis	NaOH, Na Ac, water	HPAEC	-	Au, PH-Ag/AgCl, -	PAD	0.02	[140]
2017	Glucose	Astragalus residue	-	HPAEC	TL-FC	Au, Ag, -	IPAD	74	[141]
2017	Glucuronic acid	Spirulina platensis	NaOH, Na Ac, water	HPAEC	-	Au, PH-Ag/AgCl, -	PAD	0.01	[140]
2017	Mannitol	Spirulina platensis	NaOH, Na Ac, water	HPAEC	-	Au, PH-Ag/AgCl, -	PAD	0.02	[140]
2017	Mannose	Spirulina platensis	NaOH, Na Ac, water	HPAEC	-	Au, PH-Ag/AgCl, -	PAD	0.021	[140]
2017	Rhamnose	Spirulina platensis	NaOH, Na Ac, water	HPAEC	-	Au, PH-Ag/AgCl, -	PAD	0.02	[140]
2017	Ribose	Spirulina platensis	NaOH, Na Ac, water	HPAEC	-	Au, PH-Ag/AgCl, -	PAD	0.02	[140]

2017	Sucrose	Spirulina platensis	NaOH, Na Ac, water	HPAEC	-	Au, PH-Ag/AgCl, -	PAD	0.02	[140]
2017	Xylose	Spirulina platensis	NaOH, Na Ac, water	HPAEC	-	Au, PH-Ag/AgCl, -	PAD	0.01	[140]
2017	Xylose	Astragalus residue	-	HPAEC	TL-FC	Au, Ag, -	IPAD	91	[141]
2017	Cellobiose	Astragalus residue	-	HPAEC	TL-FC	Au, Ag, -	IPAD	91	[141]
2018	Galactose	Galactooligosaccharides	PBS	HPAEC	-	Au, pH-Ag/AgCl, -	PAD	300	[142]
2018	Glucose	Galactooligosaccharides	PBS	HPAEC	-	Au, pH-Ag/AgCl, -	PAD	300	[142]
2018	Lactose	Galactooligosaccharides	PBS	HPAEC	-	Au, pH-Ag/AgCl, -	PAD	300	[142]
Sulfur containing compounds									
1998	Ampicillin	Milk	ACN, Na Ac	RP-LC	TL-FC	Au, Ag/AgCl, Pt	IPAD	10	[143]
1998	Cephapirin	Milk	ACN, Na Ac	RP-LC	TL-FC	Au, Ag/AgCl, Pt	IPAD	20	[143]
1999	Sulfur contains antibiotics	Pharmaceutical capsule	NaAc, CH_3CN, MeOH; 3.7	HPLC	TL-FC	Au, PH-Ag/AgCl, Ti	IPAD	8	[144]
2001	Cephalosporin	Pharmaceutical tablets	KOH	RP-HPLC	TL-FC	Au, pH, Ti	IPAD	-	[53]
2001	Lincomycin	Pharmaceutical tablets	KOH	RP-HPLC	TL-FC	Au, pH, Ti	IPAD	-	[53]
2005	Thio-based additives	Pharmaceutical	NaOAc buffer, CH_3CN; 4.5	HPLC	TL-FC	Au, Ag/AgCl, Pt	PAD	0.2-1	[145]
Monitoring bioprocess									
1997	Monosaccharide	Wheat starch	NaOH	HPAEC	-	-, Ag/AgCl, -	IPAD	-	[146]
1998	Maltosaccharides	Maize starch	NaOH, Na Ac	HPAEC	TL-FC	Au, -, -	PAD	-	[147]

1998	Monosaccharide	PP in human serum	PBS	HPLC	-	-	PAD	-	[148]
2005	N-linked oligosaccharide	Immunoglobulin G	NaOH, Na Ac, water	HPAEC	-	Au, Ag/AgCl, -	PAD	-	[149]
2005	Oligosaccharide	MA in sea water	NaOH, Na Ac	HPAEC	TL-FC	Au, pH-Ag/AgCl	PAD	-	[149]
2008	Monosaccharide	Natural cyclodextrins	ACN, water	HPLC	-	Au, -, -	PAD	-	[150]
2008	Monosaccharide	Yeast	NaOH	HPAEC	-	-	PAD	-	[151]
2011	Asiaticoside	CA leaf, ointment	-	RP-HPAEC	-	Au, Ag/AgCl, -	PAD	0.05	[152]
2011	Madecassoside	CA leaf, ointment	Ethanol, ACN	RP-HPAEC	-	Au, Ag/AgCl, -	PAD	0.05	[152]
2012	Monosaccharide	Carbohydrates	NaOAc, NaOH	HPAEC	-	Au, -, -	PAD	-	[153]
2015	Hyaluronan oligosaccharide	Commercial	water, NaOH	HPAEC	-	Au, Ag/AgCl, -	PAD	-	[154]
2016	Arabinan oligosaccharide	Commercial	NaOH, Na Ac, water	HPAEC	-	-	PAD	7-25	[155]
2016	Galactan oligosaccharide	Commercial	NaOH, Na Ac, water	HPAEC	-	-	PAD	10-25	[155]
2016	Oligosaccharide	Human milk	NaOH, NaOAc	HPAEC	-	-	PAD	-	[156]
Acid-soluble biomass-derived compounds									
2015	2,6-dimethoxyphenol	Commercial	NaOH, NaOAc	HPAEC	-	Au, AgCl, -	PAD	140	[157]
2015	3,5-dim-4-hyd	Commercial	NaOH, NaOAc	HPAEC	-	Au, AgCl, -	PAD	140	[157]
2015	4-met-oxyben-alc	Commercial	NaOH, NaOAc	HPAEC	TL-FC	Au, AgCl, -	PAD	140	[157]
Antioxidants									

2010	Ascorbic acid	Pharmaceutical tablets	AA, PAB, H_2SO_4; 1.6/4.7	FIA	-	Au/GC, Ag/AgCl, Pt	PAD	19.80	[78]
2014	Ascorbic acid	Commercial	KCl	-	-	rGO-GC, Ag/AgCl, Pt	PAD	123	[11]
2014	Ascorbic acid	Commercial	PPB; 7	-	-	Au/rGO/GC, SCE, Pt	PAD	8.9×10^7	[11]
2018	Sinapic acid, tyrosol	-	Methanol, B-RB	FIA	-	GC, Ag/AgCl, Pt	MPAD	-	[158]
Phenolic antioxidants									
2015	4-Hydroxycumarin	Commercial	SPP, Me, β-CD; 2	HPLC	TL-FC	Au, H, SS	PAD	25	[159]
2015	Caffeic acid	Commercial	SPP, Me, β-CD; 2	HPLC	TL-FC	Au, H, SS	PAD	75	[159]
2015	Catequin	Commercial	SPP, Me, β-CD; 2	HPLC	TL-FC	Au, H, SS	PAD	16	[159]
2015	Chlorogenic acid	Commercial	SPP, Me, β-CD; 2	HPLC	TL-FC	Au, H, SS	PAD	378	[159]
2015	Ferulic acid	Commercial	SPP, Me, β-CD; 2	HPLC	TL-FC	Au, H, SS	PAD	170	[159]
2015	Gallic acid	Commercial	SPP, Me, β-CD; 2	HPLC	TL-FC	Au, H, SS	PAD	29	[159]
2015	Myricetin	Commercial	SPP, Me, β-CD; 2	HPLC	TL-FC	Au, H, SS	PAD	43	[159]
2015	q-coumaric acid	Commercial	SPP, Me, β-CD; 2	HPLC	TL-FC	Au, H, SS	PAD	34	[159]
2015	Quercetin	Commercial	SPP, Me, β-CD; 2	HPLC	TL-FC	Au, H, SS	PAD	35	[159]
2015	Quercitrin	Commercial	SPP, Me, β-CD; 2	HPLC	TL-FC	Au, H, SS	PAD	23	[159]
2015	Resveratrol	Commercial	SPP, Me, β-CD; 2	HPLC	TL-FC	Au, H, SS	PAD	23	[159]
2015	Rutin	Commercial	SPP, Me, β-CD; 2	HPLC	TL-FC	Au, H, SS	PAD	79	[159]
Environmental Protection Agency (EPA) priority pollutants									

2005	Pentachlorophenol	Water	PPB; 12.4	CE	-	Au, Ag, Pt	PAD	225	[160]
2005	Phenol	Water	PPB; 12.4	CE	-	Au, Ag, Pt	PAD	82	[160]
2015	1,5-Di-O-caf-lqu acid	Commercial	AA, ACN; 6	LC	TL-FC	GC, Ag/AgCl, SS	PAD	0.2	[161]
2015	3,4-Di-O-caf-lqu acid	Commercial	AA, ACN; 6	LC	TL-FC	GC, Ag/AgCl, SS	PAD	0.4	[161]
2015	3,5-Di-O-caf-qu acid	Commercial	AA, ACN; 6	LC	TL-FC	GC, Ag/AgCl, SS	PAD	0.2	[161]
2015	3-Hydroxytyrosol	Commercial	AA, ACN; 6	LC	TL-FC	GC, Ag/AgCl, SS	PAD	0.008	[161]
2015	4,5-Di-O-caf-lqu acid	Commercial	AA, ACN; 6	LC	TL-FC	GC, Ag/AgCl, SS	PAD	0.3	[161]
2015	4,6-dinitro-o-cresol	Water	PPB; 12.4	CE	-	Au, Ag, Pt	PAD	130	[160]
2015	Apigetrin	Commercial	AA, ACN; 6	LC	TL-FC	GC, Ag/AgCl, SS	PAD	0.01	[161]
2015	Caffeic acid	Commercial	AA, ACN; 6	LC	TL-FC	GC, Ag/AgCl, SS	PAD	0.014	[161]
2015	Catechol	Commercial	AA, ACN; 6	LC	TL-FC	GC, Ag/AgCl, SS	PAD	0.006	[161]
2015	Chlorogenic acid	Commercial	AA, ACN; 6	LC	TL-FC	GC, Ag/AgCl, SS	PAD	0.03	[161]
2015	Cinaroside	Commercial	AA, ACN; 6	LC	TL-FC	GC, Ag/AgCl, SS	PAD	0.4	[161]
2015	Criptochlorogenic acid	Commercial	AA, ACN; 6	LC	TL-FC	GC, Ag/AgCl, SS	PAD	0.07	[161]
2015	Cynarin	Commercial	AA, ACN; 6	LC	TL-FC	GC, Ag/AgCl, SS	PAD	0.05	[161]
2015	Ferulic acid	Commercial	AA, ACN; 6	LC	TL-FC	GC, Ag/AgCl, SS	PAD	0.013	[161]
2015	Neochlorogenic acid	Commercial	AA, ACN; 6	LC	TL-FC	GC, Ag/AgCl, SS	PAD	0.02	[161]
2015	Oleuropein	Commercial	AA, ACN; 6	LC	TL-FC	GC, Ag/AgCl, SS	PAD	0.016	[161]
2015	p-Coumaric acid	Commercial	AA, ACN; 6	LC	TL-FC	GC, Ag/AgCl, SS	PAD	0.003	[161]

2015	Syringic acid	Commercial	AA, ACN; 6	LC	TL-FC	GC, Ag/AgCl, SS	PAD	0.005	[161]
2015	Tyrosol	Commercial	AA, ACN; 6	LC	TL-FC	GC, Ag/AgCl, SS	PAD	0.004	[161]
2015	Verbascoside	Commercial	AA, ACN; 6	LC	TL-FC	GC, Ag/AgCl, SS	PAD	0.016	[161]
Nonsteroidal anti-inflammatory drugs									
2006	Acetaminophen	Blood	Borate buffer; 11.5	CE	-	Au, Ag, Pt	PAD	0.19	[162]
2006	DCF	Blood	Borate buffer; 11.5	CE	-	Au, Ag, Pt	PAD	0.23	[162]
2006	DFS	Blood	Borate buffer; 11.5	CE	-	Au, Ag, Pt	PAD	0.26	[162]
2006	Salicylic acid	Blood	Borate buffer; 11.5	CE	-	Au, Ag, Pt	PAD	0.23	[162]
Aliphatic carboxylate									
2015	Biotin	Commercial	NaOH	HPAEC	TL-FC	Au, pH-Ag/AgCl, Ti	In. PAD	2-6	[163]
2015	Gabapentin	Commercial	NaOH	HPAEC	TL-FC	Au, pH-Ag/AgCl, Ti	In. PAD	3-8	[163]
2015	Lysin	Commercial	NaOH	HPAEC	TL-FC	Au, pH-Ag/AgCl, Ti	In. PAD	1-2	[163]
2015	Methionine	Commercial	NaOH	HPAEC	TL-FC	Au, pH-Ag/AgCl, Ti	In. PAD	2-4	[163]
2015	Vegabatin	Commercial	NaOH	HPAEC	TL-FC	Au, pH-Ag/AgCl, Ti	In. PAD	1-3	[163]
Renal function markers									
2003	Creatine	Urine	Borate buffer; 9.4	CE	-	Au, Ag/AgCl, Pt	PAD	250	[164]

2003	Creatinine	Urine	Borate buffer; 9.4	CE	-	Au, Ag/AgCl, Pt	PAD	80	[164]
2003	Uric acid	Urine	Borate buffer; 9.4	CE	-	Au, Ag/AgCl, Pt	PAD	270	[164]
Synthetic colorant in food									
2003	Brilliant blue	Food	H_2SO_4	FIA	-	BDD, Ag/AgCl, SS	MPAD	-	[164]
2003	Sunset yellow	Food	H_2SO_4	FIA	-	BDD, Ag/AgCl, SS	MPAD	-	[164]
2003	Tartrazine	Food	H_2SO_4	FIA	-	BDD, Ag/AgCl, SS	MPAD	-	[164]
β-agonists drug									
2006	Clenbuterol	Commercial	-	FIA	-	BBD/Ag/AgCl/Pt	PAD	0.3	[165]
2006	Salbutamol	Commercial	-	FIA	-	BBD/Ag/AgCl/Pt	PAD	0.1	[165]
2006	Terbutaline	Commercial	-	FIA	-	BBD/Ag/AgCl/Pt	PAD	0.5	[165]
Miscellaneous									
2002	Aliphatic organic acid	Food, beverages	$HClO_4$	HPLC	TL-FC	Pt, Ag/AgCl, SS	PAD	0.5-7	[166]
2003	Furosemide	Commercial	ACN, NaH_2PO_4	FIA/HPLC	TL-FC	SCF, Ag/AgCl, Pt	PAD	0.17	[21]
2004	Acrolein	Vegetable oils	$HClO_4$	LC	TL-FC	Pt, Ag/AgCl, SS	PAD	8.41	[167]
2004	Chlortetracycline	Pharmaceutical tablets	PDHP, NaOH; 5-10	FIA	TL-FC	Au, Ag/AgCl, Pt	PAD	1-100	[20]
2004	Doxycycline	Pharmaceutical tablets	PDHP, NaOH; 5-10	FIA	TL-FC	Au, Ag/AgCl, Pt	PAD	1-100	[20]

2004	Formalin	Food	ACN, water	FIA	-	Au, Ag/AgCl, Pt	PAD	0.013	[168]
2004	Thiols	Commercial	Borate, NaOH; 9.4	CE	-	C, Pt , -	PAD	7.5	[128]
2005	Bromide	Infant formula	NaOH	AEC	TL-FC	Ag, Ag/AgCl, Ti	PAD	5	[16]
2005	Cyanide	Infant formula	NaOH	AEC	TL-FC	Ag, Ag/AgCl, Ti	PAD	2	[16]
2005	Iodide	Infant formula	NaOH	AEC	TL-FC	Ag, Ag/AgCl, Ti	PAD	5	[16]
2005	Sulfide	Infant formula	NaOH	AEC	TL-FC	Ag, Ag/AgCl, Ti	PAD	1	[16]
2005	Tetracycline antibiotics	Food	ACN, PPB; 2.50	HPLC	TL-FC	BBD/Ag/AgCl/Pt	PAD	50-100	[169]
2005	Thiocyanate	Infant formula	NaOH	AEC	TL-FC	Ag, Ag/AgCl, Ti	PAD	10	[16]
2006	Acrylamide	Food	H_2SO_4	HPLC	TL-FC	Pt, Ag/AgCl, SS	PAD	1.44	[18]
2006	Acrylic acid	Food	H_2SO_4	HPLC	TL-FC	Pt, Ag/AgCl, SS	PAD	3.24	[18]
2006	Ethyl glucuronide	Urine	AA, ACN	RP-HPLC	-	Au, Ag/AgCl, SS	PAD	30	[170]
2006	Orotic acid	Milk	NaOH, $NaNO_3$	AEC	TL-FC	Au, pH-Ag/AgCl, Ti	APAD	8.0	[171]
2007	Cyanide	Drinking water	NaOH, water	AEC	-	Ag, pH-Ag/AgCl, -	PAD	1.0	[172]
2007	Imipramine	Pharmaceutical tablets	LiCl, IHCl	FIA	-	-, Ag/AgCl, Pt	PAD	280	[173]
2007	Tacrine	Pharmaceutical tablets	LiCl, IHCl	FIA	-	-, Ag/AgCl, Pt	PAD	19.80	[174]
2008	Paracetamol	Pharmaceutical tablets	AA, PAB, H_2SO_4; 1.6/4.7	FIA	-	Au/GC, Ag/AgCl, Pt	MPAD	19.80	[76]
2010	Butalyted hydroxyanisole	Food	Ethanol, KNO_3; 1.50	FIA	-	BDD, Ag/AgCl, -	MPAD	0.03	[175]
2010	Butalyted hydroxytoluene	Food	Ethanol, KNO_3; 1.50	FIA	-	BDD, Ag/AgCl, -	MPAD	0.40	[175]
2011	Caffeine	Pharmaceutical tablets	AA, Acetate buffer; 4.7	FIA	-	BDD, Ag/AgCl, Pt	MPAD	0.87	[57]

2011	Paracetamol	Pharmaceutical tablets	AA, Acetate buffer; 4.7	FIA	-	BDD, Ag/AgCl, Pt	MPAD	0.66	[57]
2012	Astragalin	Plant	ACN, water	RP-HPLC	-	Au, Ag/AgCl, -	PAD	360	[176]
2012	Astragolaside	Plant	ACN, water	RP-HPLC	-	Au, Ag/AgCl, -	PAD	20	[176]
2012	Lisinopril	Human plasma	NaOH	AEC	TL-FC	Au, pH-Ag/AgCl, -	IPAD	0.12	[177]
2014	Iodine	Serum and urine	-	AEC	-	-	PAD	82-145	[178]
2015	2-methylimidazole	Beverages	PPB; 12.4	RP-HPLC	TL-FC	Au, pH, -	IPAD	20	[179]
2015	4-methylimidazole	Beverages	PPB; 12.4	RP-HPLC	TL-FC	Au, pH, -	IPAD	15	[179]
2015	5-hyd-met-fur	Beverages	PPB; 12.4	RP-HPLC	TL-FC	Au, pH, -	IPAD	100	[179]
2015	5-hyd-met-fur	Sugarcane bagasse	AA, acetate buffer; 4.7	HPLC	WJ-FC	Ni-GC, Palladium, Pt	PAD	-	[180]
2015	Caffeic acid	Commercial	AA, ACN; 6	-	TL-FC	GC, Ag/AgCl, Pt	PAD	14	[181]
2015	Caffeine	Commercial	ACN, PPB; 7	FIA	-	BDD, -, -	MPAD	0.15	[77]
2015	Clenbuterol	Commercial	AA, ACN; 6	-	TL-FC	GC, Ag/AgCl, Pt	PAD	0.1	[181]
2015	Cyanide	Liquor sample	KOH	IC	-	Ag, pH-Ag/AgCl, Ti	PAD	1	[182]
2015	Furanic aldehydes	Sugarcane bagasse	AA, Acetate buffer; 4.7	HPLC	WJ-FC	Ni-GC, Pd, Pt	PAD	3.8×10^7	[180]
2015	Gluconate	Nuclear waste	ACN, water	HPAEC	-	Au, -, -	PAD	-	[183]
2015	Ibuprofen	Commercial	ACN, PPB; 7	FIA	-	BDD, -, -	MPAD	0.16	[77]
2015	Myoinositol	Infant formula	NaOH, Na Ac, water	AEC	-	Au, Ag/AgCl, Ti	PAD, QPAD	-	[184]
2015	Paracetamol	Commercial	ACN, PPB; 7	FIA	-	BDD, -, -	MPAD	0.163	[77]
2016	8-Chlorotheophylline	Commercial	H_2SO_4	BIA	-	BDD, Ag/AgCl, Pt	MPAD	40.7	[185]

2016	Diphenhydramine	Commercial	H_2SO_4	BIA	-	BDD, Ag/AgCl, Pt	MPAD	45.96	[185]
2016	Etimicin sulfate	Commercial	ACN, TFA, NaOH; 3.5	LC	-	Au, pH-Ag/AgCl, Ti	PAD	81	[186]
2016	Prazosin	Pharmaceutical	PPB; 4	FIA	-	BDD, Ag/AgCl, Pt	MPAD	31.77	[187]
2016	Pyridoxine	Commercial	H_2SO_4	BIA	-	BDD, Ag/AgCl, Pt	MPAD	91.35	[185]
2017	Ami-met-pho acid	Drinking Water	ACN, water, TFA	HPAEC	WJ-FC	Au, Pt, -	IPAD	< 1	[188]
2017	Cyanide	Urine / Saliva	NaOH, NaCN	IC	-	-	PAD	0.1-0.5	[189]
2017	Glyphosate, AMPA	Drinking Water	ACN, water, TFA	HPAEC	WJ-FC	Au, Pt, -	IPAD	1	[188]
2017	Keratan sulfate	SCS	NaOH	HPAEC	-	-	PAD	-	[190]
2017	Lactic acid	Sugarcane Vinasse	NaOH, CH_3COONa, water	HPAEC	-	Ni-BDD	PAD	1×10^8	[191]
2017	Malic acid	Sugarcane Vinasse	NaOH, CH_3COONa, water	HPAEC	-	Ni-BDD	PAD	8.1×10^4	[191]
2017	N-linked glycans	Glycoproteins	-	HPAEC	-	Au, pH-Ag/AgCl, -	PAD	-	[188]
2017	Tartaric acid	Sugarcane Vinasse	NaOH, CH_3COONa, water	HPAEC	-	Ni-BDD	PAD	4.2×10^4	[191]
2017	Warfarin	Pharmaceutical	PPB; 7	FIA	-	BBD/Ag/AgCl/-	MPAD	154	[192]
2015	Tramadol	Pharmaceutical	H_2SO_4	FIA	-	BDD, Ag/AgCl, SS	MPAD	10.5	[193]
2015	8-chlorotheophylline	Pharmaceutical	ACN, H_3PO_4	BIA	-	BDD, Ag/AgCl, Pt	MPAD	40	[185]
2015	Acetaminophen	Pharmaceutical	H_2SO_4	FIA	-	BDD, Ag/AgCl, SS	MPAD	4.5	[193]
2015	Captopril	Pharmaceutical	Acetic acid/acetate buffer	BIA	-	BDD, Ag/AgCl, Pt	MPAD	189	[194]
2015	Diphenhydramine	Pharmaceutical	ACN, H_3PO_4	BIA	-	BDD, Ag/AgCl, Pt	MPAD	45	[185]
2015	Enalapril	Pharmaceutical	H_2SO_4	FIA	WJ-FC	BDD, Ag/AgCl, SS	MPAD	3.76	[195]

2015	Hydrochlorothiazide	Pharmaceutical	H_2SO_4	FIA	WJ-FC	BDD, Ag/AgCl, SS	MPAD	59.5	[195]
2015	Hydrochlorothiazide	Pharmaceutical	Acetic acid/acetate buffer	BIA	-	BDD, Ag/AgCl, Pt	MPAD	113	[194]
2015	Myo-Inositol	Food	NaOH	HPLC	TL-FC	Au, -, -	PAD	-	[196]
2015	Pyridoxine	Pharmaceutical	ACN, H_3PO_4	BIA	-	BDD, Ag/AgCl, Pt	MPAD	91	[185]
2016	Sucrose acetates	6-O-acetyl sucrose	ACN, water	HPLC	-	Au, Ag/AgCl, SS	PAD	8.4	[197]
2017	Fructooligosaccharides	Onion	Water, NaOH, NaOAc	HPAEC	-	Au, -, -	PAD	-	[198]
2017	Isoflavonoids	Astragali Radix	ACN, water	RP-HPLC	-	-	IPAD	-	[199]
2017	Triterpene saponins	Astragali Radix	ACN, water	RP-HPLC	-	-	IPAD	-	[199]
2018	Chlorine ions	Milk	Na_2SO_4	FIA	-	Au, Ag/AgCl, Pt	PAD	5000	[200]
2018	5-HIAA	Commercial	$HClO_4$, CH_3COONa	RP- HPLC	TL-FC	-	IPAD	6×10^{-5}	[111]
2018	Allura red	Candy	H_2SO4	FIA	TL-, WJ-FC	BDD, Ag/AgCl, SS	MPAD	122	[201]
2018	Amfepramone	Dietary supplements	Ammonium acetate	RP-HPLC	-	-	PAD	2720	[202]
2018	Andhomovanillic acid	Commercial	$HClO_4$, CH_3COONa	RP-HPLC	TL-FC	-	IPAD	0.0024	[111]
2018	Bisacodyl	Dietary supplements	Ammonium acetate	RP-HPLC	-	-	PAD	740	[202]
2018	Caffeine	Dietary supplements	Ammonium acetate	RP-HPLC	-	-	PAD	320	[202]
2018	Clonazepam	Dietary supplements	Ammonium acetate	RP-HPLC	-	-	PAD	260	[202]
2018	Colchicine	Pharmaceutical, urine	-	FIA	-	BDD, Ag/AgCl, Pt	MPAD	8.3, 25	[203]
2018	Diazepam	Dietary supplements	Ammonium acetate	RP-HPLC	-	-	PAD	430	[202]
2018	DOPAC	Commercial	$HClO_4$, CH_3COONa	RP-HPLC	TL-FC	-	IPAD	2×10^{-5}	[111]

2018	Fenproporex	Dietary supplements	Ammonium acetate	RP-HPLC	-	-	PAD	40	[202]
2018	Fluoxetine	Dietary supplements	Ammonium acetate	RP-HPLC	-	-	PAD	310	[202]
2018	Furosemide	Dietary supplements	Ammonium acetate	RP-HPLC	-	-	PAD	120	[202]
2018	Indigo carmine	Candy	H_2SO_4	FIA	TL-, WJ-FC	BDD, Ag/AgCl, SS	MPAD	700	[201]
2018	Lorazepam	Dietary supplements	Ammonium acetate	RP-HPLC	-	-	PAD	120	[202]
2018	Midazolam	Dietary supplements	Ammonium acetate	RP-HPLC	-	-	PAD	150	[202]
2018	Oxcarbazepine	Pharmaceutical	Acetate buffer	FIA	WJ-FC	BDD, Ag/AgCl, Pt	MPAD	4.2-10.3	[204]
2018	Serotonin (5-HT)	Commercial	$HClO_4$, CH_3COONa	RP-HPLC	TL-FC	-	IPAD	5×10^{-5}	[111]
2018	Sertraline	Dietary supplements	Ammonium acetate	RP-HPLC	-	-	PAD	920	[202]
2018	Sildenafil	Dietary supplements	Ammonium acetate	RP-HPLC	-	-	PAD	1600	[202]
2018	Tadalafil	Dietary supplements	Ammonium acetate	RP-HPLC	-	-	PAD	230	[202]
2018	Verapamil	Pharmaceutics, urine	H_2SO_4	FIA	-	BDD, Ag/AgCl, Pt	MPAD	7.2	[205]
2018	Yohimbine	Dietary supplements	Ammonium acetate	RP-HPLC	-	-	PAD	70	[202]

Application: Di-O-caf-lqu acid: Di-O-caffeoylquinic acid; 3,5-dim-4-hyd: 3,5-dimethoxy-4-hydroxybenzaldehyde; 4-met-oxyben-alc: 4-methoxybenzylalcohol; 5-hyd-met-fur: 5-hydroxymethylfurfural; Ami-met-pho acid: Aminomethylphosphonic acid; C filled PTFE: carbon filled polytetrafluoroethylene; CA: Centella asiatica; DCF: Diclofenac (sodium o-2,6-dichloroanilino-phenyl acetate); DFS: Diflunisal (5-(2,4 difluorophenyl) salicylic acid); FA: Furanic aldehydes; MA: Mannuronan alginate.

Sample matrix: SCS: Sodium Chondroitin sulfate

Solvent: AA: Acetic acid; ACN: Acetonitrile; BaAc: Barium acetate, CH_3COONa: Sodium acetate trihydrate; EtOH: Ethanol; $HClO_4$: Perchloric acid HFBA: Heptafluorobutyric acid; IHCl: Imipramine hydrochloride; MeOH: Methanol; MSA: Methanesulfonic acid; Na Ac: Sodium Acetate; Na phosphate: Sodium phosphate; OA: Oxalic acid; B-RB: Britton-Robinson buffer; PAB: Potassium acetate buffer; PBS: Phosphate-buffered saline; PDHP: Potassium dihydrogen phosphate; PDHP: Potassium dihydrogen phosphate; PFPA: Pentafluoropropionic acid; PPA: Phosphoric acid; PPB: Phosphate buffer.

SOSP: Sodium-1-octanesulphonate; SPP: Sodium phosphate; SS: Sodium sulphate; TFA: Trifluoroacetic acid; THF: Tetrahydrofuran; β-CD: β-cyclodextrin.

Instrument: BIA: Batch injection analysis; HPAEC: High performance anion exchange chromatography; HPCEC: High performance cation exchange chromatography; RP-LC: Reversed phase liquid chromatography.

Electrode: WE: Working electrode; RE: Reference electrode; AE: Auxiliary electrode; BBD: Boron-doped diamond; GC: Glassy carbon; rGO: reduced graphene oxide; H: Hydrogen; PP: Pichia pastoris; PP: Polyphenol; SCE: Standard calomel electrode; SCF: Single carbon fibre; SS: Stainless steel.

EC mode: In. PAD: Indirect PAD; IPAD: Integrated PAD; MPAD: Multiple PAD; QPAD: Quadrupole PAD; SPAD: Six-potential PAD.

7. Future directions

3D printed flow cells with integrated versatile and exchangeable electrodes can be made commercially available for EC detection [206]. The strength of 3D printing designs is the ease of creation and the flexibility of the design. These devices consist of removable and reusable polymer-based body parts and fittings and allow the various electrode materials (such as carbon, gold, platinum, and silver) to be easily added to a threaded receiving port printed on the device. The technology spans a wide range of applications such as NO detection, neurotransmitter detection, and measuring oxygen tension in a stream of red blood cells [206]. Erkal *et al.* [206] utilised 3D printed microfluidic EC detectors for an AD of dopamine and nitrite in FIA platform. However, we haven't yet observed the applications of 3D printing in PAD techniques. Additionally, use of NMs such as zirconium dioxide nanoparticles was reported to facilitate simple modification of electrodes, increased electroactive surface areas, good electrical conductivity, and better EC response for the determination of propranolol [39]. Therefore, we envisage that in near future the rapid evolution of 3D printed EC detectors and the incorporation of NMs in EC detection will speed the development of enhanced EC detection including PAD in flow-based systems. We also envisage that in near future multi-modal EC detection (including a combination of PAD with PPD [207], PAD with AD [50] as well as a combination of various PAD cycles discussed in section 3) can gain attention to address detection of analytes that cannot be detected in one particular EC detection mode.

8. Conclusions

Over the last three decades, PAD has served as an electroanalytical detection technique for the determination of various organic aliphatic compounds using CE, FIA, and LC separation methods. Some unique advances of PAD techniques such as pulsed potential cleaning, low-cost instrumentation, minimal reagent usage, high sensitivity and high selectivity have expanded the range of applications of PAD in the field of analytical chemistry. Disposable microelectrodes have opened new horizons for the field of PAD, providing equal or better detection limits, and higher reproducibility and calibration linearity than with non-disposable electrodes. Additionally, the application of NMs-based EC detection has been reported to exhibit greater conductivity, improved catalytic effects during EC reactions, enhancement of faster electron transfer between electrode surfaces, and the ability to perform as reactants in EC analysis. The growing interest in utilising metal nanomaterial properties, 3D printing, and multi-modal detection in EC technology over the last two decades is gradually leading towards establishing advanced pulsed EC detection of wide range of analytes in biological, and complex sample matrices especially electro-inactive aliphatic organic compounds such as formic acid, acetic acid, maleic acid and β-cyclodextrin complexes.

Acknowledgements

The authors acknowledge the University of Tasmania for the financial support from Tasmania Graduate Research Scholarships (TGRS) to demonstrate research ability awarded to MAI. MM acknowledge the Australian Research Council (ARC) Future Fellowship (FT120100559) for the financial support of this research. MAI immensely grateful to all co-authors and Dr Ruth Amos (editor) for their comments on an earlier version of the manuscript that greatly helped to improve the manuscript.

Chapter 2. Miniaturised EC detector for capillary to standard analytical systems

Capillary gap flow cell as capillary-end electrochemical detector in flow-based analysis

Muhammed Ariful Islam [a], Shing Chung Lam [a, b], Yan Li [a], Mostafa A. Atia [a], Parvez Mahbub [a, c], Pavel N. Nesterenko [a, d], Brett Paull [a, b], Mirek Macka [a, e, f, *]

[a] Australian Centre for Research on Separation Science (ACROSS), School of Natural Sciences, University of Tasmania, Private Bag 75, Hobart 7001, Australia

[b] ARC Training Centre for Portable Analytical Separation Technologies (ASTech), School of Natural Sciences, University of Tasmania, Private Bag 75, Hobart 7001, Australia

[c] Institute for Sustainable Industries and Liveable Cities, Victoria University, Footscray Park Campus, Melbourne 3011, Australia

[d] Laboratory of Adsorption and Gas Chromatography, Chemistry Department, Lomonosov Moscow State University, 1-3 Leninskie Gory, 119991 Moscow, Russian Federation

[e] Department of Chemistry and Biochemistry, Mendel University in Brno, Zemedelska 1, CZ-613 00 Brno, Czech Republic

[f] Central European Institute of Technology, Brno University of Technology, Purkynova 123, CZ-612 00 Brno, Czech Republic

* Email: mirek.macka@utas.edu.au

Graphical abstract

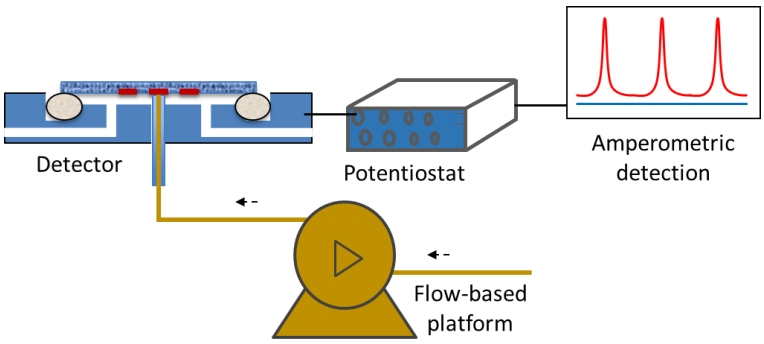

Highlights

- Gap flow cell (gap-FC) characterised and demonstrated as a capillary-end electrochemical detector.
- Gap-FC capillary outlet-electrode gap distance of just 30 µm.
- Gap-FC characterised for current, efficiency and effective cell volume.
- Highest efficiency 11% and lowest effective cell volume 35 nL achieved at 30 µm gap distance.
- Analytical performances compared with UV detection in capillary and standard LC.
- Gap-FC achieved lowest LODs of ascorbic acid, 2,3-dihydroxybenzoic acid and pyrocatechol to date.

Abstract

A gap flow cell (gap-FC) as a capillary-end electrochemical (EC) detector, incorporating exchangeable screen-printed electrodes, that facilitates adjustment of the gap distance between the capillary outlet and working electrode down to 30 µm was

investigated. The analytical performance of the gap-FC was assessed in terms of detector response (current), the efficiency of EC conversion of ferrocyanide, and effective cell volume, as a function of flow rate and gap distance, within a range of 0.1-200 µL min^{-1} and 30-100 µm, respectively. As a result, an efficiency of EC conversion within the range of ~1.5-11% (~3-16 times higher than wall-jet FC), at an effective cell volume of ~30-75 nL, was achieved. The gap-FC was applied as a liquid chromatography EC detector, coupled with standard and capillary format liquid chromatographs, where the analytical performance of gap-FC was compared with that of a UV detector. With the standard LC, the sensitivity for ascorbic acid, 2,3-dihydroxybenzoic acid and pyrocatechol, was greater than with the UV detector, with limits of detection (LODs) one order of magnitude lower for the gap-FC (0.10 µM, 0.09 µM, 0.19 µM, respectively, RSD 1.35-3.8 %, n=9, linearity r^2 ~0.99 for concentration range 1-100 µM). LODs of test electroactive solutes using the gap-FC were ~2 times lower than LODs reported in existing literature using standard EC detectors, including wall-jet and thin-layer FCs.

Keywords

Conversion efficiency

Effective cell volume

Flow-based analysis

Gap distance

Gap flow cell

1. Introduction

The prospect of low-cost and miniaturised detection has led to the use of electrochemical (EC) detectors in flow-based analytical systems such as flow injection analysis (FIA), capillary electrophoresis, and liquid chromatography (LC) [29, 44, 45, 208-210]. However, incorporating EC detectors in flow-based systems is challenging, specifically when attempting the physical and chemical characterisation of the EC detector. Wang [209] discussed the design, principles and applications of EC detectors for microfluidic-based systems. Xu et al. [210] reported a novel microelectrode design, fabrication methods, versatility of EC techniques for identifying of biochemical processes, and applications such as in situ analysis, point-of-care testing and portable analysers for complex sample matrices. The most commonly used EC detector is thin-layer flow cell (TL-FC). In TL-FC, the solution flows through a thin flat channel parallel to the working electrode (WE) surface [4-6]. In another type of commonly used EC detector is wall-jet FC (WJ-FC) [7], where the solution stream is directed perpendicularly to the plane of WE [8] through a small orifice and forms a jet that impinges on the electrode surface [9].

There exist a number of significant drawbacks and research challenges associated with the existing TL- and WJ-FC as EC detectors. These include difficulties in miniaturisation of the system [1-3], frequent repolishing of the electrode [32], and low efficiency of EC conversion, typically 4-5% [10]. Additionally, there are technical issues such as a lack of experimentally determined effective cell volume (V_E) data for the different gap distance (capillary outlet-electrode) in existing EC detectors [31, 34, 35, 211], as well as the necessity of cleaning the electrode surface during or after the experiment, and lack of EC detectors capable of being coupled with chromatographic separation platforms operating at flow rates within the nano- to millilitre per minute range [1, 10, 31-35]. The existing mechanisms of TL- and WJ-FC in terms of layer and jet formation is reported in Hubbard *et al*. [212], Gunasingham [1], and Patthy *et al.* [32] respectively, which stipulate rigid construction of the

EC detection FCs. In flow-based analytical systems, variations in the rigid construction of TL- and WJ-FC such as adjustment of effective cell volume, flow rates as well as the incorporation of miniaturised electrodes made of different materials are required.

Recently, BVT Technologies has designed a new EC detector (termed gap-FC in this study), which enables the use of exchangeable electrodes in a flow-through arrangement. The inherent features of this new gap-FC for EC detection overcome some of the above-mentioned difficulties associated with EC detectors in flow-based systems. Unlike TL- and WJ-FC, the gap-FC enables simple adjustment of the gap distance between the surface of the WE and the capillary orifice, down to a few microns, to facilitate the formation of a very thin layer of electrolyte on the electrode surface. At very low flow rates and small gap distances, the gap-FC can be used to precisely investigate current dependencies, efficiency % of EC conversion, and the exact V_E. As the gap-FC also incorporates exchangeable electrodes, specifically screen-printed electrodes (SPEs), the choice of potential WE materials is extensive. SPEs are typically inexpensive, simple, reliable to operate with high selectivity and precision [39], and offer a quick response and high sensitivity [213]. Additionally, the new gap-FC is small in size, robust, and relatively low cost (<$800), which makes it an ideal solution for portable and miniaturised analytical systems.

Comparing the design of gap-FC with TL- and WJ-FC designs, we emphasize that gap-FC is not similar to either TL- or WJ-FC. In TL-FC, the flow direction is horizontal to electrode surface whereas, in WJ-FC the flow direction is vertical to the electrode surface. Recently, we have published a review paper [29], where the flow profiles in EC FCs were schematically illustrated. Compared to TL- and WJ-FC, gap-FC enables adjustment of the gap distance between the surface of the WE and the capillary orifice, down to a few microns, to facilitate the formation of a very thin layer of electrolyte on the electrode surface which resulted the effective cell volume of the gap FC. One can expect all the advantages of thin layer FC in gap-FC with the added advantage of controlling the effective cell volume. According to literature, the WJ-FC were constructed with minimum gap distances in 0.125-10 mm range and minimum flow rate in 0.7-19.6 mL min^{-1} range [1, 8]. The construction of gap-FC accommodates very low flow rates (0.1-200 µL min^{-1} in this study) and minimal gap distance (30-100 µm in this study). We emphasize that in our study of the gap-FC, a layer is formed inside at such low flow rates and gap distance, for which we demonstrated the accurate measurement of the resulting effective cell volume inside the gap-FC. We acknowledge that at high flow rates in mL range and at larger gap distance in mm range, the gap-FC may act as WJ-FC, however, these configurations were deemed unsuitable for miniaturised capillary platforms in this study.

There is a significant number of publications covering the topic FIA coupled with SPEs, where most of these works illustrated the application of the techniques [34, 35, 214-217]. Additionally, researchers employed biologically modified electrodes in micro FCs for AD in flow mode [214-217], however without demonstrating their effective coupling with separation platforms, mainly due to lack of characterisation of these EC biosensors in terms of detector response (current), the efficiency of EC conversion, and V_E, at a range of flow rates and gap distances. We emphasize the fact that a detailed performance analysis of these EC detectors [34, 35] is the prerequisite for their coupling with separation platforms [214-217]. To date, studies on detailed performance analysis of miniaturised EC detectors that could be effectively coupled with FIA, capillary and standard LC systems are limited in their number and scope.

The aim of this study was to evaluate the performance of miniaturised EC detector (i.e., gap-FC) in EC detection for the first time and then demonstrate its application within the performance range when coupled with flow-based systems, specifically FIA, capillary and standard LC. Therefore, within this work, we investigated the analytical performance of the gap-FC

incorporating SPEs using a simple FIA set-up, in terms of detector response (current), the efficiency of EC conversion, and V_E, at a range of flow rates and gap distances. Having the performance range of the gap-FC characterised, we then investigated the analytical application of the gap-FC in capillary and standard LC. SPEs were reported as in-house/commercially available exchangeable electrodes used in EC sensors/biosensors [26, 34], and hence, in our study we employed commercially available SPEs as exchangeable electrodes in gap FC. The electroactive species, namely, ascorbic acid, 2,3-dihydroxybenzoic acid, pyrocatechol and dopamine were used as test solutes in this study. These solutes were previously reported in different flow-based analysis systems using EC detectors and therefore allowed direct comparison with previous works [3, 76, 218, 219]. The analytical application of the gap-FC in LC was also investigated, comparing the detection sensitivity of the gap-FC with EC detectors reported in the literature, as well as with a standard UV detector.

2. Experimental

2.1 Chemicals

Analytical grade standards and reagents were used in this study. These were potassium ferrocyanide trihydrate ($K_4Fe(CN)_6.3H_2O$, Ajax, Australia), sodium hydroxide (NaOH, Sigma-Aldrich, Sweden), dopamine, ascorbic acid, 2,3-dihydroxybenzoic acid (2,3-DHBA), pyrocatechol, citric acid, sodium citrate dihydrate (Sigma-Aldrich, USA), acetonitrile (ACN, 99.8% HPLC grade, VWR, Australia), and milli-Q water (Millipore, USA). HPLC grade solvents were used for all separations. All test solutes and mixtures were freshly prepared in the same solvent such as ACN and citrate buffer used for the LC mobile phase.

2.2 Instrumentation

A simple micro-flow injection analysis (μFIA) platform was assembled using a LabSmith uProcess™ microfluidic system (LabSmith, USA). The platform consisted of two programmable microsyringe pumps (LabSmith model: SPS01) with 100 μL glass syringes, one four port valve ('L' pattern flow, and 2 positions switching valve, LabSmith model: AV201-C360) and one injector valve (LabSmith model: AV303-C360). All pumps and switching valves were connected via PEEK tubing (Polyether ether ketone, 150 μm i.d., 360 μm o.d.) on a LabSmith uProcess™ Breadboard. LabSmith uProcess™ software was used for controlling the various components and the volumetric flow rate of microsyringe pumps [220]. The gap-FC was investigated using a polyimide coated fused silica capillary (100 μm i.d., 360 μm o.d., length 7-12 cm, TSP100375, Polymicro Technologies™, USA) to connect the injector valve and the gap-FC. The gap-FC itself was a three-electrode FC configuration, of dimensions - length 30 x width 16 x height 17 ± 0.05 mm, and model FC5 in PEEK (BVT Technologies, Czech Republic; see Fig. 6, SI Fig. S1, Fig. S2, and section S1). A TraceDec® capacitively-coupled contactless conductivity detector (C^4D, Innovative Sensor Technologies GmbH, Austria) was incorporated into the set-up to allow peak area comparisons for V_E calculations. The full instrumental scheme is shown in SI (see Fig. S3).

Both capillary and standard LC platforms were used in this study. The capillary LC (Dionex ultimate 3000 Nano HPLC, Thermo Scientific™, USA) consisted of a thermostated reversed-phase (RP) capillary column (SGE ProteCol C18 G 123 column, length 15 cm x i.d 150 μm, particles size 3 μm, 120 Å, Trajan Scientific and Medical, Australia), a multi-wavelength UV-Vis photometric detector (UltiMate™ 3000 VWD variable wavelength detector, path length: 10 mm, cell volume: 45 nL, Dionex™ Thermo Scientific™, USA) and injector valve (MV303-C360, LabSmith, USA). The capillary LC platform was operated using Chromeleon 6.8 software (Thermo Scientific™, USA). The standard LC platform (Alliance Waters 2690 HPLC, Waters, USA) consisted of

thermostated RP column (YMC Pac Pro C18, length 25 cm x i.d. 4.6 mm, pore size 5 µm, YMC Co. Ltd, Japan), UV detector (Waters 996 PDA detector, path length: 10 mm, cell volume: 8 µL, Waters, USA) and injector valve (SM4, Waters, USA). The standard LC was operated by the Empower software (Waters, USA). The gap-FC was coupled to both capillary and standard LCs.

AD was performed under optimised conditions, where +800 mV using a platinum (Pt) as WE, with a flow rate of 1 µL min^{-1} in the capillary LC set-up, and 0.6 mL min^{-1} with the standard LC, using a capillary i.d of 100 µm, and a gap distance of 30 µm. We have observed a higher UV signal (peak height) at 254 nm for ascorbic acid, and at 280 nm for 2,3-DHBA, pyrocatechol, and dopamine. Therefore, we used both 254 nm and 280 nm for UV detection in this study.

EC detection in both FIA and LC platforms was performed using the commercially available SPEs $AC_1W_2R_S$ as an exchangeable EC sensor of dimensions - length 25.40 x width 7.26 x height 0.63 ± 0.05 mm (BVT Technologies, Czech Republic). The electrode consisted of Pt as WE (diameter: 2 mm), silver (Ag) as a reference electrode (RE), and Pt as the auxiliary electrode. The potential at WE, which is measured versus the RE, is determined by the element metal of RE and the active species concentration in the electrolyte. In our study, we used screen-printed silver as a RE and the wet form of electrolyte ($[Fe(CN)_6]^{4-}$ in NaOH solution). The form of the electrolyte, had no effect on the reference potential [221]. The SPEs materials and fabrication details are discussed in recent reviews by Li *et al.* [213] and Couto *et al.* [13]. The O-ring of the FC ensured no back mixing of the flowing solution (see video link in SI section S1.1). A potentiostat (model ER466CE, eDAQ Pty Ltd, Australia) was connected to the gap-FC and operated with eDAQ software (eDAQ Pty Ltd, Australia) to perform EC detection.

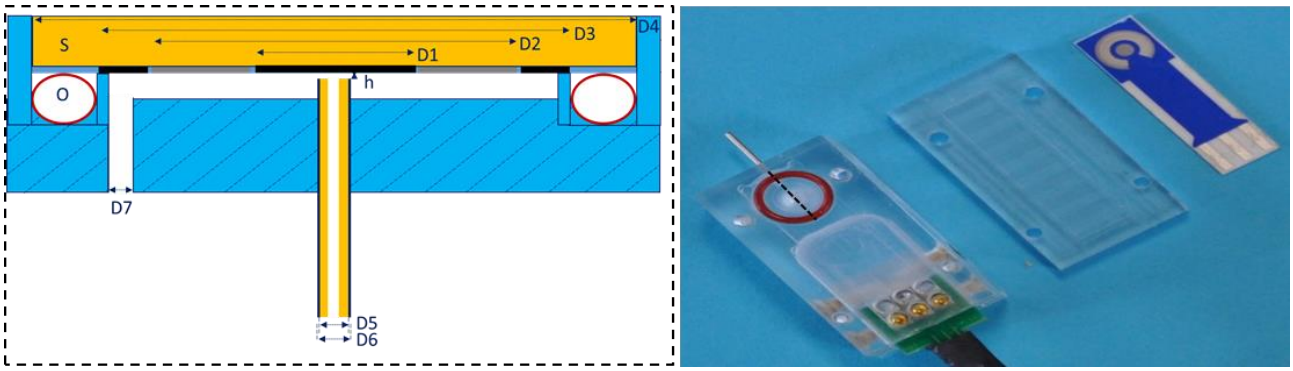

Fig. 6. Gap-FC with SPEs (plan view and a cross-section of measurement part, where D1: working electrode 2.05 mm, D2: reference electrode 4.60 mm, D3: auxiliary electrode 5.95 mm, D4: dielectric layer 7.65 mm, D5: passage for capillary 0.36 mm, D6: hole for capillary 0.4 mm, D7: waste 0.3 mm, h: gap distance, O: O-ring, S: SPEs thickness 0.63 mm).

3. Results and discussions

FIA was used to characterise the gap-FC in terms of detector response, the efficiency of EC conversion, and V_E. For experimental investigations, we used low concentration of $[Fe(CN)_6]^{4-}$, which is highly electroactive as well as the most commonly used solute for the study of EC detection. In addition to EC detection in our study, we also incorporated C^4D for gap-FC characterisation. The low concentration of $[Fe(CN)_6]^{4-}$ was suitable to use in C^4D platform in terms of detector sensitivity. Therefore, we have used 10 nM concentration of $[Fe(CN)_6]^{4-}$. Observations of the baseline did not reveal any considerable fluctuations with the flow of the eluent in our study. This characterisation was undertaken prior to demonstrating the practical analytical application of the gap-FC in capillary and standard LCs.

3.1 Characterisation of gap-FC

3.1.1 Detector response (current)

The combined dependence of current on flow rate and gap distance for the gap-FC is shown in Fig. 7.

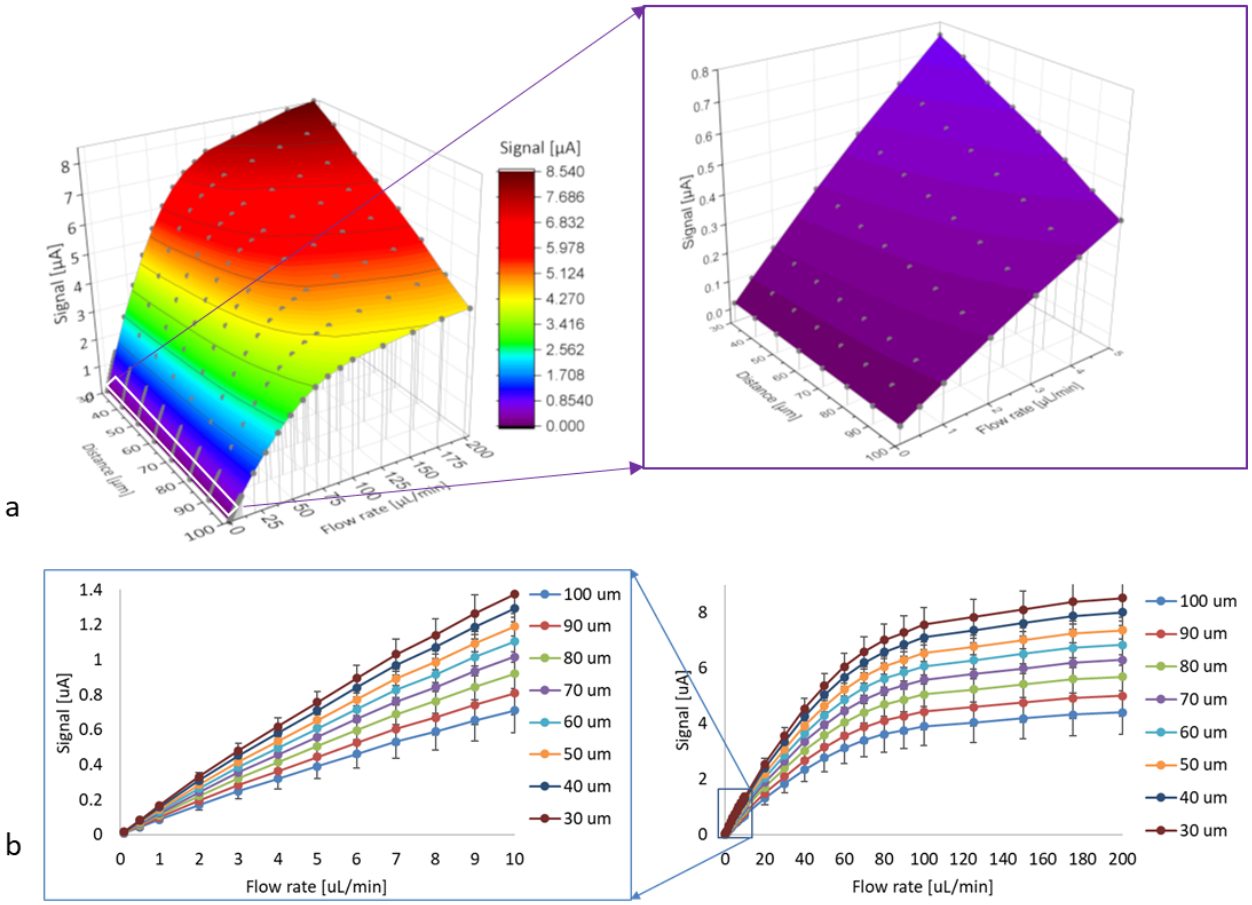

Fig. 7. Dependency of current on flow rate and gap distance, respectively (a. 3D graph and b. 2D graph). Conditions: solvent: water; flow rate: 0.1-200 µL min^{-1}; solute: 10 nM $[Fe(CN)_6]^{4-}$ in 0.04 M NaOH; sample injection volume: 3 µL; capillary (injector-gap-FC): i.d 100 µm, length 7 cm; gap distances: 30-100 µm; and AD potential: +650 mV.

The current in EC detector depends on the number of moles of solute that are oxidised or reduced at the WE. Obviously, flow velocity has a significant impact on the efficiency of this process. We observe in Fig. 7 that at low (0-20 µL min^{-1}) and high (>20-200 µL min^{-1}) flow rates, the signal always increased with a decrease in gap distance. At higher flow rates due to high sharper peaks with less dispersion in the fluidic path [222], detector response continued to increase but at a reduced rate. At flow rates above 75-100 µL min^{-1}, the response could be approximately doubled through reduction of the gap distance from 100 down to 30 µm. The rate of change of signal with flow rate below 20 µL min^{-1} at a fixed gap distance of 30-100 µm was appeared linear (see Fig. 7). The theoretical current in EC detectors can be expressed by equations 1 and 2 [10, 223].

$$I_0 = QCF \qquad (2)$$

$$I_0 = nAF\frac{dN}{dt} \qquad (3)$$

Where, I_0 = Theoretical current corresponding to full conversion at WE surface, Q = Flow rate [L min^{-1}], C = Concentration [mol L^{-1}], F = Faraday constant 96,485 [C mol^{-1}], n = number of electrons transferred per mole of solute, A = Electrode geometric or projected area [m^2], N = Number of moles of solute oxidised or reduced, and t = time [min].

By combining equations 1 and 2, we can derive equation 3, where we can attribute the increased rate of change of the number of moles (dN/dt) at the electrode surface with the increased flow rate (Q), considering C and n as constants.

$$QC = nA\frac{dN}{dt} \qquad (4)$$

Equations 1-2 doesn't contain any parameter related to the gap distance. Here higher currents were observed at smaller gap distances, although noise remained almost constant for all gap distances (see SI section S3.1.4). Furthermore, we attribute the fact that the residence time of solute (i.e., $K_4Fe(CN)_6.3H_2O$) at the electrode surface reduces with decreasing gap distance. The increased responses from different analytes in terms of peak heights and widths at lower gap distances in EC detectors have also been observed and reported by Yamada *et al.* [8], Gunasingham [1], and Ji *et al.* [224]. Gunasingham [1] has previously shown this effect, noting that the short residence time caused increased peak current (signal) for some analyte (o-aminophenol, p-aminophenol and p-phenylenediamine), whereas decreased peak current for some other analyte (2,6-diisopropylphenol, 3-isopropylphenol and phenol). Gunasigham [1] attributed the alteration of the radial velocity profile of different analytes at the detection cell at a lower gap distance as a reason for this increase or decrease of peak current. Therefore, the analyte type is chosen in our study also played a role in the increased signal at lower gap distance. In this investigation, the dependencies are clearly demonstrating that current can be maximised at the lowest gap distance of 30 µm and can be further increased with the increase of flow rate at this lowest gap distance.

3.1.2 EC conversion efficiency

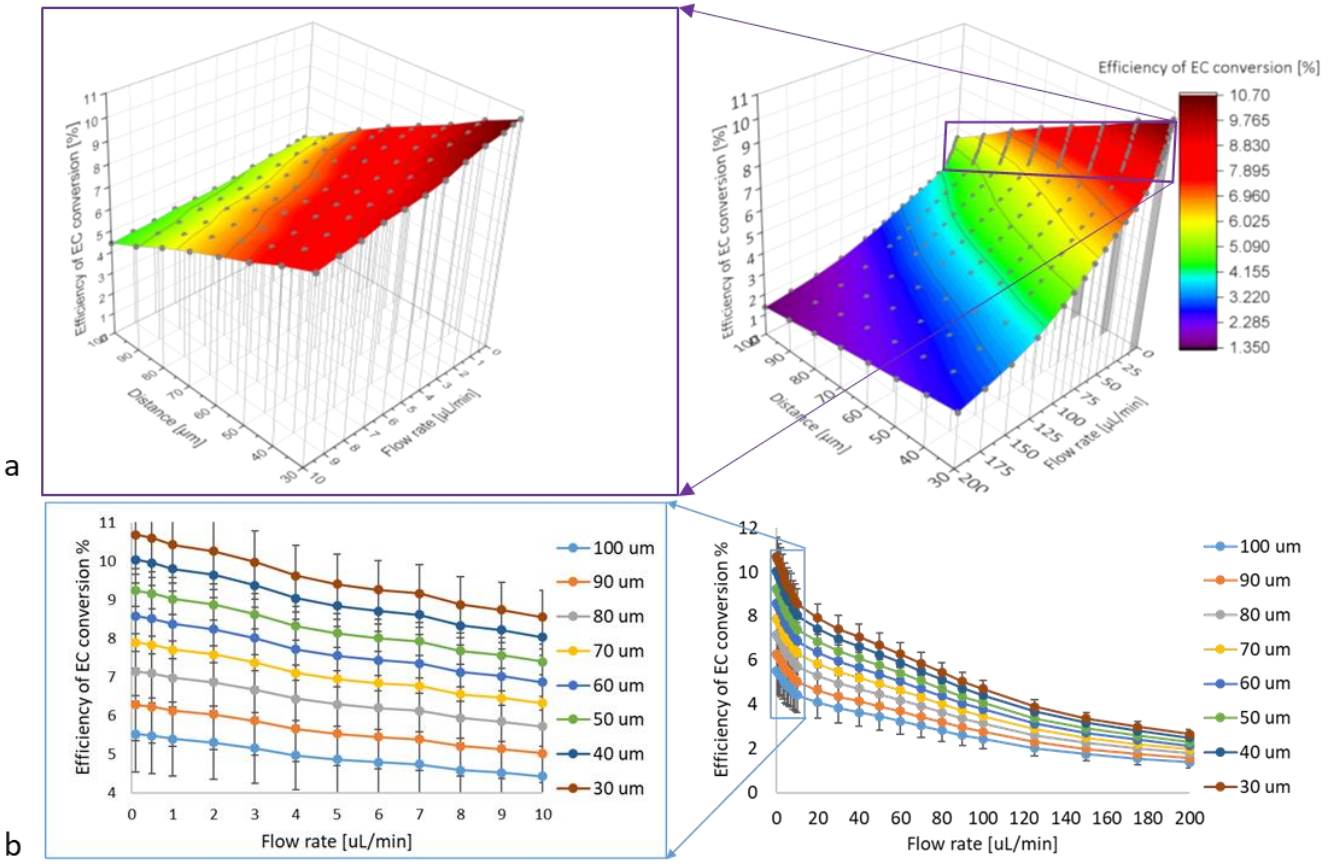

Fig. 8. The dependency of the efficiency of EC conversion % on flow rate and gap distance (a. 3D graph and b. 2D graph). Conditions: solvent: water; flow rate: 0.1-200 µL min^{-1}; solute: 10 nM $[Fe(CN)_6]^{4-}$ in 0.04 M NaOH; sample injection volume: 3 µL; capillary (injector-gap-FC): i.d 100 µm, length 7 cm; gap distances: 30-100 µm; and AD potential: +650 mV.

The dependence of EC conversion efficiency upon gap distance for solute $[Fe(CN)_6]^{4-}$ was determined across the range of 30 to 100 µm, with the resulting efficiency data shown in Fig. 8. Counter to the above overall signal enhancement with flow rate, the EC conversion efficiency observed to drop rapidly with the flow.

The ratio of measured current I to the theoretical current I_0 corresponds to the EC conversion efficiency of the FC according to equation 4.

$$\eta = \frac{I}{I_0} = \frac{I}{QcF} \qquad (5)$$

Where, η = EC conversion efficiency [%], I = Measured current [A].

The reduction of the EC conversion efficiency at the increased flow rate in Fig. 8 illustrates the inverse relationship between the efficiency of EC FCs with the flow rates described in equation 4 [10]. Krejci *et al.* [10] has previously shown this effect, noting that lower flow rates provide longer residence time and thus increased substrate conversion efficiency. Here, this effect is further eventuated with an increase in gap distance, as shown in Fig. 7 and Fig. 8. For the flow rates used in this study, EC conversion efficiencies ranged from ~1.5 % at 200 µL min^{-1} to 11 % at 0.10 µL min^{-1}. However, the EC conversion efficiencies with the gap-FC were ~3-16 times higher than those reported for a WJ-FC, for flow rates ranging from 1.5 to 200 µL min^{-1} [10].

Finally, the above characterisation studies confirmed that the minimum gap distance of 30 µm at the lowest flow rate of 0.10 µL min^{-1} showed maximum EC conversion efficiency for the gap-FC.

3.1.3 Effective cell volume

In this study, the V_E of gap-FC was experimentally determined by varying the flow rate and gap distance. For a given set of conditions (such as flow rate, gap distance, and length of the capillary) simultaneous peak responses for the test solute $[Fe(CN)_6]^{4-}$ were obtained using both on-capillary C^4D and the gap-FC as EC detector, from a single injection. From the peak response (i.e., the height of the peaks), the total volume was calculated by multiplying the flow rate and time at half of the peak height [225] (see SI Fig. S4). In general, for a certain flow rate and gap distance, two sets of total volumes can be obtained from C^4D and gap-FC by varying the length of the capillary. Detailed measurement and calculations of V_E are discussed in section 3.1.3 and SI section S2.2.

The V_E of the gap-FC varied across the range of 35-75 nL for different gap distances (30-80 µm) and flow rates investigated in this study (see Fig. 9). Gunasingham [1] reported that small V_E reduce band spreading and enhance EC conversion efficiency. In this study, the maximum EC conversion efficiency of 11% was obtained at 30 µm gap distance and a flow rate of 0.5 µL min^{-1} (see Fig. 8). This relatively high EC conversion rate was achieved at an V_E of ~35 nL, as illustrated in Fig. 9(a). In the past, the V_E of alternative EC detectors have been calculated based on applying a simplified method for a known detector geometry, by multiplying electrode surface area and gap distance [31, 33, 211]. In this present study, V_E has been measured experimentally, through varying gap distance and flow rate. The experimentally determined V_E of 35 nL for the gap-FC is the lowest amongst those reported V_E of EC detectors [31, 33, 211] and more importantly, the only experimentally confirmed V_E to-date, which produced an EC conversion efficiency of ~11%.

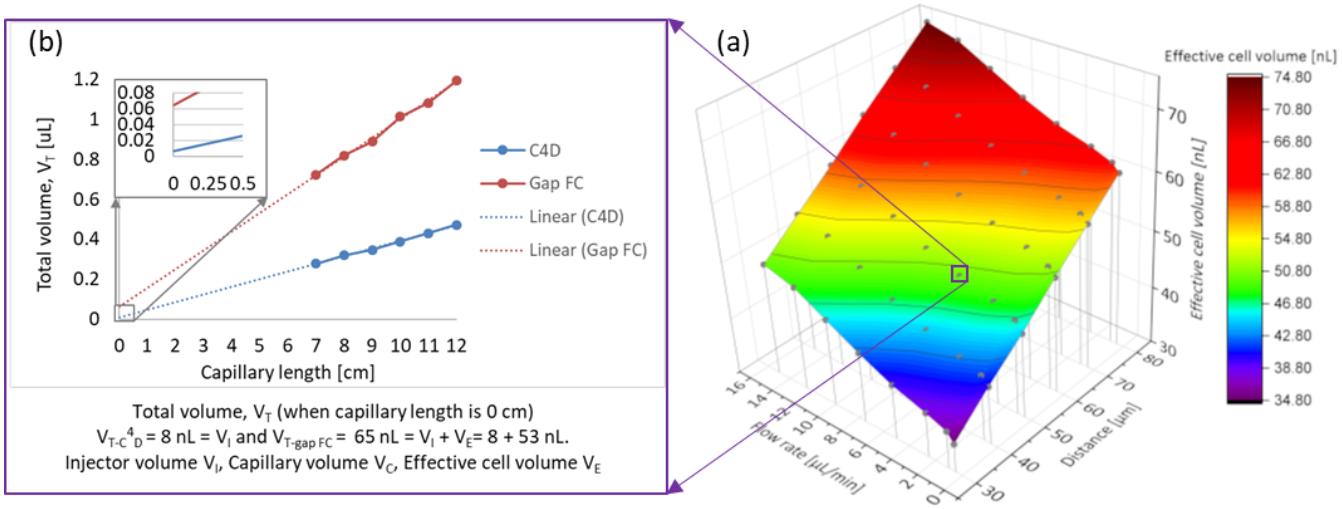

Fig. 9. (a) Dependency of effective cell volume on flow rate and gap distance, respectively. Conditions: solvent: water; flow rate: 0.5-15 µL min^{-1}; solute: 10 nM $[Fe(CN)_6]^{4-}$ in 0.04 M NaOH; sample injection volume: 3 µL; capillary (injector-gap-FC): i.d 100 µm, length 7-12 cm; gap distances: 30-80 µm; and AD potential: +650 mV. (b) Calculated V_E for flow rate 5 µL min^{-1}, and gap distance 50 µm, which plotted as a single point in the 3D graph.

3.2 Analytical applications

In this study, to demonstrate compatibility across a wide range of flow rates, the analytical applications of the gap-FC were investigated in combination with both capillary LC, and standard LC systems (the latter with simultaneous UV absorbance detection). The separations were developed under isocratic conditions, and the system parameters, such as mobile phase flow rate, column to detector capillary i.d, gap distance, and applied potential, were optimised using chromatographic peak signal-to-noise ratio (S/N, see SI section S3). Under optimised conditions calibration curves for test solutes were constructed for each LC format.

3.2.1 Standard LC-UV-EC

The chromatograms of target solutes using standard LC-UV-EC system are illustrated in Fig. 10.

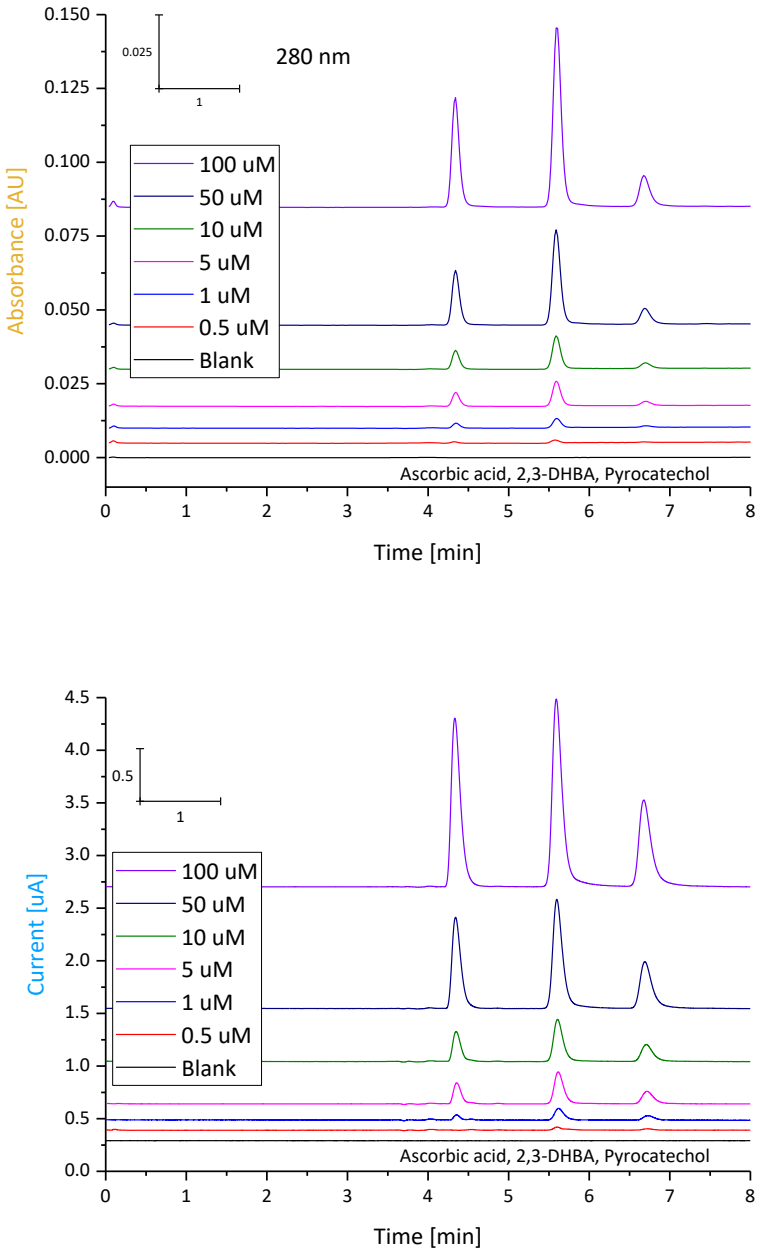

Fig. 10. Chromatograms showing separations of ascorbic acid, 2,3-DHBA, and pyrocatechol using standard platform. Conditions: mobile phase (v/v=60:20:20): ACN: water:25 mM citrate buffer, pH 3.5; elution: isocratic; flow rate: 0.6 mL min^{-1}; sample injection volume: 10 µL; LC column (injector-UV detector): YMC Pac Pro C18 RP column (length: 25 cm, i.d: 4.6 mm, particles size: 5 µm), column oven temperature: 25 °C; pressure: ~1050 psi (~73 bar); capillary (UV-gap-FC) i.d: 100 µm, length: 7 cm; gap distance: 30 µm; WE: Pt; and AD applied potential: +800 mV. UV absorbance wavelength: 280 nm. See 254 nm UV absorbance graph in SI (Fig. S13).

Table 2. Comparison of analytical performance of gap-FC with UV detector in standard LC platform.

Detector	Analyte	Void Volume [a] [mL]	Peak asymmetry factor [b]	Peak efficiency (plate number [c]/ column length) [N m^{-1}]	Peak FWHM [min]	Baseline noise (3SD) 5-10 min	LOD [d] [µM]	RSD [%]
UV	Ascorbic acid	0.1	1.1-1.3	39800-62000	0.12-0.16	0.22 [mAU] (254 nm) 0.15 [mAU] (280 nm)	0.37	1.1-4.8
	2,3-DHBA						0.83	
	Pyrocatechol						4.90	
Gap-FC	Ascorbic acid	-	1.0-1.2	36300-55400	0.10-0.13	1.5 [nA]	0.10	1.3-4.9
	2,3-DHBA						0.09	
	Pyrocatechol						0.19	

[a] Void volume calculated by multiplying flow rate and the elution time for mobile phase or unretained solute when the first baseline disturbance is observed [50]. [b] Peak asymmetry factor, $A_s = \frac{w_R}{w_L}$, where w_R is the distance from the peak midpoint (perpendicular from the peak highest point to baseline) to the trailing edge of the peak and w_L is the distance from the leading edge of the peak to the peak midpoint measured at 10 % of peak height [50]. [c] Plate number, $N_P = 5.54\,(\frac{t_R}{w_{h/2}})^2$, where t_R is retention time and $w_{h/2}$ is width of the peak at half height [50]. [d] Limit of detection (LOD) was calculated by dividing the standard deviation of peak signals of fortified blank samples close to the expected LODs by the slopes of the corresponding calibration curves [50]. LODs calculated at 254 nm for ascorbic acid and 280 nm for 2,3-DHBA and pyrocatechol.

The calibration curves for both UV and EC detections were plotted using peak heights for each solute (see Fig. S13). The LODs values of EC detection were ~4-25 times lower than those obtained with UV detection). The LODs obtained for the gap-FC were 0.10 µM, 0.09 µM, 0.19 µM for ascorbic acid, 2,3-DHBA and pyrocatechol, respectively (see Table 2).

However, the performances of gap-FC in terms of peak asymmetry, peak efficiency and peak FWHM are compared with UV detector in this platform (see Table 2). The delay time between chromatograms ~1-2s, the loss of efficiency (~9-11%), ~2-3% peak broadening in gap-FC was given by the connecting pathways [226], geometry [48] and the effective volume of FC [50].

3.2.2 Capillary LC-EC

The chromatograms of test solutes using the capillary LC-EC system are shown in Fig. 11. The calibration curves for capillary LC peaks using either UV absorbance or EC detection (not simultaneous) were plotted based on peak height response (see SI Fig. S10 and Fig. S11). Once again LODs were 1.63 µM, 1.96 µM, and 2.66 µM for dopamine, 2,3-DHBA, and pyrocatechol, respectively, using the gap-FC. In this case, these LODs were at least one order of magnitude higher than those obtained with UV detection (see Table 3). We emphasise the fact that there is literature that reported sub-nanomolar LODs for similar analytes where LODs were expressed as the standard deviations of baseline noise (e.g., Gu *et al.* [227]). In this study, we calculated the LODs as the ratio of the standard deviation of baseline noise to the slope of the corresponding calibration curves [50]. The resulting differences in LODs between the standard and capillary format LC systems reflect the response dependencies characterised within section 3.1. However, the performances of gap-FC in terms of peak asymmetry, peak efficiency and peak FWHM are compared with UV detector in this platform (see Table 3).

Table 4 compares the analytical performance of the gap-FC used here with the standard LC and capillary LC formats, with other reported data for flow-through EC detectors [76, 219]. The LODs for the gap-FC EC detector in standard LC were at least one order of magnitude lower than those obtained in the capillary LC-EC system for 2,3-DHBA, and pyrocatechol. More importantly, the LODs obtained with the gap-FC were ~2 times lower than the EC detectors reported by Santos *et al.* [76] for ascorbic acid and Pluangklang *et al.* [219] for 2,3-DHBA, and pyrocatechol, respectively (see Table 4).

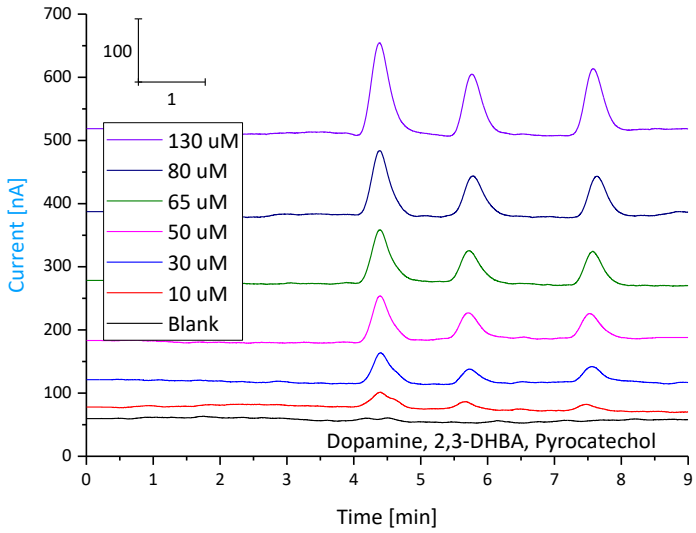

Fig. 11. Chromatograms showing separations of dopamine, 2,3-DHBA, and pyrocatechol using capillary LC platform. Conditions: mobile phase (v/v=20:80): acetonitrile:25 mM citrate buffer, pH 3.5; elution: isocratic; flow rate: 1 µL min^{-1}; sample injection loop: i.d: 25 µm, volume: 174 nL; capillary LC column (injector-capillary inlet): ProteCol C18 RP column (length: 15 cm, i.d: 150 µm, particles size: 3 µm), column oven temperature: 35 °C; pressure: ~110 bar; capillary (column-gap-FC): i.d 100 µm, length 15 cm; gap distance: 30 µm; WE: Pt; and AD applied potential: +800 mV.

Table 3. Comparison of analytical performance of gap-FC with UV detector in capillary LC platform.

Detector	Analyte	Void Volume [a] [µL]	Peak asymmetry factor [b]	Peak efficiency (plate number [c] / column length) [N m^{-1}]	Peak FWHM [min]	Baseline noise (3SD) 5-10 min	LOD [d] [µM]	RSD [%]
UV	Dopamine	0.2	1-1.2	24800-32200	0.25	0.02 [mAU] (254 nm) 0.04 [mAU] (280 nm)	0.20	2.5-4.5
	2,3-DHBA						0.29	
	Pyrocatechol						0.19	
Gap-FC	Dopamine	-	1.1-1.3	19200-25100	0.29	0.54 [nA]	1.63	3.2-4.9
	2,3-DHBA						1.96	
	Pyrocatechol						2.66	

[a, b, c, d] Calculation details are given in Table 2.

Table 4. Comparison of performance of gap-FC with other reported EC detectors in flow-based analysis systems.

Platform-EC method	Potential [mV]	Flow rate [mL min^{-1}]	Solvent (v/v), pH	Linearity [µM]	LOD [µM]	Ref.
FIA-pulsed AD	400	0.6	0.1 M acetic acid/ acetate, pH 4.7	28.5-140	0.11 [a]	[76]
Standard LC-AD	800	0.3	25 mM citrate buffer, pH 3.5:ACN (20:80)	0.25-125	0.18 [b] 0.23 [c]	[219]
Standard LC-AD	800	0.6	25 mM citrate buffer, pH 3.5:water:ACN (20:20:60)	0.50-100	0.10 [a] 0.09 [b] 0.19 [c]	This work
Capillary LC-AD		0.001	25 mM citrate buffer, pH 3.5:ACN (20:80)	10-200	1.96 [b] 2.66 [c]	

[a] Ascorbic acid, [b] 2,3-DHBA, and [c] Pyrocatechol.

4. Conclusions

In this study, a new gap-FC has been characterised in terms of detector response, EC conversion efficiency, and effective cell volume for flow-based analysis. The highest reported EC conversion (~11%) at the lowest reported effective cell volume (35

nL) was achieved. The gap-FC provided EC measurements with high repeatability, high sensitivity, and was readily applied within flow-based analytical systems across a wide flow rate range. The analytical performance in terms of sensitivity and LODs values of standard LC-EC was ~4-25 times lower than the capillary LC-UV, capillary LC-EC, and standard LC-UV systems for test solutes, namely ascorbic acid, 2,3-DHBA, and pyrocatechol. Additionally, for the standard LC platform, ~2 times lower LODs were obtained than those reported to-date using alternative EC detectors, such as those based upon TL- and WJ-FCs.

Acknowledgements

The authors acknowledge the University of Tasmania for the financial support in the form of a Tasmania Graduate Research Scholarships (TGRS) awarded to MAI. MM acknowledges the Australian Research Council (ARC) Future Fellowship (FT120100559) for the financial support of this research. SCL wishes to acknowledge the Australian Research Council for the provision of a post-graduate scholarship under Grant IC140100022. Thanks to Dr. Petr Smejkal for his technical support and Farhan Cecil, Aleksandra Koreshkova and Dr. Vipul Gupta for their initial technical guidance for using flow-based systems. The author MAI dedicates the paper to his spouse Mrs Merin Nigar for her continued support to keep things in perspective that made the completion of this work possible.

Supplementary information (SI)

The supporting information content includes:

1. Gap-FC: body parts construction, gap distance adjustment, and gap-, TL- and WJ-FC comparisons.
2. FIA platform: instrumentation and calculation of effective cell volume.
3. Separation platforms: capillary LC-UV and LC-EC systems, and standard LC-UV-EC system.
    3.1. Capillary LC-UV and LC-EC systems: optimisation of parameters such as mobile phase, buffer pH, flow rate, capillary i.d., gap distance, applied potential and calibration plots.
    3.2. Standard LC-UV-EC system: optimisation of flow rate and calibration plots.

1. Gap-FC

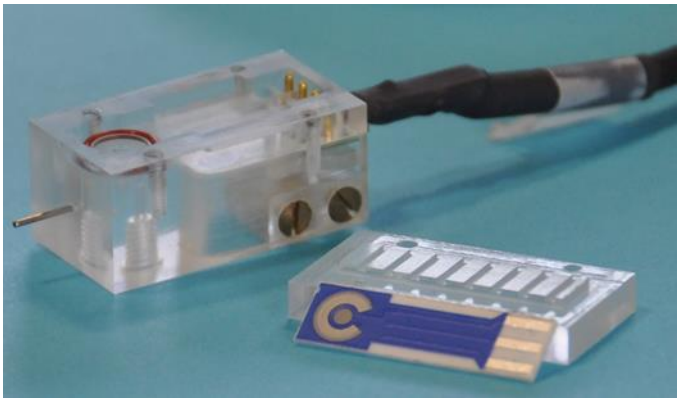

Fig. S1. The gap-FC (elevation view)

The visual inspection of bubbles and space around the WE were captured by using an optical microscope (model: AM4113T-GFBW, Dino-Lite digital microscope, USA. Experimental conditions: 1 mM Rhodamine 6G dye (Sigma-Aldrich, USA), flow rate: 10 µL min^{-1}, LabSmith microsyringe pump, solvent: water, capillary (injector-gap-FC as EC detector): i.d: 100 µm, and gap distance: 30 µm. For this purpose, semi-transparent Poly(methyl methacrylate (PMMA) gap-FC was used instead of PEEK material-based gap-FC that used for experimental investigations. See web link:

https://www.youtube.com/watch?v=GIWNc4xCr8E

1.1 Body parts construction

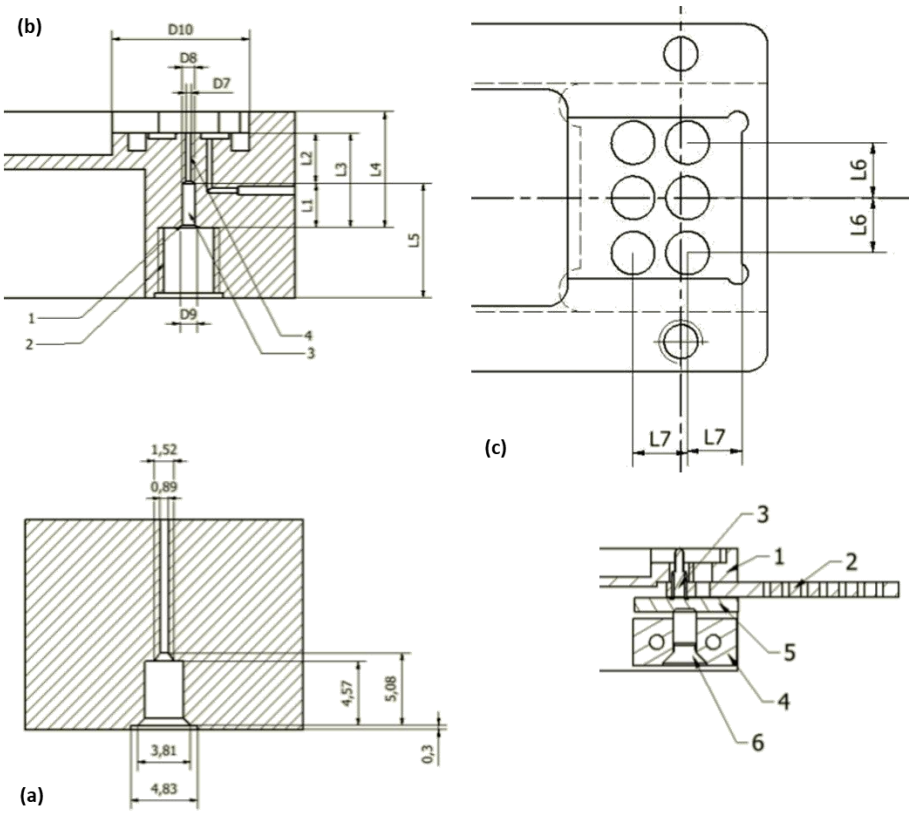

Fig. S2. The gap-FC: (a) connection of capillary, (b) measuring part (1. cone for tightening, 2. screw for coupling screw, 3. hole for tightening of sealing of capillary, 4. hole for capillary insertion), and (c) SPEs connector (1. body part of gap-FC, 2. printed circuit board with contacts, 3. gold plated contacts, 4. supporting desk, 5. insulating spacer, and 6. screw M3 for fastening of printed brand with contacts). Dimensions: D7: 0.4 mm, D8: 0.95 mm, D9: 1.52 mm, D10: 5.6 mm, L1: 2.9 mm, L2: 3 mm, L3: 5.9 mm, L4: 7.4 mm, L5: 8.5 mm, L6: 2.54 mm, L7: 2.5 mm, h1: 0.4 mm, and h2: 0.005-0.015 mm.

1.2 Gap distance adjustment

One of the key features of gap-FC is to facilitate a quick and accurate method to adjust the gap distance between the electrode and capillary orifice. To adjust the gap distance, the commercially available as well as mechanically durable thin steel (part number: 412092, Kincrome Australia Pty Ltd.) with vendor specified thickness was used as a spacer. The spacer was cut into the same diameter of the electrode. In the cell, the spacer was placed between the capillary orifice and electrode. The upper part of the cell and capillary were locked with screws and the built-in system for fastening the capillary. Finally, the upper part of the cell was opened to take out the spacer and locked again that confirms the desired gap distance between the working electrode and the capillary orifice. We used an external marker on the capillary to double check the gap distance by measuring the shift of the marker when the spacer was taken out using an optical microscope (model: AM4113T-GFBW, Dino-Lite digital microscope, USA). We used commercially available steel sheet with thicknesses varying from 30 µm (minimum thickness available from vendors) to 100 µm. We measured the spacer thickness for at least 5 times (30±0.02 µm) before placing the spacer between capillary outlet and electrode inside gap-FC.

2. FIA platform

2.1 Instrumentation

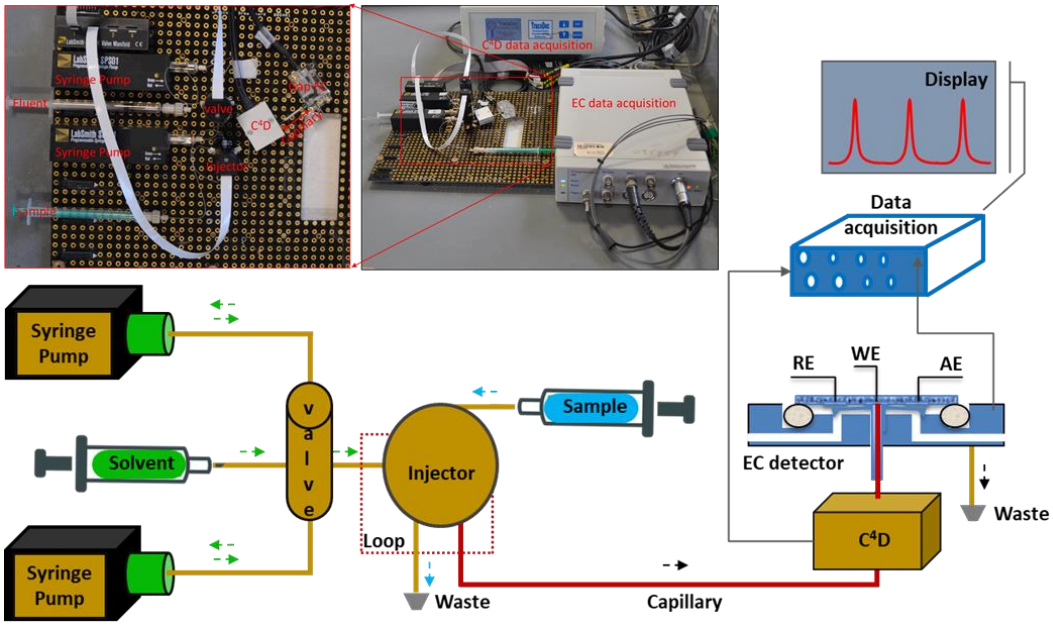

Fig. S3. Schematic flow diagram of µFIA platform.

2.2 Effective cell volume

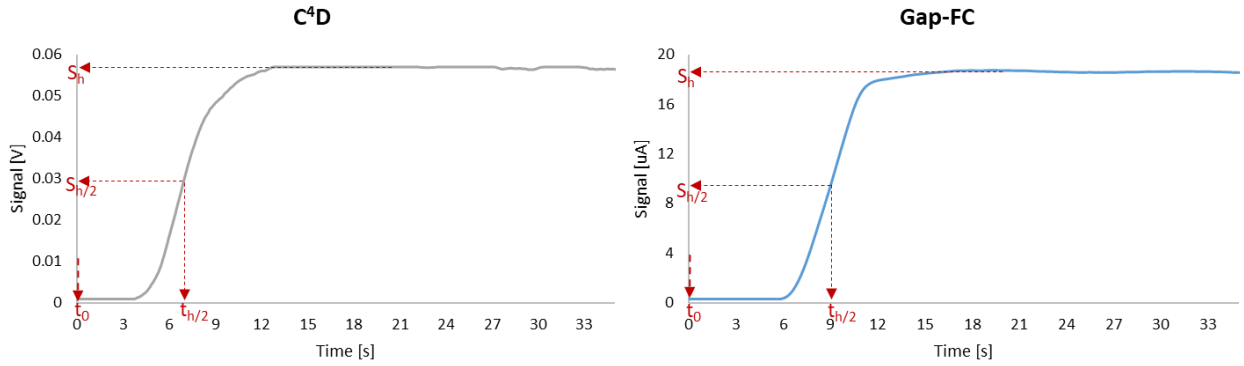

Fig. S4. Demonstration of calculating the response times ($t_{h/2}$) in gap-FC and C^{4}D detectors from the measured peak signals (S_h) at flow rate 5 µL min^{-1}, capillary length: 7 cm and gap distance: 50 µm. Conditions: solvent: water, flow rate: 5 µL min^{-1}; solute: 10 nM $[Fe(CN)_6]^{4-}$ in 0.04 M NaOH; sample injection volume 3 µL; capillary (injector-gap-FC): i.d 100 µm, length 7 cm; gap distance: 50 µm; and AD potential: +650 mV. t_0 is initial time, $t_{h/2}$ is time at half of signal height, $S_{h/2}$ is half of signal height, S_h is signal height.

The effective cell volume, V_E of gap-FC can be measured by varying the length of the capillary from injector to detector in X-axis and total volume ($V_T = V_I + V_C + V_E$) obtained from the detector signal in Y-axis. V_T is the total of injector volume i.e. void volume of the injector V_I, capillary volume V_C, and V_E. For a given length of the capillary (see Fig. S4), V_T can be calculated from the detector signal by considering time at half of the signal height and flow rate. In X-axis when the length of the capillary is zero, $V_{T-C^4D} = V_I$ *and* $V_{T-gap-FC} = V_I + V_E$. Finally, V_E of gap-FC can be calculated by subtracting the value of V_I from the value of $V_{T-gap-FC}$ in Y-axis.

Table S1. Total volume calculation of C^{4}D and gap-FC at capillary length 7 cm and gap distance 50 µm.

Detector	Time at half of peak height, $t_{h/2}$ [s]	Flow rate, Q [µL min-1]	Total volume, V_T ($t_{h/2}$ x Q) [nL]
C4D	7	5	583
Gap-FC	9	5	750

3. Analytical applications

3.1 Capillary LC-UV/LC-EC

In this study, the parameters were investigated to optimise the experimental conditions (see sections 3.1.1–3.1.5). The optimum conditions (composition of organic mobile phase and pH of buffer) selected were same as conditions trialled by Pluangklang *et al.* [219]. Statistical analysis was undertaken to compare the experimental conditions and results (see Table 4).

3.1.1 Optimisation of mobile phase

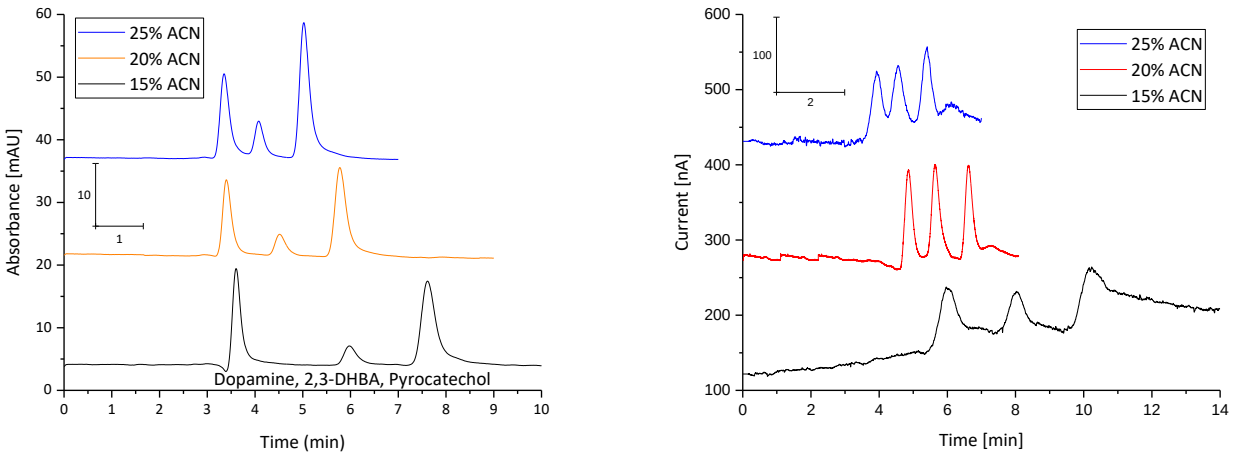

Fig. S5. Dependency of solute response on organic solvent ratio. Conditions: mobile phase (v/v=15:85, 20:80, and 25:75): acetonitrile:25 mm citrate buffer, pH 3.5; elution: isocratic; flow rate: 1 µL min^{-1}; solute concentration: 80 µM; sample injection loop: i.d: 25 µm, volume: 174 nL; capillary LC column (injector-UV or EC detector): ProteCol C18 RP column (length: 15 cm, i.d: 150 µm, particles size: 3 µm), column oven temperature: 35 ºC; pressure: ~110 bar; UV absorbance wavelength: 280 nm; capillary (column-gap-FC): i.d 100 µm, length 15 cm; gap distance: 30 µm; WE: Pt; and AD applied potential: +800 mV.

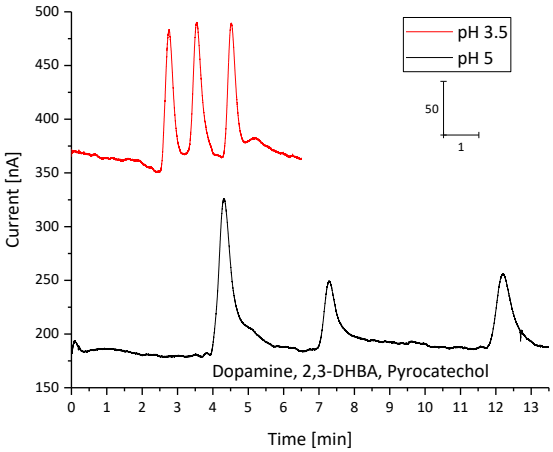

Fig. S6. Dependency of solute response on pH of mobile phase. Conditions: mobile phase (v/v=20:80): acetonitrile:25 mm citrate buffer, pH 3, and 5; elution: isocratic; flow rate: 1.5 µL min^{-1}; solute concentration: 80 µM; sample injection loop: i.d: 25 µm, volume: 174 nL; capillary LC column (injector-UV or EC detector): ProteCol C18 RP column (length: 15 cm, i.d: 150 µm, particles size: 3 µm), column oven temperature: 35 ^{o}C; pressure: ~110 bar; capillary (column-gap-FC): i.d 100 µm, length 15 cm; gap distance: 30 µm; WE: Pt; and AD applied potential: +800 mV.

3.1.2 Optimisation of flow rate

The different flow rate was investigated by observing peak response in the EC detector. The increase of flow rate increases the pressure of the column, and the pressure of the column was limited by column specification. The pressure ~110, and 150 bar pressures were observed for the flow rate 1 µL min^{-1}, and 1.5 µL min^{-1}, respectively. The maximum S/N ratio obtained for flow rate 1 µL min^{-1} in EC detector considering pressure limit of the column.

3.1.3 Optimisation of capillary i.d

The maximum S/N ratio obtained for capillary i.d (capillary LC column-gap-FC) 100 µm.

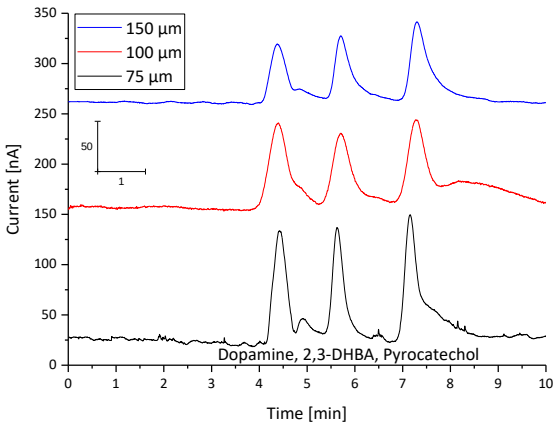

Fig. S7. Dependency of solute response capillary on internal diameter (i.d). Conditions: mobile phase (v/v=20:80): acetonitrile:25 mM citrate buffer, pH 3.5; elution: isocratic; flow rate: 1 µL min^{-1}; solute concentration: 80 µM; sample injection loop: i.d: 25 µm, volume: 174 nL; capillary LC column (injector-UV or EC detector): ProteCol C18 RP column (length: 15 cm, i.d: 150 µm, particles size: 3 µm), column oven

temperature: 35 °C; pressure: ~110 bar; capillary (column-gap-FC): i.d 75, 100, and 150 µm, length 15 cm; gap distance: 30 µm; WE: Pt; and AD applied potential: +800 mV.

Table S2. The dependency of solute response on capillary internal diameter (i.d).

Capillary i.d (capillary LC column-gap-FC) [µm]									
Solute	75	100	150	75	100	150	75	100	150
	Peak height [nA]			Peak width [min]			S/N [nA]		
							5 x baseline noise 1-2 min [nA]		
							9.8	3.4	3.2
Dopamine	111	84	58	0.31	0.36	0.42	11	25	18
2,3-DHBA	113	73	65	0.24	0.32	0.40	12	22	20
Pyrocatechol	127	86	80	0.27	0.36	0.38	13	27	25

3.1.4 Optimisation of gap distance

The maximum S/N ratio obtained for gap distance 30 µm.

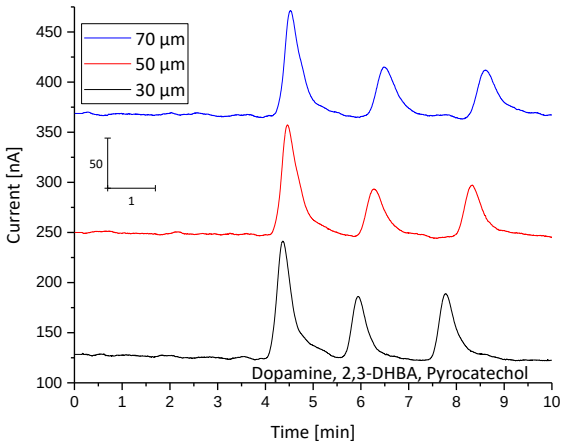

Fig. S8. Dependency of solute response on gap distance. Conditions: mobile phase (v/v=20:80): acetonitrile:25 mM citrate buffer, pH 3.5; elution: isocratic; flow rate: 1 µL min^{-1}; solute concentration: 80 µM; sample injection loop: i.d: 25 µm, volume: 174 nL; capillary LC column (injector-UV or EC detector): ProteCol C18 RP column (length: 15 cm, i.d: 150 µm, particles size: 3 µm), column oven temperature: 35 °C; pressure: ~110 bar; capillary (column-gap-FC): i.d 100 µm, length 15 cm; gap distance: 30, 50, and 70 µm; WE: Pt; and AD applied potential: +800 mV.

Table S3. Dependency of solute response on gap distance.

Gap distance (capillary outlet-electrode) [µm]									
Solute	30	50	70	30	50	70	30	50	70
	Peak height [nA]			Peak width [min]			S/N [nA]		
							5 x baseline noise 1-2 min [nA]		
							3	2.6	2.5
Dopamine	114	108	102	0.32	0.36	0.37	42	40	37
2,3-DHBA	61	42	41	0.33	0.40	0.43	20	16	15
Pyrocatechol	59	47	42	0.35	0.38	0.44	19	18	17

3.1.5 Optimisation of applied potential

The maximum S/N ratio obtained for AD applied potential +800 mV.

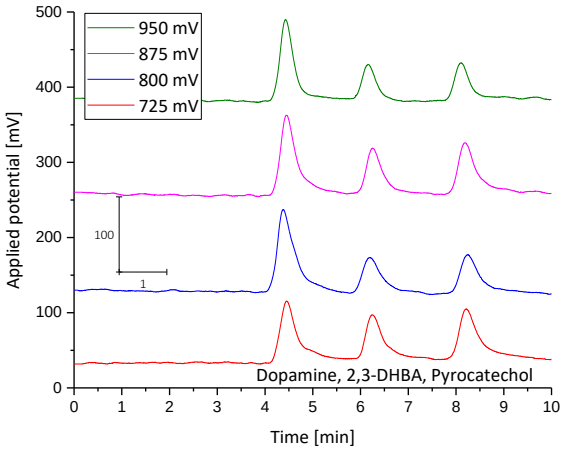

Fig. S9. Dependency of solute response on applied potential. Conditions: mobile phase (v/v=20:80): acetonitrile:25 mM citrate buffer, pH 3.5; elution: isocratic; flow rate: 1 µL min^{-1}; solute concentration: 80 µM; sample injection loop: i.d: 25 µm, volume: 174 nL; capillary LC column (injector-UV or EC detector): ProteCol C18 RP column (length: 15 cm, i.d: 150 µm, particles size: 3 µm), column oven temperature: 35 °C; pressure: ~110 bar; capillary (column-gap-FC): i.d 100 µm, length 15 cm; gap distance: 30 µm; WE: Pt; and AD applied potential: 650-950 mV.

Table S4. Dependency of solute response on applied potential.

Applied potential [mV]															
Solute	650	725	800	875	950	650	725	800	875	950	650	725	800	875	950
	Peak height [nA]					Peak area [nA min]					S/N [nA]				
Dopamine	72	80	113	105	106	28	32	42	40	35	152	167	238	220	222
2,3-DHBA	59	58	60	59	47	21	24	22	23	17	123	121	126	125	99
Pyrocatechol	64	66	65	66	48	28	30	27	15	16	135	138	136	140	101

3.1.6 Calibration plots

The calibration plots of capillary LC-UV and LC-EC.

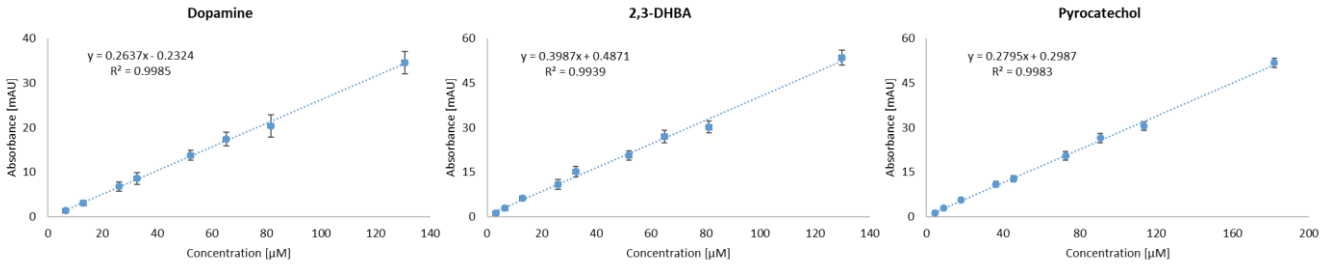

Fig. S10. Calibration plots of capillary LC-UV system. Conditions: Mobile phase (v/v=20:80): acetonitrile:25 mM citrate buffer pH 3.5; elution: isocratic; flow rate: 1 µL min^{-1}; solute concentration: 5-180 µM; sample injection loop: i.d: 25 µm, volume: 174 nL; capillary LC column (injector-UV detector): ProteCol C18 RP column (length: 15 cm, i.d: 150 µm, particles size: 3 µm), column oven temperature: 35 °C; pressure: ~110 bar; and UV absorbance wavelength: 280 nm.

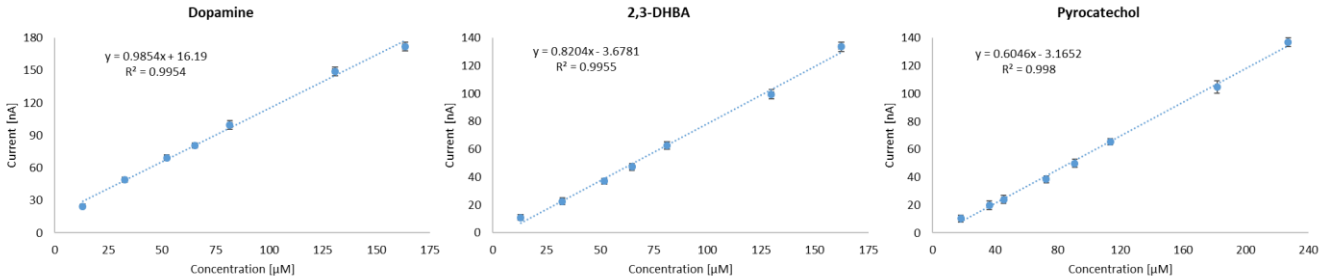

Fig. S11. Calibration plots of capillary LC-EC system. Conditions: Mobile phase (v/v=20:80): acetonitrile:25 mM citrate buffer, pH 3.5; elution: isocratic; flow rate: 1 µL min^{-1}; solute concentration: 10-225 µM; sample injection loop: i.d: 25 µm, volume: 174 nL; capillary LC column (injector- EC detector): ProteCol C18 RP column (length: 15 cm, i.d: 150 µm, particles size: 3 µm), column oven temperature: 35 °C; pressure: ~110 bar; capillary (column-gap-FC): i.d 100 µm, length 15 cm; gap distance: 30 µm; WE: Pt; and AD applied potential: +800 mV.

3.2 Standard LC-UV-EC

3.2.1 Optimisation of flow rate

The maximum S/N values obtained for flow rate 0.6 mL min^{-1} (see SI Fig. S12).

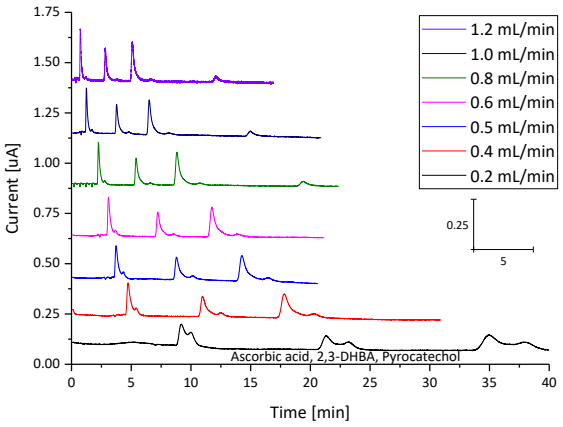

Fig. S12. Dependency of solute response on flow rate. Conditions: mobile phase (v/v=60:20:20): ACN: water:25 mM citrate buffer, pH 3.5; elution: isocratic; flow rate: 0.2-1.2 mL min^{-1}; solute concentration: 100 µM; sample injection volume: 10 µL; LC column (injector-UV detector): YMC Pac Pro C18 RP column (length: 25 cm, i.d: 4.6 mm, particles size: 5 µm), column oven temperature: 25 °C; pressure: ~1050 psi (~73 bar); capillary (UV-gap-FC) i.d: 100 µm, length: 7 cm; gap distance: 30 µm; WE: Pt; and AD applied potential: +800 mV.

Table S5. Dependency of solute response on flow rate.

Flow rate [mL min^{-1}]							
Solute	0.2	0.4	0.5	0.6	0.8	1	1.2
	5 x baseline noise 1-2 min [nA]						
	1.7	2.1	1.9	1.8	2.25	3.7	4.4
	S/N [nA]						
Dopamine	61	77	85	105	92	60	57
2,3-DHBA	40	48	59	67	60	39	37
Pyrocatechol	44	57	66	82	73	47	44

3.2.2 Calibration plots

In standard LC-UV-EC system, the maximum S/N values obtained for flow rate 0.6 mL min^{-1} (see SI Fig. S12). The parameters such as capillary i.d (UV-gap-FC) 100 µm, gap distance 30 µm, and AD applied potential +800 mV were same as used in capillary LC platform. Under these optimised conditions, the calibration curves of UV and EC detector (see SI Fig. S13) showed the linearity from 0.50-100 µM for all solutes, respectively.

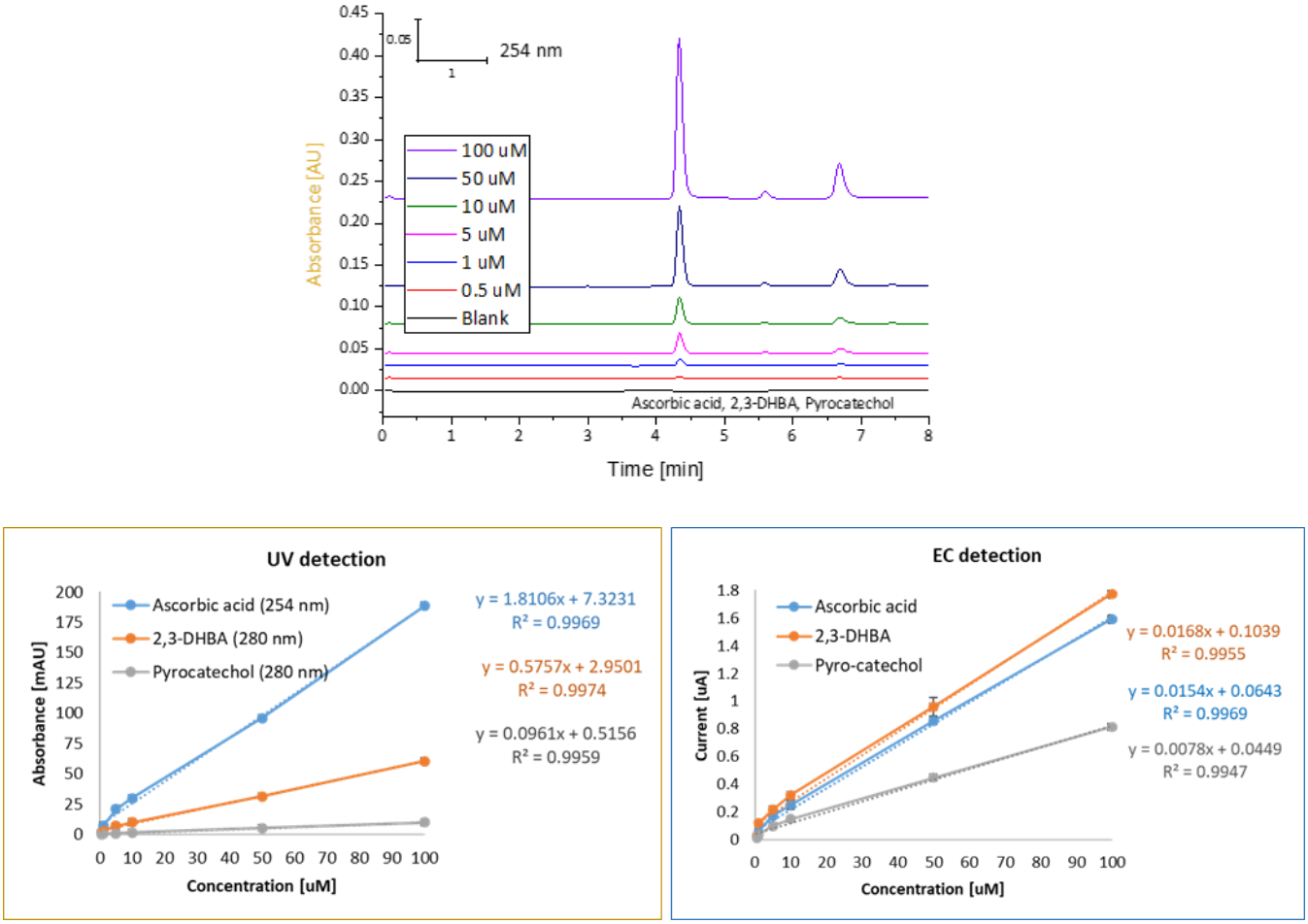

Fig. S13. Calibration plot in standard LC-UV-EC systems. Conditions: mobile phase (v/v=60:20:20): ACN: water:25 mM citrate buffer, pH 3.5; elution: isocratic; flow rate: 0.6 mL min^{-1}; sample injection volume: 10 µL; LC column (injector-UV detector): YMC Pac Pro C18 RP column (length: 25 cm, i.d: 4.6 mm, particles size: 5 µm), column oven temperature: 25 °C; pressure: ~1050 psi (~73 bar); UV absorbance wavelength: 254 nm and 280 nm; capillary (UV-gap-FC) i.d: 100 µm, length: 7 cm; gap distance: 30 µm; WE: Pt; and AD applied potential: +800 mV.

Chapter 3. Rapidly modified and highly stable electrodes for sensitive detection

Electrochemical characterisation of nanoparticulate zirconium dioxide-on-gold electrode for electrochemical detection in flow-based analytical systems

Muhammed Ariful Islam [a], Mostafa A. Atia [a], Mirek Macka [a, b, c], Brett Paull [a, d], Parvez Mahbub [a, e, *]

[a] Australian Centre for Research on Separation Science (ACROSS), School of Natural Sciences, University of Tasmania, Private Bag 75, Hobart 7001, Australia

[b] Department of Chemistry and Biochemistry, Mendel University in Brno, Zemedelska 1, CZ-613 00 Brno, Czech Republic

[c] Central European Institute of Technology, Brno University of Technology, Purkynova 123, CZ-612 00 Brno, Czech Republic

[d] ARC Training Centre for Portable Analytical Separation Technologies (ASTech), School of Natural Sciences, University of Tasmania, Private Bag 75, Hobart 7001, Australia

[e] Institute for Sustainable Industries and Liveable Cities, Victoria University, Footscray Park Campus, Melbourne 3011, Australia

* Email: parvez.mahbub@utas.edu.au

Graphical abstract

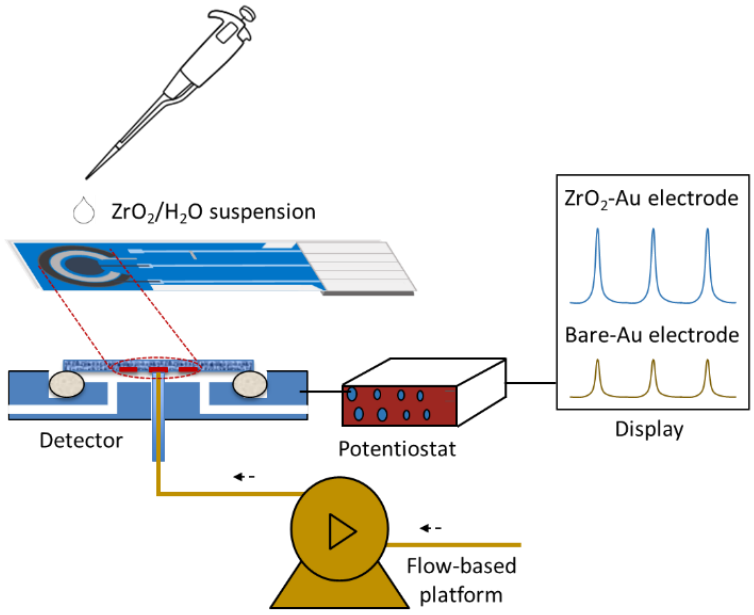

Highlights

- Electrochemical characterisation of nanoparticulate ZrO_2-on-Au is investigated for flow-based analysis.
- Electrochemical reversibility and 100% increase of effective surface area are achieved in ZrO_2-Au.
- LODs of ascorbic acid, 2,3-dihydroxybenzoic acid, and pyrocatechol are the lowest achieved to-date.
- Stability of ZrO_2-Au electrode in continuous-flow system is the highest reported to-date (8.5 hr).

Abstract

The modification of gold (Au) electrode using zirconium dioxide nanoparticles (ZrO_2 NPs) has been investigated for enhanced electrochemical (EC) detection in flow-based analytical systems. The average size of ZrO_2 NPs deposited in a facile procedure on the Au electrode surface was calculated as 22.5±7 nm. Redox behaviour of a test solute, ferrocyanide $[Fe(CN)_6]^{4-}$, on the bare- and ZrO_2-Au electrodes was initially investigated using cyclic voltammetry. From the voltammograms of bare- and ZrO_2-Au electrodes, the EC reversibility values and effective surface area were experimentally determined for the first-time in this study. Further, EC reversibility and 100% increase in effective electrode surface area were confirmed in ZrO_2-Au electrode through investigating the detection response (current). The EC performance of the ZrO_2-Au electrode was then investigated in amperometric detection of selected electroactive solutes separated by reversed-phase HPLC. The limits of detection (LODs), based upon an injection volume of 10 µL for ascorbic acid, 2,3-dihydroxybenzoic acid and pyrocatechol were 0.09 µM, 0.04 µM, and 0.10 µM, respectively (RSD 2.5 %, n= 9, r^2 = 0.99 for concentration range 1-100 µM). These LODs for the ZrO_2-Au electrode were 2-times lower for 2,3-DHBA, and pyrocatechol than the lowest LODs reported in the literature for EC detection in HPLC. The ZrO_2-Au electrode demonstrated satisfactory repeatability of preparation, detection reproducibility and high stability (8.5 hr) during continuous-flow in FIA and 45 days during intermittent use with HPLC, at flow rate of 0.6 mL min^{-1}. This work has demonstrated a comprehensive EC characterisation of Au electrode with nanoparticulate ZrO_2 for flow-based analytical systems.

Keywords

Electrochemical detection

Flow-based analytical systems

Nanomaterials

Zirconium dioxide

1. Introduction

The use of nanomaterials (NMs) [40, 228-233] as electrode surface modifiers for enhanced electrochemical (EC) detection, has become one of the hottest fields of research in electroanalytical chemistry. The increasing interest in NMs is driven by their unique chemical and physical properties [58, 229]. For example, NMs act as electrocatalysts by decreasing the overpotential of many EC reactions and increasing the electrical conductivity of modified surfaces by enhancement of faster transfer of electrons in EC analysis [58, 229, 234]. Kleijn *et al.* [235] also reported the use of NMs on electrode surface resulting in an increased rate of mass-transport to the electrode surface via the formation of diffusion layers above each NP or NPs agglomerates. These properties make them extremely suitable for augmenting the performance of EC detection in terms of larger effective surface areas and better EC response (in terms of peak current, EC reversibility, and EC conversion efficiency) [229], including when used within flow-based analytical platforms, such as flow injection analysis (FIA), capillary electrophoresis, and high-performance liquid chromatography (HPLC) [29, 236]. The most reported NMs used for electrode modification in flow-based analytical systems have been silver (Ag) [229], gold (Au) [11, 19, 229], nickel (Ni) [12, 191], platinum (Pt) [229], boron (B)-doped diamond [165, 192, 237], iron (Fe) oxide-reduced graphene oxide [11, 238], and manganese (Mn) dioxide [229]. These

materials are widely used due to their high electrical conductivity (Ag > Au > Ni > Fe > Pt > Mn > B [239]) as well as due to the inert properties.

The drawbacks associated with the use of NMs for conventional or disposable electrode modification process include time consuming multiple steps in modification techniques such as electrodeposition [11, 12] and sol-gel processes [13, 14], the requirement of polishing the electrode surface before modification [11, 19, 38], the use of reagents to enhance the porosity of the electrode surface [240], the requirement of technical skills for modification [11-14], and the limited stability of the modified electrode surface, usually 5-7 days [15, 16]. Most recent reports on the preparation and/or modification of electrodes with NMs have drawbacks such as use of large quantities of NMs (e.g. *ca.* 965 mg in [38]) together with expensive modification techniques [11-14, 19, 40, 165, 191, 240]. Further, to-date the EC reversibility, effective surface area, and stability of the NMs modified-electrode surface in continuous-flow has not been experimentally investigated [39, 40], and the often limited stability of modified-electrode surfaces [15, 16] significantly hinders the potential of using modified-electrodes in flow-based analytical systems [11, 39, 40, 241, 242]. Therefore, the integration of disposable electrodes with flow-based analytical systems requires accurate characterisation of bare and modified surface areas in terms of current, EC reversibility, effective surface area, and stability of the modified-electrode surface in continuous-flow as well as intermittent use within an analytical platform.

In this context, zirconium dioxide nanoparticles (ZrO_2 NPs) have been reported in the literature as electrocatalyst [39, 50, 234, 242-249] for use in EC techniques in stopped-flow mode such as cyclic voltammetry (CV), linear sweep voltammetry, and differential pulse voltammetry , particularly due to the ZrO_2 NPs' stability upon the modified electrode surface [39, 50, 242], good electrical conductivity (Pt > Zr > Mn [239]), high strength and resistance to fracturing, high melting point, low thermal conductivity and high corrosion resistance, as well as the fact that the ZrO_2 NPs are non-toxic [39, 248]. In 2017, Mohammadizadeh *et al.* [39] reported ZrO_2 NPs-modified porous graphite surfaces with a better EC response for the determination of propranolol using CV, LSV, and DPV. In 2015, Gholivand *et al.* [249] proposed a new electrode composed of a ZrO_2 NPs carbon-paste electrode modified with 3-(4'-amino-3'-hydroxybiphenyl-4-yl)-acrylic acid for the determination of hydrazine in aqueous solutions using CV. In 2013, Mazloum-Ardakani *et al.* [234] prepared a mobil crystalline material/ZrO_2 NPs-modified carbon-paste electrode that required no additional electron transfer mediator or reagent, for simultaneous and selective CV determination of epinephrine and acetaminophen. Some interesting applications of ZrO_2 NPs in different research fields have been reported such as their use as catalysts in gas-sensing, use in photocatalysis, wastewater treatment, and as stable column packing materials for elevated temperatures [39, 50, 244-246]. However, to-date there have been no reports of using ZrO_2 NPs-modified electrodes for EC detection in analytical flow techniques (such as HPLC and FIA). The use of low-cost ZrO_2 NPs to modify disposable electrodes [13, 213] can be beneficial in terms of a rapid modification process (approx. 10 min) for the formation of the porous electrode surface that can provide a larger electro-active surface area for an enhanced EC response (current) [39, 234, 242, 249] and facilitate reversible (Nernstian) EC reaction [39, 250, 251]. In addition, the use of ZrO_2 NPs can increase the stability and corrosion resistance [39, 248] properties of the electrode in flow-based analysis.

Therefore, the aim of this study was to investigate EC detection using disposable Au electrode modified with ZrO_2 NPs (termed here as ZrO_2-Au) within flow-based analytical systems. We also aimed to demonstrate the enhanced EC performance using CV in terms of peak current, resulting EC reversibility and effective surface area. Additionally, we demonstrated enhanced amperometric response (current) using the disposable ZrO_2-Au electrode with a miniaturised EC detector coupled to an HPLC

for detection of electroactive analytes including ascorbic acid (considered as an antioxidant [218]), 2,3-dihydroxybenzoic acid (2,3-DHBA, a biological marker for the detection and quantification of $OH^{\bullet}$ radicals [252]), and pyrocatechol (a possible human carcinogen classified by International Agency for Research on Cancer (IARC) [253]). The stability test of ZrO_2-Au electrode is also investigated for continuous-flow in FIA and intermittent use in HPLC.

2. Experimental

2.1 Chemicals

Analytical grade standards and reagents were used in this study. These were potassium ferrocyanide trihydrate ($K_4Fe(CN)_6.3H_2O$, Ajax, Australia), potassium chloride (KCl, Sigma-Aldrich, Sweden), ascorbic acid, 2,3-dihydroxybenzoic acid (2,3-DHBA), pyrocatechol, citric acid, sodium citrate dihydrate (Sigma-Aldrich, USA), acetonitrile (ACN, 99.8% HPLC grade, VWR, Australia), and milli-Q water (Millipore, USA). HPLC grade solvents were used for all separations. All test solutes and mixtures were freshly prepared in ACN and citrate buffer which was used as HPLC mobile phase. The suspension of ZrO_2 NPs (10 wt. % in H_2O, Sigma-Aldrich, USA) was used for preparation of ZrO_2-Au electrode.

2.2 Instrumentation

A simple CV platform was assembled using a uProcess (LabSmith™, USA) microfluidic system. The platform consisted of two programmable microsyringe pumps (model: SPS01) with 100 µL glass syringes, one four port valve ('L' pattern flow, and a two-position switching valve, model: AV201-C360). All pumps and switching valves were connected via PEEK tubing (Polyether ether ketone, 150 µm i.d., 360 µm o.d.) on a uProcess™ Breadboard. The software uProcess™ was used for controlling the various components and the volumetric flow rate of the microsyringe pumps [220]. A polyimide coated fused silica capillary (100 µm i.d., 360 µm o.d., length 7 cm, TSP100375, Polymicro Technologies™, USA) was used to connect the switching valve and the EC detector gap flow cell (gap-FC) [236]. The full instrumental scheme is shown in the SI (see Fig. S14).

The HPLC (Alliance Waters 2690, Waters, USA) consisted of an injector valve (SM4, Waters, USA), a thermostatted reversed-phase (RP) column (YMC Pac Pro C18, length 25 cm x i.d. 4.6 mm, pore size 5 µm, YMC Co. Ltd, Japan), and an UV detector (model: 996 PDA detector, path length: 10 mm, cell volume: 8 µL, Waters, USA). The HPLC was operated by Empower software (Waters, USA). The gap-FC was coupled to HPLC as illustrated in SI Fig. S15. In UV detector, we have observed a higher signal (peak height) at 254 nm for ascorbic acid, and at 280 nm for 2,3-DHBA, pyrocatechol, and dopamine. Therefore, we used both 254 nm and 280 nm for UV detection in this study.

The EC detection in both CV and HPLC configurations was performed using the commercially available screen-printed electrodes of dimensions: length 25.40 x width 7.26 x height 0.63 ± 0.05 mm (model: sensor $AC_1W_2R_S$, BVT Technologies, Czech Republic). The electrode consisted of a Au working electrode (diameter: 2 mm), a Ag reference electrode, and a Pt auxiliary electrode. Further details of electrode materials and fabrication can be found in recent reviews by Li *et al.* [213] and Couto *et al.* [13]. A potentiostat (model ER466CE, eDAQ Pty Ltd, Australia) was connected to the gap-FC and operated with eDAQ software (eDAQ Pty Ltd, Australia) to perform EC detection. Transmission electron microscopy (TEM, model: HT7700, Hitachi, Japan) and scanning electron microscopy (SEM, model: Hitachi SU70, Hitachi, Japan) were utilised for characterising the modified electrode surface in terms of size distribution and morphology of ZrO_2 NPs in this study.

2.3 Modification of electrode

The bare-Au surface was rinsed thoroughly with water and dried with inert nitrogen gas. The surface of the Au was coated with 10 µL aliquot of the filtrated ZrO_2 NPs/H_2O suspension (10 wt. % in H_2O) and the solvent was allowed to evaporate for approx. 10 min at room temperature 20 °C. The ZrO_2 NPs were attached to the electrode surface by physical adsorption (i.e. weak Van der Waals forces) [254].

2.4 ZrO_2 NPs size distribution

The TEMs of ZrO_2 NPs (see SI Fig. S16) and SEMs of bare- and ZrO_2-Au electrodes surface (see SI Fig. S17) are given in SI. The histogram illustrated in SI Fig. S18 shows a Gaussian distribution of size (diameter) of ZrO_2 NPs. The mean diameter of ZrO_2 NPs was calculated to be 22.5±7 nm using a Gaussian model (Origin 2016, OriginLab Corporation, USA) from the histogram. The resulting 22.5±7 nm diameter of ZrO_2 NPs confirmed that the agglomeration effect of ZrO_2 NPs from the ZrO_2/H_20 suspension on Au surface was insignificant. The porosity as discussed in [255, 256], was calculated by measuring particle density [257] and bulk density of ZrO_2 NPs [258] (approx. 94.5 %, for detail calculation see SI section 2). The formation of porous surface by the ZrO_2 NPs was also observed in SEM (see SI Fig. S17).

3. Results and discussions

Initially, CV was performed to study the EC behaviour of species involved in redox (reduction and oxidation) reactions at electrodes [259]. From voltammograms of bare- and ZrO_2-Au electrodes, the peak current, EC reversibility, and effective surface area are compared in the following section. This investigation was undertaken prior to demonstrating the analytical application of ZrO_2-Au electrode in FIA and HPLC for enhanced EC detection of target solutes. The AD in FIA and HPLC was performed under optimised conditions reported in Islam *et al.* [236], with a flow rate of 0.6 mL min^{-1}, capillary i.d. 100 µm (UV-gap FC), and a gap distance (capillary outlet-electrode) of 30 µm. Additionally, the optimised applied potential +800 mV was obtained for ZrO_2-Au electrode in terms of signal-to-noise (S/N, see SI Fig. S23).

3.1 Cyclic voltammetry

The peaks response (current) for the EC redox behaviour of potassium ferrocyanide at bare- and ZrO_2-Au electrodes are shown in Fig. 12. The redox peak currents of ±50 µA at ±160 mV obtained for the bare-Au, which were *ca.* 100% increased to ±100 µA at ±185 mV for ZrO_2-Au electrode with the same scan rate of 700 mV s^{-1}. In our study, the use of ZrO_2 NPs on Au electrode surface resulted in an increased rate of mass-transport to the electrode surface via the formation of diffusion layers above each NP or NP-agglomerate. These diffusion layers result in a larger effective surface area, higher electrical conductivity, and a better EC response at the modified electrode (ZrO_2-Au) compared to the bare electrode (Au) [229]. We also attribute this increase of peak current to the formation of a porous electrode surface that increased the electro-active surface area, and facilitated reversible (Nernstian) EC reaction [39, 250, 251].

EC reversibility can be achieved when the redox reaction is at equilibrium, no side reactions take place and electron transfer kinetics are fast to keep the surface concentrations of redox-active species at certain values expected by the Nernst equation [250]. Nie *et al.* [251] suggested EC reversibility as the difference in peak potentials as shown in equation 1.

$$\Delta E_P = E_{P_c} - E_{P_a} = \frac{59}{n} \qquad (1)$$

where, ΔE_P (in mV) = difference in peak potentials, E_{P_a}= anodic peak potential, and E_{P_c}= cathodic peak potential, and n= the number of electrons transferred.

The complete EC reversibility can be achieved when ΔE_P= 59 mV (when, n= 1 in this study) and the peak current (oxidation/reduction) ratio is equal to 1 [251]. We observed E_{P_a} and E_{P_c} from Fig. 12 and calculated ΔE_P of $[Fe(CN)_6]^{4-}$ for bare- and ZrO_2-Au electrodes as *ca.* 10 mV and 59 mV, respectively (where, n = 1) by employing equation 1. In accord with the calculations of Nie *et al.* [251] only the values from the oxidation (+) and reduction (–) potentials were added without including the positive or negative signs of the potentials. This evaluation of peak potentials shows that a complete EC reversibility was achieved by using ZrO_2-Au electrode (where, ΔE_P = 59 mV). We attribute the increase of ΔE_P values from 10 mV to 59 mV by using ZrO_2 NPs for the formation of porous electrode surface.

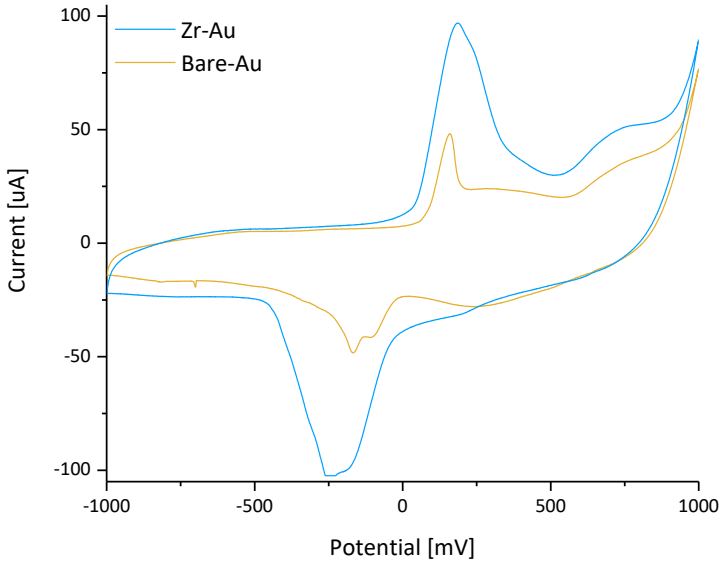

Fig. 12. The cyclic voltammogram of 100 µM $[Fe(CN)_6]^{4-}$ in 0.1 M KCl at a scan rate 700 mV s^{-1} for bare- and ZrO_2-Au electrodes. The voltammogram for the EC redox reaction of $[Fe(CN)_6]^{4-}$ was investigated from -1 V to 1 V at scan rates 10-800 mV s^{-1} (see SI Fig. S19). Two overlaid cathodic peaks were observed due to the presence of impurities in KCl (see further explanations of overlaid cathodic peaks in SI Fig. S20).

In the reversible redox analysis, we observed the different peak current at bare- and ZrO_2-Au electrode for same geometrical surface area of electrode (*ca.* 2 mm^2 in this study). Therefore, the effective surface area [260, 261] of bare- and ZrO_2-Au electrodes were calculated using the Randles-Sevcik equation (equation 2) [240, 262-264] for a reversible redox analysis.

$$i_p = 269\, ACn^{3/2}D^{1/2}v^{1/2} \qquad (2)$$

where, i_p = peak current [A], A = effective surface area [mm^2], C = concentration [mM], D = diffusion coefficient [$cm^2\ s^{-1}$], and v = potential scan rate [V s^{-1}].

The peak current for the EC redox reaction of $[Fe(CN)_6]^{4-}$ was investigated over a wide range of potential scan rates from 10 to 800 mV s^{-1} (see SI Fig. S19). The anodic peak currents reflected the oxidation of $[Fe(CN)_6]^{4-}$ to $[Fe(CN)_6]^{3-}$, and were measured at +160 mV. The plots of current vs. square root of scan rate for both bare- and ZrO_2-Au electrodes are illustrated in Fig. 13.

The resulting peak current for the reversible redox analysis can be defined by Equation 2. According to the equation, the magnitude of peak current has a linear dependence on the concentration of the test solute and the square root of the potential scan rate. Here, a linear fit with A equal to slope/$269Cn^{3/2}D^{1/2}$ was obtained [240] for the test solute, 100 µM $[Fe(CN)_6]^4$. A was calculated to be 135 mm^2 and 270 mm^2 for bare- and ZrO_2-Au electrodes, respectively (where, slope (i_p [A]/$v^{1/2}$[V s^{-1}])= 0.0001 for bare-Au and 0.0002 for ZrO_2-Au electrode in Fig. S15, C= 100 µM (i.e., 0.1 mM) $[Fe(CN)_6^{4-}]$, n= 1, and diffusion coefficient, $D^{1/2}$= 0.0027 cm^1 $s^{-1/2}$ [240, 262-264]). The results obtained for the ZrO_2-Au electrode indicates a 100% increase of A which is due to the presence of ZrO_2 NPs on the surface of the Au. Importantly, the changes in effective surface area of using modified electrode is experimentally determined for the first time amongst the reported EC detection studies to-date [39, 234, 249]. This investigation also showed the resulting current obtained in EC detection is influenced by the effective surface area rather than the geometrical surface area of electrode. The comparison between voltammograms of bare- and ZrO_2-Au electrode (see Fig. 12 and Fig. S19) demonstrates the beneficial effect of ZrO_2 for the enhanced EC response of target solutes (such as ascorbic acid, 2,3-DHBA, and pyrocatechol in this study) by minimising the capacitance of double layer [265, 266] (see SI section 3.2). These characterisations can be beneficial specially for miniaturised flow-based analytical systems (such as µFIA-EC and capillary-LC-EC, see our previous work [236]), where ZrO_2-Au can provide enhanced EC signal (current) to overcome the limitations of measuring effective cell volume and EC conversion efficiency, when flow rate < 0.1 µL min^{-1}.

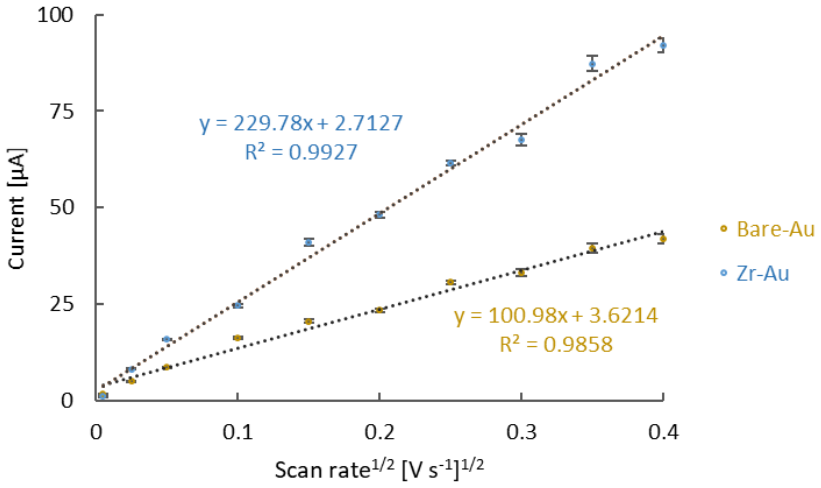

Fig. 13. Anodic peak current of 100 µM $[Fe(CN)_6]^{4-}$ in 0.1 M KCl for bare- and ZrO_2-Au electrodes. Conditions: peak current measured at +160 mV and potential scan rate ranging from 10 to 800 mV s^{-1} (n= 3). At zero scan rate, charging current resulting from the double layer effects [20, 267] was observed during the measurement.

3.2 HPLC-UV-EC

In this study, the analytical application of ZrO_2-Au electrode was investigated for enhanced EC detection of test solutes, namely ascorbic acid, 2,3-dihydroxybenzoic acid and pyrocatechol. Under optimised conditions, the chromatograms of test solutes using ZrO_2-Au electrode in HPLC are illustrated in Fig. 14.

The calibration curves for both UV and EC detection were plotted using peak heights for each solute (see SI Fig. S24). There was a significant difference observed in the limits of detection (LODs) obtained using UV and EC detection. The LOD values from EC detection were approx. 4-49 times lower than those obtained with UV detection at 254 nm and 280 nm. The LODs obtained for the AD using the ZrO_2-Au electrode were 0.09 µM, 0.04 µM, and 0.10 µM for ascorbic acid, 2,3-DHBA, and pyrocatechol, respectively (see Table 5, n= 9, determination coefficient r^2= 0.99 for 1-100 µM). Furthermore, the LODs obtained using the ZrO_2-Au electrode in a HPLC-EC system are comparable with the lowest reported for EC detection using unmodified Pt electrode in flow-based analytical systems. The calculated LODs are about 2-times lower than the lowest reported LODs in our previous work [236] for 2,3-DHBA, and pyrocatechol as illustrated in Table 5. In this study, we observed 95 to 180-times improvement of current at 800 mV while comparing the voltammograms of solutes (ascorbic acid, 2,3-DHBA, and pyrocatechol, see SI Fig. S21) using bare- and ZrO_2-Au electrode. The results from Table 5 also provide a significant reduction (*ca.* 3-times) of the baseline noise and enhanced peak efficiency *ca.* 4-8% compared to reported EC detection in flow-based analytical systems [236] for all solutes, namely ascorbic acid, 2,3-dihydroxybenzoic acid and pyrocatechol.

The Student's t-test and F-test were conducted to express confidence intervals of LODs in our study compared with HPLC-AD work reported by Pluangklang *et al.* [219]. The value of t-test and F-test were calculated using the equations (see SI section 4.3) given by Harris [50]. The calculated confidence level ranged from 90 to 95% for 2,3-DHBA, and pyrocatechol. The F-test resulted two standard deviations are significantly different for 2,3-DHBA (where, $F_{\text{calculated}}$ 4.3 > F_{table} 3.39), however the difference is insignificant for pyrocatechol ($F_{\text{calculated}}$ 3.09 < F_{table} 3.39).

The performance of gap-FC in terms of peak asymmetry, peak efficiency and peak FWHM were also compared with a UV detector in this platform (see Table 5). The delay time between chromatograms for UV and EC detection in this study were 4.9-5 s, the peak efficiency decreased 1.5-6% in EC detection and approx. 2.5% peak broadening was also observed for the EC detector. We attribute these insignificant differences in peak efficiency and broadening in EC detector due to the connecting pathways [226], geometry [48] and effective volume of the FC [50]. EC detection in our previous studies also reported minor differences in peak efficiency and broadening compared to the UV detection [236].

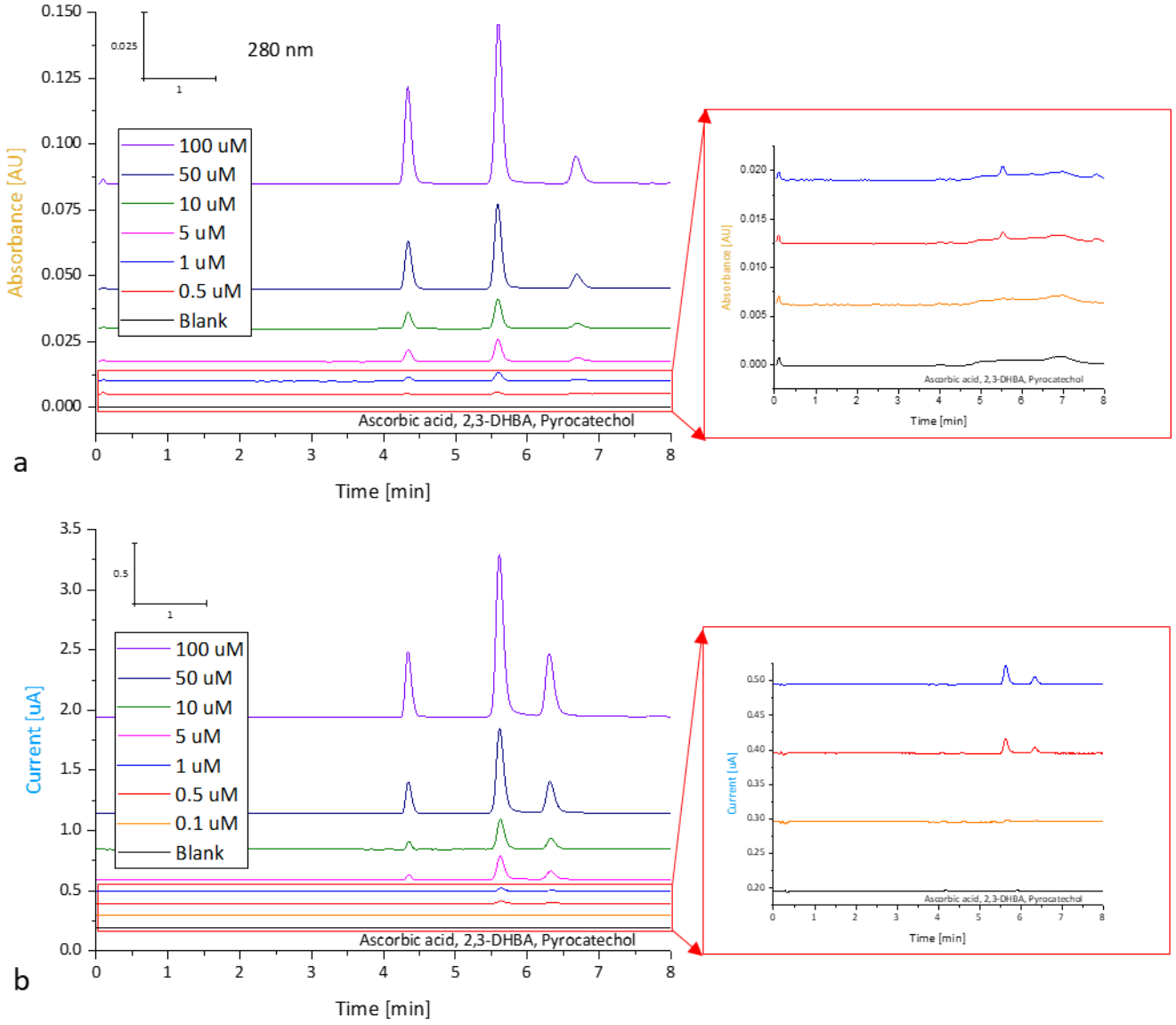

Fig. 14. Chromatograms showing separations of ascorbic acid, 2,3-DHBA, and pyrocatechol using a HPLC (a. UV detection, and b. EC detection). Conditions: mobile phase (v/v= 60:20:20): ACN: water:25 mM citrate buffer (pH 3.5), elution: isocratic, flow rate: 0.6 mL min^{-1}, sample injection volume: 10 µL, HPLC column (injector-UV detector): YMC Pac Pro C18 reversed-phase column (length: 25 cm, i.d: 4.6 mm, particles size: 5 µm), column oven temperature: 25 °C, pressure: *ca.* 1050 psi (73 bar), capillary (UV-gap-FC) i.d: 100 µm (length: 7 cm), gap distance: 30 µm, WE: ZrO_2-Au, potential: +800 mV. UV absorbance wavelength: 254 nm (see SI Fig. S24) and 280 nm.

Table 5. Comparison of the analytical performance of EC and UV detection in a HPLC. *

Detector (WE)	Analyte	Void Volume [a] [mL]	Peak asymmetry factor [b]	Peak efficiency (plate number [c]/column length) [N m^{-1}]	Peak FWHM [min]	Baseline noise (SD)	LOD [d] [µM]	RSD [%]	Sensitivity [e]	Ref.
UV	Ascorbic acid	0.1	1.1-1.3	39900-62000	0.12-0.16	0.07 [mAU] (254 nm) 0.05 [mAU] (280 nm)	0.37	1.1-4.8	1.9	This work
	2,3-DHBA						0.83		0.6	
	Pyrocatechol						4.90		0.1	
EC (Pt)	Ascorbic acid	-	1.0-1.2	36000-55500	0.10-0.13	0.5 [nA]	0.10	1.3-4.9	15.9	[236]
	2,3-DHBA						0.09		17.8	
	Pyrocatechol						0.20		8.1	
EC (ZrO_2-Au)	Ascorbic acid	-	1.2-1.3	39300-58000	0.09-0.13	0.16 [nA]	0.09	1.6-2.8	5.5	This work
	2,3-DHBA						0.04		13.4	
	Pyrocatechol						0.10		5.1	

* Solvent (v/v): 25 mM citrate buffer, pH 3.5:ACN (20:80), flow rate: 0.6 mL min^{-1}, and applied potential: 800 mV.

[a] Void volume calculated by multiplying flow rate and the elution time for mobile phase or unretained solute when the first baseline disturbance is observed [50].

[b] Peak asymmetry factor, $A_s = \frac{w_R}{w_L}$, where w_R is the distance from the peak midpoint (perpendicular from the peak highest point to baseline) to the trailing edge of the peak and w_L is the distance from the leading edge of the peak to the peak midpoint measured at 10 % of peak height [50].

[c] Plate number, $N_P = 5.54\ (\frac{t_R}{w_{h/2}})^2$, where t_R is retention time and $w_{h/2}$ is width of the peak at half height [50].

[d] LODs were calculated by dividing the three-times of standard deviation (SD) of a blank response (noise level) by the slopes of the corresponding calibration curves [50]. In UV detection, LODs calculated at 254 nm for ascorbic acid and 280 nm for 2,3-DHBA, and pyrocatechol.

[d] Sensitivity was calculated from 0.1 to 100 µM in this study (0.5-100 µM in our previous work [236]). The sensitivity units are mAu $µM^{-1}$ (UV detection) and nA $µM^{-1}$ (EC detection).

3.3 Stability tests

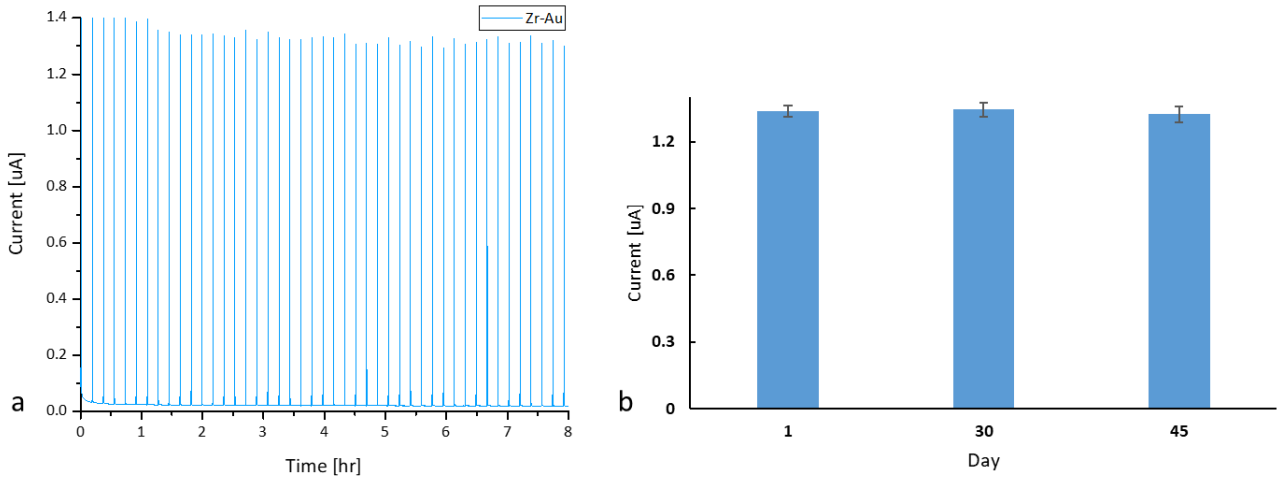

Fig. 15. Stability test of ZrO_2-Au electrode (a) continuous-flow in FIA and (b) intermittent use with HPLC. Conditions (a): solute: 100 µM 2,3-DHBA, mobile phase (v/v= 60:20:20): ACN:water:25 mM citrate buffer (pH 3.5), elution: isocratic, flow rate: 0.6 mL min^{-1}, sample injection volume: 1 µL, capillary (UV-gap-FC) i.d: 100 µm (length: 7 cm), gap distance: 30 µm, WE: ZrO_2-Au, potential: +800 mV. Conditions (b): same conditions for 2,3-DHBA in Fig. 14. The modified electrodes were stored at room temperature (ca. 20 °C) in an air-tight container with silica beads supplied by vendor during intermittent use of the electrodes with HPLC (up to 45 days).

The stability of the ZrO_2-Au electrode surface was tested in FIA and HPLC at room temperature (*ca.* 20 °C). In the FIA platform (see Fig. 15), 100 µM of 2,3-DHBA was continuously injected at flow rate 0.6 mL min^{-1} (50 injections, with 10 min analysis time per injection). It was observed that the ZrO_2-Au electrode was stable for 8.5 hr at 0.6 mL min^{-1} (RSD *ca.* 2.6%) in continuous-flow. Most EC measurements reported stability of modified electrodes ranging ca. 5-7 days [15, 16]. However, there are no reports on stability of modified electrodes when used in continuous-flow modes such as in FIA to date. The analysis time reported in EC detection in continuous flow modes using FIA ranged up to ten minutes [29, 30]. As our measured stability of the modified electrode was significantly higher than those reported in previous studies [29, 30], we did not continue the stability test in continuous mode beyond 8.5 hours in FIA.

The reproducibility of stability achieved via FIA as shown in Fig. 15a was translated to HPLC experiments by repeating the injection of the 2,3-DHBA 5 times each on 3 different days (day 1, day 30, and day 45) and is illustrated in Fig. 15b. The resulting sensitivity 13.35 nA μM^{-1} (RSD 2.7%) shows the stability of ZrO_2-Au electrode was 45 days in the HPLC. The demonstrated stability of ZrO_2-Au electrode in a flow-based analytical platforms is the highest amongst the modified EC sensors reported [15, 16] to-date.

3.4 Real sample analysis

To demonstrate the applicability of the ZrO_2-Au electrode to real sample analysis, tap water from chemistry laboratory and river water samples obtained from the Derwent River (Hobart, Australia) were spiked with ascorbic acid, 2,3-DHBA, and pyrocatechol. Then, amperometric current of real samples at the ZrO_2-Au electrode in HPLC were recorded under optimized conditions. The results are summarized in Table 6 and the calculated recovery values were in the range of 98-102.5%. Therefore, the ZrO_2-Au electrode can be applied for practical and low-cost analysis of target solutes in water using flow-based analytical system.

Table 6. Determination of ascorbic acid, 2,3-DHBA, and pyrocatechol in real water samples (n= 3).

Solutes	Added [μM]	Tap water		River water	
		Found [μM]	Recovery [%]	Found [μM]	Recovery [%]
Ascorbic acid	0	0	-	0.09 ± 0.02	-
	0.5	0.49 ± 0.03	98	0.49 ± 0.03	98.7
	1	1 ± 0.03	99.6	1 ± 0.04	100.3
	5	5.07 ± 0.04	101.3	5.07 ± 0.03	101.5
2,3-DHBA	0	0	-	0	-
	0.5	0.5 ± 0.03	99.3	0.5 ± 0.01	99.7
	1	1 ± 0.02	99.6	1.01 ± 0.02	100
	5	5.02 ± 0.04	100.4	5.04 ± 0.03	100.7
Pyrocatechol	0	0	-	0.1 ± 0.05	-
	0.5	0.49 ± 0.02	98.7	0.5 ± 0.01	100
	1	1.01 ± 0.02	100.7	1.02 ± 0.02	101.7
	5	5.09 ± 0.08	101.8	5.12 ± 0.03	102.5

4. Conclusions

In this study, a comprehensive EC characterisation of Au electrode with nanoparticulate ZrO_2 is investigated for flow-based analytical systems. Voltammograms show that ZrO_2-Au electrode provides faster electron transfer rates, with current and effective surface area increased by approx. 100% compared to the bare-Au, for enhanced redox abilities towards the test solute. We demonstrate the use of ZrO_2 NPs-modified electrodes for EC detection in flow-based analytical systems including HPLC and FIA for the first time. Using AD in HPLC, we obtained LOD values for the test solutes (2,3-DHBA, and pyrocatechol) which were approx. 2 times lower than reported LODs to-date. The results provided *ca.* 3 times reduction in baseline noise compared to previously reported EC detection. Moreover, the ZrO_2-Au electrode demonstrated good repeatability, reproducibility, and stability for 8.5 hr in continuous-flow in FIA and 45 days during intermittent use with HPLC at flow rate of 0.6 mL min^{-1}.

Acknowledgements

The authors acknowledge the University of Tasmania for the financial support in the form of a Tasmania Graduate Research Scholarships (TGRS) awarded to MAI. MM acknowledges the Australian Research Council (ARC) Future Fellowship (FT120100559) for the financial support of this research. The authors like to show gratitude to the Dr

Sandrin T. Feig, (Laboratory Analyst – SEM and X-Ray Microanalysis, Central Science laboratory, University of Tasmania), and Dr Olivier Bibari (Senior Technical Officer – TEM, Medicine, University of Tasmania) for their technical support in this research. MAI is immensely grateful to all co-authors and Dr Ruth Amos (Senior Editor, Fix My English) for their comments on an earlier version of the manuscript that greatly helped to improve the manuscript.

Supplementary information (SI)

The supporting information content includes:

1. Instrumentation: schematic flow diagrams (CV and HPLC-UV-EC).
2. ZrO2 NPs characterisation: TEM, SEM, ZrO2 NPs size distribution, and porosity.
3. Cyclic voltammetry: peak current, and selection of electrode.
4. HPLC-UV-EC: optimisation of applied potential, and calibration plots.

1. Instrumentation

1.1 Cyclic voltammetry

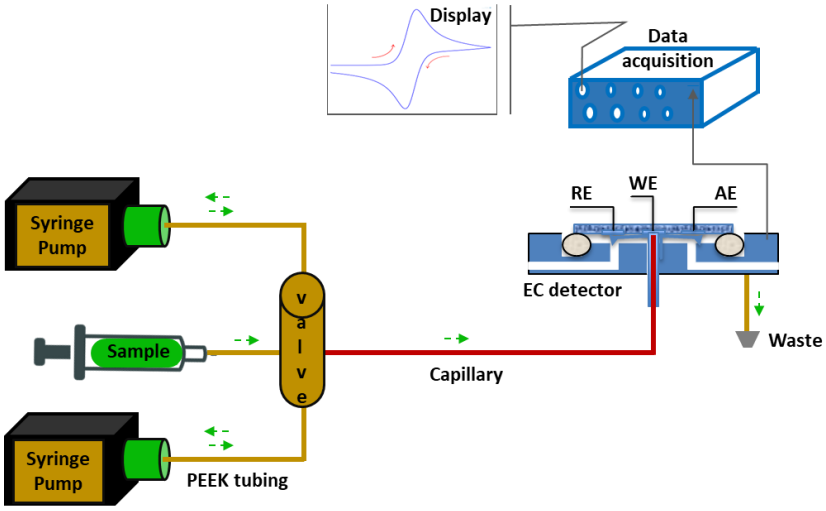

Fig. S14. Schematic flow diagram of CV platform.

1.2 HPLC-UV-EC

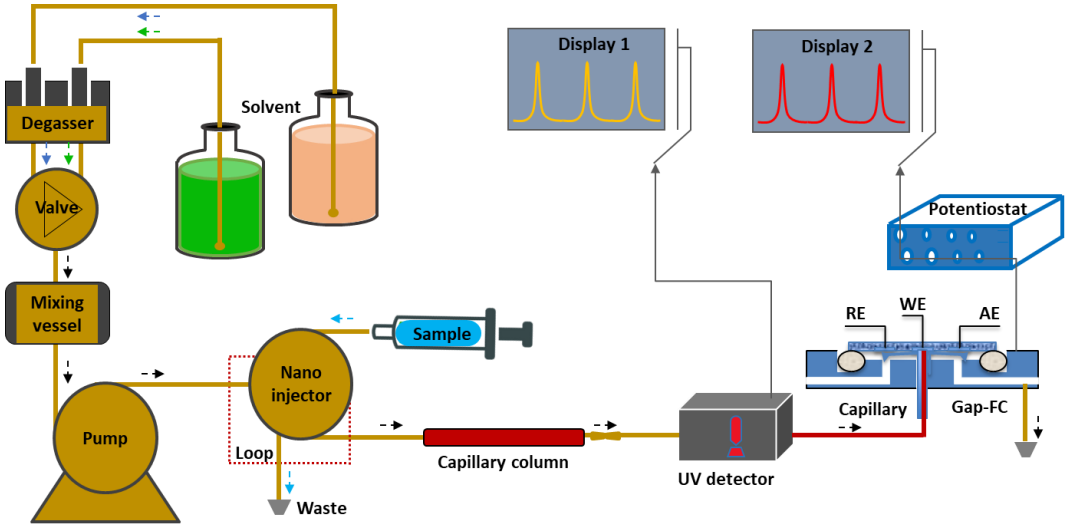

Fig. S15. Schematic flow diagram of HPLC-UV-EC platform.

2. ZrO_2 NPs characterisation

2.1 TEM

The morphology of the ZrO_2 NPs was investigated by TEM (see Fig. S16). Typical TEM images of dark spots correspond to ZrO_2 NPs, which are isolated from each other by the light features of the carbon matrix. The ZrO_2 NPs was highly dispersed in the carbon matrix and formed a homogeneous film. The ZrO_2 NPs were spherical in shape with a size distribution range of 25-35 nm.

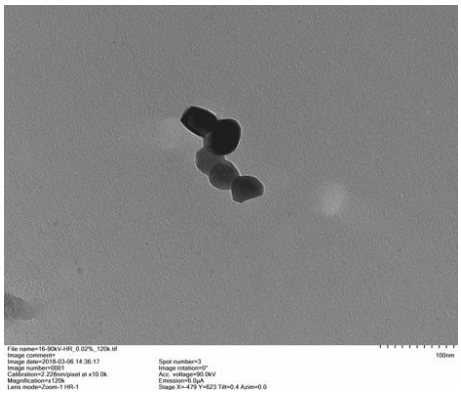

Fig. S16. Morphology of ZrO_2 NPs analysed by TEM. Conditions: acceleration voltage 90 KV, magnification 120 K.

2.2 SEM

The SEM demonstrates the surface morphology change between bare- and ZrO_2-Au electrode (see Fig. S17). The ZrO_2 NPs size distribution at ZrO_2-Au electrode surface was approx. 15-30 nm and formed fine nanoparticle clusters (*ca.* 50 nm) with a relatively high surface particle density.

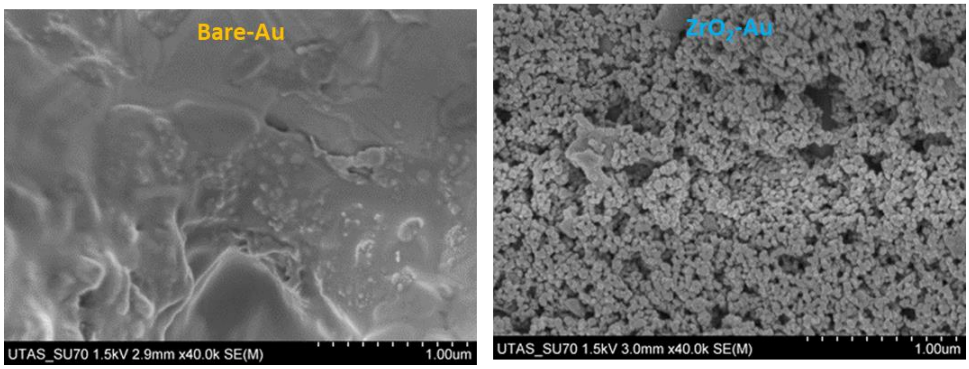

Fig. S17. SEM of bare- and ZrO_2-Au electrodes. Conditions: acceleration voltage 1.5 KV, magnification 40 K and magnification distance 3 mm.

2.3 ZrO_2 NPs size distribution

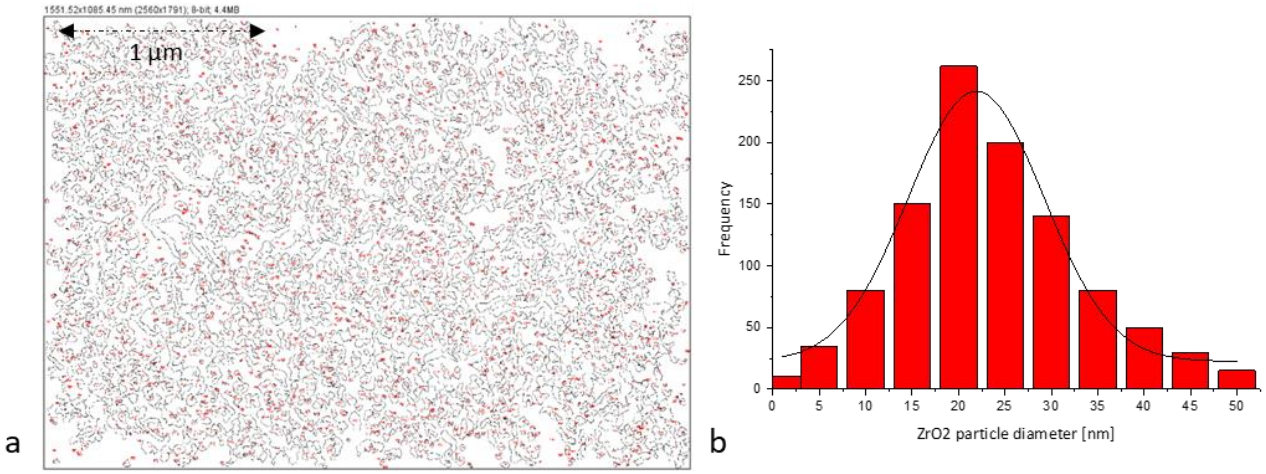

Fig. S18. ZrO_2 NPs size distribution. (a) Extracted image from SEM of ZrO_2-Au electrode using ImageJ software to calculate ZrO_2 NPs size distribution using a Gaussian model. (b) The size (diameter) distribution of ZrO_2 NPs using a Gaussian model.

2.4 Porosity

The particle density was calculated using below equation and method discussed by Blake [257].

Particle density, $\rho_P = \frac{\rho_w (W_s - W_a)}{(W_s - W_a) - (W_{sw} - W_w)}$

where, ρ_w = density of the water at room temperature, W_s = oven-dry weight of flask plus sample, W_a = weight of oven-dry flask, W_{sw} = weight of flask plus sample plus distilled water needed to fill the flask when it contains the sample, and W_w = weight of flask filled with distilled water at room temperature.

The porosity [255] was calculated using the below equation reported by He *et al.* [256].

Porosity = $(1 - \frac{Particle\ density}{Bulk\ density})$ x 100

The calculated particle density (0.32 g cm^{-3}) and bulk density (5.89 g cm^{-3} [258]) of ZrO_2 NPs resulted the porosity ca. 94.50 %.

3. Cyclic voltammetry

3.1 Voltammograms

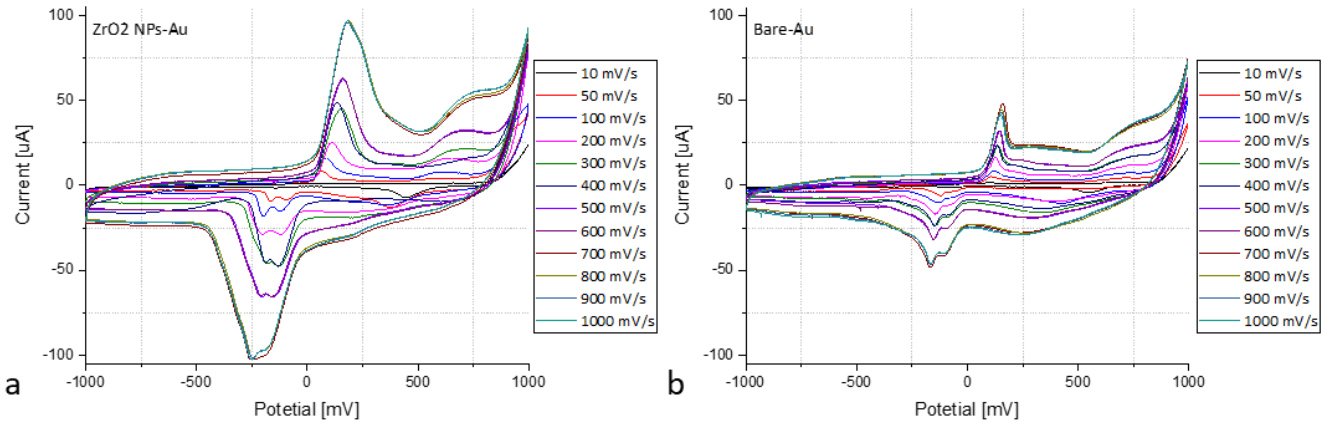

Fig. S19. The voltammogram of 100 µM $[Fe(CN)_6]^{4-}$ in 0.1 M KCl at scan rate 10-1000 mV s^{-1}. (a) bare- and (b) ZrO_2-Au electrode.

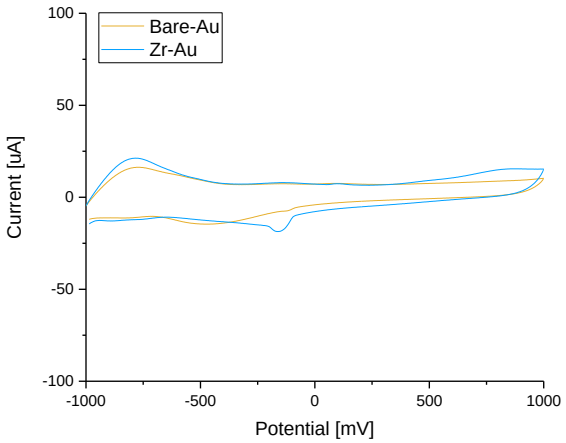

Fig. S20. The voltammogram of blank (i.e., 0.1 M KCl in the absence of $[Fe(CN)_6]^{3-}$) at scan rate 700 mV s^{-1} in bare- and ZrO_2-Au electrode. The unexpected cathodic (reduction) peak was observed due to the presence of impurities in KCl.

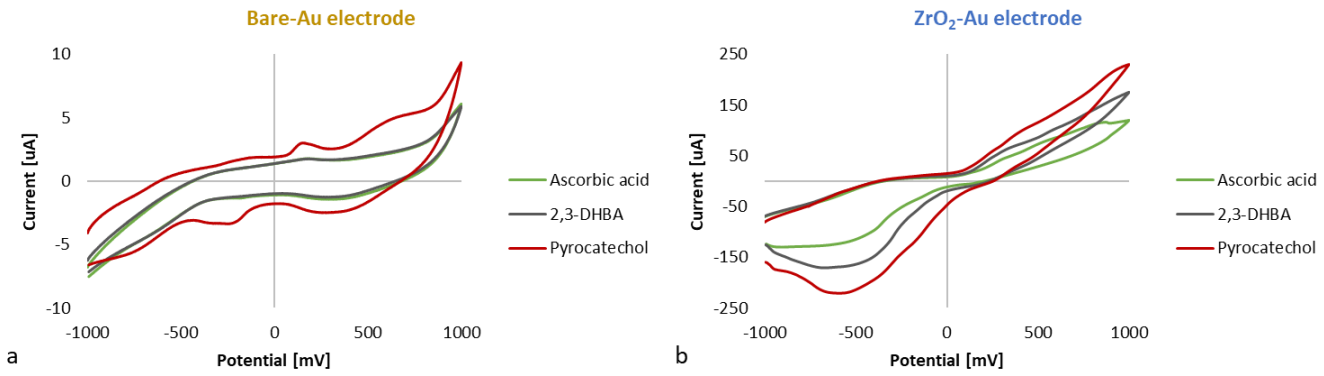

Fig. S21. The voltammogram of 100 µM solutes (ascorbic acid, 2,3-DHBA, and pyrocatechol) in 25 mM in citrate buffer (pH 3.5) at scan rate 400 mV s^{-1}.

3.2 Capacitance of double layer

The capacitance of double layer before and after the electrode modification was discussed by Silva *et al.* [265]. The capacitance of double layer at bare- and ZrO_2-Au electrodes was calculated using the below equation reported by Lämmel *et al.* [266].

$$C = {}^{I}/_{v}$$

where C = capacitance [F], I = current measured at a plateau [A], and v = potential scan rate [V s^{-1}].

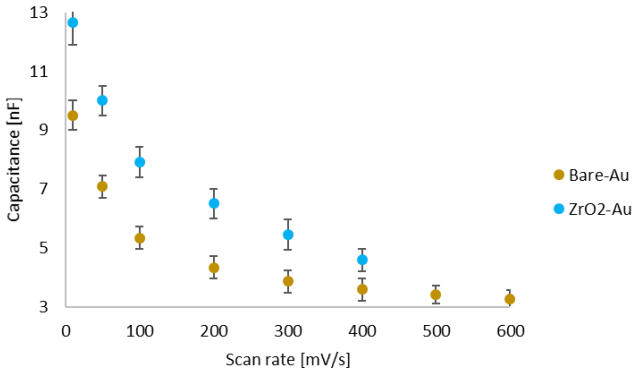

Fig. S22. The capacitance of double layer at bare- and ZrO_2-Au electrode.

The capacitance was calculated from the voltammograms by running the scan rate dependency from 10 to 1000 mV s^{-1} (see Fig. S19). The resulting capacitance was decreased with the increase of scan rate (see Fig. S22). The capacitance was insignificant after 600 mV s^{-1} (at bare-Au electrode) and 400 mV s^{-1} (at ZrO_2-Au electrode). At higher scan rate the double layer cannot be completely charged according to the applied voltage [266]. This investigation shows that the double layer capacitance was higher after modification with ZrO_2 which suggests increased electroactive surface area of the working electrode (Au) after modification with ZrO_2.

4. HPLC-UV-EC

4.1 Optimisation of potential

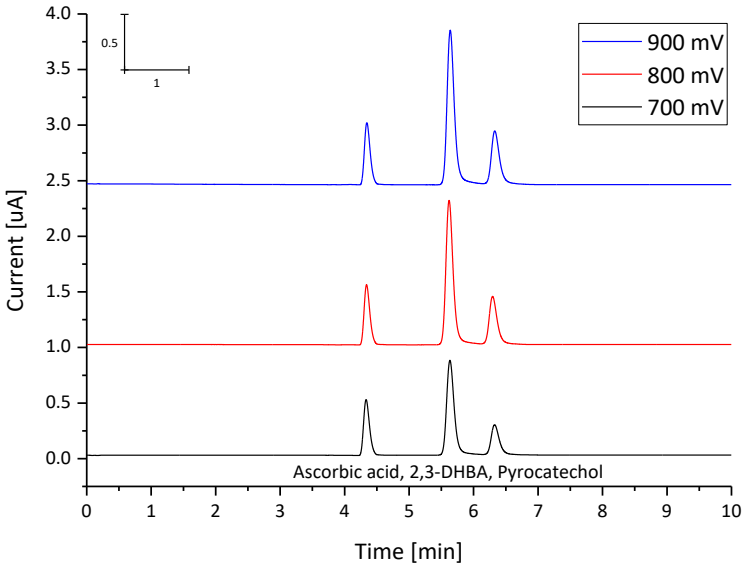

Fig. S23. Optimisation of applied potential of ZrO_2-Au electrode in a HPLC. Conditions: mobile phase (v/v= 60:20:20):ACN:water:25 mM citrate buffer (pH 3.5), elution: isocratic, flow rate: 0.6 mL min^{-1}, sample injection volume: 1 µL, HPLC column (injector-detector): YMC Pac Pro C18 reversed-phase column (length: 25 cm, i.d: 4.6 mm, pore size: 5 µm), column oven temperature: 25 °C, capillary (UV-EC detector) i.d: 100 µm (length: 7 cm), gap distance: 30 µm, WE: ZrO_2-Au, and potential: 700-900 mV.

Table S6. Dependency of solute response on applied potential.

Applied potential [mV]						
Solute	700	800	900	700	800	900
	Peak height [nA]			S/N [nA]		
Ascorbic acid	0.50	0.55	0.55	375	391	202
2,3-DHBA	0.85	1.28	1.34	638	916	489
Pyrocatechol	0.27	0.42	0.61	202	301	168

4.2 Calibration plots

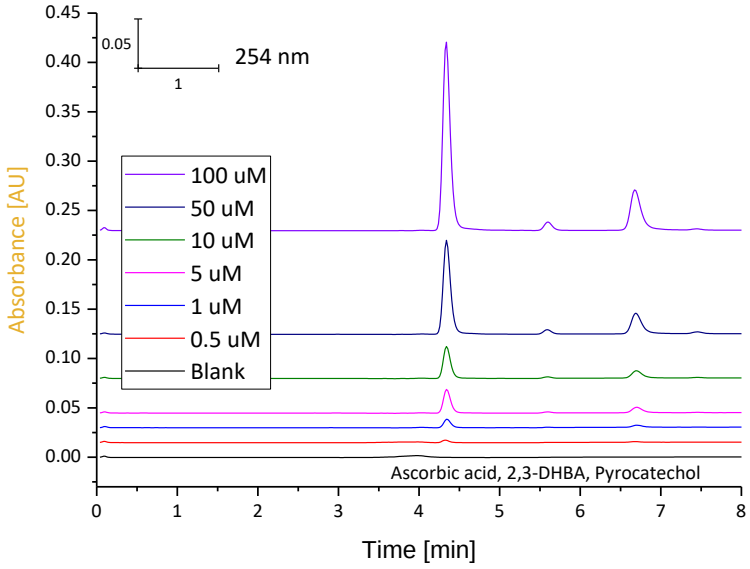

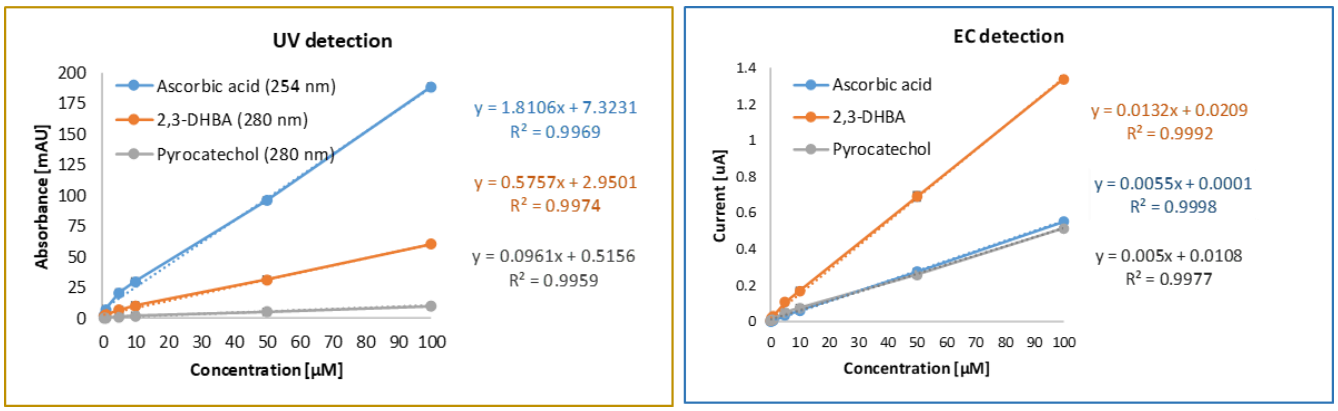

Fig. S24. Chromatograms showing separations of ascorbic acid, 2,3-DHBA, and pyrocatechol using HPLC (UV detection at 254 nm). Calibration plots of UV and EC detection. Conditions: see Fig. 14.

4.3 Student's *t*-test and F-test

The Student's t-test and F-test calculation details were reported by Harris [50]. If the standard deviations are not same for sets of measurements, below equations are needed to follow:

$$t_{Calculated} = \frac{x_1 - x_2}{\sqrt{(S_1^2/n_1 + S_2^2/n_2)}}$$

$$\text{Degree of freedom} = \frac{(S_1^2/n_1 + S_2^2/n_2)^2}{\frac{(S_1^2/n_1)^2}{n_1+1} + \frac{(S_2^2/n_2)^2}{n_2+1}}$$

$$F_{Calculated} = S_1^2/S_2^2$$

where, x_1 and x_2 = averages, s_1 and s_2 = standard deviations, n_1 and n_2 = number of measurements.

Chapter 4. Fast-pulsed waveform for miniaturised flow-through EC detection

Fast pulsed amperometric waveform for miniaturised flow-through electrochemical detection: Application in monitoring graphene oxide reduction

Muhammed Ariful Islam [a], Aleksandra N. Koreshkova [a], Vipul Gupta [a, b], Trevor Lewis [a, b], Mirek Macka [a, c, d], Brett Paull [a, b], Parvez Mahbub [a, e, *]

[a] Australian Centre for Research on Separation Science (ACROSS), School of Natural Sciences, University of Tasmania, Private Bag 75, Hobart 7001, Australia

[b] ARC Centre of Excellence for Electromaterials Science (ACES), School of Natural Sciences, University of Tasmania, Private Bag 75, Hobart 7001, Australia

[c] Central European Institute of Technology, Brno University of Technology, Purkynova 123, CZ-612 00 Brno, Czech Republic

[d] Department of Chemistry and Biochemistry, Mendel University in Brno, Zemedelska 1, CZ-613 00 Brno, Czech Republic

[e] Institute for Sustainable Industries and Liveable Cities, Victoria University, Footscray Park Campus, Melbourne 3011, Australia

* Email: parvez.mahbub@utas.edu.au

Graphical abstract

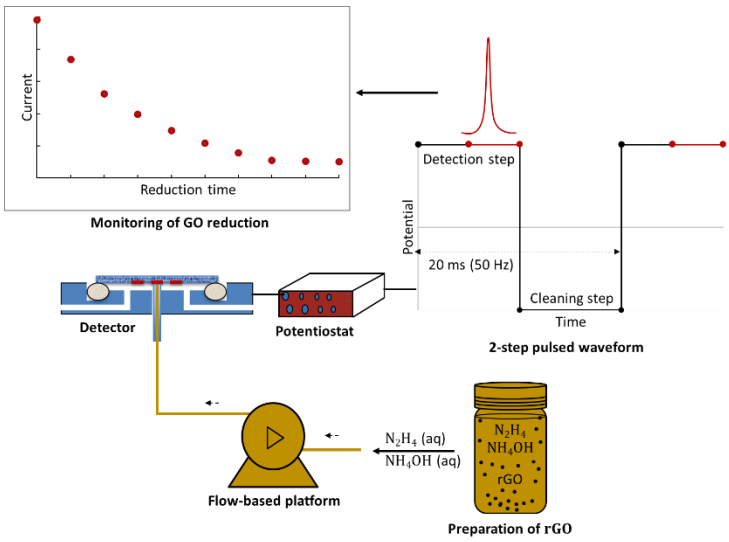

Highlights

- A novel waveform (2-step, 20 ms, 50 Hz) 15-45 times faster frequency than previously developed.
- The detection limit of hydrazine (0.8 nM) is approx. 6 times lower than the lowest LOD reported to date.
- The reduction of GO is monitored in a miniaturised electrochemical system for the first time.
- The reaction half-lives, endpoints, and % yields in the GO reduction process are investigated.

Abstract

A fast pulsed waveform (2-steps at +400 mV and -400 mV, 10 ms each, 50 Hz cycle repetition, and current sampling time 1 ms) was developed incorporated within a miniaturised EC detector, and used to demonstrate the pulsed amperometric detection (PAD) of hydrazine in a flow-based analytical system. In contrast to standard amperometric detection (AD), a subsequent surface oxide reduction step was applied within the PAD waveform. The PAD applied within a simple flow-injection analysis (FIA) method provided a limit of detection (LOD) just as low as 0.8 nM of hydrazine (RSD 5%, n= 9, linearity r^2 = 0.99 for 1 nM-100 µM), which is one order of magnitude lower than the lowest LOD reported to date. Significantly, the LOD was obtained using 5-20 times lower electrode surface area, flow rate, and sample volume, than in previous methods, with 15 times faster cycle repetition frequency than alternative PAD based studies reported in literature. Practical application of the PAD waveform was demonstrated by monitoring the temporal consumption of reducing agents during graphene oxide reduction experiments, separated using chromatographic methods (hydrazine in IC and ascorbic acid in HPLC).

Keywords

Pulsed amperometric detection

Miniaturised flow-based electrochemical detection

Hydrazine and ascorbic acid

Graphene oxide reduction

1. Introduction

Amperometric detection (AD) has become one of the most frequently employed electrochemical (EC) detection techniques in flow-based analysis, including flow injection analysis (FIA), high-performance liquid chromatography (HPLC), and ion chromatography (IC) [29, 45, 209, 236]. In such applications, AD as an EC detection technique is employed to detect target analytes in a liquid stream, measuring current at a fixed or variable potential [26]. The usual analysis time for the above variety of methods typically ranges from one to ten minutes [26, 41, 236]. To retain the electroactivity of electrodes in AD as well as to overcome the capacity gap of AD in terms of the lengthy duration of applied potential (similar to the analysis time, approx. ten minutes), a pulsed potential waveform used for pulsed amperometric detection (PAD) is now commonly applied during amperometric measurements [29, 30]. PAD uses variable potentials during oxidation and subsequent reduction steps that facilitate potentiostatic cleaning and reactivation of the electrode surface after each measurement cycle, with the pulse duration on a time scale of milliseconds [29, 30]. Kotnik *et al.* [17] achieved a frequency of 2 Hz for the detection of carbohydrates, and envisaged that the prospect of obtaining a 50 Hz potential cycle could be a great benefit in fast eluting flow-based analytical systems (such as IC). The development of a fast pulse waveform is challenging, particularly due to limitations of data acquisition capability at high frequency (in the range of 50 Hz corresponding to a cycle duration of only 20 ms) [17], and the loss of useful data when a long reduction step (such as 560 ms reported in [18]) is incorporated within a miniaturised EC detection system coupled with fast eluting flow-based analytical systems [18, 21]. In addition, challenges arise due to the long cleaning time required for the removal of large oxide layers from the electrode surface resulting from the use of high potential values (700-1250 mV [19-21]), high flow rates (1-1.2 mL min^{-1} [17-21]), and high sample volumes (20 µL [21]). Such limitations have resulted in a maximum calculated frequency of *ca.* 3.3 Hz [21] to date for 2-steps pulsed waveforms [17-

21]. Low frequency waveforms result in longer analysis time, and consequently the formation of large surface oxide layers and low stability of electrodes. The development of high frequency waveform incorporated within a miniaturised flow-through EC detector could be an advantage for rapid analysis of target solute (such as hydrazine [42], which has gained huge interest for different applications). It has been shown that conventional pulsed EC detection can benefit flow based analytical systems, such as in capillary electrophoresis [207].

Hydrazine has been widely used as pesticide, oxygen scavenger, corrosion inhibitor, rocket fuel [268, 269], and reducing agent in chemical reactions (e.g., reduction of graphene oxide, GO) [42]. However, hydrazine has significant toxicity, is carcinogen, and has been reported to cause serious damage to the liver, kidneys, and central nervous system [270-272]. Numerous analytical methods have been developed for the detection of hydrazine in various matrices, including chemiluminescence [273], colorimetric [274], fluorometric [275], spectrophotometric [275], and titrimetric [276] based approaches. However, these methods have mostly reported limits of detection (LODs) in the micromolar to millimolar range, and require specific reagents and/or complex derivatization processes, or suffer from significant matrix effects in real samples [22]. In terms of EC detection of hydrazine, the majority of the reported methods used cyclic voltammetry (CV) [277-280] in stopped-flow mode for relatively sensitive detection of hydrazine. In addition, there have been a limited number of reports of AD [22, 281-288] based upon modified electrodes for sensitive detection of hydrazine in FIA. The drawbacks associated with those existing AD based methods include the large cell volumes of the EC detector (20 mL reported in [288]), a large surface area of the disposable electrodes (16 mm^2 reported in [22]), high flow rates (*ca.* 3 mL min^{-1}), and large sample volume injected (100 µL in [22], resulting in LODs only in the range of 5-320 nM [22, 281-288]. Compared to AD, the prospect of PAD as an EC detection technique in flow-based analysis of hydrazine is very promising, delivering improved electroactivity of the electrode [26, 29], higher amperometric signal, rapid establishment of stable baseline, and long-term analytical reproducibility [18], as well as generally high detection sensitivity to electroactive analytes [22, 29, 283, 284]. Larson *et al.* [289] and Christison *et al.* [290] reported prolonged/complex pulse waveforms (600-999 ms) within large conventional EC detectors (cell volume < 0.5 µL) for the detection of hydrazine. However, to-date, to the authors' best knowledge, fast and sensitive pulsed amperometric waveforms for the detection of hydrazine, delivered within a miniaturised EC detector for flow-based analytical systems, has not been reported.

As mentioned earlier, hydrazine is often used as a reducing agent for the synthesis of reduced graphene oxide (rGO). rGO has attracted attention in many areas [42, 291-294], as it exhibits a number of unique properties. For example, it can acts as a flexible conductor [295], has unusual electronic properties such as an anomalous quantum Hall effect, high carrier mobility at relatively high charge carrier concentrations [296], relatively impermeable to gases, and optical transparency [292]. rGO is also used in numerous applications such as supercapacitors [42], highly conductive transparent layers [292], high-strength low-weight nanocomposites used in satellites and aircrafts [295], and photovoltaic devices [294]. An exact measurement of the reductant (i.e., hydrazine) consumption during the reduction of GO, and of the point of complete reduction, could provide efficiency savings in such processing at increased scale, improved homogeneity, and quality of future rGO based materials [297]. This is significant as the exact mechanism of GO reduction is still not fully understood [292]. Furthermore, our group has recently reported that reduction of GO can be easily studied by monitoring the concentration of the reducing agent during the reduction process [297]. In recent years, ascorbic acid has also been presented as a viable alternative reducing agent for this purpose [42]. Recently, we reported [41, 236] upon the highly sensitive EC detection of ascorbic acid (approx. 4 times lower

than UV detection) using a miniaturised gap flow cell (gap-FC) as EC detector, incorporating disposable electrodes. Therefore, herein the application of PAD to deliver a complete and accurate assessment of the relative performance of hydrazine and ascorbic acid as reducing agents for GO reduction, in terms of reaction half-lives, endpoints, and % yields, is presented.

Therefore, the aim of this study was to develop a novel, fast PAD waveform incorporated within a miniaturised EC detector for the sensitive detection of hydrazine in flow-based analytical systems. The analytical application of the developed waveform was demonstrated by monitoring the consumption of reducing agents (hydrazine and ascorbic acid) during the GO reduction process. The concentration of reducing agents were monitored through chromatographic methods (hydrazine in IC and ascorbic acid in HPLC) coupled with the miniaturised EC detection system incorporating the developed fast pulsed waveform.

2. Experimental

2.1 Chemicals

Analytical grade standards and reagents were used in this study. These were hydrazine monohydrate 65% (Sigma-Aldrich, Germany), ammonia 25% solution (i.e., ammonium hydroxide, NH_4OH, density 0.89 g mL^{-1}, Chem-Supply, Australia), sodium phosphate monobasic and sodium phosphate dibasic heptahydrate (Sigma-Aldrich, USA) for preparation of the phosphate buffer solution (PBS), Dionex methanesulfonic acid eluent generator cartridges (Thermo Fisher Scientific, USA)) for IC analysis, and milli-Q water (Millipore, USA). All test solutes and mixtures were freshly prepared in the same solvent as used for flow-based analytical systems. Smolenkov *et al.* [298] reports that hydrazine is completely protonated in buffer solution at pH ≤ 7. Gas-tight vials with PTFE/silicon septa (Supelco, USA) were used for sample preparation. The GO suspension (17 mg mL^{-1}) was provided by the University of Wollongong, Australia.

The reducing agents (hydrazine and ascorbic acid), were used to monitor the GO reduction process as shown by Fernández-Merino *et al.* [42], where ammonia solution was used to promote the colloidal stability of rGO [42] as well as to minimise the aggregation of the rGO sheets [293, 299]. Millipore membrane filters (Filter type HA, 0.45 µm pore size) were used for vacuum filtration of rGO. A suspension of ZrO_2 nanoparticles (10 wt. % in H_2O, Sigma-Aldrich, USA) was used for the modification of electrodes.

2.2 Instrumentation

The FIA-EC (FIA-AD and FIA-PAD) platform was assembled using an HPLC pump (PN 700001352, Waters, USA) and an injector valve (6-port 2 position, model SM4, Waters, USA). The miniaturised gap flow cell (i.e., gap-FC [236]) as the EC detector was connected to the injector valve using a polyimide coated fused silica capillary (100 µm i.d., 360 µm o.d., length 7 cm, PN TSP100375, Polymicro Technologies™, USA). The full instrumental schematic diagram of FIA-is shown in the Supporting Information (SI, see Fig. S26).

For monitoring the reduction of GO with hydrazine, IC-PAD was employed for the detection of hydrazine. The IC platform (ICS 2000, Dionex, USA) consisted of thermostatted cation-exchange columns (Dionex IonPac CG16 guard column: length 5 cm x i.d. 5 mm and CS16 analytical column: 25 cm x i.d. 5 mm, PN 057573, Thermo Fisher Scientific, USA) for the target analyte $N_2H_5^+$, and a manual injector valve (6-port 2 position, model 7000, Coati, USA). A reusable glass syringe with gas-tight plunger (250 µL, Trajan, Australia) was used for manual sample loading into the injector valve from the 15 mL reaction vessel (a mixture of 0.1 mg mL^{-1} GO, 2 mM hydrazine monohydrate, and 2 µL mL^{-1} 25% ammonia solution at 95^{O} C [42]) at regular time intervals.

The syringe was used with a disposable PTFE syringe filter (pore size 0.45 µm) to filter rGO from the sample mixture of hydrazine and ammonia solution. The gap-FC was connected to the IC column using a capillary (the same as used in FIA). The IC was operated by Chromeleon 6.8 software (Thermo Fisher Scientific, USA). The detailed instrumental schematic diagram of the IC-PAD is shown in the SI (see Fig. S27).

For monitoring the reduction of GO with ascorbic acid, HPLC-PAD was employed for the detection of ascorbic acid. The HPLC platform (Alliance Waters 2690, Waters, USA) consisted of a thermostatted reversed-phase column (YMC Pac Pro C18: length 25 cm x i.d. 4.6 mm, pore size 5 µm, YMC Co. Ltd, Japan), and an injector valve (model SM4, Waters, USA). A plastic syringe (1 mL) was used for manual sample loading into the HPLC auto sampler from the 15 mL reaction vessel (a mixture of 0.1 mg mL^{-1} GO, 2 mM ascorbic acid, and 2 µL mL^{-1} 25% ammonia solution at 95^{O} C [42]) at regular time intervals. The syringe was used with a disposable PTFE syringe filter (pore size 0.45 µm) to filter rGO from the sample mixture of ascorbic acid and ammonia solution. The gap-FC was connected to the HPLC column using a capillary (the same as used in FIA). The HPLC was operated by Empower software (Waters, USA). The full instrumental schematic diagram of the HPLC-PAD platform is shown in SI (see Fig. S28).

EC detection was performed using commercially available disposable screen-printed electrodes as exchangeable EC sensors of dimensions: length 25.40 x width 7.26 x height 0.63 ± 0.05 mm (PN AC1WxRS, BVT Technologies, Czech Republic). The sensors $AC_1W_1R_S$ used gold (Au) and $AC_1W_2R_S$ used platinum (Pt) as the working electrode (WE, diameter: 2 mm), both used silver as the reference electrode, and Pt as the auxiliary electrode. The electrodes were modified with ZrO_2 nanoparticles, as discussed in detail in our recent work [41]. The screen-printed electrodes' material and fabrication details are discussed by Li *et al.* [213] and Couto *et al.* [13]. A potentiostat (model ER466CE, eDAQ Pty Ltd, Australia; data acquisition capability of 1.92 Gbit s^{-1} at 120 MHz frequency) was connected to the gap-FC and operated with eDAQ software (eDAQ Pty Ltd, Australia) to perform various EC detection techniques such as CV in stopped-flow mode, as well as AD and PAD in flow-based analytical systems. All EC investigations were performed using a capillary i.d. of 100 µm, and gap distance (capillary outlet-electrode) of 30 µm as optimised in our previous work [236].

2.3 Selection of electrode and hydrazine oxidation potential

CV [240, 250] was performed to study the electrochemical response for the blank (0.1 M PBS, pH 7) and 1 mM hydrazine (in 0.1 M PBS, pH 7) at the electrode surface (Au, Pt, ZrO_2-Au and ZrO_2-Pt, see Fig. 16 and see Fig. S25 for full instrumental schematic diagram of CV in SI). The Pt electrode (bare and modified) acts as relatively active electrocatalyst compared to a Au electrode (bare and modified), as shown for both the blank (see Fig. 16a) and hydrazine (see Fig. 16b). The electrochemistry of hydrazine at the Pt electrode surface was discussed by Aldous *et al.* [300], who demonstrated that the presence of platinum oxides remaining from preceding oxidative scans resulted in a greater oxidation of hydrazine occurring up to *ca.* 400 mV, as compared to an oxide-free Pt electrode. In our study, we also observed an enhancement in hydrazine oxidation with oxide layer deposited on Pt up to 400 mV. After 400 mV, hydrazine oxidation was substituted by water oxidation, and more oxide layers were deposited on the Pt. The oxidation of hydrazine upon ZrO_2-Pt was *ca.* 2-10 times higher than other electrode surfaces (Au, Pt, and ZrO_2-Au) at +400 mV. The ZrO_2 nanoparticles act as electrocatalysts [41] on electrode surface resulted in an increased rate of mass-transport to the electrode surface via the formation of diffusion layers above each NP or NP-agglomerate. These diffusion layers result in a larger effective surface area, higher electrical conductivity, and a better EC

response at the modified electrode (ZrO_2-Pt) compared to the bare electrode (Pt). Finally, ZrO_2-Pt electrode and 400 mV (as hydrazine oxidation potential) were selected for further investigations in PAD.

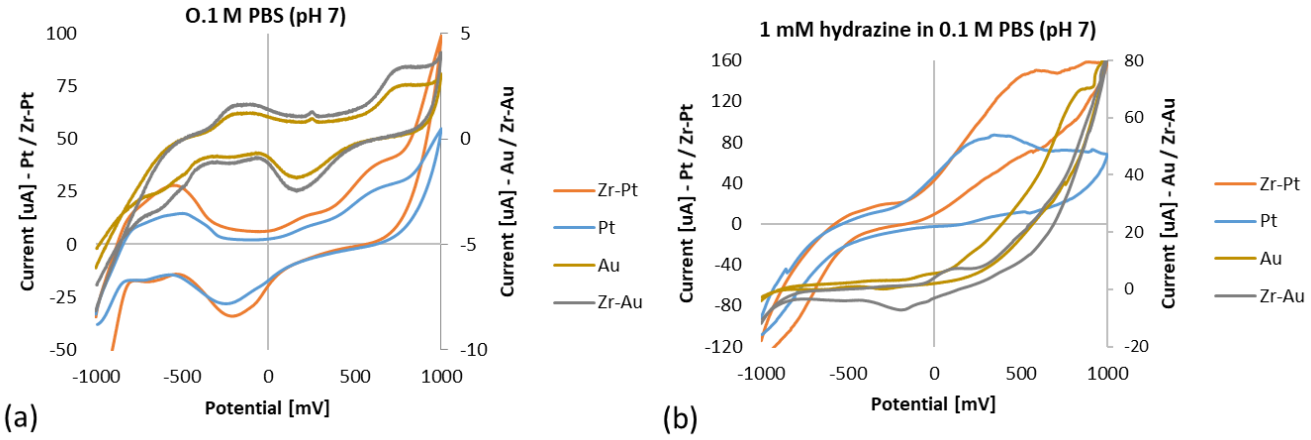

Fig. 16. Dependency of (a) blank and (b) hydrazine response at electrodes (Au, Pt, ZrO_2-Au and ZrO_2-Pt). Conditions: solvent: 0.1 M PBS (pH 7) and scan rate 100 mV s^{-1}.

3. Results and discussions

Initially, CV and AD were performed for the selection of electrode type (material), solvent, detection potential, flow rate, and sample volume. The optimised conditions were used for the development of fast pulsed waveforms and sensitive detection of hydrazine in FIA. The analytical application of the waveform was demonstrated by monitoring the consumption of hydrazine in IC and ascorbic acid in HPLC respectively, during the GO reduction process.

3.1 Fast pulsed waveform design

The primary objective for the design of 2-step PAD waveform was to investigate a high frequency potential cycle resulting from the generated pulses, allowing fast cycle repetition and thus high enough frequency of individual signal data points during signal acquisition in chromatography. For the exploration and development of a fast waveform, we placed an emphasis on short analysis times, without compromising the electrode cleaning of surface oxide, the electrode stability, and the high sensitivity to our target solute (hydrazine), in our miniaturised EC detection system (see section 2.2 “Instrumentation”). Our EC detection system generated signal data of ~1Kbit s^{-1} for a 20 ms pulse at 50 Hz, with optimised low potential values, flow rates, and sample volumes (see SI section 4) compared to other 2-step waveform reports [17-21]. Our waveform (total 20 ms cycle, see Fig. 17) achieved 15-45 times faster frequency (50 Hz) than previously reported for 2-step PAD waveforms (frequency ranged 1.1-3.3 Hz) [17-21] and to the authors’ knowledge this waveform has been developed in a miniaturised EC detection system (see our previous work [236]) for the first time.

In the initial detection step (see Fig. 17), the signal (i.e., faradaic current) decreases due to charging current resulting from the double layer effect (also known as the capacitance effect) during detection time, t_{det} [20, 267]. Therefore, to minimise double layer effects, we investigated a delay time, t_{del} in the range of 1-9 ms of the detection step (see SI

Fig. S32). We established an optimal value of t_{del} in terms of signal to noise (S/N) as 5 ms (see SI Table S8). The resulting value of integration time, t_{int} (t_{det}-t_{del}) was 5 ms, where the voltage was proportional to the optimal current (i.e., maximum faradaic

current with minimal attenuation of amperometric signal due to charging current) [301]. The measurements of optimal current were repeated, corresponding to the frequency of t_{int}, which varied from 52.63 Hz to 100 Hz (see SI Table S8).

The electrodes form oxide layer or monolayers under electrochemical oxidation conditions [302]. In the subsequent reduction step, the reduction potential (E_{red}) was optimised to achieve dissolution of the oxide layer from the electrode surface, and enhanced cleaning of the electrode. The optimisation of E_{red} was performed by calculating the oxidative current and corresponding S/N at three different E_{red} (see SI Fig. S33 and Table S9). At a -400 mV E_{red}, we obtained the maximum oxidative current for hydrazine oxidation as well as maximum S/N. Additionally, Sung *et al.* [106] suggested utilising shorter reduction times to enable the recording of narrow peaks in flow-based analytical systems (such as FIA). In this reduction step, an efficient dissolution of surface oxide layer would result in an optimal current during t_{int} as discussed before. Therefore, we applied an E_{red} from -100 to -600 mV at t_{red} 10 ms and observed that E_{red} = -400 mV gave the optimal current during t_{int} (see SI Table S9). At this optimal E_{red}, we also investigated reduction times (t_{red}) from 5-10 ms to establish enhanced cleaning of the electrode (see SI Table S8).

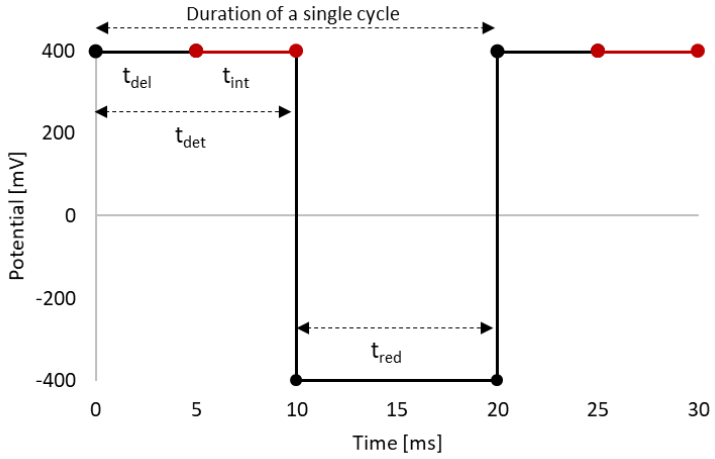

Fig. 17. Generated 2-step PAD waveform. Conditions: detection potential, E_{det} +400 mV (delay time, t_{del} 5 ms and integration time, t_{int} 5 ms), reduction potential, E_{red} -400 mV (reduction time, t_{red} 10 ms), and frequency 50 Hz.PAD of hydrazine in FIA

In this study, the developed waveform was investigated for miniaturised flow-through EC detection of hydrazine. Under the optimised conditions, the responses of the test solute (hydrazine) were measured at different concentrations, and a calibration curve was plotted using peak heights (see Fig. 18). The LOD of hydrazine obtained in FIA-PAD was 2.5 times lower than the LOD obtained in FIA-AD (see Table 7, n= 9, and determination coefficient r^2 = 0.99 for concentration range 1 nM - 100 µM for PAD and 10 nM - 100 µM for AD).

Table 7 illustrates the benefits of using the fast pulsed waveform compared to reported AD [22, 273, 297, 303] and PAD with slower waveforms [17-21] in terms of the greater stability of the electrode (*ca.* 5 hr in continuous-flow of 0.4 mL min^{-1}, see Fig. S35), an increased linearity range (0.001 uM - 0.1 mM), high sensitivity (*ca.* 5 times), and lower LODs (*ca.* 100 times) for hydrazine detection. We also observed an improved S/N ratio resulting from our fast pulses (see Table S8). Furthermore, the PAD investigation was undertaken with a 5 times lower surface area (2 mm^2) of the disposable electrode (ZrO_2-Pt) allowing lower effective detection volumes in flow methods such as HPLC, a 6 times lower flow rate (0.4 mL min^{-1}), and a 20 times lower sample volume (5 µL) compared to that of Ayaz *et al.* [22] who previously reported lowest LOD 80 nM of hydrazine in FIA-AD.

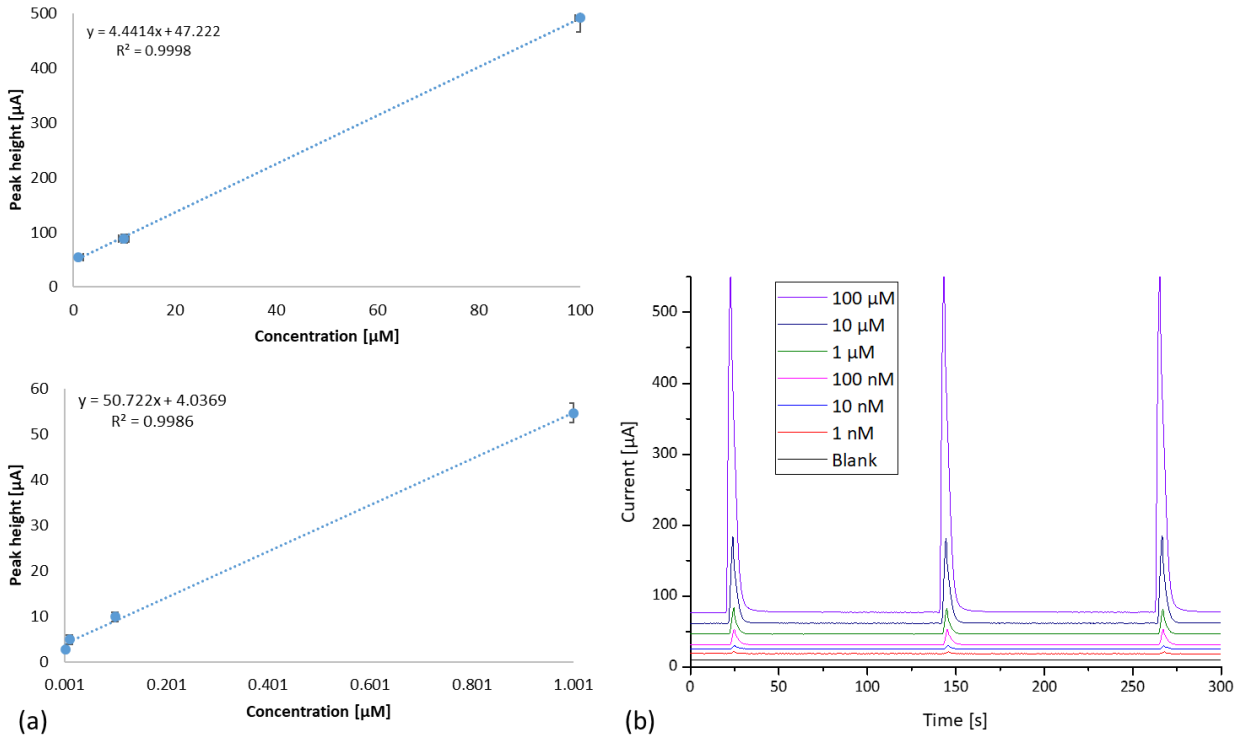

Fig. 18. Hydrazine response in FIA-PAD showing (a) calibration plot (n= 9) and (b) three repetitive continuous injections. Conditions: mobile phase: 0.1 M PBS (pH 7), flow rate: 0.4 mL min^{-1}, sample volume: 5 µL, capillary (injector-gap-FC) i.d: 100 µm (length: 7 cm), gap distance: 30 µm, and WE: ZrO_2-Pt. PAD waveform: see Fig. 17.

Table 7. Comparison of analytical performance for hydrazine in flow-based analytical systems.

Method	Electrode	Solvent	Flow rate [mL min^{-1}]	Potential [mV]	Sample volume [µL]	Noise [nA]	Linearity range [µM - mM]	Sensitivity [µA $µM^{-1}$]	LOD [µM]	Ref.
FIA-AD	Pcv-PGE	PBS, pH 9	2.4	+ 100	100	-	0.25 - 0.5	0.032 [c]	0.08	[22]
FIA-AD [b]	ZrO_2-Pt	PBS, pH 7	0.4	+ 400	7.5	16	0.01 - 1	0.433 [c]	0.005 [a]	This work
FIA-Chemiluminescence	-	Sodium dichloroisocyanurate	3.8	-	-	-	-	-	0.2	[273]
FIA-PAD	ZrO_2-Pt	PBS, pH 7	0.4	+ 400	5	13	0.001 - 0.1	0.495 [c]	0.0008 [a]	This work
IC-AD	Pt	Borate buffer	0.8	+700	5	-	10 - 4	-	3	[297]
IC-AD	-	HCl, L-lysine	0.77	+600	100	-	-	-	0.015	[303]
IC-PAD	ZrO_2-Pt	Methanesulfonic acid	0.4	+400	5	13	0.01 - 1	0.544 [c]	0.18	This work

[a] LODs = three standard deviations (3SD) of a blank response (noise level)/slopes of the corresponding calibration curves [50].

[b] FIA-AD: see details in SI section 3.

[c] Sensitivity= slope of calibration curve (change in signal / change in analyte concentration) [50].

Pcv-PGE: Pyrocatechol violet modified pencil graphite electrode.

3.2 Study of GO reduction in IC-PAD and HPLC-PAD

The analytical application of the developed waveform was demonstrated by monitoring the consumption of reducing agents (hydrazine and ascorbic acid) during the reduction of GO. At regular time intervals, the samples were collected manually from the reaction vessel and injected into the chromatographic platforms (i.e, IC for hydrazine and HPLC for ascorbic acid) connected to the miniaturised EC detection system (for details see section 2.2 "Instrumentation").

The reducing agents signal (i.e., faradaic current during t_{int}) vs. retention time was plotted at 3 min reaction time intervals in the GO reduction process (see Fig. 19a and Fig. 20a). The changes in signal of reducing agents was observed for different reaction times. The corresponding concentrations of reducing agents were calculated and plotted against reduction time intervals of each analyte separately (see Fig. 19b and Fig. 20b) for the determination of reaction endpoint. As illustrated in Fig. 19b and Fig. 20b, the concentrations of reducing agents decreased at a fast rate (as illustrated by the fast rate of change of the slope of the reaction kinetics curve) up to a certain point in the chemical reaction, and then at a slower rate (as illustrated by the slow rate of change of the slope of the reaction kinetics curve) until reaching the reaction endpoint. The reaction endpoint, or the point at which no rate of change of the slope of the reaction kinetics curve is observed, was for hydrazine at 21 min (see Fig. 19b) and 27 min (Fig. 20b).

The half-life of a chemical reaction is a useful measure to characterise the chemical reaction kinetics curve [304]. The half-life of a chemical reaction is the point in time where the initial concentration of reactant is reduced by half compared to its initial concentration [304]. From this definition, three half-life times for ascorbic acid and no half-life for hydrazine were observed in Fig. 19b and Fig. 20b. This confirms the very different nature of the two reducing agents used in our study in terms of their redox potentials in GO reduction. The nature of reactants can affect the rate of reaction and result in different reduction times for different reactants under the same experimental conditions [305].

At the endpoint in Fig. 19b and Fig. 20b, the final concentrations of the reducing agents were different because of the difference in redox potentials of reducing agents (hydrazine 360 mV [306] and ascorbic acid 240 mV at pH 7 [307]) during the GO reduction process. The strong reducing agent hydrazine with higher redox potential reduced the GO more readily than the ascorbic acid, as a result fast reduction of GO (i.e. less time was taken to reduce 0.1 mg mL $^{-1}$ GO (Time 21 min, see Fig. 19b) and high % yield of RGO (*ca.* 52%, see Table S12) and consequently less consumption of hydrazine in the reaction (0.9 mM hydrazine consumed at endpoint, see Fig. 19b) were observed. On the other hand, the weaker reducing agent ascorbic acid with lower redox potential reduced 0.1 mg mL $^{-1}$ GO at a slow rate (Time 27 min, see Fig. 20b) giving a low % yield of RGO (*ca.* 34%, see Table S12)) and consequently high consumption of ascorbic acid in the reaction (1.8 mM ascorbic acid consumed at the endpoint, see Fig. 20b). Fernández-Merino *et al.* [42] reported that ascorbic acid can be an ideal substitute for hydrazine in the large-scale preparation of rGO without comparing the reaction half-lives, GO reduction endpoint, % yields, and cost of reducing agents (*ca.* 2 times higher consumption of ascorbic acid compared to hydrazine).

The EC detection (here with the pulsed waveform as well as the similar study performed by our group [297]) has overcome the contradictory reports of GO reduction endpoints using hydrazine such as 15 min [42] and 60 min [293] when UV-vis absorption spectroscopy was used. These contradictions are likely due to the UV absorbance of the GO functional groups (such as hydroxyl, epoxide, carbonyl, and carboxyl [294]) across a wide spectral range (230-270 nm) [293]. Additionally, X-ray photoelectron spectroscopy as well as Fourier-transformation infrared spectroscopy studies gave a GO reduction endpoint as 3 hr [294] under

the same conditions. XPS and FTIR are highly controlled systems and slow data acquisition techniques [308, 309], which require long time periods to analyse the samples compared to our developed miniaturised electrochemical detection system. In XPS, one must also be concerned about X-ray radiation damage to the sample at such long exposures and XPS must be compatible with an ultra-high vacuum environment (ca. 1×10^{-9} Torr) [1]. In our study, the EC detection system for monitoring the GO reduction process without requirement of highly-controlled pH and expensive reagent-dependent derivatisation as required in a fluorescence-based assay [310, 311], and there was interference effects from excess ammonia as observed in the spectrophotometric method [312]. Furthermore, our investigations may be beneficial for the quality control of GO reduction, as Gilje *et al.* [313] has reported the requirement of reduced GO collected at different reduction times for various applications in electronic devices.

In further study, the GO reduction time (see SI Fig. S40) obtained with the developed pulsed waveform were found in correspondence with a similar study performed by our group on a commercial Dionex ED40 EC detector (reported in [297]). The study demonstrated the significance of hydrazine monitoring to evaluate GO reduction process. The successful use of a miniaturised EC detector (gap-FC) incorporating disposable electrode [41, 236] and pulsed waveform to monitor the concentration of hydrazine and ascorbic acid during GO reduction should facilitate the development of a miniaturised on-line system to study the process. This would encourage future investigations into the poorly understood mechanism and kinetics of reducing GO sheets.

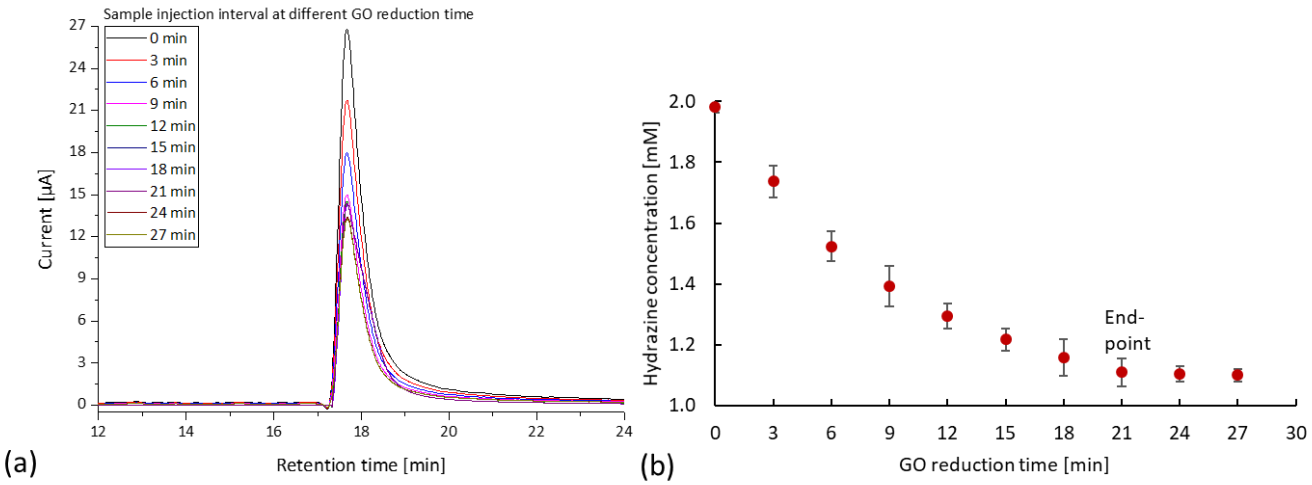

Fig. 19. Monitoring reduction of 0.1 mg mL^{-1} GO using 2 mM hydrazine (2 µL mL^{-1} 25% NH_4OH to adjust pH 9-10) in IC-PAD platform showing (a) chromatograms and (b) determined hydrazine concentrations (n= 3). Conditions: solvent: 30 mM methanesulfonic acid, flow rate: 0.6 mL min^{-1}, sample volume: 5 µL, IC column: IonPac CG16 and CS16 (length: 5 and 25 cm, i.d: 5 mm), column oven temperature: 30 °C, pressure: *ca.* 1015 psi (70 bar), capillary (column-gap-FC): i.d 100 µm (length: 7 cm), gap distance: 30 µm, and WE: ZrO_2-Pt. PAD waveform: see Fig. 17. At 21 minutes, the reaction does not proceed further although there is a small amount of hydrazine remaining in the solution.

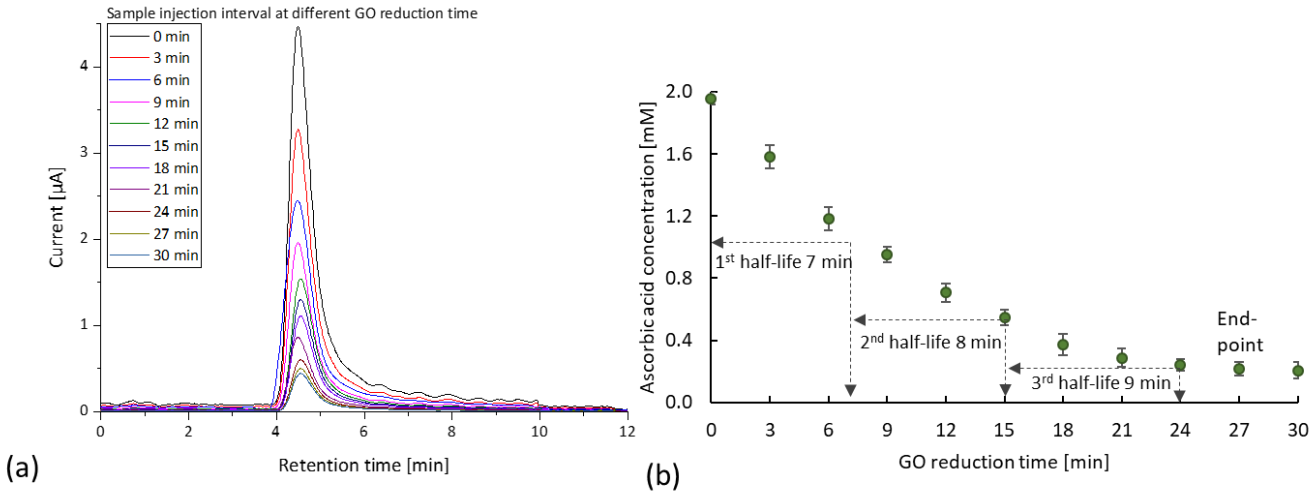

Fig. 20. Monitoring reduction of 0.1 mg mL^{-1} GO using 2 mM ascorbic acid (2 µL mL^{-1} 25% NH_4OH to adjust pH 9-10) in an HPLC-PAD platform, showing (a) chromatograms and (a) determined hydrazine concentrations (n= 3). Conditions: mobile phase (v/v=60:20:20): ACN: water:25 mM citrate buffer solution, pH 3.5, elution: isocratic, flow rate: 0.6 mL min^{-1}, sample volume: 5 uL, HPLC column: YMC Pac Pro C18 reversed-phase column (length: 25 cm, i.d: 4.6 mm, particles size: 5 µm), column oven temperature: 25 °C, pressure: *ca.* 1050 psi (73 bar), capillary (column-gap-FC) i.d: 100 µm (length: 7 cm), gap distance: 30 µm, and WE: ZrO_2-Au. PAD waveform: see Fig. 17. At 27 minutes, the reaction does not proceed further although there is a small amount of ascorbic acid remaining in the solution.

4. Conclusions

This work shows that a fast PAD can be designed for rapid repeated measurements in dynamic systems such as here in analytical flow systems including FIA and IC/LC. The herein developed fast PAD waveform (2-steps at +400 mV and -400 mV, 10 ms each, 50 Hz cycle repetition) is demonstrated for PAD of hydrazine in flow-based analytical systems for the first-time. The LOD of hydrazine obtained was 0.8 nM, which is one order of magnitude lower than the lowest LOD reported in the literature so far. Significantly, the LOD was obtained by using 5-20 times lower key experimental parameters (including electrode surface area, flow rate, sample volume, and faster PAD frequency) than in previous studies. The faster PAD frequency could be of great benefit serving to minimise the loss of useful data when a long reduction (i.e., electrode cleaning) step is incorporated within a miniaturised EC detection system coupled with fast eluting flow-based analytical systems. Furthermore, we demonstrated an analytical application of the developed waveform by monitoring the consumption of reducing agents (hydrazine and ascorbic acid) during the GO reduction process. We observed different reaction half-lives, endpoints and % yields for hydrazine (-, 21 min, and 52%) and ascorbic acid (7 min, 27 min, and 34%) respectively, during the reduction of GO.

Acknowledgements

The authors acknowledge the University of Tasmania for financial support in the form of a Tasmania Graduate Research Scholarship (TGRS) awarded to MAI. MM acknowledges the Australian Research Council (ARC) Future Fellowship (FT120100559) for the financial support of this research. MAI is immensely grateful to all co-authors and Dr Ruth Amos (Senior Editor, Fix My English) for their comments on an earlier version of the manuscript that greatly helped to improve the manuscript.

Supplementary information (SI)

The supporting information content includes:

5. Instrumentation: Cyclic voltammetry, FIA-AD, FIA-PAD, IC-PAD, and HPLC-PAD.
6. Cyclic voltammetry (CV): Selection of solvent and pH of solvent.
7. AD of hydrazine in FIA: Optimisation of detection potential, flow rate, and sample volume, calibration plot, and repetitive continuous injections.
8. PAD of hydrazine in FIA: Fast pulsed waveform design, flow rate, sample volume, and stability and repeatability test.
9. Study of GO reduction in IC-PAD and HPLC-PAD: Optimisation of flow rate, calibration plots, and % yields.
10. Extended study of GO reduction in IC-PAD: Calibration plot and monitoring reduction of GO.

1. Instrumentation

1.1 Cyclic voltammetry

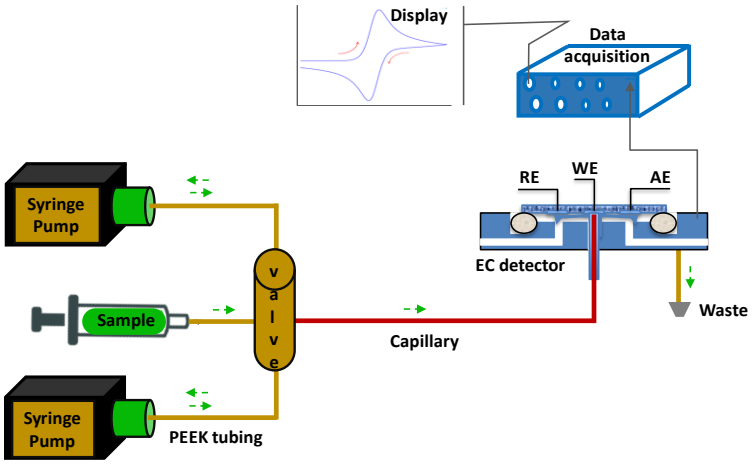

Fig. S25. Schematic flow diagram of CV.

1.2 FIA-AD and FIA-PAD

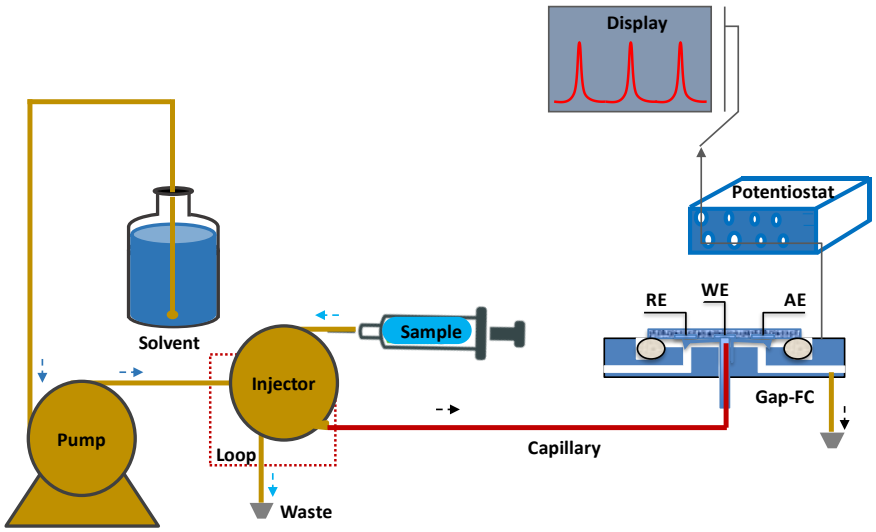

Fig. S26. Schematic flow diagram of FIA-AD and FIA-PAD.

1.3 IC-PAD

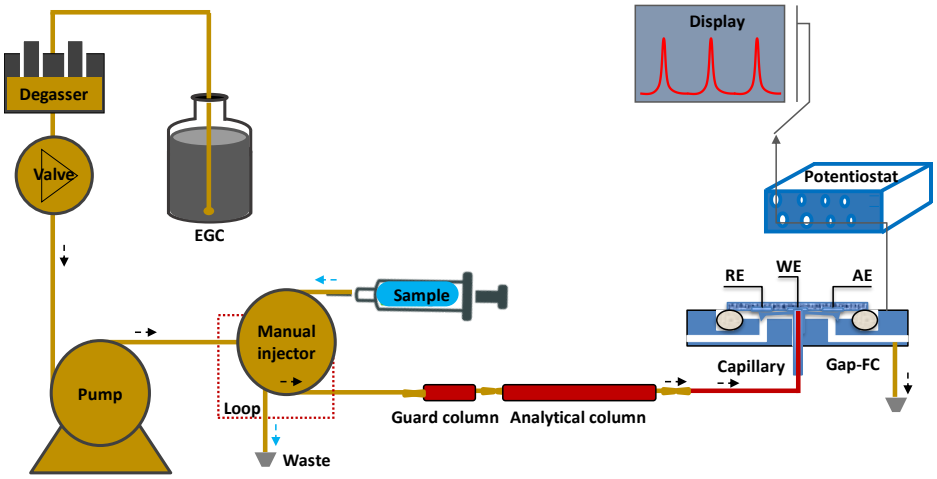

Fig. S27. Schematic flow diagram of IC-PAD.

1.4 HPLC-PAD

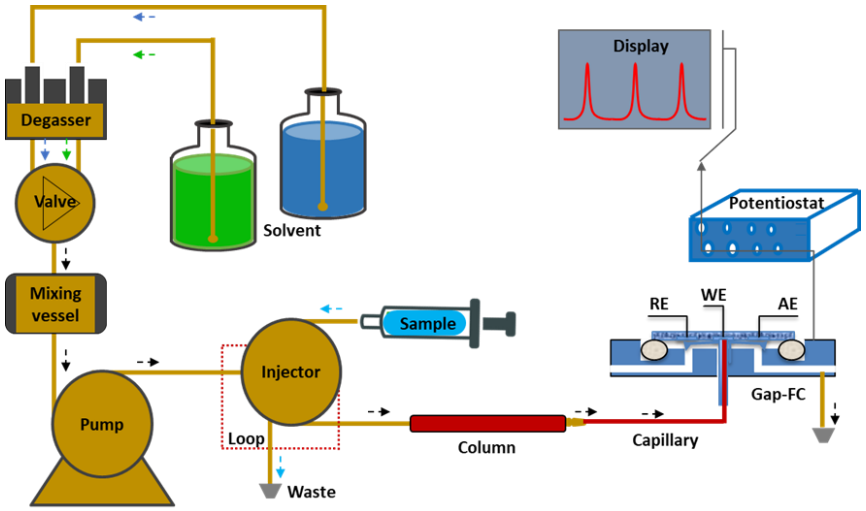

Fig. S28. Schematic flow diagram of HPLC-PAD.

2. Cyclic voltammetry

A simple CV platform was assembled using a µProcess (LabSmith™, USA) microfluidic system as reported in our previous work [41]. The CV is often the first EC experiment has been performed to study the behaviour of species involved in redox reactions at electrode surface [240, 250]. The EC redox behaviour of hydrazine for solvent (KCl, $NaOH$, citrate buffer solution, and phosphate buffer solution), and solvent pH (in the range of 3-9) were investigated in this study. The CV was performed over a wide range of potential from -1 V to 1 V at scan rate 100 mV s^{-1}.

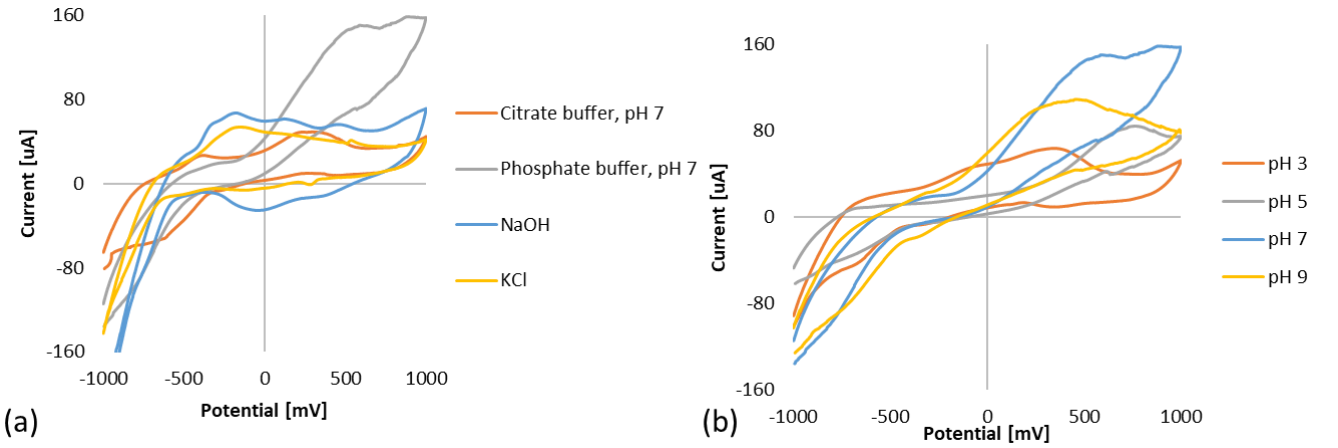

Fig. S29. Dependency of 1 mM hydrazine response on (a) solvent and (b) pH of solvent (0.1 M PBS). Conditions: WE: ZrO_2-Pt and scan rate 100 mV s^{-1}.

3. AD of hydrazine in FIA

3.1 Optimisation of parameters

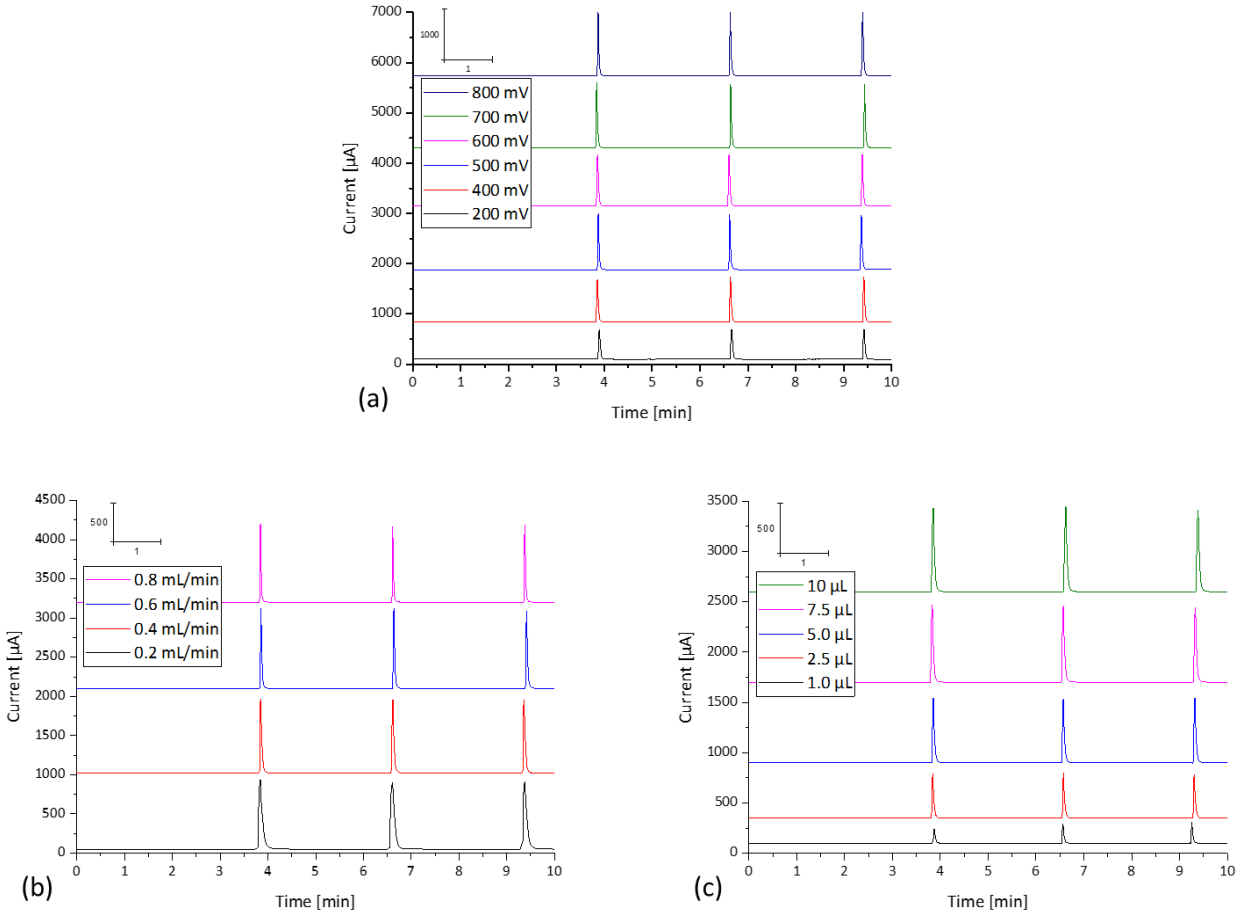

Fig. S30. Dependency of 1 mM hydrazine response on (a) AD potential, (b) flow rate, and (c) sample volume in FIA-AD. Conditions: solvent: 0.1 M PBS (pH 7), flow rate: 0.6 mL min^{-1} (a, c), sample volume: 10 µL (a, b), capillary (injector-gap-FC): i.d 100 µm (length: 7 cm), gap distance: 30 µm, WE: ZrO_2-Pt, and potential: +400 mV (b, c).

Table S7. Dependency of 1 mM hydrazine response on AD potential, flow rate, and sample volume in FIA-AD platform.

Potential [mV]	S/N		Flow rate [mL min^{-1}]	S/N		Volume [µL]	S/N
200	14858		0.2	35522		1	12923
400	15325		0.4	37800		2.5	14167
500	6248		0.6	33744		5	16000
600	3250		0.8	24617		7.5	17037
700	2417					10	16633
800	1742						

3.2 Calibration plot of hydrazine in FIA-AD

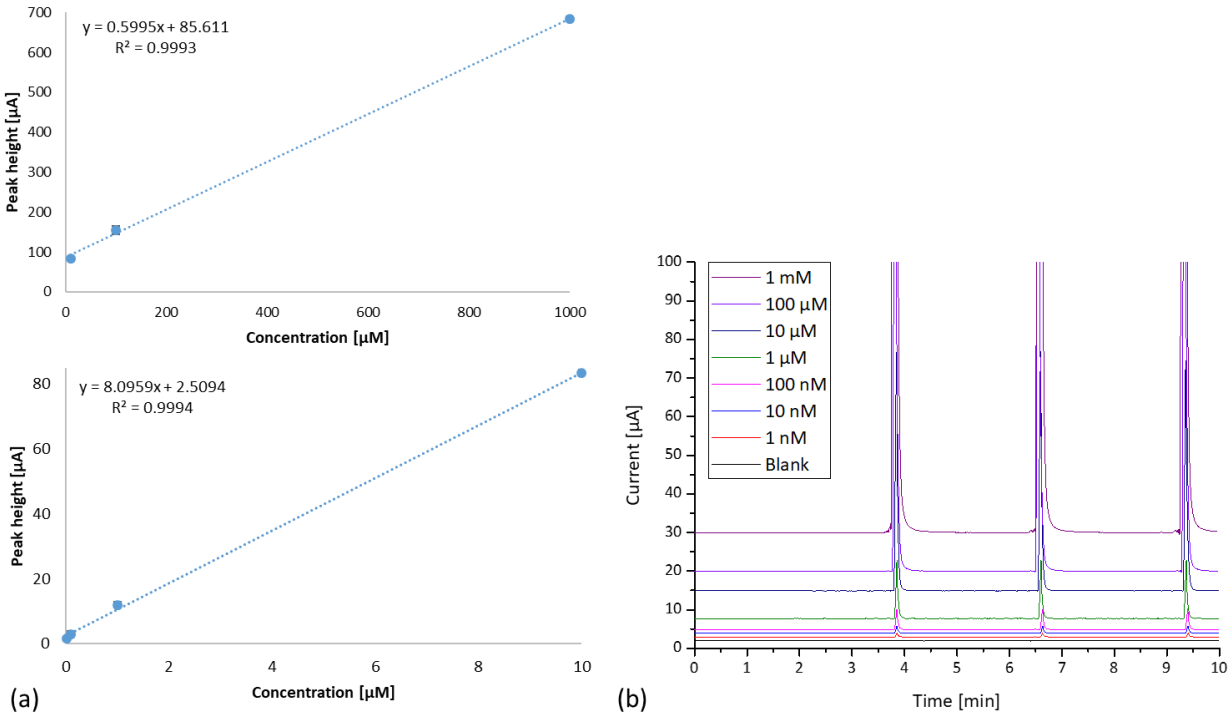

Fig. S31. Hydrazine response in FIA-AD showing (a) calibration plot (n= 9) and (b) three repetitive continuous injections. Conditions: mobile phase: 0.1 M PBS (pH 7), flow rate: 0.4 mL min^{-1}, sample volume: 7.5 µL, capillary (injector-gap-FC) i.d: 100 µm (length: 7 cm), gap distance: 30 µm, WE: ZrO_2-Pt, and potential: +400 mV.

4. PAD of hydrazine in FIA

4.1 Fast pulsed waveform design

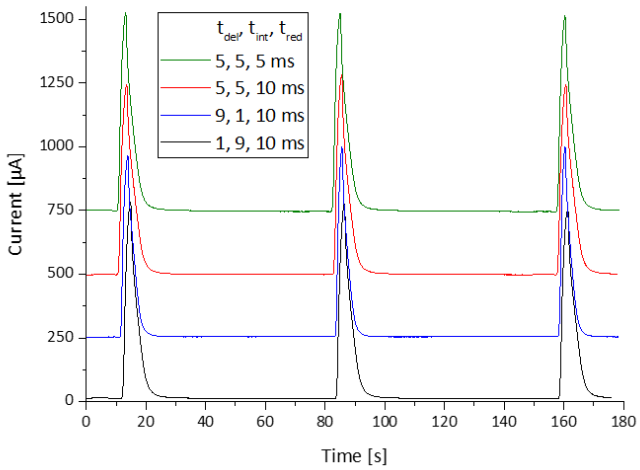

Fig. S32. Dependency of 1 mM Hydrazine response on fast pulsed waveform design (target frequency at least 50 Hz) in FIA-PAD. Conditions: mobile phase: 0.1 M PBS (pH 7), flow rate: 0.4 mL min^{-1}, sample volume: 7.5 µL, capillary (injector-gap-FC) i.d: 100 µm (length: 7 cm), gap distance: 30 µm, and WE: ZrO_2-Pt. PAD waveform: E_{det} +400 mV, t_{del} 1-9 ms, t_{int} 1-9 ms , E_{red} -400 mV , t_{red} 5-10 ms (c).

Table S8. Dependency of 1 mM Hydrazine response on fast pulsed waveform design (target frequency at least 50 Hz) in FIA-PAD.

Time [ms]			Potential [mV]		Frequency [Hz]		S/N
Delay	Integration	Reduction	Oxidation	Reduction	Integration time	Pulsed waveform	
1	9	10	+ 400 [a]	- 400	90.90	50	1893
5	5	10			66.67	50	3277
9	1	10			52.63	50	1618
5	5	5			100	66.67	1533
[a] Oxidation potential +400 mV was selected from AD in terms of S/N.							

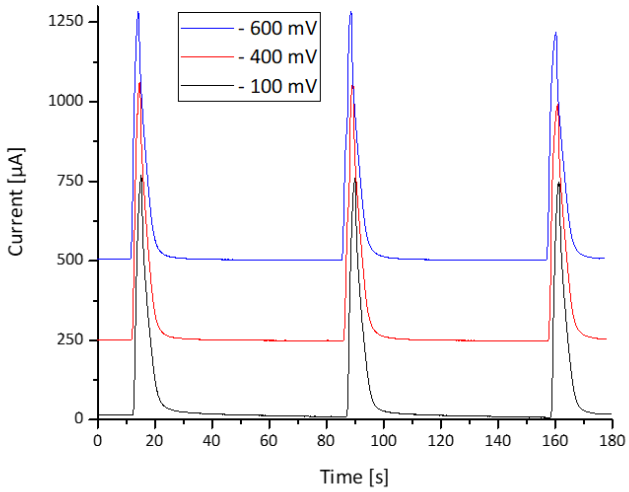

Fig. S33. Dependency of 1 mM Hydrazine response on reduction potential in FIA-PAD. Conditions: mobile phase: 0.1 M PBS (pH 7), flow rate: 0.4 mL min^{-1}, sample volume: 5 µL, capillary (injector-gap-FC) i.d: 100 µm (length: 7 cm), gap distance: 30 µm, and WE: ZrO_2-Pt. PAD waveform: see Fig. 17 and E_{red} -100 to -600 mV.

Table S9. Dependency of 1 mM Hydrazine response on reduction potential in FIA-PAD.

Time [ms]			Potential [mV]		Frequency [Hz]	S/N
Delay	Integration	Reduction	Oxidation	Reduction		
5	5	10	+ 400	- 100	50	1980
				- 400		3277
				- 600		2785

4.2 Optimisation of parameters

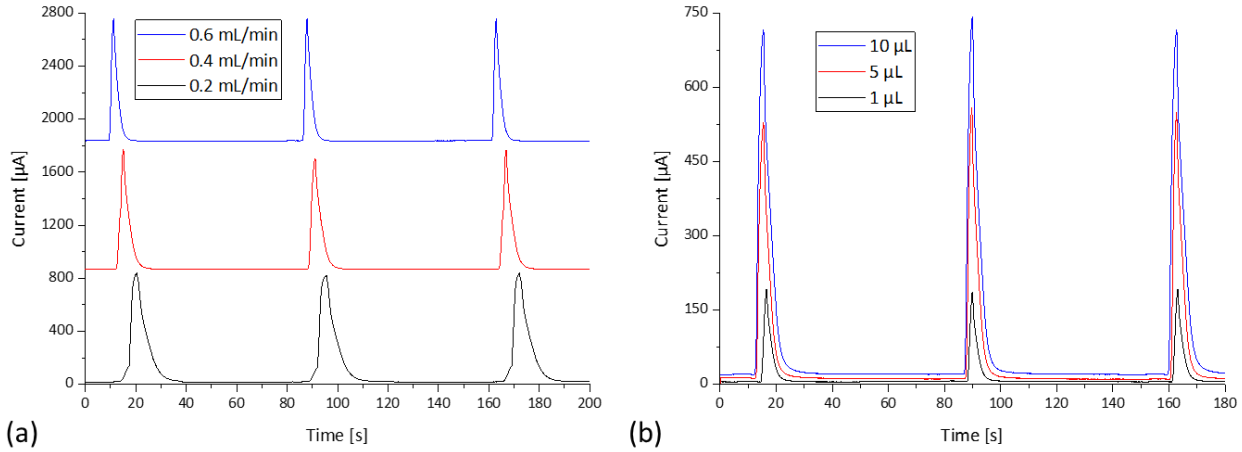

Fig. S34. Dependency of 1 mM Hydrazine response on (a) flow rate and (b) sample volume in FIA-PAD. Conditions: mobile phase: 0.1 M PBS (pH 7), flow rate: 0.2-0.6 mL min^{-1} (a) and 0.4 mL min^{-1} (b), sample volume: 5 µL (a) and 1-10 µL (b), capillary (injector-gap-FC) i.d: 100 µm (length: 7 cm), gap distance: 30 µm, and WE: ZrO_2-Pt. PAD waveform: see Fig. 17.

Table S10. Dependency of 1 mM hydrazine response on flow rate and sample volume in FIA-PAD platform.

Flow rate [mL min^{-1}]	S/N		Volume [µL]	S/N
0.2	4022		1	1021
0.4	4149		5	2268
0.6	2112		10	2060

4.3 Stability and repeatability test

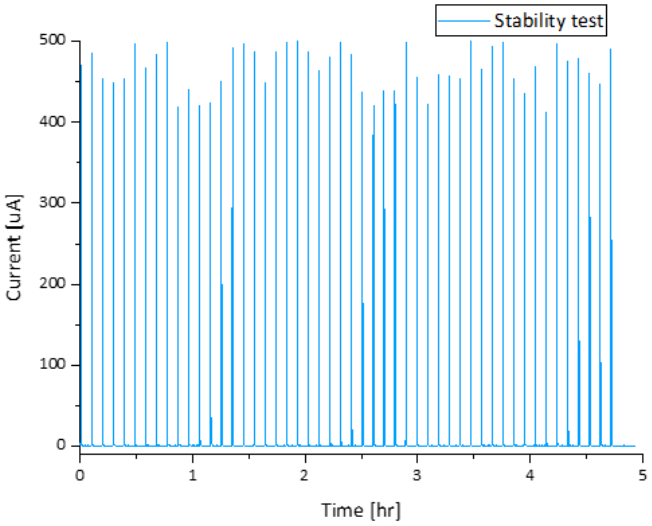

Fig. S35. Stability test of electrode and repeatability test of Hydrazine response (n= 50) in FIA-PAD. Conditions: solute: 100 µM hydrazine, mobile phase: 0.1 M PBS (pH 7), flow rate: 0.4 mL min^{-1}, sample volume: 5 µL, capillary (injector-gap-FC) i.d: 100 µm (length: 7 cm), gap distance: 30 µm, and WE: ZrO_2-Pt. PAD waveform: see Fig. 17.

A comparison of hydrazine responses for 50 repetitive continuous injection of 5 µL was observed for the developed 2-step PAD waveform (see SI Fig. S35). There are no significant differences between the peaks signal (height) obtained at room temperature (*ca.* 20 °C). Under optimised conditions, the average peak current of 100 µM hydrazine was equals 466±25.3 µA (RSD 5.4%, n=50). This investigation also ensures that the application of short reduction step (potential -400 mV, and time 10 ms) in pulse sequence restores the electrode surface activity as well as retains it free from undesirable reaction products during the period of *ca.* 5 hr in continuous-flow of 0.4 mL min^{-1}. The proposed PAD waveform enhances less t_{int}, and easy online cleaning process to an extended lifetime of disposable electrodes.

5. Study of GO reduction in IC-PAD and HPLC-PAD

5.1 Flow rate optimisation

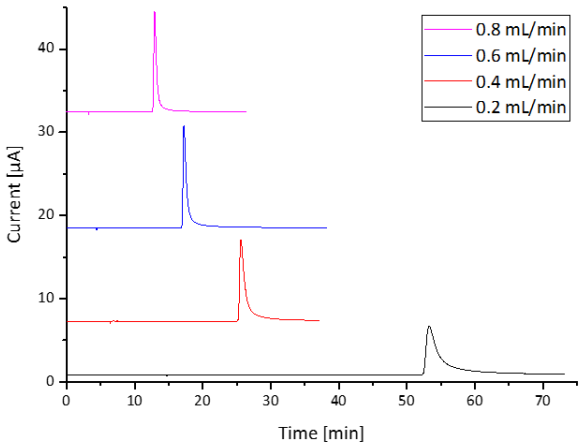

Fig. S36. Dependency of 1 mM hydrazine response on flow rate in IC-PAD. Conditions: solvent: 30 mM methanesulfonic acid, flow rate: see graph, sample volume 5 µL, IC column (injector-gap-FC): IonPac GS6 guard column and CS16 cation-exchange analytical column (length: 5 cm and 25 cm, i.d: 5 mm), column oven temperature: 30 °C, pressure: *ca.* 400-1400 psi (27-98 bar), capillary (injector-gap-FC): i.d 100 µm (length: 7 cm), gap distance: 30 µm, WE: ZrO_2-Pt, and potential: +400 mV.

Table S11. Dependency of 1 mM hydrazine response on flow rate in terms of S/N and plate no. in IC-PAD platform.

Flow rate [mL min^{-1}]	Noise [nA] (0-10 min)	S/N	Plate no. [N m-1]
0.2	7.5	750	1715
0.4	16.1	590	1750
0.6	18.8	630	1790
0.8	21.2	550	1420

For rGO study in IC-PAD platform, the flow rate (0.6 mL min^{-1}) was optimised in terms of S/N (see Table S11), however, in HPLC platform the investigations were performed with optimised flow rate 0.6 mL min^{-1} and potential +800 mV as reported in our previous work [41].

5.2 Calibration plot of hydrazine in IC-PAD

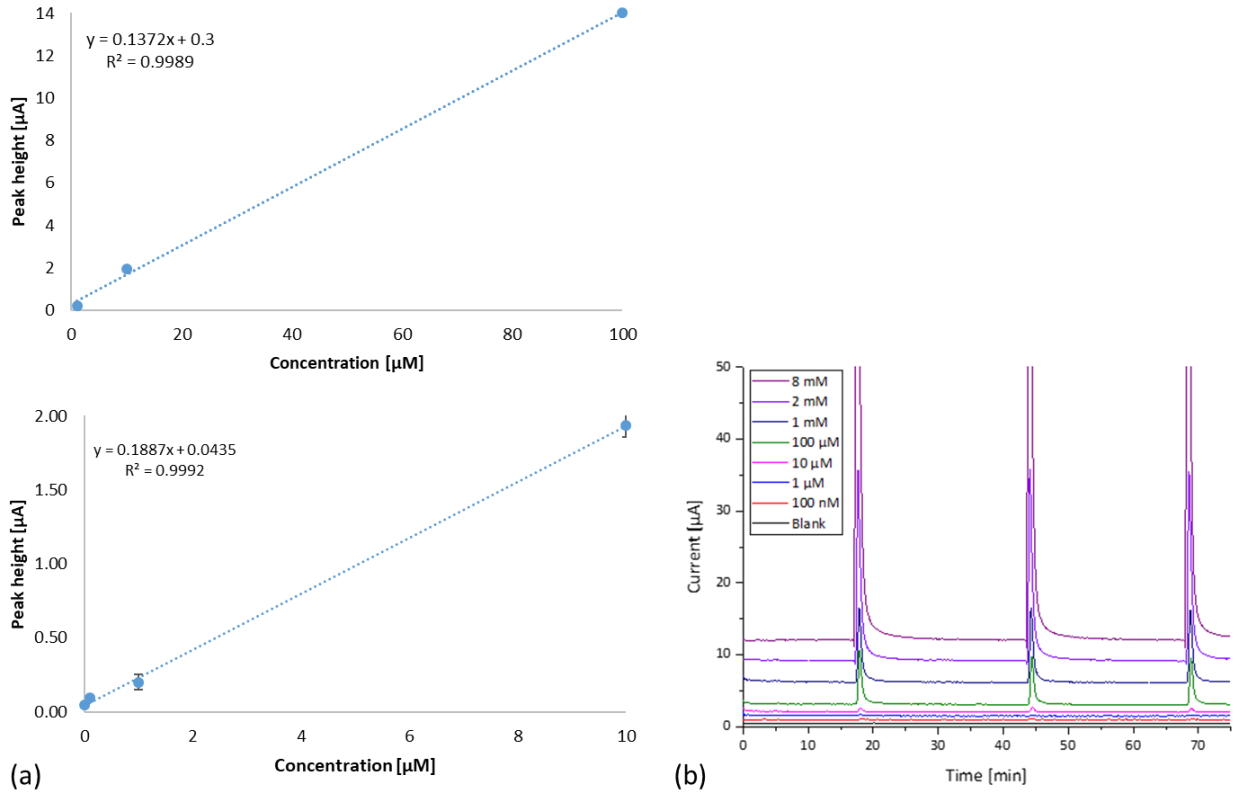

Fig. S37. (a) Calibration plot and (b) three repetitive continuous injections of 10 nM-10 mM hydrazine (2 µL mL^{-1} 25% NH_4OH to adjust pH 9-10) in IC-PAD. Conditions: see Fig. 19. PAD waveform: see Fig. 17.

5.3 Calibration plot of ascorbic acid in IC-PAD

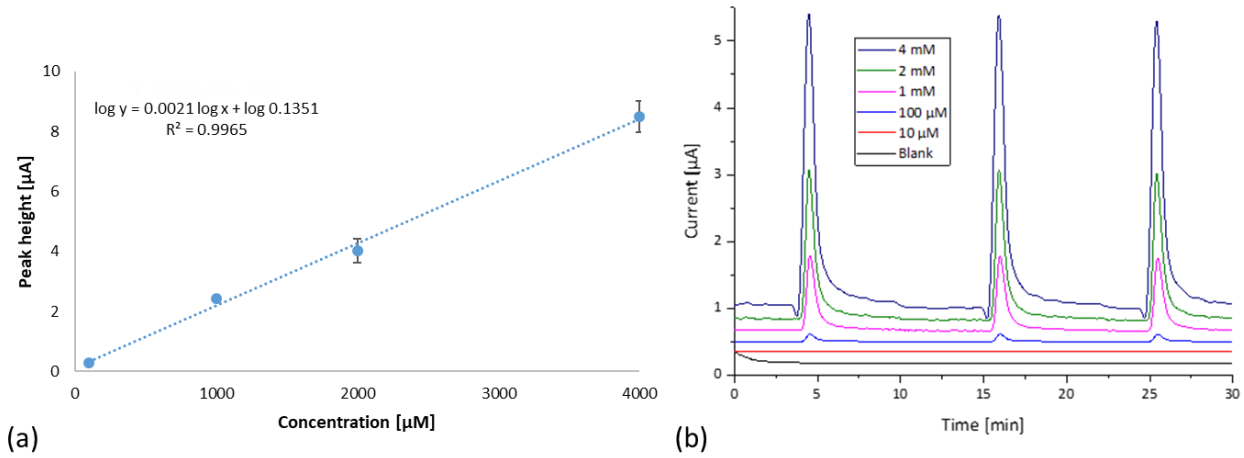

Fig. S38. (a) Calibration plot and (b) three repetitive continuous injections of 10 µM-4 mM ascorbic acid (2 µL mL^{-1} 25% NH_4OH to adjust pH 9-10) in HPLC-PAD. Conditions: see Fig. 20. PAD waveform: see Fig. 17.

5.4 % yield of GO

Table S12. Calculation of GO % yield (at endpoints of Fig. 19b and Fig. 20b) in gravimetric method (n= 3).

Graphene oxide (GO)	Using hydrazine	Using ascorbic acid
Weight of GO before reaction, W_b	1.50 ± 0.01 mg	1.50 ± 0.02 mg
Weight of reduced GO after reaction, W_a	0.79 ± 0.03 mg	0.51 ± 0.02 mg
% yield in gravimetric method ($\frac{W_a}{W_b} x\ 100$)	52 ± 1.70 %	34 ± 1.10 %

6. Extended study of GO reduction in IC-PAD

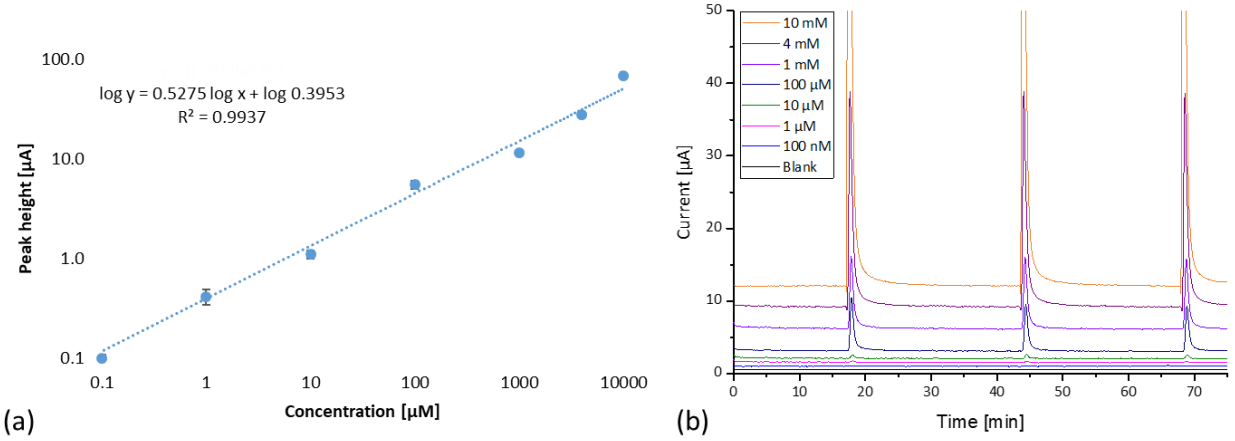

Fig. S39. (a) Calibration plot and (b) three repetitive continuous injections 100 nM-10 mM hydrazine (+ 0.25 M 30% NH_4OH at 80 ^{0}C) in IC-PAD. Conditions: solvent: 30 mM methanesulfonic acid, flow rate: 0.6 mL min^{-1}, sample volume 5 µL, IC column: IonPac CG16 and CS16 (length: 5 and 25 cm, i.d: 5 mm), column oven temperature: 30 ^{o}C, pressure: *ca.* 1015 psi (70 bar), capillary (column-gap-FC): i.d 100 µm (length: 7 cm), gap distance: 30 µm, and WE: ZrO_2-Pt. PAD waveform: see Fig. 17.

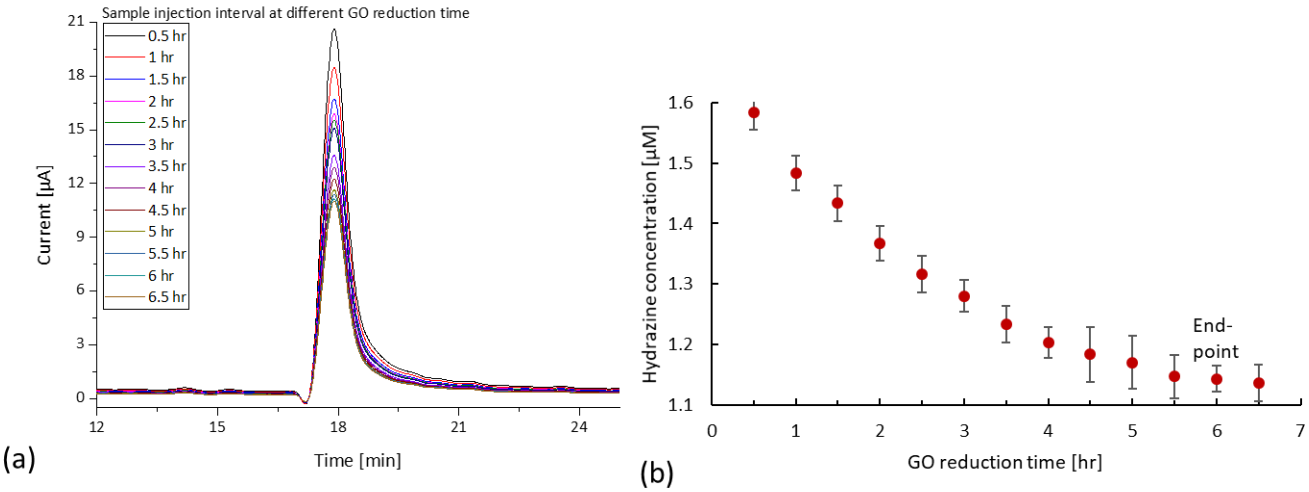

Fig. S40. Monitoring reduction of 2 mg mL^{-1} GO using 1.6 mM hydrazine (+ 0.25 M 30% NH_4OH at 80 ^{0}C) in IC-PAD showing (a) calibration plot and (b) determined hydrazine concentrations. Conditions: solvent: 30 mM methanesulfonic acid, flow rate: 0.6 mL min^{-1}, sample volume 5

µL, IC column: IonPac CG16 and CS16 (length: 5 and 25 cm, i.d: 5 mm), column oven temperature: 30 °C, pressure: *ca.* 1015 psi (70 bar), capillary (column-gap-FC): i.d 100 µm (length: 7 cm), gap distance: 30 µm, and WE: ZrO_2-Pt. PAD waveform: see Fig. 17. At 6 hr, the reaction does not proceed further although there is a small amount of hydrazine remaining in the solution.

Conclusions and future directions

In this program of research, an advanced miniaturised EC detection method for flow-based analytical systems has been explored, developed, characterised and applied. Advances have been achieved using this new miniaturised FC (i.e., gap-FC), which can be rapidly modified and used with highly stable disposable electrodes (i.e., ZrO_2 NPs-Au and -Pt), and with fast-pulsed waveforms (2-step, 20 ms, 50 Hz), within a variety of flow-based systems, from capillary to standard format systems. The key findings of this research and directions for further investigations are discussed below.

1. Miniaturised EC detector for capillary to standard analytical systems

The gap-FC, incorporating disposable electrodes, performed effectively as a robust and low cost (< $800) miniaturised EC detector for various flow-based analytical systems, such as FIA, capillary-LC, and standard-LC (see Chapter 3). The FC enabled very simple precise control of the gap distance (30 – 200 µm), for the formation of different thicknesses of the electrode layer. The gap-FC design delivered all of advantages of other widely used EC detectors (such as TL-FC and WJ-FC), with the added advantage of controlling the efficiency of EC conversion and effective cell volume, which can now be varied with gap distance and flow rate. Additionally, for the first time the gap-FC was applied in combination with different analytical systems, operating at flow rates from nano- to millilitre per minute range. In FIA, with adjustment to the lowest gap distance (30 µm) and lower flow rate (0.5 µL min^{-1}), the gap-FC achieved the highest efficiency (*ca.* 16-times) and lowest effective cell volume (35 nL) reported to-date. In capillary-LC, at a flow rate of 1 µL min^{-1} and a gap distance of 30 µm, the gap-FC was shown to be up to one order of magnitude more sensitive than a UV detector under similar conditions for a series of test solutes. In standard-LC, at a high flow rate 0.6 mL min^{-1} and a gap distance of 30 µm, the sensitivity for test solutes was four- to 25-times greater than those reported to-date using alternative EC and UV detectors. This study also demonstrated for the first time that current can be maximised with the lowest gap distance (30 µm) and can be further increased with an increase of flow rate.

2. Rapidly modified and highly stable electrodes for sensitive detection

Rapidly modified and highly stable disposable electrodes were investigated for improved performance of the gap-FC (see Chapter 4). A simple and low-cost electrode-modification process has been demonstrated in this study, only requiring approximately 10 minutes to evaporate the suspension (10 µL aliquot of filtered ZrO_2 NPs/H_2O) from the electrode surface at room temperature (20°C). The effective surface area of the electrodes (bare and modified), EC reversibility, and the stability of the modified electrodes in continuous flow have been experimentally determined for the first time. This investigation determined that the current obtained in EC detection is influenced by the effective surface area, rather than the geometrical surface area of the electrode. A 100% increase of effective surface area, 95- to 180-fold increase in current, and EC reversibility were achieved using the modified electrodes due to the formation of a porous electrode surface and minimisation of the capacitance of the double layer using ZrO_2 NPs. The highest (8.5 hours) stability for modified electrodes under continuous flow conditions, with twice higher sensitivity to the test solutes than that reported to-date, was achieved. These investigations also showed that modified electrodes can be used as a replacement for bare electrodes in gap-FC to overcome the limitations of measuring effective cell volume and EC conversion efficiency, when the flow rate is less than 0.1 µL min^{-1} (see Chapter 3).

3. Fast-pulsed waveform for miniaturised flow-through EC detection

A fast-pulsed waveform (2-step, 20 ms, 50 Hz) for use within the gap-FC and with the developed disposable modified electrodes was investigated to further advance miniaturised EC detection for flow-based analytical systems (see Chapter 5). The developed

high-frequency waveform (15- to 45-times faster than previously reported) showed benefits for use with fast flow-through systems (such as FIA, LC, and IC in this study), significantly reducing the loss of useful data by replacing long cleaning steps (such as 560 ms) with a step of just 10 ms, and reducing experimental parameters (including electrode surface area, flow rate, and sample volume) five- to 20-fold, compared to previous studies reported in the literature. This high frequency waveform resulted reduced integration time, reduced the formation of surface oxide layers, and demonstrated the highest (*ca*. 5 hr) electrode stability in continuous flow compared to previous reported waveforms. The waveform improves the electroactivity of the electrode and provided rapid establishment of baseline stability, providing the highest sensitivity (*ca.* five times), and lowest LODs (*ca.* 100 times) for the test solute (i.e., hydrazine) reported to date. The benefits of the advanced miniaturised EC detection system were demonstrated by overcoming the contradictory reports of consumption of reducing agents, reduction endpoints, and yield % for different GO reducing agents.

4. Future directions

The advanced miniaturised EC detection system described, developed and applied herein will certainly be beneficial for wider research and development in the fields of analytical, bioanalytical and chemical sciences. Our studies have highlighted how further investigations could include the following directions:

- The rapidly modified and highly stable electrode as EC sensor could be advantageous for rapid, portable and on-the-fly alkane gas detection in combination with microcontrollers in large emission sites such as bushfire sites, mining sites and landfills.
- The fast-pulsed waveform could be of great benefit in reducing the loss of data collection in fast-eluting flow-based analytical systems. The system may be useful for gas sensing, where large data collection is still very challenging. Some interesting applications of the system could be in photocatalysis and wastewater treatment.
- The system could be applied for pharmaceutical and biomedical sample analysis and could be an ideal alternative for the numerous analytical methods where specific reagents and/or complex derivatization processes are required, or which suffer from significant matrix effects in real samples.
- The system could be utilised for environmental sample analysis (such as surface water, sea water, waste water, sediment, and soil) and may thus assist in further studies targeted at lower-cost and less time-consuming detection processes for Perfluoroalkyl acids (PFAAs) than the regularly used LC-MS system. LC-MS is effective for PFAA analysis but is a very expensive and time-consuming process to perform, and typically not suited to portable or at-site analysis.
- The system could be employed for EC detection of antimicrobials such as tetracyclines.
- Other metal-oxide NM-modified microelectrodes could be of great benefit for analysis of environmental samples.
- The system could be applied to investigate the reduction kinetics and the order of the reaction for various reducing agents utilised for the reduction of GO.
- A compact advanced miniaturised EC detection system could be developed by upgrading the current compact potentiostat (in the form of a USB stick directly connected to a smartphone) with complex pulsed amperometric waveform generation facilities.

References

[1] H. Gunasingham, Large-volume wall-jet cells as electrochemical detectors for high-performance liquid chromatography, Anal. Chim. Acta, 159 (1984) 139-147.

[2] P. Laevers, A. Hubin, H. Terryn, J. Vereecken, A wall-jet electrode reactor and its application to the study of electrode reaction mechanisms Part I: Design and construction, J. Appl. Electrochem., 25 (1995) 1017-1022.

[3] Y. Zhou, H. Yan, Q. Xie, S. Huang, J. Liu, Z. Li, M. Ma, S. Yao, Simultaneous analysis of dopamine and homovanillic acid by high-performance liquid chromatography with wall-jet/thin-layer electrochemical detection, Analyst, 138 (2013) 7246-7253.

[4] D.T. Chin, C.H. Tsang, Mass transfer to an impinging jet electrode, J. Electrochem. Soc., 125 (1978) 1461-1470.

[5] D.T. Chin, R.R. Chandran, Ring disk electrodes with an impinging jet, J. Electrochem. Soc., 128 (1981) 1904-1912.

[6] W.J. Albery, S. Bruckenstein, Uniformly accessible electrodes, J. Electroanal. Chem., 144 (1983) 105-112.

[7] K.C. Honeychurch, Design and application of liquid chromatography dual electrode detection, Electrochemistry, 13 (2016) 1-20.

[8] J. Yamada, H. Matsuda, Limiting diffusion currents in hydrodynamic voltammetry: III. Wall jet electrodes, J. Electroanal. Chem., 44 (1973) 189-198.

[9] Z. Niegreisz, L. Szücs, J. Fekete, G. Horvai, K. Tóth, E. Pungor, Modifications of the wall-jet electrochemical detector for liquid chromatography and flow analysis, J. Chromatogr., 316 (1984) 451-459.

[10] J. Krejci, I. Ventrubova, L. Jezova, J. Fischer, J. Barek, Testing of electrochemical efficiency of wall-jet cell FC2 as a tool for detection of electrochemically oxidisable biomarkers, Int. J. Electrochem. Sci., 10 (2015) 4922-4927.

[11] C. Wang, J. Du, H. Wang, C.e. Zou, F. Jiang, P. Yang, Y. Du, A facile electrochemical sensor based on reduced graphene oxide and Au nanoplates modified glassy carbon electrode for simultaneous detection of ascorbic acid, dopamine and uric acid, Sensors Actuators B: Chem., 204 (2014) 302-309.

[12] J.L. da Silva, M.A. Beluomini, N.R. Stradiotto, Determination of furanic aldehydes in sugarcane bagasse by high-performance liquid chromatography with pulsed amperometric detection using a modified electrode with nickel nanoparticles, J. Sep. Sci., 38 (2015) 3176-3182.

[13] R.A.S. Couto, J.L.F.C. Lima, M.B. Quinaz, Recent developments, characteristics and potential applications of screen-printed electrodes in pharmaceutical and biological analysis, Talanta, 146 (2016) 801-814.

[14] S.-W. Ui, I.-S. Choi, S.-C. Choi, Synthesis of high surface area mesoporous silica powder using anionic surfactant, ISRN Mater. Sci., 2014 (2014) 1-6.

[15] V.P. Hanko, J.S. Rohrer, Determination of tobramycin and impurities using high-performance anion exchange chromatography with integrated pulsed amperometric detection, J. Pharm. Biomed. Anal., 40 (2006) 1006-1012.

[16] J. Cheng, P. Jandik, N. Avdalovic, Pulsed amperometric detection of sulfide, cyanide, iodide, thiosulfate, bromide and thiocyanate with microfabricated disposable silver working electrodes in ion chromatography, Anal. Chim. Acta, 536 (2005) 267-274.

[17] D. Kotnik, M. Novič, W.R. LaCourse, B. Pihlar, Cathodic re-activation of the gold electrode in pulsed electrochemical detection of carbohydrates, J. Electroanal. Chem., 663 (2011) 30-35.

[18] I.G. Casella, M. Pierri, M. Contursi, Determination of acrylamide and acrylic acid by isocratic liquid chromatography with pulsed electrochemical detection, J. Chromatogr. A, 1107 (2006) 198-203.

[19] V. Carralero, A. González-Cortés, P. Yáñez-Sedeño, J. Pingarron, Pulsed amperometric detection of histamine at glassy carbon electrodes modified with gold nanoparticles, Electroanalysis, 17 (2005) 289-297.

[20] T. Charoenraks, S. Palaharn, K. Grudpan, W. Siangproh, O. Chailapakul, Flow injection analysis of doxycycline or chlortetracycline in pharmaceutical formulations with pulsed amperometric detection, Talanta, 64 (2004) 1247-1252.

[21] A. Guzmán, L. Agüí, M.a. Pedrero, P. Yáñez-Sedeño, J.M. Pingarrón, Flow injection and HPLC determination of furosemide using pulsed amperometric detection at microelectrodes, J. Pharm. Biomed. Anal., 33 (2003) 923-933.

[22] S. Ayaz, Y. Dilgin, Flow injection amperometric determination of hydrazine based on its electrocatalytic oxidation at pyrocatechol violet modified pencil graphite electrode, Electrochim. Acta, 258 (2017) 1086-1095.

[23] W. Dungchai, O. Chailapakul, C.S. Henry, Electrochemical detection for paper-based microfluidics, Anal. Chem., 81 (2009) 5821-5826.

[24] T. You, X. Yang, E. Wang, Applications of microelectrodes in capillary electrophoresis/electrochemical detection, Electroanalysis, 11 (1999) 459-464.

[25] P.T. Kissinger, C. Refshauge, R. Dreiling, R.N. Adams, An electrochemical detector for liquid chromatography with picogram sensitivity, Anal. Lett., 6 (1973) 465-477.

[26] W. Siangproh, W. Leesutthipornchai, W. Dungchai, O. Chailapakul, Electrochemical detection for flow-based system: A Review, J. Flow Injection Anal., 26 (2009) 5-25.

[27] W.R.t. Vandaveer, S.A. Pasas-Farmer, D.J. Fischer, C.N. Frankenfeld, S.M. Lunte, Recent developments in electrochemical detection for microchip capillary electrophoresis, Electrophoresis, 25 (2004) 3528-3549.

[28] L. Jiang, Y. Lu, Z. Dai, M. Xie, B. Lin, Mini-electrochemical detector for microchip electrophoresis, Lab Chip, 5 (2005) 930-934.

[29] M.A. Islam, P. Mahbub, P.N. Nesterenko, B. Paull, M. Macka, Prospects of pulsed amperometric detection in flow-based analytical systems - A review, Anal. Chim. Acta, 1052 (2019) 10-26.

[30] J. Fedorowski, W.R. LaCourse, A review of pulsed electrochemical detection following liquid chromatography and capillary electrophoresis, Anal. Chim. Acta, 861 (2015) 1-11.

[31] O. Niwa, M. Morita, B.P. Solomon, P.T. Kissinger, Carbon film based ring-disk and split-disk dual electrodes as detectors for microbore liquid chromatography, Electroanalysis, 8 (1996) 427-433.

[32] M. Patthy, R. Gynnge, J. Salát, Comparison of the design and performance charateristics of the wall-jet type and thin-layer type electrochemical detectors, J. Chromatogr., 241 (1982) 131-139.

[33] L. Szücs, G. Horvai, J. Fekete, B. Pungor, Band broadening in a wall-jet type electrochemical detector for liquid chromatography, Microchim. Acta, 96 (1988) 259-267.

[34] L.M. Ochiai, D. Agustini, L.C.S. Figueiredo-Filho, C.E. Banks, L.H. Marcolino-Junior, M.F. Bergamini, Electroanalytical thread-device for estriol determination using screen-printed carbon electrodes modified with carbon nanotubes, Sensors Actuators B: Chem., 241 (2017) 978-984.

[35] M. Castaño-Álvarez, M.T. Fernández-Abedul, A. Costa-García, Analytical performance of CE microchips with amperometric detection, Instrum Sci. Technol., 34 (2006) 697-710.

[36] M.A. Islam, S.C. Lam, P. Mahbub, P.N. Nesterenko, B. Paull, M. Macka, Electrochemical detection in miniaturised capillary separation platforms: Gap cell for amperometric detection for portable liquid chromatography, XVIII. Workshop of Biophysical Chemists and Electrochemists, Masaryk University, 2018, pp. 12.

[37] W.R. LaCourse, S.J. Modi, Microelectrode applications of pulsed electrochemical detection, Electroanalysis, 17 (2005) 1141-1152.

[38] S.Z. Mohammadi, H. Beitollahi, E.B. Asadi, Electrochemical determination of hydrazine using a ZrO_2 nanoparticles-modified carbon paste electrode, Environ. Monit. Assess., 187 (2015) 122.

[39] N. Mohammadizadeh, S.Z. Mohammadi, M. Kaykhaii, Highly sensitive amperometric detection of propranolol using graphite screen printed electrode modified with zirconium dioxide nanoparticles, Anal. Bioanal. Electrochem., 9 (2017) 277-285.

[40] G.A. Ruiz-Córdova, S. Khan, L.M. Gonçalves, M.I. Pividori, G. Picasso, T.S. Maria Del Pilar, Electrochemical sensing using magnetic molecularly imprinted polymer particles previously captured by a magneto-sensor, Talanta, 181 (2017) 19-23.

[41] M.A. Islam, M.A. Atia, M. Macka, B. Paull, P. Mahbub, Electrochemical characterisation of nanoparticulate zirconium dioxide-on-gold electrode for electrochemical detection in flow-based analytical systems, Electrochim. Acta, 318 (2019) 61-68.

[42] M.J. Fernández-Merino, L. Guardia, J.I. Paredes, S. Villar-Rodil, P. Solís-Fernández, A. Martínez-Alonso, J.M.D. Tascón, Vitamin C is an ideal substitute for hydrazine in the reduction of graphene oxide suspensions, J. Phys. Chem. C, 114 (2010) 6426-6432.

[43] M.A. Islam, A.N. Koreshkova, V. Gupta, T. Lewis, M. Macka, B. Paull, P. Mahbub, Fast pulsed amperometric waveform for miniaturised flow-through electrochemical detection: Application in monitoring graphene oxide reduction, Electrochim. Acta, 328 (2019) 135087.

[44] D.C. Johnson, S.G. Weber, A.M. Bond, R.M. Wightman, R.E. Shoup, I.S. Krull, Electroanalytical voltammetry in flowing solutions, Anal. Chim. Acta, 180 (1986) 187-250.

[45] P. Jandik, P.R. Haddad, P.E. Sturrock, Electrochemical detectors for ion chromatographic analysis: A critical review, Crit. Rev. Anal. Chem., 20 (1988) 1-74.

[46] W.R. LaCourse, Pulsed electrochemical detection in high performance liquid chromatography, Wiley, New York, 1997.

[47] P. Jandik, J. Cheng, N. Avdalovic, Analysis of amino acid–carbohydrate mixtures by anion exchange chromatography and integrated pulsed amperometric detection, J. Biochem. Bioph. Methods, 60 (2004) 191-203.

[48] M. Trojanowicz, Recent developments in electrochemical flow detections—a review: Part ii. Liquid chromatography, Anal. Chim. Acta, 688 (2011) 8-35.

[49] C. Corradini, A. Cavazza, C. Bignardi, High-performance anion-exchange chromatography coupled with pulsed electrochemical detection as a powerful tool to evaluate carbohydrates of food interest: Principles and applications, J. Carbohydr. Chem., 2012 (2012) 1-13.

[50] D.C. Harris, Quantitative chemical analysis, Seventh ed., W. H. Freeman and Company, New York, 2007.

[51] O.J. Guy, K.-A.D. Walker, Graphene functionalization for biosensor applications, in: S.E. Saddow (Ed.) Silicon carbide biotechnology, Elsevier 2016, pp. 85-141.

[52] P. Kissinger, W.R. Heineman, Laboratory Techniques in Electroanalytical Chemistry, revised and expanded, CRC press, Boca Raton, 1996.

[53] V.P. Hanko, W.R. Lacourse, C.O. Dasenbrock, J.S. Rohrer, Determination of sulfur-containing antibiotics using high-performance liquid chromatography with integrated pulsed amperometric detection, Drug Dev. Res., 53 (2001) 268-280.

[54] G.G. Neuburger, D.C. Johnson, Comparison of the pulsed amperometric detection of carbohydrates at gold and platinum electrodes for flow injection and liquid chromatographic systems, Anal. Chem., 59 (1987) 203-204.

[55] D.S. Austin-Harrison, D.C. Johnson, Pulsed amperometric detection based on direct and indirect anodic reactions: A review, Electroanalysis, 1 (1989) 189-197.

[56] M.P. Olson, L.R. Keating, W.R. LaCourse, Indirect pulsed electrochemical detection of amino acids and proteins following high performance liquid chromatography, Anal. Chim. Acta, 652 (2009) 198-204.

[57] W.C. Silva, P.F. Pereira, M.C. Marra, D.T. Gimenes, R.R. Cunha, R.A.B. da Silva, R.A.A. Munoz, E.M. Richter, A simple strategy for simultaneous determination of paracetamol and caffeine using flow injection analysis with multiple pulse amperometric detection, Electroanalysis, 23 (2011) 2764-2770.

[58] E. Katz, I. Willner, J. Wang, Electroanalytical and bioelectroanalytical systems based on metal and semiconductor nanoparticles, Electroanalysis, 16 (2004) 19-44.

[59] W.R. LaCourse, D.C. Johnson, Optimization of waveforms for pulsed amperometric detection (PAD) of carbohydrates following separation by liquid chromatography, Carbohydr. Res., 215 (1991) 159-178.

[60] T.J. Paskach, H.-P. Lieker, P.J. Reilly, K. Thielecke, High-performance anion-exchange chromatography of sugars and sugar alcohols on quaternary ammonium resins under alkaline conditions, Carbohydr. Res., 215 (1991) 1-14.

[61] P. Edwards, K. Haak, A pulsed amperometric detector for ion chromatography, Am. Lab., 15 (1983) 78.

[62] J. Polta, D. Johnson, The direct electrochemical detection of amino acids at a platinum electrode in an alkaline chromatographic effluent, J. Liq. Chromatogr., 6 (1983) 1727-1743.

[63] J.A. Polta, D.C. Johnson, K.E. Merkel, Liquid chromatographic separation of aminoglycosides with pulsed amperometric detection, J. Chromatogr. A, 324 (1985) 407-414.

[64] D. Gilroy, Oxide growth at platinum electrodes in H2SO4 at potentials below 1.7 V, J. Electroanal. Chem., 71 (1976) 257-277.

[65] T.Z. Polta, D.C. Johnson, Pulsed amperometric detection of sulfur compounds: Part i. Initial studies of platinum electrodes in alkaline solutions, J. Electroanal. Chem., 209 (1986) 159-169.

[66] D.G. Williams, D.C. Johnson, Pulsed voltammetric detection of arsenic (III) at platinum electrodes in acidic media, Anal. Chem., 64 (1992) 1785-1789.

[67] J.K. Sanders, Pulsed Electrochemical Detection in High-Performance Liquid Chromatography (LaCourse, William R.), J. Chem. Educ., 75 (1998) 1555.

[68] M.E. Johll, D.G. Williams, D.C. Johnson, Activated pulsed amperometric detection of cysteine at platinum electrodes in acidic media, Electroanalysis, 9 (1997) 1397-1402.

[69] R.D. Rocklin, A.P. Clarke, M. Weitzhandler, Improved long-term reproducibility for pulsed amperometric detection of carbohydrates via a new quadruple-potential waveform, Anal. Chem., 70 (1998) 1496-1501.

[70] W.R. LaCourse, Pulsed electrochemical detection: waveform evolution, LC GC North America, 29 (2011) 584-593.

[71] P.J. Vandeberg, D.C. Johnson, Pulsed electrochemical detection of cysteine, cystine, methionine, and glutathione at gold electrodes following their separation by liquid chromatography, Anal. Chem., 65 (1993) 2713-2718.

[72] R.W. Andrews, R.M. King, Selection of potentials for pulsed amperometric detection of carbohydrates at gold electrodes, Anal. Chem., 62 (1990) 2130-2134.

[73] L.E. Welch, W.R. LaCourse, D.A. Mead, D.C. Johnson, T. Hu, Comparison of pulsed coulometric detection and potential-sweep-pulsed coulometric detection for underivatized amino acids in liquid chromatography, Anal. Chem., 61 (1989) 555-559.

[74] A.P. Clarke, P. Jandik, R.D. Rocklin, Y. Liu, N. Avdalovic, An integrated amperometry waveform for the direct, sensitive detection of amino acids and amino sugars following anion-exchange chromatography, Anal. Chem., 71 (1999) 2774-2781.

[75] T.R.I. Cataldi, C. Campa, G.E. De Benedetto, Carbohydrate analysis by high-performance anion-exchange chromatography with pulsed amperometric detection: The potential is still growing, Fresenius J. Anal. Chem., 368 (2000) 739-758.

[76] W. Torres Pio dos Santos, E.G. Nascimento de Almeida, A. Ferreira, H. Eustáquio, D.T. Gimenes, E.M. Richter, Simultaneous flow injection analysis of paracetamol and ascorbic acid with multiple pulse amperometric detection, Electroanalysis, 20 (2008) 1878-1883.

[77] S.C. Chaves, P.N.C. Aguiar, L.M.F.C. Torres, E.S. Gil, R.C.S. Luz, F.S. Damos, R.A.A. Munoz, E.M. Richter, W.T.P. dos Santos, Simultaneous determination of caffeine, ibuprofen, and paracetamol by flow-injection analysis with multiple-pulse amperometric detection on boron-doped diamond electrode, Electroanalysis, 27 (2015) 2785-2791.

[78] D.T. Gimenes, W.T.P. dos Santos, R.A.A. Munoz, E.M. Richter, Internal standard in flow injection analysis with amperometric detection, Electrochem. Commun., 12 (2010) 216-218.

[79] B. Fleet, C.J. Little, Design and evaluation of electrochemical detectors for HPLC, J. Chromatogr. Sci., 12 (1974) 747-752.

[80] H. Gunasingham, T. Chin-Huat, Conducting organic salt amperometric glucose sensor in continuous-flow monitoring using a wall-jet cell, Anal. Chim. Acta, 229 (1990) 83-91.

[81] H. Gunasingham, K. Ang, C. Ngo, Stripping voltammetry of thin mercury films at the wall-jet electrode, Anal. Chem., 57 (1985) 505-508.

[82] W.J. Albery, C.M. Brett, The wall-jet ring-disc electrode: Part I. Theory, J. Electroanal. Chem., 148 (1983) 201-210.

[83] H. Gunasingham, B. Fleet, Wall-jet electrode in continuous monitoring voltammetry, Anal. Chem., 55 (1983) 1409-1414.

[84] Y.L. Huang, S.B. Khoo, M.G. Yap, Flow-injection analysis—wall-jet electrode system for monitoring glucose and lactate in fermentation broths, Anal. Chim. Acta, 283 (1993) 763-771.

[85] J. Wang, H.D. Dewald, A Porous-jet Flow-through electrode, Talanta, 29 (1982) 453-456.

[86] G.G. Neuburger, D.C. Johnson, Pulsed coulometric detection of carbohydrates at a constant detection potential at gold electrodes in alkaline media, Anal. Chim. Acta, 192 (1987) 205-213.

[87] R.E. Roberts, D.C. Johnson, Variation in PED response at a gold microelectrode as a function of waveform parameters when applied to alditols and carbohydrates separated by capillary electrophoresis, Electroanalysis, 7 (1995) 1015-1019.

[88] M.B. Jensen, D.C. Johnson, Fast wave forms for pulsed electrochemical detection of glucose by incorporation of reductive desorption of oxidation products, Anal. Chem., 69 (1997) 1776-1781.

[89] J.O. Howell, R.M. Wightman, Ultrafast voltammetry and voltammetry in highly resistive solutions with microvoltammetric electrodes, Anal. Chem., 56 (1984) 524-529.

[90] T.K. Chen, Y.Y. Lau, D.K. Wong, A.G. Ewing, Pulse voltammetry in single cells using platinum microelectrodes, Anal. Chem., 64 (1992) 1264-1268.

[91] T.J. O'Shea, S.M. Lunte, W.R. LaCourse, Detection of carbohydrates by capillary electrophoresis with pulsed amperometric detection, Anal. Chem., 65 (1993) 948-951.

[92] W. Lu, R.M. Cassidy, Pulsed amperometric detection of carbohydrates separated by capillary electrophoresis, Anal. Chem., 65 (1993) 2878-2881.

[93] P.L. Weber, T. Kornfelt, N. Klausen, S.M. Lunte, Characterization of glycopeptides from recombinant coagulation factor VIIa by high-performance liquid chromatography and capillary zone electrophoresis using ultraviolet and pulsed electrochemical detection, Anal. Biochem., 225 (1995) 135-142.

[94] L.A. Holland, S.M. Lunte, Capillary electrophoresis coupled to electrochemical detection: A review of recent advances, Anal. Commun., 35 (1998) 1H-4H.

[95] W.R. Lacourse, G.S. Owens, Pulsed electrochemical detection of nonchromophoric compounds following capillary electrophoresis, Electrophoresis, 17 (1996) 310-318.

[96] C.D. García, C.S. Henry, Coupling capillary electrophoresis and pulsed electrochemical detection, Electroanalysis, 17 (2005) 1125-1131.

[97] A. Paulus, A. Klockow, Detection of carbohydrates in capillary electrophoresis, J. Chromatogr. A, 720 (1996) 353-376.

[98] J. Cheng, P. Jandik, N. Avdalovic, Use of disposable gold working electrodes for cation chromatography–integrated pulsed amperometric detection of sulfur-containing amino acids, J. Chromatogr. A, 997 (2003) 73-78.

[99] L. Liang, Y. Cai, S. Mou, J. Cheng, Comparisons of disposable and conventional silver working electrode for the determination of iodide using high-performance anion-exchange chromatography with pulsed amperometric detection, J. Chromatogr. A, 1085 (2005) 37-41.

[100] J. Cheng, P. Jandik, X. Liu, C. Pohl, Pulsed amperometric detection waveform with disposable thin-film platinum working electrodes in high performance liquid chromatography, J. Electroanal. Chem., 608 (2007) 117-124.

[101] K. Sato, J.-Y. Jin, T. Takeuchi, T. Miwa, K. Suenami, Y. Takekoshi, S. Kanno, Integrated pulsed amperometric detection of glufosinate, bialaphos and glyphosate at gold electrodes in anion-exchange chromatography, J. Chromatogr. A, 919 (2001) 313-320.

[102] C. Thiele, M. Gänzle, R. Vogel, Sample preparation for amino acid determination by integrated pulsed amperometric detection in foods, Anal. Biochem., 310 (2002) 171-178.

[103] D.A. Martens, K.L. Loeffelmann, Soil amino acid composition quantified by acid hydrolysis and anion chromatography–pulsed amperometry, J. Agric. Food. Chem., 51 (2003) 6521-6529.

[104] T.R. Cataldi, G. Telesca, G. Bianco, Improved determination of taurine by high-performance anion-exchange chromatography with integrated pulsed amperometric detection (HPAEC-IPAD), Anal. Bioanal. Chem., 378 (2004) 804-810.

[105] J.D. Russell, J.M. Dolphin, M.D. Koppang, Selective analysis of secondary amino acids in gelatin using pulsed electrochemical detection, Anal. Chem., 79 (2007) 6615-6621.

[106] X. Sun, X. Yang, E. Wang, Determination of biogenic amines by capillary electrophoresis with pulsed amperometric detection, J. Chromatogr. A, 1005 (2003) 189-195.

[107] R. Possari, R.F. Carvalhal, R.K. Mendes, L.T. Kubota, Electrochemical detection of cysteine in a flow system based on reductive desorption of thiols from gold, Anal. Chim. Acta, 575 (2006) 172-179.

[108] B.M. De Borba, J.S. Rohrer, Determination of biogenic amines in alcoholic beverages by ion chromatography with suppressed conductivity detection and integrated pulsed amperometric detection, J. Chromatogr. A, 1155 (2007) 22-30.

[109] G. Favaro, P. Pastore, G. Saccani, S. Cavalli, Determination of biogenic amines in fresh and processed meat by ion chromatography and integrated pulsed amperometric detection on Au electrode, Food Chem., 105 (2007) 1652-1658.

[110] A. Wong, A.M. Santos, O. Fatibello-Filho, Simultaneous determination of dopamine and cysteamine by flow injection with multiple pulse amperometric detection using a boron-doped diamond electrode, Diamond Relat. Mater., 85 (2018) 68-73.

[111] M. Oh, E. Huh, M.S. Oh, J.S. Jeong, S.P. Hong, Development of a diagnostic method for Parkinson's disease by reverse-phase high-performance liquid chromatography coupled with integrated pulsed amperometric detection, J. Pharm. Biomed. Anal., 153 (2018) 110-116.

[112] E. Adams, J. Dalle, E. De Bie, I. De Smedt, E. Roets, J. Hoogmartens, Analysis of kanamycin sulfate by liquid chromatography with pulsed electrochemical detection, J. Chromatogr. A, 766 (1997) 133-139.

[113] E. Adams, D. Puelings, M. Rafiee, E. Roets, J. Hoogmartens, Determination of netilmicin sulfate by liquid chromatography with pulsed electrochemical detection, J. Chromatogr. A, 812 (1998) 151-157.

[114] K. Kaiser, R. Benner, Determination of amino sugars in environmental samples with high salt content by high-performance anion-exchange chromatography and pulsed amperometric detection, Anal. Chem., 72 (2000) 2566-2572.

[115] J. Szunyog, E. Adams, E. Roets, J. Hoogmartens, Analysis of tobramycin by liquid chromatography with pulsed electrochemical detection, J. Pharm. Biomed. Anal., 23 (2000) 891-896.

[116] J. Szunyog, E. Adams, K. Liekens, E. Roets, J. Hoogmartens, Analysis of a formulation containing lincomycin and spectinomycin by liquid chromatography with pulsed electrochemical detection, J. Pharm. Biomed. Anal., 29 (2002) 213-220.

[117] D. Debremaeker, E. Adams, E. Nadal, B. Van Hove, E. Roets, J. Hoogmartens, Analysis of spectinomycin by liquid chromatography with pulsed electrochemical detection, J. Chromatogr. A, 953 (2002) 123-132.

[118] S. Palaharn, T. Charoenraks, N. Wangfuengkanagul, K. Grudpan, O. Chailapakul, Flow injection analysis of tetracycline in pharmaceutical formulation with pulsed amperometric detection, Anal. Chim. Acta, 499 (2003) 191-197.

[119] L. Xi, G. Wu, Y. Zhu, Analysis of etimicin sulfate by liquid chromatography with pulsed amperometric detection, J. Chromatogr. A, 1115 (2006) 202-207.

[120] N. Zawilla, J. Diana, J. Hoogmartens, E. Adams, Analysis of neomycin using an improved liquid chromatographic method combined with pulsed electrochemical detection, J. Chromatogr. B, 833 (2006) 191-198.

[121] N.H. Zawilla, B. Li, J. Hoogmartens, E. Adams, Improved reversed-phase liquid chromatographic method combined with pulsed electrochemical detection for the analysis of amikacin, J. Pharm. Biomed. Anal., 43 (2007) 168-173.

[122] G. Brajanoski, J. Hoogmartens, K. Allegaert, E. Adams, Determination of amikacin in cerebrospinal fluid by high-performance liquid chromatography with pulsed electrochemical detection, J. Chromatogr. B, 867 (2008) 149-152.

[123] V. Manyanga, J. Hoogmartens, E. Adams, Development and validation of an improved reversed-phase liquid chromatographic method combined with pulsed electrochemical detection for the analysis of netilmicin, J. Sep. Sci., 33 (2010) 1897-1903.

[124] Y. Yuan, S. Chopra, X. Deng, M. Zhang, X. Fan, C. Hu, S. Jin, A. Van Schepdael, E. Adams, Analysis of micronomicin by liquid chromatography with pulsed electrochemical detection, J. Chromatogr. A, 1295 (2013) 90-98.

[125] T.R. Cataldi, G. Margiotta, L. Iasi, B. Di Chio, C. Xiloyannis, S.A. Bufo, Determination of sugar compounds in olive plant extracts by anion-exchange chromatography with pulsed amperometric detection, Anal. Chem., 72 (2000) 3902-3907.

[126] N. Torto, B. Lobelo, L. Gorton, Determination of saccharides in wastewater from the beverage industry by microdialysis sampling, microbore high performance anion exchange chromatography and integrated pulsed electrochemical detection, Analyst, 125 (2000) 1379-1381.

[127] R.L. Marple, X. Li, W.R. LaCourse, Pulsed electrochemical detection of aryl- and alkylglycosides following reversed-phase liquid chromatography, J. Liq. Chromatogr. Rel. Technol., 27 (2004) 1695-1710.

[128] C.D. García, C.S. Henry, Enhanced determination of glucose by microchip electrophoresis with pulsed amperometric detection, Anal. Chim. Acta, 508 (2004) 1-9.

[129] Y. Cai, J. Liu, Y. Shi, L. Liang, S. Mou, Determination of several sugars in serum by high-performance anion-exchange chromatography with pulsed amperometric detection, J. Chromatogr. A, 1085 (2005) 98-103.

[130] C.D. García, G. Engling, P. Herckes, J.L. Collett, C.S. Henry, Determination of levoglucosan from smoke samples using microchip capillary electrophoresis with pulsed amperometric detection, Environ. Sci. Technol., 39 (2005) 618-623.

[131] G. Engling, C.M. Carrico, S.M. Kreidenweis, J.L. Collett Jr, D.E. Day, W.C. Malm, E. Lincoln, W.M. Hao, Y. Iinuma, H. Herrmann, Determination of levoglucosan in biomass combustion aerosol by high-performance anion-exchange chromatography with pulsed amperometric detection, Atmos. Environ., 40 (2006) 299-311.

[132] J.-S. Jeong, H.-J. Kwon, Y.-M. Lee, H.-R. Yoon, S.-P. Hong, Determination of sugar phosphates by high-performance anion-exchange chromatography coupled with pulsed amperometric detection, J. Chromatogr. A, 1164 (2007) 167-173.

[133] A.P. Ranwala, W.B. Miller, Analysis of nonstructural carbohydrates in storage organs of 30 ornamental geophytes by high-performance anion-exchange chromatography with pulsed amperometric detection, New Phytol., 180 (2008) 421-433.

[134] H.-J. Sim, J.-S. Jeong, H.-J. Kwon, T.H. Kang, H.M. Park, Y.-M. Lee, S.Y. Kim, S.-P. Hong, HPLC with pulsed amperometric detection for sorbitol as a biomarker for diabetic neuropathy, J. Chromatogr. B, 877 (2009) 1607-1611.

[135] N.-H. Kim, J.-S. Jeong, H.-J. Kwon, Y.-M. Lee, H.-R. Yoon, K.R. Lee, S.-P. Hong, Simultaneous diagnostic method for phenylketonuria and galactosemia from dried blood spots using high-performance liquid chromatography-pulsed amperometric detection, J. Chromatogr. B, 878 (2010) 1860-1864.

[136] C.A. Fisher, T. Christison, M. Verma, H. Yang, L. Lopez, Fast determination of lactose and lactulose in dairy products using a 4 mu m particle column and high-performance anion-exchange chromatography with pulsed amperometric detection, Abstracts of Papers of the American Chemical Society, 247 (2014).

[137] H. Lee, V.L. de MeloSilva, Y. Liu, D. Barile, Short communication: Quantification of carbohydrates in whey permeate products using high-performance anion-exchange chromatography with pulsed amperometric detection, J Dairy Sci., 98 (2015) 7644-7649.

[138] M.A. Khan, M. Nadeem, A. Rakha, S. Shakoor, A. Shehzad, M.R. Khan, Structural characterization of oat bran (1→3), (1→4)-β-d-glucans by lichenase hydrolysis through high-performance anion exchange chromatography with pulsed amperometric detection, Int. J. Food Prop., 19 (2016) 929-935.

[139] D.J. Ellingson, P. Anderson, D.P. Berg, Analytical method for sugar profile in pet food and animal feeds by high-performance anion-exchange chromatography with pulsed amperometric detection, J. AOAC Int., 99 (2016) 342-352.

[140] D. Zhao, F. Feng, F. Yuan, J. Su, Y. Cheng, H. Wu, K. Song, B. Nie, L. Yu, F. Zhang, Simultaneous determination of 13 carbohydrates using high-performance anion-exchange chromatography coupled with pulsed amperometric detection and mass spectrometry, J. Sep. Sci., 40 (2017) 1843-1854.

[141] Y. Zhang, J.R. Wu, Q.H. Ni, H. Dong, Multicomponent quantification of astragalus residue fermentation liquor using ion chromatography-integrated pulsed amperometric detection, Exp. Ther. Med., 14 (2017) 1526-1530.

[142] H. Lin, S.X. Li, C.X. Xu, M.L. Pang, S.L. Wang, Simultaneous determination of galactose, glucose, lactose and galactooligosaccharides in galactooligosaccharides raw materials by highperformance anion-exchange chromatography with pulsed amperometric detection, Food Chem., 263 (2018) 29-36.

[143] C.O. Dasenbrock, W.R. LaCourse, Assay for cephapirin and ampicillin in raw milk by high-performance liquid chromatography − integrated pulsed amperometric detection, Anal. Chem., 70 (1998) 2415-2420.

[144] W.R. LaCourse, C.O. Dasenbrock, Pulsed electrochemical detection of sulfur-containing antibiotics following high performance liquid chromatography, J. Pharm. Biomed. Anal., 19 (1999) 239-252.

[145] S.J. Modi, W.R. LaCourse, R.E. Shansky, Determination of thio-based additives for biopharmaceuticals by pulsed electrochemical detection following HPLC, J. Pharm. Biomed. Anal., 37 (2005) 19-25.

[146] N. Torto, L. Gorton, G. Marko-Varga, T. Laurell, On-Line Monitoring of Enzymatic Bioprocesses by Microdialysis Sampling, Anion Exchange Chromatography, and Integrated Pulsed Electrochemical Detection, in: G.M. Campbell, C. Webb, S.L. McKee (Eds.) Cereals: Novel Uses and Processes, Springer US, Boston, MA, 1997, pp. 63-67.

[147] K. Koch, R. Andersson, P. Åman, Quantitative analysis of amylopectin unit chains by means of high-performance anion-exchange chromatography with pulsed amperometric detection, J. Chromatogr. A, 800 (1998) 199-206.

[148] W. Ohtani, T. Ohda, A. Sumi, K. Kobayashi, T. Ohmura, Analysis of Pichia pastoris components in recombinant human serum albumin by immunological assays and by HPLC with pulsed amperometric detection, Anal. Chem., 70 (1998) 425-429.

[149] S. Ballance, S. Holtan, O.A. Aarstad, P. Sikorski, G. Skjåk-Bræk, B.E. Christensen, Application of high-performance anion-exchange chromatography with pulsed amperometric detection and statistical analysis to study oligosaccharide distributions–a complementary method to investigate the structure and some properties of alginates, J. Chromatogr. A, 1093 (2005) 59-68.

[150] T. Toropainen, P. Jarho, M. Lehtonen, P. Keski-Rahkonen, H. Raatikainen, T. Järvinen, Quantitative analysis of natural cyclodextrins by high-performance liquid chromatography with pulsed amperometric detection: Application to cell permeation study, J. Chromatogr. B, 867 (2008) 90-98.

[151] T.A. Stadheim, H. Li, W. Kett, I.N. Burnina, T.U. Gerngross, Use of high-performance anion exchange chromatography with pulsed amperometric detection for O-glycan determination in yeast, Nat. Protoc., 3 (2008) 1026.

[152] H.-J. Kwon, J.-H. Park, G.-T. Kim, Y.-D. Park, Determination of madecassoside and asiaticoside contents of C. asiatica leaf and C. asiatica-containing ointment and dentifrice by HPLC-coupled pulsed amperometric detection, Microchem. J., 98 (2011) 115-120.

[153] Z. Zhang, N.M. Khan, K.M. Nunez, E.K. Chess, C.M. Szabo, Complete monosaccharide analysis by high-performance anion-exchange chromatography with pulsed amperometric detection, Anal. Chem., 84 (2012) 4104-4110.

[154] M. Rothenhöfer, M. Grundmann, G. Bernhardt, F.-M. Matysik, A. Buschauer, High performance anion exchange chromatography with pulsed amperometric detection (HPAEC-PAD) for the sensitive determination of hyaluronan oligosaccharides, J. Chromatogr. B, 988 (2015) 106-115.

[155] D. Wefers, M. Bunzel, Arabinan and galactan oligosaccharide profiling by high-performance anion-exchange chromatography with pulsed amperometric detection, J. Agric. Food Chem., 64 (2016) 4656-4664.

[156] A. Lie, L.H. Pedersen, Analysis of human milk oligosaccharides using high-performance anion-exchange chromatography with pulsed amperometric detection, 11th Danish Conference on Biotechnology and Molecular Biology, 2016.

[157] N. Anders, H. Humann, B. Langhans, A.C. Spieß, Simultaneous determination of acid-soluble biomass-derived compounds using high performance anion exchange chromatography coupled with pulsed amperometric detection, Anal. Methods, 7 (2015) 7866-7873.

[158] D. Bavol, A. Economou, J. Zima, J. Barek, H. Dejmkova, Simultaneous determination of sinapic acid and tyrosol by flow-injection analysis with multiple-pulse amperometric detection, Monatsh. Chem., 149 (2018) 1679-1684.

[159] G.D. da Silveira, M.J. Motta, L.S. Müller, O. Lameira, M.L. Athayde, M. Piana, M.B.d. Rosa, C. Viana, L.M. de Carvalho, Determination of phenolic antioxidants in Amazonian medicinal plants by HPLC with pulsed amperometric detection, J. Liq. Chromatogr. Rel. Technol., 38 (2015) 1259-1266.

[160] Y. Ding, C.D. Garcia, Pulsed amperometric detection with poly(dimethylsiloxane)-fabricated capillary electrophoresis microchips for the determination of EPA priority pollutants, Analyst, 131 (2006) 208-214.

[161] A. Natale, D. Nardiello, C. Palermo, M. Muscarella, M. Quinto, D. Centonze, Development of an analytical method for the determination of polyphenolic compounds in vegetable origin samples by liquid chromatography and pulsed amperometric detection at a glassy carbon electrode, J. Chromatogr. A, 1420 (2015) 66-73.

[162] Y. Ding, C.D. Garcia, Determination of nonsteroidal anti-inflammatory drugs in serum by microchip capillary electrophoresis with electrochemical detection, Electroanalysis, 18 (2006) 2202-2209.

[163] L.R. Keating, W.R. LaCourse, Indirect pulsed electrochemical detection of aliphatic carboxylate-containing analytes following high performance anion-exchange chromatography, Talanta, 146 (2016) 594-602.

[164] C.D. García, C.S. Henry, Direct determination of carbohydrates, amino acids, and antibiotics by microchip electrophoresis with pulsed amperometric detection, Anal. Chem., 75 (2003) 4778-4783.

[165] R.A. Medeiros, B.C. Lourencao, R.C. Rocha-Filho, O. Fatibello-Filho, Flow injection simultaneous determination of synthetic colorants in food using multiple pulse amperometric detection with a boron-doped diamond electrode, Talanta, 99 (2012) 883-889.

[166] I.G. Casella, M. Gatta, Determination of aliphatic organic acids by high-performance liquid chromatography with pulsed electrochemical detection, J. Agric. Food. Chem., 50 (2002) 23-28.

[167] I.G. Casella, M. Contursi, Quantitative analysis of acrolein in heated vegetable oils by liquid chromatography with pulsed electrochemical detection, J. Agric. Food. Chem., 52 (2004) 5816-5821.

[168] S. Ngamchana, W. Surareungchai, Sub-millimolar determination of formalin by pulsed amperometric detection, Anal. Chim. Acta, 510 (2004) 195-201.

[169] T. Charoenraks, S. Chuanuwatanakul, K. Honda, Y. Yamaguchi, O. Chailapakul, Analysis of tetracycline antibiotics using HPLC with pulsed amperometric detection, Anal. Sci., 21 (2005) 241-245.

[170] R. Kaushik, W.R. LaCourse, B. Levine, Determination of ethyl glucuronide in urine using reversed-phase HPLC and pulsed electrochemical detection (Part II), Anal. Chim. Acta, 556 (2006) 267-274.

[171] T.R. Cataldi, D. Nardiello, R. Ciriello, A. Guerrieri, Pulsed electrochemical detection of orotic acid by an activated potential waveform at a gold working electrode following anion-exchange chromatography, J. Chromatogr. A, 1107 (2006) 130-138.

[172] T.T. Christison, J.S. Rohrer, Direct determination of free cyanide in drinking water by ion chromatography with pulsed amperometric detection, J. Chromatogr. A, 1155 (2007) 31-39.

[173] J. Ortuño, A. Gil, C. Sanchez-Pedreno, Flow-injection pulse amperometric detection based on ion transfer across a water-plasticized polymeric membrane interface for the determination of imipramine, Sensors Actuators B: Chem., 122 (2007) 369-374.

[174] J.A. Ortuño, C. Rueda, Flow-injection amperometric determination of tacrine based on ion transfer across a water–plasticized polymeric membrane interface, Sensors, 7 (2007) 1185-1192.

[175] R.A. Medeiros, B.C. Lourencao, R.C. Rocha-Filho, O. Fatibello-Filho, Simple flow injection analysis system for simultaneous determination of phenolic antioxidants with multiple pulse amperometric detection at a boron-doped diamond electrode, Anal. Chem., 82 (2010) 8658-8663.

[176] H.-J. Kwon, Y.-D. Park, Determination of astragalin and astragaloside content in Radix Astragali using high-performance liquid chromatography coupled with pulsed amperometric detection, J. Chromatogr. A, 1232 (2012) 212-217.

[177] Y.X. Liu, D. Shou, M.L. Chen, Z.D. Chen, P.M. Zhang, Y. Zhu, Determination of lisinopril using anion exchange chromatography with integrated pulsed amperometric detection, Chin. Chem. Lett., 23 (2012) 335-338.

[178] A. Błażewicz, M. Klatka, W. Dolliver, R. Kocjan, Determination of total iodine in serum and urine samples by ion chromatography with pulsed amperometric detection–Studies on analyte loss, optimization of sample preparation procedures, and validation of analytical method, J. Chromatogr. B, 962 (2014) 141-146.

[179] X.B. Xu, D.B. Liu, S.J. Yu, P. Yu, Z.G. Zhao, Separation and determination of 4-methylimidazole, 2-methylimidazole and 5-hydroxymethylfurfural in beverages by amino trap column coupled with pulsed amperometric detection, Food Chem., 169 (2015) 224-229.

[180] J.L. da Silva, M.A. Beluomini, N.R. Stradiotto, Determination of furanic aldehydes in sugarcane bagasse by high-performance liquid chromatography with pulsed amperometric detection using a modified electrode with nickel nanoparticles, J. Sep. Sci., 38 (2015) 3176-3182.

[181] D. Nardiello, C. Palermo, A. Natale, M. Quinto, D. Centonze, Pulsed amperometric detection at glassy carbon electrodes: A new waveform for sensitive and reproducible determination of electroactive compounds, Anal. Chim. Acta, 894 (2015) 1-6.

[182] W. Wu, Q. Xiao, P. Zhang, M. Ye, Y. Wan, H. Liang, Rapid measurement of free cyanide in liquor by ion chromatography with pulsed amperometric detection, Food Chem., 172 (2015) 681-684.

[183] L. du Bois de Maquillé, P. Wund, L. Renaudin, C. Gautier, A. Jardy, J. Vial, D. Thiébaut, P. Fichet, F. Goutelard, Determination of gluconate in nuclear waste by high-performance liquid chromatography: comparison of pulsed amperometric detection and electrospray mass spectrometry detection, J. Radioanal. Nucl. Chem., 306 (2015) 213-220.

[184] S. Zhang, L. Huang, H. Li, X. Chen, F. Wang, D. Zhang, Y. Zhu, A flexible ion chromatography column-switching system with a switching time window (STW) calibration program for the determination of myo-inositol in infant formula by pulsed amperometric detection, Anal. Methods, 7 (2015) 2830-2838.

[185] J.M. Freitas, T. da Costa Oliveira, D.T. Gimenes, R.A. Munoz, E.M. Richter, Simultaneous determination of three species with a single-injection step using batch injection analysis with multiple pulse amperometric detection, Talanta, 146 (2016) 670-675.

[186] Y. Wu, W. Zhao, X. Zhu, F. Wang, M. Zhang, X. Fan, Y. Yuan, C. Hu, X. Deng, E. Adams, Improved liquid chromatography combined with pulsed electrochemical detection for the analysis of etimicin sulfate, J. Sep. Sci., 39 (2016) 1471-1479.

[187] T.d.J. Guedes, M.F. Alecrim, F.M. Oliveira, A.B. Lima, S.L. Barbosa, W.T.P. dos Santos, Determination of prazosin in pharmaceutical samples by flow injection analysis with multiple-pulse amperometric detection using boron-doped diamond electrode, J. Solid State Electrochem., 20 (2016) 2445-2451.

[188] Z. Szabo, J.R. Thayer, Y. Agroskin, S. Lin, Y. Liu, K. Srinivasan, J. Saba, R. Viner, A. Huhmer, J. Rohrer, D. Reusch, R. Harfouche, S.H. Khan, C. Pohl, In-depth analyses of native N-linked glycans facilitated by high-performance anion exchange chromatography-pulsed amperometric detection coupled to mass spectrometry, Anal. Bioanal. Chem., 409 (2017) 3089-3101.

[189] E. Jaszczak, S. Narkowicz, J. Namieśnik, Ż. Polkowska, Determination of cyanide in urine and saliva samples by ion chromatography with pulsed amperometric detection, Monatsh. Chem., 148 (2017) 1645-1649.

[190] S. Bottelli, G. Grillo, E. Barindelli, A. Nencioni, A. Di Maria, T. Fossati, Validated high-performance anion-exchange chromatography with pulsed amperometric detection method for the determination of residual keratan sulfate and other glucosamine impurities in sodium chondroitin sulfate, J. Chromatogr. A, 1505 (2017) 43-49.

[191] G.C. Sedenho, J.L. da Silva, M.A. Beluomini, A.C. de Sá, N.R. Stradiotto, Determination of electroactive organic acids in sugarcane vinasse by high performance anion-exchange chromatography with pulsed amperometric detection using a nickel nanoparticle modified boron-doped diamond, Energy Fuels, 31 (2017) 2865-2870.

[192] T. de Jesus Guedes, G. Antônio Reis Andrade, A. Barbosa Lima, R. Amorim Bezerra da Silva, W. Torres Pio dos Santos, Simple and fast determination of warfarin in pharmaceutical samples using boron-doped diamond electrode in bia and fia systems with multiple pulse amperometric detection, Electroanalysis, 29 (2017) 2340-2347.

[193] A.M. Santos, F.C. Vicentini, L.C.S. Figueiredo-Filho, P.B. Deroco, O. Fatibello-Filho, Flow injection simultaneous determination of acetaminophen and tramadol in pharmaceutical and biological samples using multiple pulse amperometric detection with a boron-doped diamond electrode, Diamond Relat. Mater., 60 (2015) 1-8.

[194] D.T. Gimenes, M.C. Marra, J.M. de Freitas, R.A. Abarza Muñoz, E.M. Richter, Simultaneous determination of captopril and hydrochlorothiazide on boron-doped diamond electrode by batch injection analysis with multiple pulse amperometric detection, Sensors Actuators B: Chem., 212 (2015) 411-418.

[195] B.C. Lourencao, R.A. Medeiros, O. Fatibello-Filho, Simultaneous determination of antihypertensive drugs by flow injection analysis using multiple pulse amperometric detection with a cathodically pretreated boron-doped diamond electrode, J. Electroanal. Chem., 754 (2015) 154-159.

[196] L.D. Butler-Thompson, W.A. Jacobs, K.J. Schimpf, J. Austad, L. Basumallick, W.U. Bolong, L. Chen, S. Christiansen, C. Domer, D. Ellingson, G. Lautenschlager, I. Malaviole, S. Purachaka, G. Wang, F. Xong, Determination of myo-inositol in infant, pediatric, and adult formulas by liquid chromatography-pulsed amperometric detection with column switching: Collaborative study, final action 2011.18, J. AOAC Int., 98 (2015) 1666-1678.

[197] W.W. Yan, N.N. Wang, P.M. Zhang, J.J. Zhang, S.C. Wu, Y. Zhu, Analysis of sucrose acetates in a crude 6-O-acetyl sucrose product by on-line hydrolysis-high-performance liquid chromatography with pulsed amperometric detection, J. Chromatogr. A, 1449 (2016) 71-77.

[198] T. Pohnl, C. Bottcher, H. Schulz, M. Sturtz, S. Widder, R. Carle, R.M. Schweiggert, Comparison of high performance anion exchange chromatography with pulsed amperometric detection (HPAEC-PAD) and ultra-high performance liquid chromatography with evaporative light scattering (UHPLC-ELSD) for the analyses of fructooligosaccharides in onion (Allium cepa L.), J. Food Compost. Anal., 63 (2017) 148-156.

[199] S.-M. Lee, J.-S. Jeong, H.-J. Kwon, S.-P. Hong, Quantification of isoflavonoids and triterpene saponins in Astragali Radix, the root of Astragalus membranaceus, via reverse-phase high-performance liquid chromatography coupled with integrated pulsed amperometric detection, J. Chromatogr. B, 1070 (2017) 76-81.

[200] X. Chen, B. Chu, H. Xi, J. Xu, L. Lai, H. Peng, D. Deng, G. Huang, Determination of chlorine ions in raw milk by pulsed amperometric detection in a flow injection system, J. Dairy Sci., 101 (2018) 9647-9658.

[201] P.B. Deroco, R.A. Medeiros, R.C. Rocha-Filho, O. Fatibello-Filho, Selective and simultaneous determination of indigo carmine and allura red in candy samples at the nano-concentration range by flow injection analysis with multiple pulse amperometric detection, Food Chem., 247 (2018) 66-72.

[202] D.T. Muratt, L.S. Muller, T. Dal Molin, C. Viana, L.M. de Carvalho, Pulsed amperometric detection of pharmacologic adulterants in dietary supplements using a gold electrode coupled to HPLC separation, Anal. Methods, 10 (2018) 2226-2233.

[203] D.A.R. Moreira, F.M. de Oliveira, D.M. Pimentel, T.J. Guedes, R.C.S. Luz, F.S. Damos, A.C. Pereira, R.A.B. da Silva, W.T.P. dos Santos, Determination of colchicine in pharmaceutical formulations and urine by multiple-pulse amperometric detection in an fia system using boron-doped diamond electrode, J. Braz. Chem. Soc., 29 (2018) 1796-1802.

[204] A.B. Lima, F.M. de Oliveira, T.d.J. Guedes, R.M.F. Sousa, R.A.A. Munoz, W.T.P. dos Santos, Altered electrochemistry of oxcarbazepine on cathodically treated boron-doped diamond electrode: Selective detection by pulsed amperometric detection coupled to flow-injection analysis, Electrochim. Acta, 260 (2018) 564-570.

[205] A.B. Lima, L.F. Ferreira, S.L. Barbosa, E.D. Gil, R.A.B. da Silva, W.T.P. dos Santos, Selective determination of verapamil in pharmaceutics and urine using a boron-doped diamond electrode coupled to flow injection analysis with multiple-pulse amperometric detection, Electroanalysis, 30 (2018) 1872-1877.

[206] J.L. Erkal, A. Selimovic, B.C. Gross, S.Y. Lockwood, E.L. Walton, S. McNamara, R.S. Martin, D.M. Spence, 3D printed microfluidic devices with integrated versatile and reusable electrodes, LChip, 14 (2014) 2023-2032.

[207] P. Zakaria, M. Macka, G. Gerhardt, P.R. Haddad, Pulsed potentiometric detection in capillary electrophoresis using platinum electrodes, Analyst, 125 (2000) 1519-1523.

[208] M. Ryvolová, J. Preisler, F. Foret, P.C. Hauser, P. Krásenský, B. Paull, M. Macka, Combined contactless conductometric, photometric, and fluorimetric single point detector for capillary separation methods, Anal. Chem., 82 (2010) 129-135.

[209] J. Wang, Electrochemical detection for microscale analytical systems: a review, Talanta, 56 (2002) 223-231.

[210] X. Xu, S. Zhang, H. Chen, J. Kong, Integration of electrochemistry in micro-total analysis systems for biochemical assays: Recent developments, Talanta, 80 (2009) 8-18.

[211] K. Šlais, D. Kouřilová, Electrochemical detector with a 20 nl volume for micro-columns liquid chromatography, Chromatographia, 16 (1982) 265-266.

[212] A.T. Hubbard, D.G. Peters, Electrochemistry in thin layers of solution, C R C Critical Reviews in Anal. Chem., 3 (1973) 201-242.

[213] M. Li, Y.-T. Li, D.-W. Li, Y.-T. Long, Recent developments and applications of screen-printed electrodes in environmental assays—A review, Anal. Chim. Acta, 734 (2012) 31-44.

[214] J.-G. Guan, Y.-Q. Miao, J.-R. Chen, Prussian blue modified amperometric FIA biosensor: one-step immunoassay for α-fetoprotein, Biosens. Bioelectron., 19 (2004) 789-794.

[215] M. Quinto, I. Losito, F. Palmisano, C.G. Zambonin, Disposable interference-free glucose biosensor based on an electropolymerised poly(pyrrole) permselective film, Anal. Chim. Acta, 420 (2000) 9-17.

[216] S. Gáspár, X. Wang, H. Suzuki, E. Csöregi, Amperometric biosensor-based flow-through microdetector for microdialysis applications, Anal. Chim. Acta, 525 (2004) 75-82.

[217] F.R. Caetano, E.A. Carneiro, D. Agustini, L.C.S. Figueiredo-Filho, C.E. Banks, M.F. Bergamini, L.H. Marcolino-Junior, Combination of electrochemical biosensor and textile threads: A microfluidic device for phenol determination in tap water, Biosens. Bioelectron., 99 (2018) 382-388.

[218] P.J. O'Connell, C. Gormally, M. Pravda, G.G. Guilbault, Development of an amperometric l-ascorbic acid (Vitamin C) sensor based on electropolymerised aniline for pharmaceutical and food analysis, Anal. Chim. Acta, 431 (2001) 239-247.

[219] T. Pluangklang, J.B. Wydallis, D.M. Cate, D. Nacapricha, C.S. Henry, A simple microfluidic electrochemical HPLC detector for quantifying Fenton reactivity from welding fumes, Anal. Methods, 6 (2014) 8180-8186.

[220] Y. Li, M. Dvorak, P.N. Nesterenko, R. Stanley, N. Nuchtavorn, L.K. Krcmova, J. Aufartova, M. Macka, Miniaturised medium pressure capillary liquid chromatography system with flexible open platform design using off-the-shelf microfluidic components, Anal. Chim. Acta, 896 (2015) 166-176.

[221] F.J. Ansuini, J.R. Dimond, Factors affecting the accuracy of reference electrodes, NACE International, Houston, Texas (USA), 1994.

[222] M. Bicking, Technical Resources, Troubleshooting HPLC Separation Issues, Crawford Scientific™ Ltd., Lanarkshire, 2018. https://www.crawfordscientific.com/technical/chromatography-technical-tips/hplc-chromatography-tips/troubleshooting-hplc-separation-issues.

[223] E.J. Calvo, Chapter 1 Fundamentals. The Basics of Electrode Reactions, in: C.H. Bamford, R.G. Compton (Eds.) Comprehensive Chemical Kinetics, Elsevier 1986, pp. 1-78.

[224] H. Ji, E. Wang, Amperometric detection at a carbon-fibre array ring/glassy-carbon disk electrode in a wall-jet cell, Talanta, 38 (1991) 73-80.

[225] E.S. Ng, N.W. Chan, D.F. Lewis, O. Hindsgaul, D.C. Schriemer, Frontal affinity chromatography-mass spectrometry, Nat. Protoc., 2 (2007) 1907-1917.

[226] K. Štulík, V. Pacáková, Electrochemical detection in HPLC. Part. 1. Principles, techniques and instrumentation, Food / Nahrung, 29 (1985) 501-516.

[227] H. Gu, E.L. Varner, S.R. Groskreutz, A.C. Michael, S.G. Weber, In vivo monitoring of dopamine by microdialysis with 1 min temporal resolution using online capillary liquid chromatography with electrochemical detection, Anal. Chem., 87 (2015) 6088-6094.

[228] M. Steinhart, Introduction to nanotechnology. By Charles P. Poole, Jr. and Frank J. Owens, Angew. Chem. Int. Ed., 43 (2004) 2196-2197.

[229] X. Luo, A. Morrin, A.J. Killard, M.R. Smyth, Application of nanoparticles in electrochemical sensors and biosensors, Electroanalysis, 18 (2006) 319-326.

[230] J. Wang, Nanomaterial-based electrochemical biosensors, Analyst, 130 (2005) 421-426.

[231] G. March, T.D. Nguyen, B. Piro, Modified electrodes used for electrochemical detection of metal ions in environmental analysis, Biosensors, 5 (2015) 241-275.

[232] Z. Taleat, A. Khoshroo, M. Mazloum-Ardakani, Screen-printed electrodes for biosensing: a review (2008–2013), Microchim. Acta, 181 (2014) 865-891.

[233] V. Bhalla, S. Carrara, P. Sharma, Y. Nangia, C. Raman Suri, Gold nanoparticles mediated label-free capacitance detection of cardiac troponin I, Sensors Actuators B: Chem., 161 (2012) 761-768.

[234] M. Mazloum-Ardakani, A. Dehghani-Firouzabadi, N. Rajabzade, M.A. Sheikh-Mohseni, A. Benvidi, M. Abdollahi-Alibeik, MCM/ZrO_2 nanoparticles modified electrode for simultaneous and selective voltammetric determination of epinephrine and acetaminophen, J. Iran. Chem. Soc., 10 (2013) 1-5.

[235] S.E.F. Kleijn, S.C.S. Lai, M.T.M. Koper, P.R. Unwin, Electrochemistry of nanoparticles, Angew. Chem. Int. Ed., 53 (2014) 3558-3586.

[236] M.A. Islam, S.C. Lam, Y. Li, M.A. Atia, P. Mahbub, P.N. Nesterenko, B. Paull, M. Macka, Capillary gap flow cell as capillary-end electrochemical detector in flow-based analysis, Electrochim. Acta, 303 (2019) 85-93.

[237] C. Karuwan, T. Mantim, P. Chaisuwan, P. Wilairat, K. Grudpan, P. Jittangprasert, Y. Einaga, O. Chailapakul, L. Suntornsuk, O. Anurukvorakun, Pulsed amperometry for anti-fouling of boron-doped diamond in electroanalysis of β-agonists: application to flow injection for pharmaceutical analysis, Sensors, 6 (2006) 1837-1850.

[238] T. Peik-See, A. Pandikumar, H. Nay-Ming, L. Hong-Ngee, Y. Sulaiman, Simultaneous electrochemical detection of dopamine and ascorbic acid using an iron oxide/reduced graphene oxide modified glassy carbon electrode, Sensors, 14 (2014) 15227-15243.

[239] Periodic table technical data, Wolfram Research Inc., http://periodictable.com/Elements/079/data.wt.html (accessed July 2018).

[240] P.K.Q. Nguyen, Cyclic voltammetric and square wave anodic stripping voltammetric analysis of lead and cadmium utilizing the novel titanium dioxide/zirconium dioxide/tween 80 carbon paste composite electrode, Wright State University, Dayton, USA, 2013, pp. 1-160.

[241] P.K.Q. Nguyen, S.K. Lunsford, Electrochemical response of carbon paste electrode modified with mixture of titanium dioxide/zirconium dioxide in the detection of heavy metals: Lead and cadmium, Talanta, 101 (2012) 110-121.

[242] N.M. Ahmad, J. Abdullah, N.A. Yusof, A.H. Ab Rashid, S. Abd Rahman, M.R. Hasan, Amperometric biosensor based on zirconium oxide/polyethylene glycol/tyrosinase composite film for the detection of phenolic compounds, Biosensors, 6 (2016) 31-44.

[243] Y. Zhang, X. Chen, W. Yang, Direct electrochemistry and electrocatalysis of myoglobin immobilized in zirconium phosphate nanosheets film, Sensors Actuators B: Chem., 130 (2008) 682-688.

[244] I.A. Rutkowska, A. Wadas, P.J. Kulesza, Mixed layered WO_3/ZrO_2 films (with and without rhodium) as active supports for PtRu nanoparticles: enhancement of oxidation of ethanol, Electrochim. Acta, 210 (2016) 575-587.

[245] G.K. Sidhu, R. Kumar, Role of anionic and cationic surfactants on the structural and dielectric properties of ZrO_2 nanoparticles, Appl. Surf. Sci., 392 (2017) 598-607.

[246] J. Li, Y. Hu, P.W. Carr, Fast separations at elevated temperatures on polybutadiene-coated zirconia reversed-phase material, Anal. Chem., 69 (1997) 3884-3888.

[247] H. Karimi-Maleh, M. Moazampour, A.A. Ensafi, S. Mallakpour, M. Hatami, An electrochemical nanocomposite modified carbon paste electrode as a sensor for simultaneous determination of hydrazine and phenol in water and wastewater samples, Environ. Sci. Pollut. Res., 21 (2014) 5879-5888.

[248] I.M. Ibrahim, M.E. Moustafa, M.R. Abdelhamid, Effect of organic acids precursors on the morphology and size of ZrO_2 nanoparticles for photocatalytic degradation of Orange G dye from aqueous solutions, J. Mol. Liq., 223 (2016) 741-748.

[249] M.B. Gholivand, A. Azadbakht, A novel hydrazine electrochemical sensor based on a zirconium hexacyanoferrate film-bimetallic Au–Pt inorganic–organic hybrid nanocomposite onto glassy carbon-modified electrode, Electrochim. Acta, 56 (2011) 10044-10054.

[250] Voltammetric methods, Electrochemical methods, LibreTexts libraries, The California State University

https://chem.libretexts.org/LibreTexts/Northeastern/11%3A_Electrochemical_Methods/11.4%3A_Voltammetric_Methods (01.04.2019).

[251] Z. Nie, C.A. Nijhuis, J. Gong, X. Chen, A. Kumachev, A.W. Martinez, M. Narovlyansky, G.M. Whitesides, Electrochemical sensing in paper-based microfluidic devices, Lab Chip, 10 (2010) 477-483.

[252] 2,3-Dihydroxybenzoic acid, National Centre for Biotechnology Information, U.S. National Library of Medicine, Rockville Pike, USA.

[253] Pyrocatechol, National Center for Biotechnology Information, U.S. National Library of Medicine, Rockville Pike, USA.

[254] C.-c. Jiang, Y.-k. Cao, G.-y. Xiao, R.-f. Zhu, Y.-p. Lu, A review on the application of inorganic nanoparticles in chemical surface coatings on metallic substrates, RSC Advances, 7 (2017) 7531-7539.

[255] L. Ghasemi-Mobarakeh, D. Semnani, M. Morshed, A novel method for porosity measurement of various surface layers of nanofibers mat using image analysis for tissue engineering applications, J. Appl. Polym. Sci., 106 (2007) 2536-2542.

[256] W. He, Z. Ma, T. Yong, W.E. Teo, S. Ramakrishna, Fabrication of collagen-coated biodegradable polymer nanofiber mesh and its potential for endothelial cells growth, Biomaterials, 26 (2005) 7606-7615.

[257] G.R. Blake, Particle density, in: W. Chesworth (Ed.) Encyclopedia of Soil Science, Springer Netherlands, Dordrecht, 2008, pp. 504-505.

[258] Zirconium oxide nanopowder, US Research Nanomaterials Inc., Houston, TX 77084, USA.

[259] N. Elgrishi, K.J. Rountree, B.D. McCarthy, E.S. Rountree, T.T. Eisenhart, J.L. Dempsey, A Practical Beginner's Guide to Cyclic Voltammetry, J. Chem. Educ., 95 (2018) 197-206.

[260] V. Fragkou, Y. Ge, G. Steiner, D. Freeman, N. Bartetzko, A.P. Turner, Determination of the real surface area of a screen-printed electrode by chronocoulometry, Int. J. Electrochem. Sci, 7 (2012) 6214-6220.

[261] S. Trasatti, O.A. Petrii, Real surface area measurements in electrochemistry, J. Electroanal. Chem., 327 (1992) 353-376.

[262] D. Sawyer, W. Heineman, J. Beebe, Chemistry experiments for instrumental analysis, John Wiley & Sons, Inc., New York, 1984.

[263] J. Moldenhauer, M. Meier, D.W. Paul, Rapid and direct determination of diffusion coefficients using microelectrode arrays, J. Electrochem. Soc., 163 (2016) H672-H678.

[264] J. Krejci, Z. Sajdlova, V. Nedela, E. Flodrova, R. Sejnohova, H. Vranova, R. Plicka, Effective surface area of electrochemical sensors, J. Electrochem. Soc., 161 (2014) B147-B150.

[265] L.M. Da Silva, L.A. De Faria, J.F.C. Boodts, Determination of the morphology factor of oxide layers, Electrochim. Acta, 47 (2001) 395-403.

[266] C. Lämmel, M. Schneider, M. Weiser, A. Michaelis, Investigations of electrochemical double layer capacitor (EDLC) materials – a comparison of test methods, Materialwiss. Werkstofftech., 44 (2013) 641-649.

[267] Y. Lin, H. Zhao, F. Yu, J. Yang, Design of an Extended Experiment with Electrical Double Layer Capacitors: Electrochemical Energy Storage Devices in Green Chemistry, Sustainability, 10 (2018) 3630-3638.

[268] J.E. Troyan, Properties, production, and uses of hydrazine, Ind. Eng. Chem., 45 (1953) 2608-2612.

[269] B. Toth, A review of the natural occurrence, synthetic production and use of carcinogenic hydrazines and related chemicals, In Vivo, 14 (2000) 299-319.

[270] B. Toth, Toxicities of hydrazines: a review, In Vivo, 2 (1988) 209-242.

[271] M. Matsumoto, H. Kano, M. Suzuki, T. Katagiri, Y. Umeda, S. Fukushima, Carcinogenicity and chronic toxicity of hydrazine monohydrate in rats and mice by two-year drinking water treatment, Regul. Toxicol. Pharm., 76 (2016) 63-73.

[272] S. Parodi, S.D. Flora, M. Cavanna, A. Pino, L. Robbiano, C. Bennicelli, G. Brambilla, DNA-damaging activity in vivo and bacterial mutagenicity of sixteen hydrazine derivatives as related quantitatively to their carcinogenicity, Cancer Res., 41 (1981) 1469.

[273] A. Safavi, M.A. Karimi, Flow injection chemiluminescence determination of hydrazine by oxidation with chlorinated isocyanurates, Talanta, 58 (2002) 785-792.

[274] A.M. El-Brashy, L.A. El-Hussein, Colorimetric determination of some important hydrazine derivatives, Anal. Lett., 30 (1997) 609-622.

[275] A.D. Smolenkov, I.A. Rodin, O.A. Shpigun, Spectrophotometric and fluorometric methods for the determination of hydrazine and its methylated analogues, J. Anal. Chem., 67 (2012) 98-113.

[276] S.S. Yamamura, J.H. Sikes, Analysis of ammonia-hydrazine mixtures for both components, Anal. Chem., 35 (1963) 1958-1960.

[277] Z. Wei, Z. Hai, M.K. Akbari, J. Hu, L. Hyde, S. Depuydt, F. Verpoort, S. Zhuiykov, Ultrasensitive, sustainable, and selective electrochemical hydrazine detection by ALD-developed two-dimensional WO_3, ChemElectroChem, 5 (2018) 266-272.

[278] A. Benvidi, M. Nikmanesh, M. Dehghan Tezerjani, S. Jahanbani, M. Abdollahi, A. Akbari, A. Rezaeipoor-Anari, A comparative study of various electrochemical sensors for hydrazine detection based on imidazole derivative and different nano-materials of MCM-41, RGO and MWCNTs: Using net analyte signal (NAS) for simultaneous determination of hydrazine and phenol, J. Electroanal. Chem., 787 (2017) 145-157.

[279] J.W. Wu, T.T. Zhou, Q. Wang, A. Umar, Morphology and chemical composition dependent synthesis and electrochemical properties of MnO2-based nanostructures for efficient hydrazine detection, Sensors Actuators B: Chem., 224 (2016) 878-884.

[280] Z. Zhao, Y. Wang, P. Li, S. Sang, W. Zhang, J. Hu, K. Lian, A highly sensitive electrochemical sensor based on Cu/Cu<inf>2</inf>O@carbon nanocomposite structures for hydrazine detection, Analytical Methods, 7 (2015) 9040-9046.

[281] B.K. Jena, C.R. Raj, Ultrasensitive nanostructured platform for the electrochemical sensing of hydrazine, J. Phys. Chem. C, 111 (2007) 6228-6232.

[282] S. Rostami, S.N. Azizi, S. Ghasemi, Simultaneous electrochemical determination of hydrazine and hydroxylamine by CuO doped in ZSM-5 nanoparticles as a new amperometric sensor, New J. Chem., 41 (2017) 13712-13723.

[283] S.P. Kim, H.C. Choi, Reusable hydrazine amperometric sensor based on Nafion®-coated TiO_2–carbon nanotube modified electrode, Sensors Actuators B: Chem., 207 (2015) 424-429.

[284] S. Sakthinathan, S. Kubendhiran, S.-M. Chen, M. Govindasamy, F.M.A. Al-Hemaid, M. Ajmal Ali, P. Tamizhdurai, S. Sivasanker, Metallated porphyrin noncovalent interaction with reduced graphene oxide-modified electrode for amperometric detection of environmental pollutant hydrazine, Appl. Organomet. Chem., 31 (2017) e3703.

[285] R. Devasenathipathy, V. Mani, S.-M. Chen, Highly selective amperometric sensor for the trace level detection of hydrazine at bismuth nanoparticles decorated graphene nanosheets modified electrode, Talanta, 124 (2014) 43-51.

[286] K.R. Karuppasamy, R. Devasenathipathy, S.F. Wang, A glassy carbon electrode modified with graphene oxide decorated silver phosphate nanodentrites for amperometric determination of dissolved hydrazine, Microchimica Acta, 184 (2017) 2569-2577.

[287] L. Guo, F.M. Matysik, P. Glasser, W. Engewald, Determination of hydrazine, monomethylhydrazine, 1,1-dimethylhydrazine, and 1,2-dimethylhydrazine by nonaqueous capillary electrophoresis with amperometric detection, Electrophoresis, 26 (2005) 3341-3348.

[288] J.H. Zhao, J.X. Liu, S. Tricard, L. Wang, Y.L. Liang, L.H. Cao, J. Fang, W.G. Shen, Amperometric detection of hydrazine utilizing synergistic action of prussian blue @ silver nanoparticles/graphite felt modified electrode, Electrochim. Acta, 171 (2015) 121-127.

[289] S.L. Larson, A.B. Strong, Ion chromatography with electrochemical detection for hydrazine quantitation in environmental sample, U.S. Army Crops of Engineers, Washinton, DC, 1996. https://apps.dtic.mil/dtic/tr/fulltext/u2/a306785.pdf.

[290] T.T. Christison, B.D. Borba, J. Rohrer, Determination of morpholine, ethanolamine, and hydrazine in simulated nuclear power plant wastewater, Thermo Fisher Scientific, Sunnyvale, CA, USA, 2016. https://assets.thermofisher.com/tfs-assets/cmd/application-notes/an-247-ic-morpholine-ethanolamine-hydrazine-wasterwater-an71553-en.pdf.

[291] S. Stankovich, D.A. Dikin, R.D. Piner, K.A. Kohlhaas, A. Kleinhammes, Y. Jia, Y. Wu, S.T. Nguyen, R.S. Ruoff, Synthesis of graphene-based nanosheets via chemical reduction of exfoliated graphite oxide, Carbon, 45 (2007) 1558-1565.

[292] C.K. Chua, M. Pumera, Chemical reduction of graphene oxide: a synthetic chemistry viewpoint, Chem. Soc. Rev., 43 (2014) 291-312.

[293] D. Li, M.B. Müller, S. Gilje, R.B. Kaner, G.G. Wallace, Processable aqueous dispersions of graphene nanosheets, Nat. Nanotechnol., 3 (2008) 101.

[294] P.-G. Ren, D.-X. Yan, X. Ji, T. Chen, Z.-M. Li, Temperature dependence of graphene oxide reduced by hydrazine hydrate, Nanotechnology, 22 (2010) 055705.

[295] M. Venkanna, A.K. Chakraborty, Synthesis and characterizations of graphene oxide and reduced graphene oxide nanosheets, AIP Conf. Proc., 1591 (2014) 574-576.

[296] S. Pei, H.-M. Cheng, The reduction of graphene oxide, Carbon, 50 (2012) 3210-3228.

[297] A.N. Koreshkova, V. Gupta, A. Peristyy, P.N. Nesterenko, T. Rodemann, B. Paull, Ion chromatographic determination of hydrazine in excess ammonia for monitoring graphene oxide reduction reaction, Talanta, 205 (2019) 120081.

[298] A. Smolenkov, A. Pirogov, O. Shpigun, Separation of Hydrazine and Its Methylderivatives by Ion Chromatography with Amperometric Detection, Analytical Sciences/Supplements, 17icas (2002) i769-i772.

[299] K. Zhang, M. Cao, C. Lou, S. Wu, P. Zhang, M. Zhi, Y. Zhu, Graphene-coated polymeric anion exchangers for ion chromatography, Anal. Chim. Acta, 970 (2017) 73-81.

[300] L. Aldous, R.G. Compton, The mechanism of hydrazine electro-oxidation revealed by platinum microelectrodes: role of residual oxides, PCCP, 13 (2011) 5279-5287.

[301] R.E. Roberts, D.C. Johnson, Fast-pulsed electrochemical detection at noble metal electrodes: The frequency-dependent response at gold electrodes for chromatographically separated carbohydrates, Electroanalysis, 6 (1994) 269-273.

[302] B.E. Conway, G. Tremiliosi-Filho, G. Jerkiewicz, Independence of formation and reduction of monolayer surface oxide on Pt from presence of thicker phase-oxide layers, J. Electroanal. Chem. Interfacial. Electrochem., 297 (1991) 435-443.

[303] R. Gilbert, R. Rioux, S.E. Saheb, Ion chromatographic determination of morpholine and cyclohexylamine in aqueous solutions containing ammonia and hydrazine, Anal. Chem., 56 (1984) 106-109.

[304] S. Pervaiz, M.A. Farrukh, R. Adnan, F.A. Qureshi, Kinetic investigation of redox reaction between vitamin C and ferric chloride hexahydrate in acidic medium, Journal of Saudi Chemical Society, 16 (2012) 63-67.

[305] V. Andal, G. Buvaneswari, Effect of reducing agents in the conversion of Cu_2O nanocolloid to Cu nanocolloid, Engineering Science and Technology, an International Journal, 20 (2017) 340-344.

[306] W.C.E. Higginson, D. Sutton, P. Wright, 282. The oxidation of hydrazine in aqueous solution. Part I. The nature of 1- and 2-electron-transfer reactions, with particular reference to the oxidation of hydrazine, Journal of the Chemical Society (Resumed), (1953) 1380-1386.

[307] H. Borsook, G. Keighley, Oxidation-reduction potential of ascorbic acid (Vitamin C), Proc. Natl. Acad. Sci. U. S. A., 19 (1933) 875-878.

[308] J.D. Andrade, X-ray Photoelectron Spectroscopy (XPS), in: J.D. Andrade (Ed.) Surface and Interfacial Aspects of Biomedical Polymers: Volume 1 Surface Chemistry and Physics, Springer US, Boston, MA, 1985, pp. 105-195.

[309] S.P. Levine, Y. Li-Shi, C.R. Strang, X. Hong-Kui, Advantages and Disadvantages in the Use of Fourier Transform Infrared (FTIR) and Filter Infrared (FIR) Spectrometers for Monitoring Airborne Gases and Vapors of Industrial Hygiene Concern, Applied Industrial Hygiene, 4 (1989) 180-187.

[310] A. Rios, M. Silva, M. Valcarcel, Fluorimetric determination of ammonia, hydrazine and hydroxylamine and their mixtures by differential kinetic methods, Fresenius J. Anal. Chem., 320 (1985) 762-768.

[311] G.E. Collins, S.L. Rose-Pehrsson, Sensitive, fluorescent detection of hydrazine via derivatization with 2,3-naphthalene dicarboxaldehyde, Anal. Chim. Acta, 284 (1993) 207-215.

[312] F.M. Bauzá de Mirabó, R. Forteza, V. Cerdà, A multisyringe sequential injection method for monitoring water in the energy cogeneration system of a municipal waste incinerator, Talanta, 79 (2009) 1011-1020.

[313] S. Gilje, S. Han, M. Wang, K.L. Wang, R.B. Kaner, A chemical route to graphene for device applications, Nano Lett., 7 (2007) 3394-3398.